Titre: Title:	Three-Dimensional Microstructures of Epoxy-Carbon Nanotube Nanocomposites
Auteur: Author:	Rouhollah Dermanaki Farahani
Date:	2011
Type:	Mémoire ou thèse / Dissertation or Thesis
Référence: Citation:	Dermanaki Farahani, R. (2011). Three-Dimensional Microstructures of Epoxy-Carbon Nanotube Nanocomposites [Thèse de doctorat, École Polytechnique de Montréal]. PolyPublie. https://publications.polymtl.ca/689/

URL de PolyPublie: PolyPublie URL:	https://publications.polymtl.ca/689/
Directeurs de recherche: Advisors:	Daniel Therriault, & Martin Lévesque
Programme: Program:	Génie mécanique

UNIVERSITÉ DE MONTRÉAL

THREE-DIMENSIONAL MICROSTRUCTURES OF EPOXY-CARBON NANOTUBE NANOCOMPOSITES

ROUHOLLAH DERMANAKI FARAHANI

DÉPARTEMENT DE GÉNIE MÉCANIQUE

ÉCOLE POLYTECHNIQUE DE MONTRÉAL

THÈSE PRÉSENTÉE EN VUE DE L'OBTENTION

DU DIPLÔME DE PHILOSOPHIAE DOCTOR

(GÉNIE MÉCANIQUE)

NOVEMBRE 2011

UNIVERSITÉ DE MONTRÉAL

ÉCOLE POLYTECHNIQUE DE MONTRÉAL

Cette thèse intitulée:

THREE-DIMENSIONAL MICROSTRUCTURES OF EPOXY-CARBON NANOTUBE NANOCOMPOSITES

présentée par: DERMANAKI FARAHANI Rouhollah
en vue de l'obtention de diplôme de : Philosophiae Doctor
a été dûment acceptée par le jury d'examen constitué de :

Mme. ROSS Annie, Ph. D., présidente
M. THERRIAULT Daniel, Ph. D., membre et directeur de recherche
M. LÉVESQUE Martin, Ph. D., membre et codirecteur de recherche
M. BOUKHILI Rachid, Ph. D., membre
Mme. DENAULT Johanne, Ph. D., membre

DEDICATIONS

To my mother; for her emotional supports!

To Elham; for giving me the chance to experience the concept of love!

ACKNOWLEDGEMENTS

I wish to thank all those who supported me in the completion of this study and made the way of research smooth for me.

First of all, I would like to convey my gratitude to my advisors, Professor Daniel Therriault and Professor Martin Lévesque, who provided me with fundamental advises. They always supported me very well in my research with availability, patience and encouragement. I am very grateful for the things that I learnt from them; not only the scientific matters, but also lots of knowledge which are very helpful in all aspects of my life. It had been a true privilege to learn from such competent and sincere supervisors.

I also gratefully thank our collaborators at Institut National de la Recherche Scientifique, INRS-Énergie, Matériaux et Télécommunications, especially Professor My Ali El Khakani and Dr. Barhim Aissa for their valuable advises and for providing single-walled carbon nanotubes and their characterizations.

I owe special gratitude to the members of Laboratory for Multiscale Mechanics (LM2) research group who made the working place a fascinating area. My especial thanks are due to Dr. Hamid Dalir for his sympathy, support and many things that I have learnt from him. I would like to thank Dr. Louis Laberge Lebel for his great kindness to help me in the first year of my study.

I like to extent my thanks to the entire technical and administrative staff of the Mechanical Engineering Department at École Polytechnique de Montréal.

I would like to acknowledge financial support from FQRNT (Le Fonds Québécois de la Recherche sur la Nature et les Technologies).

I would also like to send a heartfelt acknowledgment to my friends who made all these years vey joyful with interesting, intellectual and creative ideas. Habib, Maryam, Farhad, Hadi, Hamid, Navid, Ebrahim, Hassan, Behzad …

Finally I could not have accomplished this without all the supports of my family, especially my lovely wife. They are the driving force behind all of my successes. To them I tribute a fervent thanks.

RÉSUMÉ

Dans les dernières décennies, la communauté scientifique a réalisé des efforts considérables dans le but d'avancer dans les domaines de la micro- et nanotechnologies. Cela est dû au grand potentiel de ces technologies dans une large variété d'applications, allant des composites structuraux jusqu'aux systèmes microélectromécaniques (MEMS) et à l'électronique organique. Pour de telles applications, les nanocomposites à base de polymères renforcés par des nanotubes de carbone (CNTs), plus spécifiquement les nanotubes de carbone à paroi simple, représentent un matériau prometteur grâce à ses propriétés mécaniques et électriques lorsque comparé aux résines conventionnelles. Toutefois, plusieurs défis quant au traitement et à la fabrication du nanomcomposite doivent être adressés dans l'objectif d'augmenter l'efficacité de ces nanocomposites. La production de nanotubes de carbone de haute qualité ayant un grand rapport de forme, leur dispersion dans la matrice polymère ainsi que l'amélioration de l'adhésion à l'interface sont tous des paramètres importants dans le comportement mécanique et électrique des nanocomposites. Ces paramètres pourraient être ingénieusement établis afin d'obtenir des propriétés optimales pour les micro- et macro- applications du nanocomposite. Cependant, la miniaturisation et l'optimisation des formes tridimensionnelles des systèmes en nanocomposite sont loin de leur plein potentiel, partiellement à cause du manque des techniques de fabrication adéquates.

Cette thèse présente le développement des matériaux nanocomposites pour la fabrication de microstructures tridimensionnelles (3D) en utilisant les techniques de l'écriture-directe (DW), la micro-infiltration et l'écriture directe assistée par rayonnement UV (UV-DW). La thèse adresse deux parties principales: la préparation du nanocomposite et la fabrication des structures 3D de nanocomposites. Des nanotubes de carbone à paroi simple de haute qualité ont été produits par la

méthode d'ablation lazer UV pour ensuite subir une purification chimique. En utilisant un surfactant, une fonctionnalisation non-covalente a été réalisée sur la surface des nanotubes afin d'avoir une interaction additionnelle avec la matrice polymère. Différentes stratégies de mélange ont été utilisées pour aboutir à une meilleure dispersion des nanotubes de carbone dans la matrice d'époxy tel que le brassage, l'ultrasonication et le mélange par cisaillement élevé. Une autre étape de fonctionnalisation, cette fois avec des bio-molécules, a été aussi réalisée sur la surface des nanotubes pour améliorer encore plus les propriétés des nanocomposites. Des observations par microscopie optique et microscopie électronique à balayage ont révélé que ces bio-molécules ont amélioré la dispersion des nanotubes de carbone dans la matrice. La caractérisation mécanique a démontré une amélioration considérable dans la résistance (76%) et le module de rigidité (93%) du nanocomposite par rapport à l'époxy dans son état pur, et ce en ajoutant seulement 1% massique de nanotubes de carbone bio-fonctionnalisés.

Dans la deuxième partie de la thèse, des techniques de fabrication ont été utilisées afin de façonner sur mesures les propriétés effectives des microstructures 3D du nanocomposite. Premièrement, la méthode d'écriture directe et celle de la micro-infiltration ont été utilisées pour fabriquer des microstructures 3D de poutrelles en nanocomposites. Les propriétés statiques et dynamiques des poutrelles ont été obtenues en prenant avantage du positionnement et de l'orientation 3D des nanotubes de carbone. Les poutrelles à matrice époxy avec un squelette 3D de microfibres en nanocomposite ont été fabriquées en infiltrant le nanocomposite renforcé par les nanotubes dans un réseau microfluidique tridimensionnel de canaux poreux. L'efficacité de cette approche a été étudiée systématiquement en utilisant différentes résines d'époxy. Les propriétés dépendant de la température de ces poutrelles sont différentes des propriétés individuelles de leurs constituants. La squelette des microfibres a été conçu pour offrir une

meilleure performance face à une sollicitation de flexion en positionnant les microfibres dans les régions subissant les plus hauts niveaux de contraintes.

Par la suite, le mélange de nanocomposite a été injecté dans le réseau de canaux poreux sous deux différents niveaux de pression, obtenant ainsi deux niveaux de cisaillement différents lors de l'injection. Ceci a été réalisé dans l'objectif d'aligner les nanotubes dans les microfibres des poutrelles. Des études morphologiques et des observations de microsocopie électronique à transmission ont révélé que les nanotubes sont partiellement alignées dans les canaux microfluidiques selon la direction du flux et ce pour le cas où la plus grande valeur de pression est appliquée. Les mesures de rigidité ont été comparées avec les prédictions théoriques d'un modèle micromécanique. Considérant la faible fraction massique des nanotubes (~0.2 %), les nanotubes de carbone et leur alignement partiel ont causé une amélioration considérable de la rigidité lorsque comparé avec l'époxy pur. Basé sur les résultats expérimentaux et théoriques, la méthode de fabrication présentée aide à aligner les nanotubes de carbone dans le nanocomposite grâce du flux de cisaillement et du confinement dimensionnel dans les canaux microfluidiques.

Le dernier point étudié dans la présente recherche est l'utilisation de la méthode d'écriture directe assistée par UV pour la fabrication de formes auto-portantes de nanocomposites destinées à des capteurs de déformation. La complexité des capteurs produits démontre les larges possibilités de la méthode de fabrication lorsque comparé à la méthode conventionnelle de la photolithographie. La sensibilité électromécanique du capteur a été évaluée en corrélant la résistivité mesurée aux déplacement/déformations appliqués. Des mesures de conductivité électrique révèlent que les capteurs produits sont très sensibles aux petites perturbations mécaniques, surtout lorsqu'on compare la sensibilité avec des faibles fractions de nanotubes aux capteurs traditionnels en métaux ou aux capteurs à base de films de nanocomposite.

Les procédures de préparation des nanocomposites présentées ici : la purificication des nanotubes, la fonctionnalisation non covalente, la bio-fonctionnalisation et la stratégie de mélange des nanocomposites aident à développer des nanocomposites de haute performance et étendre leurs applications et leurs fonctionnalités. Les dispositifs conûs dans le présent travail offrent une nouvelle perspective quant à la fabrication des microstructures 3D de nanocomposites et ce pour une large gamme d'applications tel que l'électronique organique, les capteurs de déformations à très haute sensibilité ainsi que d'autres applications dans le domaine aérospatial.

ABSTRACT

Over the last few decades, worldwide increasing effort has been directed towards achieving advances in micro- and nanotechnologies. This is motivated by their high potential for a wide variety of technological applications, ranging from structural composites to micro electromechanical systems (MEMS) and organic electronics. For such applications, polymer nanocomposites reinforced with carbon nanotubes (CNTs), and more specifically single-walled carbon nanotubes (SWCNTs), are promising materials compared to conventional resins due to their interesting mechanical and electrical properties. However, several fundamental processing and fabrication challenges have to be addressed in order to effectively use these nanocomposites. Production of high quality carbon nanotubes (CNTs) having large aspect ratio, their proper dispersion in polymer matrices as well as the improvement of interfacial bonding are the main parameters affecting their mechanical and electrical performance. Moreover, these materials can be engineered to deliver optimal properties for micro- and macro-devices. However, device miniaturization and three-dimensional shape optimization have not reached their full potential, partly because of the lack of suitable manufacturing techniques.

This thesis reports the development of nanocomposite materials for the fabrication of three-dimensional (3D) microstructures with direct-write (DW), micro-infiltration and UV-assisted direct-write (UV-DW) techniques. The thesis focuses on two main parts; nanocomposite preparation and nanocomposite-based 3D microstructures fabrication. High-quality SWCNTs were produced by the UV-laser ablation method and then subjected to a chemical purification. A non-covalent functionalization with a surfactant was performed for additional interaction with the matrix. Different mixing strategies including stirring, ultrasonication and high shear mixing were used to properly disperse SWCNTs within an epoxy matrix. Subsequent functionalization

with biomolecules was also applied on the nanotubes surface for improving further the nanocomposites properties. Optical and scanning electron microscope observations revealed that the biomolecules improved the nanotube dispersion into the epoxy matrix. Mechanical characterization showed that nanocomposites demonstrated considerable enhancement in both strength (by 76%) and modulus (by 93%), with respect to the bulk epoxy, with the addition of only 1 wt% of biofunctionalized-SWCNTs.

In the second part of this thesis, a few fabrication techniques have been used to tailor the overall properties of 3D microstructures. First, the DW and micro-infiltration techniques were employed to manufacture a 3D-reinforced nanocomposite. The dynamic and static mechanical properties of the beams were successfully tailored by taking advantage of nanotubes 3D positioning and orienting. To this end, epoxy composite beams reinforced with a complex nanocomposite microfibers 3D skeleton were fabricated via the micro-infiltration of carbon nanotube nanocomposites into a 3D porous microfluidic network. The effectiveness of this manufacturing approach was systematically studied by using different epoxy resins. The temperature-dependent mechanical properties of these multifunctional beams showed different features than their individual constituents. The microfibers 3D pattern was adapted to offer better performance under flexural solicitation by positioning most of the reinforcing microfibers in higher stress regions.

Subsequently, the nanocomposite suspensions were injected into the empty networks under two different controlled and constant pressures for subjecting the suspensions to different shear conditions. This procedure was performed in an attempt to control the nanotubes orientations into the 3D-reinforced beams. Morphological studies and transmission electron microscopy (TEM) observation revealed that the SWCNTs were preferentially aligned in the microchannels

along the flow direction at the higher injection pressure. The 3D-reinforced beams stiffness was compared with the theoretically predicted values obtained from a micromechanical model. Given the very low amount of nanotube added (~0.2 wt.%), the nanotubes orientation led to a considerable increase (~14%) of the nanocomposite's stiffness when compared to the neat epoxy. Based on the experimental and theoretical results, the present manufacturing technique enables the spatial orientation of nanotubes in the final product by taking advantage of shear flow combined with dimensional constraining inside the microfluidic channels.

The final point studied in this research was to use the UV-DW technique for the fabrication of 3D freestanding patterned nanocomposite strain sensors. The complexity of the manufactured sensors demonstrated the high capability of the technique when compared to conventional photolithographic technologies. The sensors electromechanical sensitivities were evaluated by correlating their measured resistivities to the applied displacements/strains. Electrical conductivity measurements revealed that the manufactured sensors are highly sensitive to small mechanical disturbances, especially for lower nanotube loadings when compared to traditional metallic or nanocomposite films.

The nanocomposite preparation procedures presented here, i.e., the nanotube purification, non-covalent functionalization, biofunctionalization and nanocomposite mixing strategies, helps toward the development of high-performance nanocomposite materials and extends their application to functional devices. The devices manufactured in this work provided a new perspective for manufacturing 3D-reinforced nanocomposite microstructures for a broad range of application such as organic electronics, highly sensitive 3D freestanding microstructured sensors and aerospace.

TABLE OF CONTENTS

DEDICATIONS iii

ACKNOWLEDGEMENTS iv

RÉSUMÉ vi

ABSTRACT x

TABLE OF CONTENTS xiii

LIST OF TABLES xx

LIST OF FIGURES xxii

LIST OF ABBREVIATIONS xxx

LIST OF APPENDICES xxxii

INTRODUCTION AND THESIS OBJECTIVE 1

CHAPTER 1: Literature review 5

1.1. Carbon nanotubes 5

1.1.1. Carbon nanotube structural characteristics 5

1.1.2. Carbon nanotube properties 7

1.1.3. Carbon nanotubes production methods 9

1.2. Carbon nanotubes-polymer nanocomposites 10

1.2.1. Mechanical reinforcement 11

1.2.1.1. Aspect ratio 11

1.2.1.2. Dispersion 12

1.2.1.3. Alignment 12

1.2.1.4. Interfacial interaction 13

1.2.2. Electrical conductivity 14

1.2.3. Nanocomposite preparation methods using thermosetting matrices 16

1.2.3.1. Nanotube purification 17

1.2.3.2. Nanotube surface treatment 18

1.2.3.3. Mixing in solution method 21

1.2.3.4. High shear mixing methods 22

1.2.4. Nanocomposite bulk properties 24

1.2.4.1. Mechanical properties 24

1.2.4.2. Electrical conductivity 27

1.2.5. Orientation of CNTs 28

1.2.6. Rheological behavior of nanocomposites with thermosetting matrices 30

1.3. Fabrication of 3D nanocomposite microstructures 31

1.3.1. Microfabrication techniques 32

1.3.2. Direct-write (DW) techniques 33

1.3.3. Photopolymers in microfabrication 35

1.3.4. UV-assisted direct-write technique 37

1.4. CNT-based nanocomposites for sensing applications 39

CHAPTER 2: Scientific approach and coherence of articles 42

2.1. Scientific approach and organization of research work 42

2.2. Article presentation and coherence with research objectives 43

2.2.1. Manufacturing 3D-reinforced beams with the micro-infiltration technique: Chapter 3-4 (Articles 1-2) 44

2.2.2. Manufacturing 3D freestanding nanocomposite microstructures with the UV-DW technique: Chapter 5-6 and appendix A and B (Articles 3-4 and proceeding papers, Appendices) 45

CHAPTER 3: Article 1: Micro-infiltration of three-dimensional porous networks with carbon nanotube-based nanocomposite for material design 48

Abstract 48

3.1. Introduction 49

3.2. Experimental 51

3.2.1. Nanocomposite preparation 51

3.2.2. Fabrication of 3D microfluidic networks 52

3.2.3. Preparation of the 3D-reinforced beams via micro-infiltration technique 55

3.2.4. Morphological and mechanical characterization 58

3.3. Results and discussion 59

3.3.1. Carbon nanotube structural characterization 59

3.3.2. Morphological characterization 60

3.3.3. Mechanical characterizations 63

3.3.3.1. Temperature-dependent mechanical properties 63

3.3.3.2. Quasi-static three-point bending 66

3.3.3.3. Tensile testing 69

3.4. Conclusion 70

3. Acknowledgments 71

3. References 72

CHAPTER 4: Article 2: Flow-induced orientation of functionalized single-walled carbon nanotubes embedded in epoxy using three-dimensional microfluidic networks 76

Abstract 76

4.1. Introduction 77

4.2. Experimental 79

4.2.1. Materials 79

4.2.2. Preparation of nanocomposites 80

4.2.3. Micro-injection of 3D microfluidic networks 80

4.2.4. Nanotube and nanocomposites morphological characterizations 82

4.2.5. Viscosity characterization 83

4.2.6. Mechanical properties 85

4.3. Mechanical modeling 85

4.4. Results and discussion 90

4.4.1. Nanotube and nanocomposite morphological characterizations 90

4.4.2. Shear rate estimation and viscosity characterization 93

4.4.3. Morphological characterization of the 3D-reinforced beams 96

4.4.4. Mechanical properties 98

4.4.5. Stiffness prediction with homogenization model 102

4.5. Conclusion 104

4. Acknowledgments 105

4. Appendix 4.A 106

4. References 107

CHAPTER 5: Article 3: Biotin-streptavidin interactions in functionalized carbon nanotube-epoxy composites 110

Abstract 110

5.1. Introduction 111

5.2. Experimental details 114

5.2.1. SWCNTs synthesis, purification and biofunctionalization 114

5.2.2. SWCNTs characterization 116

5.2.3. Nanocomposite preparation 116

5.2.4. Nanocomposite morphological characterization 117

5.2.5. Nanocomposite electrical and mechanical characterizations 118

5.3. Results and Discussion 119

5.3.1. Nanotube structural characterization 119

5.3.2. Morphology characterization 122

5.3.3. Mechanical properties 123

5.3.4. Governing interaction mechanisms 126

5.3.5. Electrical conductivity 128

5.4. Conclusions 129

5. Acknowledgements 130

5. References 130

5. Table of contents entry: 133

CHAPTER 6: Article 4: Direct-write fabrication of freestanding nanocomposite strain sensors 134

Abstract 134

6.1. Introduction 135

6.2. Experimental Details 137

6.2.1. Nanocomposite preparation and characterization 137

6.2.2. Fabrication of the sensors and their characterizations 139

6.3. Results and discussions 141

6.3.1. Carbon nanotube characterization 141

6.3.2. Nanocomposite viscosity characterizations 143

6.3.3. Sensors electromechanical sensitivity 144

6.3.3.1. Microfibers coupon 144

6.3.3.2. Microsprings network 147

6.4. Conclusions 150

6. Acknowledgements 150

6. References 151

CHAPTER 7: General Discussion 153

7.1. Incorporation of CNT into the epoxy matrix 153

7.2. 3D-reinforced composites fabricated by micro-infiltration technique 155

7.3. 3D nanocomposite microstructures fabricated by UV-DW 157

CHAPTER 8 - Conclusion and recommendations 159

REFERENCES 163

APPENDIX 180

LIST OF TABLES

Table 1.1 Mechanical properties comparison of three different structures of single-walled carbon nanotubes (Sinnott and Andrews 2001; Chae and Kumar 2006). 7

Table 1.2 Properties of carbon nanotubes compared to traditional reinforcement materials (Ear and Silverman 2007) 8

Table 1.3 Mechanical properties enhancement of the nanocomposites reinforced with functionalized SWCNTs 25

Table 1.4 Dynamic mechanical properties of epoxy-based nanocomposites reinforced with SWCNTs 26

Table 1.5 Percolation concentration threshold achieved for some SWCNT-polymer composites 27

Table 3.1 Different types of 3D-reinforced beams, prepared in this study, and their components. 57

Table 3.2 Glass transition temperature (Tg) and storage modulus at 25°C for the 3D-reinforced beams and the bulk epoxies. The E' variation for the three different types of nanocomposite-infiltrated beams compared to their corresponding neat epoxy-infiltrated beams is presented in the last column. 66

Table 3.3 Comparison of increase of storage modulus at 25°C by adding SWCNTs to epoxy matrices achieved in our work with those reported in literature. 66

Table 3.4 Flexural properties in three-point bending test for the 3D-reinforced beams and the bulk epoxies. The variation of the properties for the two different types of nanocomposite-infiltrated beams from their corresponding neat epoxy-infiltrated beams is also presented. 69

Table 3.5 Tensile properties of the 3D-reinforced beams and the bulk epoxies. The second and forth columns present the variation of the tensile properties of the two different nanocomposite-infiltrated beams from their corresponding neat epoxy-infiltrated beams. The last column lists the results obtained from rules of mixtures for each type of the infiltrated beams. 70

Table 4.1 Values of P and Q and the corresponding orientations. 88

Table 4.2 Estimation of the process-related apparent viscosity and the process-related apparent shear rate in microfluidic network. 95

Table 4.3 Mechanical properties of the resin-injected and the nanocomposite-injected beams prepared by micro-injection of the materials at two different shear rates and bulk epoxies. 101

Table 4.4 Comparison of increase of storage modulus at 25°C by adding SWCNTs to epoxy matrices achieved in our work with those reported in literature. 103

Table 4.5 Analytical Young's modulus of the resin- and NC-based microfibers with aligned, partially aligned and randomly oriented CNTs. 104

Table 4.6 Analytical and experimental Young's modulus of the resin- and NC-injected beams with aligned, partially aligned and randomly oriented CNTs. 104

Table 5.1 Comparison of the mechanical properties improvements in our work with those reported in literature. 126

Table 6.1 Electrical conductivity changes for the microfibers under applied strains. 147

Table 6.2 Electrical conductivity changes for the microsprings network under applied displacements. 150

LIST OF FIGURES

Figure 1.1 Three different structures of single-walled carbon nanotubes, a) armchair, b) zigzag and c) chiral that represents different mechanical properties and electrical conductivity (Hui, Chipara et al. 2004). 6

Figure 1.2 Schematic of the laser ablation method for the fabrication of SWCNTs using a laser beam which is pointed at a target of a graphite-Co-Ni mixture in a furnace at 1100˚C in an Argon atmosphere (Braidy, El Khakani et al. 2002)..... 10

Figure 1.3 SEM image and schematic of possible tunnelling effect among CNTs in the nanocomposite (Hu, Karube et al. 2008) 15

Figure 1.4 SEM image and schematic of CNTs percolation pathways in the nanocomposite (Li, Chen et al. 2008) 15

Figure 1.5 Topographic AFM images of SWCNT networks (a) before and (b) after 14 h of 3 M HNO_3 reflux treatment. The breakage of SWCNTs after HNO3 reflux treatment is observed (Dumitrescu, Wilson et al. 2007). 19

Figure 1.6 Schematic illustration of the procedure for solubilizing SWCNTs using porphyrins. The use of porphyrins as surfactants leads to (a) deagglomeration of nanotube bundles and (b) surface functionalization of CNTs due to carboxyl functional groups (R) (Nakashima and Fujigaya 2007). 20

Figure 1.7 Schematic representation of (a) high shear mixing in three-roll mixer and (b) region of high shear mixing between the feed and center rolls. The materials must pass through the small gap between the cylinders closely located to each other. The rolls with different speeds and different rotating directions provide high shear forces which is able to disperse nanotubes into the matrix (Thostenson and Chou 2006)..... 23

Figure 1.8 TEM micrographs of thin sections of PC/5 wt% MWCNT nanocomposites prepared along the flow direction (a) at low shear rate and (b) at high shear rate (Abbasi, Carreau et al. 2010)..... 29

Figure 1.9 Microscopic images of CNTs nanocomposites (0.035 wt% MWNCT suspensions): a) random orientation of CNTs and b) shear alignment of at shear rate of 10 s−1 (CNTs at very low fraction, 0.035 wt%, were aligned even after a small amount of shear was applied) (Rahatekar, Koziol et al. 2006)..... 30

Figure 1.10 Variation of apparent viscosity as a function of shear rate for a pure epoxy matrix and epoxy suspensions containing different wt% of CNT (Rahatekar, Koziol et al. 2006) 31

Figure 1.11 Schematic illustration of the fabrication of 3D scaffold by direct-write method: a) deposition of fugitive ink; b) ink layers after deposition; c) encapsulation with epoxy; d) resin solidification; and e) 3D microchannels after the ink removal (Therriault, Shepherd et al. 2005). 34

Figure 1.12 Schematic of a 3D-reinforced beam. An epoxy matrix is reinforced with nanotube nanocomposite microfibers located three-dimensionally using an infiltration technique (reproduced from (Laberge Lebel 2009). 35

Figure 1.13 3D Microstructures made of photopolymers manufactured with (a) and (b) stereolithography photopolymerization) (Liska, Schuster et al. 2007) and (c) and (d) two-photon absorption and two-photon absorption (Kawata, Sun et al. 2001). 37

Figure 1.14 Schematic illustration of UV-assisted direct-write method for the fabrication of the nanocomposite micro-coils. The UV-curable nanocomposite was extruded using a controlled-robot through a needle (Lebel, Aissa et al. 2010) 38

Figure 1.15 Schematic and real image of a nanocomposite strain sensor under tensile strain (Hu, Yin et al. 2011) 40

Figure 2.1 Schematic of two microfabrication approaches used to manufacture 3D nanocomposite microstructures 42

Figure 3.1 Schematic representation of the manufacturing process of a 3D-reinforced nanocomposite beam through micro-infiltration of 3D microfluidic network: (a) deposition of fugitive ink scaffold on an epoxy substrate, (b) encapsulation of the 3D ink-based scaffold using epoxy resin followed by resin solidification, (c) ink removal at 100 °C under vacuum, (d) micro-infiltration of the empty network by the nanocomposite followed by its curing. 54

Figure 3.2 (a) Isometric image of a EP2-beam/NC-UVE-infiltrated containing 0.5 wt% SWCNT/UV-epoxy nanocomposite, (b) typical cross-section of a nanocomposite-infiltrated beam, (c)-(e) schematic illustration of the fabricated beams: porous (empty microfluidic network), resin-infiltrated and nanocomposite-infiltrated beams, respectively. 57

Figure 3.3 (a) TEM image of the purified SWCNTs soot material which are either in bundles or as individual entities. (b) typical Raman spectrum of the nanotubes featuring three peaks: the radial breathing modes (RBM) at around 185 cm^{-1}, the G-band around 1600 cm^{-1} and the D-band around 1350 cm^{-1}..... 60

Figure 3.4 Optical microscopic image of a 20-µm thick film of SWCNT/UV-epoxy nanocomposites where both submicron- and micron-size aggregates are observed... 61

Figure 3.5 SEM images of the fracture surface of the 3D-reinforced beams in three-point bending test. (a) Typical fracture surface of a representative EP2-beam/UVE-

infiltrated and (b) enlarged region on the fiber surface, (c) typical fracture surface of a representative EP2-beam/NC-UVE-infiltrated and (d) enlarged region on the fiber surface. The dashed lines show the microfibers. 62

Figure 3.6 Dynamic mechanical properties of : (a) and (b) EP1-beam/UVE-infiltrated and NC-UVE-infiltrated, bulk-UVE and bulk-EP1, (c) and (d) EP2-beam/UVE-infiltrated and NC-UVE-infiltrated, bulk-UVE and bulk-EP2, and (e) and (f) EP1-beam/EP2-infiltrated and NC-EP2-infiltrated, bulk-EP2 and bulk-EP1. 65

Figure 3.7 The averaged curves of the flexural stress with respect to the flexural strain for 3D-reinforced beams and bulk-epoxies: (a) bulk-UVE, bulk-EP2 and EP2-beam/UVE-infiltrated and EP2-beam/NC-UVE-infiltrated with the nanocomposite fibers containing two different loading of SWCNT (0.5 wt% and 1wt%) and (b) bulk-EP1, bulk-EP2 and EP1-beam/EP2-infiltrated and EP1-beam/NC-EP2-infiltrated with the nanocomposite fibers containing two different loading of SWCNT (0.5 wt% and 1wt%). 67

Figure 4.1 Illustration of the manufacturing process of a 3D beam reinforced with aligned and localized SWCNTs through micro-injection of 3D microfluidic network: (a) overall dimensions of the microfluidic network beams, fabricated by the direct-writing of the fugitive ink upon epoxy encapsulation and ink removal, (b) micro-injection of the empty network with nanocomposite suspension which led to the fabrication of 3D-reinforced beams (the arrow shows the direction of micro-injection flow), (c) isometric image of a 3D-reinforced beam, (d) typical cross-section of a nanocomposite-injected beam, showing the configuration of microchannels filled with nanocomposites. 82

Figure 4.2 Schematic of homogenization steps 86

Figure 4.3 (a) Euler angles, (b) Orientation Probability Density Function (OPDF) and (c) probability of finding a CNT oriented at $\pm 10^{\circ}$ from X_2. 87

Figure 4.4 Typical TEM images of (a) the as-produced and (b) purified SWCNTs soot material. 91

Figure 4.5 (a) Raman spectra and (b) photoelectron spectra of the nanotubes before and after their chemical purification (acidic treatment)..... 92

Figure 4.6 SEM images of the fracture surface of the bulk (a) UV-epoxy and (b) its nanocomposite containing 0.5wt% purified-SWCNTs after ultrasonication and three-roll mill mixing. (c) and (d) higher magnification images of (a) and (b), respectively. 94

Figure 4.7 Viscosity-shear rate estimation of the pure UV-epoxy and its nanocomposites in microchannels using a method based on capillary viscometry. 94

Figure 4.8 SEM images of typical fracture surface of (a) a representative injected beam filled at 0.7 MPa and (b) a close-up view of an embedded microfiber. The red-pointed circles highlight the microfibers; and TEM images of SWCNT orientation state inside the microfiber along the longitudinal direction for the nanocomposite (0.5wt%)-injected beams filled at (c) low injection pressure and (d) high injection pressure and for the nanocomposite (1wt%)-injected filled at (e) low injection pressure and (f) high injection pressure (The arrows show the direction of flow in longitudinal direction of the beam)..... 98

Figure 4.9 Tensile properties of the 3D-reinforced beams: Averaged stress-strain curves of the resin- and NC-injected beams filled (a) at 0.7 MPa and (b) 4.2 MPa micro-injection pressure. 100

Figure 4.10 Schematic of proposed interaction mechanisms between SWCNTs and epoxy matrix through both carboxylic group grafting [31] and non-covalent functionalization of SWCNTs [9]. 100

Figure 5.1 Schematic representation of the UV-assisted direct-writing of nanocomposite microfibers: (a) nanocomposite extrusion through a capillary micronozzle by an applied pressure; fibers are partially cured shortly after extrusion under UV illumination, (b) close-up view of the microfibers, and (c) interfacial bonding between SWCNTs and epoxy matrix through biotin-streptavidin interactions. 114

Figure 5.2 (a) Raman spectra, (b) X-ray photoelectron spectra of as-produced (bottom) and purified (top) SWCNTs, (c) typical TEM image of as-produced SWCNTs, and (b) TEM image of P-SWCNTs. 120

Figure 5.3 (a) FT-IR spectra of (i) P-SWCNTs (bottom), (ii) aminated SWCNTs (middle), and (iii) biotinylated SWCNTs (BF-SWCNTs) (top), (b) high-resolution TEM image of a P-SWCNTs, and (c) high-resolution TEM image of a BF-SWCNTs. 121

Figure 5.4 Optical microscope images of a 20-μm thick film of the nanocomposite containing (a) 1 wt% P-SWCNTs and (b) 1 wt% BF-SWCNTs, (c) and (d) typical SEM images of the cross-section surface of the bulk nanocomposites containing 1 wt% P-SWCNTs and 1 wt% BF-SWCNTs, respectively. 123

Figure 5.5 Mechanical characterization of the nanocomposite materials: (a) optical image of a typical fabricated specimen consisting of three suspended fibers between two

rectangular pads, (b) SEM image of fracture surface of a nanocomposite fiber, (c) typical stress–strain curves and (d) histograms of modulus, strength and failure strain of the pure UV-epoxy and its associated nanocomposites..... 125

Figure 5.6 Schematics of (a) synthesis procedure of the BF-SWCNTs and (b) proposed interaction mechanisms governing the interaction of the BF-SWCNTs and the epoxy matrix by bridge formation through biotin-streptavidin interactions. 127

Figure 5.7 Measured current upon voltage application for the nanocomposite microfibers. 129

Figure 6.1 (a) Schematic representation of the UV-assisted direct-writing of nanocomposite microstructures, (b) a deposited line network similar to traditional strain gauges and (c) a microfibers coupon. To fabricate these microstructures using the UV-DW technique, the nanocomposite is extruded through a capillary micronozzle by an applied pressure and is partially cured shortly after extrusion under UV illumination. 140

Figure 6.2 (a) Typical TEM images of purified SWCNTs and (b) Raman spectra as-produced (bottom) and purified (top) SWCNTs..... 142

Figure 6.3 Process Process-related apparent viscosity of the neat UV-epoxy and its nanocomposites with respect to apparent shear rate using a method based on capillary viscometry..... 144

Figure 6.4 Electromechanical characterization of the nanocomposite microfibers under tensile strains: (a) optical image of a typical fabricated specimen consisting of three suspended fibers between two rectangular pads, (b) SEM image of fracture surface of a nanocomposite fiber, (c) typical force–displacement curves, (d) and (e) measured current upon voltage application between two pads for the nanocomposite microfibers

respectively at 1wt% and 2wt% SWCNTs loadings, (f) strain-resistivity correlated curves based on electrical resistivity changes and (g) an optical image of a microfibers coupon adhered to a structure from the pads. 146

Figure 6.5 Nanocomposite microsprings electromechanical characterization: (a) SEM image of a typical fabricated specimen consisting of four freestanding microsprings, (b) SEM image of the final configuration of the sensor (a circular pad on the top), (c) filament surface SEM image, (d) typical force–displacement curves, and (e) and (f) measured current upon voltage application between two aluminum pads for the nanocomposite microfibers respectively at 1wt% and 2wt% SWCNTs loadings and (g) displacement-resistivity correlated curves based on electrical resistivity changes for the microsprings network..... 149

LIST OF ABBREVIATIONS

Greek Symbols

σ	Stress
ε	Strain
$\dot{\gamma}_{app}$	Apparent shear rate
τ_W	Wall shear stress
η_{app}	Apparent viscosity
ω	Frequency
σ_f	Flexural strength
$\dot{\gamma}_{Nt}$	Newtonian shear rate

Roman Symbols

d	Diameter
RBM	Radial breathing mode
ID	Internal diameter
L	Length
L/D	Aspect ratio
T	Temperature
E_f	Flexural modulus
E^*	Complex modulus
E'	Storage modulus

E''	Loss modulus
T_g	Glass temperature transition
P_{mi}	Applied pressure
P_a	Absolute pressure
Q	Flow rate
b	Rabinowitch coefficient
$\tilde{\mathbf{C}}$	Effective stiffness tensor
c_i	Volume fraction
$\mathbf{S}$	Fourth-order Eshelby tensor
$g(\theta, \varphi, \beta)$	Orientation Probability Density Function
$\mathbf{R}$	Rotation matrix
$\mathbf{R}^T$	Rotation matrix transpose
V. F.	Volume fraction
wt.%	Weight percent
l	Longitudinal direction
t	Transverse direction
R	Electrical resistance

LIST OF APPENDICES

Appendix A: Carbon nanotubes/epoxy nanocomposites for UV-assisted direct-write fabrication of microstructures: mechanical and rheological studies. 180

Appendix B: Ultraviolet direct-write fabrication of chemically treated single-walled carbon nanotube nanocomposite microfibers: experimental and modeling studies. 193

INTRODUCTION AND THESIS OBJECTIVE

Background and problems

Carbon nanotubes, especially single-walled carbon nanotubes (SWCNTs) have generated considerable interest during the past few decades in both science and engineering fields due to their exceptional mechanical (Qian et al. 2002) and electrical properties (Tans et al. 1997). Due to the size order of an individual nanotube or their bulk physical state (i.e., powder of entangled structures), manufacturing and manipulation of these materials is quite challenging. The incorporation of nanotubes into polymer matrices expands their utilization in a broad range of applications such as organic electronics, sensors and actuators (Chou et al. 2008; Culpepper et al. 2010). On the other hand, CNTs confer multifunctional properties (e.g., reinforcing effect, electrical and thermal conductivities, etc) to polymers, which make their nanocomposites suitable for use in other potential applications such as electrostatic charge protection for aircraft and structural composite materials (Baughman et al. 2002). Therefore, CNT-polymer nanocomposites, and specifically nanotube-reinforced epoxy systems could exhibit high-performance properties such as high strength, lightweight and multifunctional features. However, nanotube reinforcement is still far from achieving its theoretical potential and new advances are needed to take advantage of excellent properties of carbon nanotubes. The performance of the nanocomposite materials is highly dependent on such features as the nanotubes dispersion, distribution and their orientation as well as the properties of polymer matrix used and etc. Understanding the relationships among these features and the macroscopic properties can therefore aid in the design of nanocomposite materials.

For some technological applications, manufacturing a 3D structure may be a key parameter to enhance its efficiency. For example, 3D fabrication may be useful for miniaturization of the

product in microelectronics. Several microfabrication techniques have been developed during the past decade to fabricate nanocomposite structures mostly in one- and two dimensions (1D/2D). Moreover, a few techniques with ability to fabricate a real three-dimensional nanocomposite have emerged. In particular, stereolithography and two-photon absorption techniques (resolution down to 120 nm) have been used to fabricate 3D products using photopolymers (Kawata et al. 2001; Meeusen et al. 2003). Material constraints such as low viscosity and transparency have limited the application of these techniques for the fabrication of devices based on nanotube-based nanocomposites. In addition, these techniques are far from being cost-effective. Thus, new fabrication methods would foster the utilization of the nanocomposites in their potential applications.

Objectives

The main objective of this research is to develop nanocomposite materials for the fabrication of nanocomposite-based 3D micro- and macrostructures for targeted technological applications in stronger materials and organic electronics. This dual objective implies the investigation of different nanocomposite mixing strategies to homogeneously disperse intrinsically entangled SWCNTs into a matrix and the use of suitable nanocomposite manufacturing techniques to produce 3D nanocomposite devices. This objective is coupled with understanding the structure-property relationship from nano- to macroscale which enables to design the nanocomposite preparation and fabrication process for optimal properties in the final product. The first objective of this thesis (objective 1) is to demonstrate the fabrication of a 3D-reinforced nanocomposite beam with tailored mechanical properties by infiltrating a nanocomposite suspension into a complex 3D microfluidic network. The effect of nanotubes

orientation induced by high shear flow and dimensional constraining inside the microfluidic networks on the mechanical properties of the 3D-reinforced beams is experimentally and theoretically studied (objective 2). The third objective (objective 3) is to study the effect of nanotubes functionalization with biomolecules on nanotube dispersion and also on nanocomposite mechanical and electrical properties. Benefiting from the versatility and flexibility of the UV-assisted direct-write technique, objective 4 addresses the feasibility of nanocomposite strain sensors with new 3D freestanding geometries.

Organization of the thesis

The thesis organization is the following:

A comprehensive review of the main findings about the nanotube-reinforced epoxy nanocomposites, specifically their mechanical, electrical and rheological properties in the literature is presented in Chapter 1. This section is followed by a literature survey of various microfabrication techniques, specifically those deal with using photopolymers and/or nanocomposites to manufacture 3D microdevices. The scientific approach and the coherence between the research objectives and the four scientific articles resulting from this work are summarized in Chapter 2. Chapters 3 to 6 present the four articles which have either been published or been submitted for publication in peer reviewed scientific journals. Chapter 3 (Article 1) reports on the use of a composite manufacturing approach which is based on the micro-infiltration of a 3D microfluidic network with SWCNTs-based nanocomposite suspension for the fabrication of 3D-reinforced multiscale composites. This article mainly focuses on the material design by co-patterning different epoxy matrices in a single material and also positioning nanotubes at higher stress region for optimal conditions. Chapter 4 (Article 2) deals

with an experimental and theoretical analysis for better understanding the effect of nanotube spatial orientation on the mechanical properties of the epoxy microstructured beams reinforced with SWCNT/epoxy nanocomposite. In Chapter 5 (Article 3), biotin-streptavidin interactions were used for further development of a multifunctional nanotube/epoxy composite system. This nanocomposite material was used for the fabrication of nanocomposite microfibers as an example of patterned microstructures for potential micro electromechanical systems (MEMS). Chapter 6 (Article 4) reports on the use of a SWCNTs-epoxy nanocomposite for the fabrication of two freestanding 3D patterned strain sensors with the ultraviolet-assisted direct-write technique. Finally, a general discussion is presented in Chapter 7, while conclusions and recommendations are stated in Chapter 8.

CHAPTER 1: Literature review

It is of interest to expand the utilization of carbon nanotubes for the development of multifunctional nanocomposite materials, since they can serve as reinforcements as well as sensing elements for potential applications of sensors and microelectronics. Before using these nanocomposites in their potential applications, it is important to have a basic understanding of nanotube structures, their microstructural arrangements in the polymer matrix and the polymer properties itself. For this reason, first carbon nanotubes are classified according to their structural, mechanical and electrical properties. Then different mixing procedures that may include nanotube functionalization and their mixing processes with thermosetting polymers are discussed.

This background information on carbon nanotube nanocomposites is followed by a review of the manufacturing techniques, specifically the micro-infiltration approach and the direct-write techniques for the fabrication of 3D nanocomposite micro- and macro-devices for different applications. This is coupled with a study on nanocomposite materials rheology which enables to optimize processing conditions for both microfabrication techniques as well as overall properties of the final product. Finally a literature survey concerning the utilization of nanotubes and nanotube-based nanocomposites for sensor applications is discussed.

1.1. Carbon nanotubes

1.1.1. Carbon nanotube structural characteristics

Carbon-carbon covalent bond is among the strongest bonds in nature. Consequently, a material based on a suitable arrangement of these bonds can produce a strong structure (Nakashima and Fujigaya 2007). Carbon nanotubes (CNTs) were first highlighted in 1991 by

Ijima (Ijima 1991). A carbon nanotube is a hexagonal network of carbon atoms in a form of seamless cylinder like rolled graphene layers with each end capped with a half sphere. CNTs are similar to graphite in chemical composition but they have a special tubular geometry giving them different properties with respect to the other carbon structures such as graphene.

There are two kinds of carbon nanotubes, single-walled (SW) and multi-walled (MW) carbon nanotubes. SWCNTs are individual cylinders of 1-2 nm in diameter and MWCNTs are a collection of concentric cylinders with weak van der Waals bonds between each cylinder (Breuer and Sundararaj 2004; Nakashima and Fujigaya 2007). Depending on the type of rolling up, three different structures (i.e., armchair, zigzag and chiral) are obtained for SWCNTs as shown in Figure 1.1 (Hui, Chipara et al. 2004). Their mechanical properties as well as electrical properties depend on their geometries (i.e., chirality). In particular, armchair structure shows highest electrical conductivity so called metallic nanotubes while other geometries are semiconductive. Mechanical properties of different types of SWCNTs and also MWCNTs are compared in Table 1.1. Excellent properties of nanotubes like high Young's modulus and good tensile strength and their low weight, high stability and processability have motivated the researchers to further investigate these materials over the past two decades.

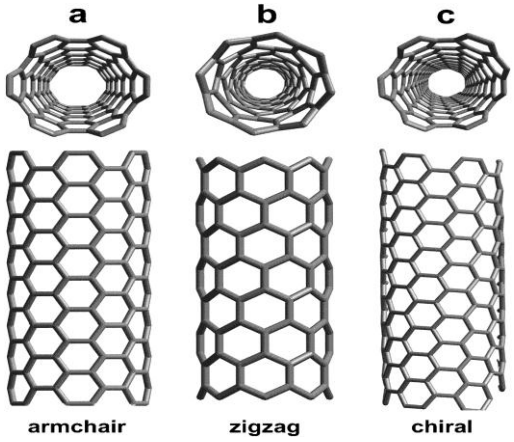

Figure 1.1 Three different structures of single-walled carbon nanotubes, a) armchair, b) zigzag and c) chiral that represents different mechanical properties and electrical conductivity (Hui, Chipara et al. 2004).

Table 1.1 Mechanical properties comparison of three different structures of single-walled carbon nanotubes (Sinnott and Andrews 2001; Chae and Kumar 2006).

Material	Armchair SWCNT	Zigzag SWCNT	Chiral SWCNT
Young's Modulus (TPa)	0.94	0.94	0.92
Tensile Strength (GPa)	126.2	94.5	75
Elongation at Break (%)	23.1	15.6-17.5	16

1.1.2. Carbon nanotube properties

The main mechanical, electrical and thermal properties of SWCNTs and some popular engineering materials are listed in Table 1.2. Due to their tubular structures, CNTs are expected to show excellent mechanical properties and to the highest strength by analogy with graphite which has high in-plane Young's modulus. The first measurement on SWCNTs was carried out by Salvetat et al. (Salvetat, Bonard et al. 1999). They obtained a modulus of ~1TPa for SWCNTs bundle with small diameter using atomic force microscopy (AFM) method. The stiffness of carbon nanotube (Young's modulus) is five times higher than that of steel, whereas its density is significantly lower. MWCNTs exhibit weaker mechanical strength and stiffness because of weak van der Waals bonds between their concentric cylinders; however, they are used in other applications where their thermal and electrical conductivity are more important than their mechanical properties (Breuer and Sundararaj 2004; Laborde-Lahoz 2005). SWCNT has superior mechanical and electrical properties but on the other hand their production is more costly and stabilizing their properties during the process with a matrix (e.g., polymers) is difficult (Ruther, Frehill et al. 2004; Moniruzzaman, Du et al. 2006; Wang, Liang et al. 2006; Sun, Warren et al. 2008; Che, Yuan et al. 2009).

Various techniques for producing SWCNTs generally generate mixtures of metallic and semiconducting SWCNTs (Li, Zhou et al. 2004; Kim, Usrey et al. 2007). Theoretically, metallic nanotubes can reach electrical current density of more than 1000 times of those of metals such as

silver and copper (Meyyappan 2005). The resistivity of SWCNTs is of the order of 10-100 μΩ.cm which is several times more conductive than conventional carbon fibers (800 μΩ.cm). The electrical properties of CNTs, similar to those of metals, make them good materials for producing electronic devices while their high aspect ratio, strength and Young's modulus have made them good choices for reinforcing purposes.

CNTs have also excellent thermal conductivity due to their graphitic structures. Experimental measurements show a thermal conductivity of 200-6000 W/m˚K. This broad range shows the effects of nanotubes quality and alignments, i.e., in the tube longitudinal axis they are conductive and in the transverse axis they are insulators (Meyyappan 2005). The value depends on the quality of the nanotubes, i.e., their properties are strongly affected by the surface defects and the presence of impurities. The value of thermal conductivity for CNTs is significantly higher than common metals like carbon steel. CNTs thermal stability (i.e., keeping their structural integrity at elevated temperatures) is estimated to be around 800˚C (Moisala, Li et al. 2006).

Table 1.2 Properties of carbon nanotubes compared to traditional reinforcement materials (Ear and Silverman 2007)

Materials	Specific gravity (g/cm3)	Tensile Strength (GPa)	Elastic Modulus (GPa)	Thermal conductivity (W/m K)	Electrical Resistivity (μΩ cm)
SWCNTs	1.4	65	1000	6000	30-100
MWCNTs	2.6	1.5	850	7400	150
Conventional carbon fiber	2.2	4	550	70	800
IM7 carbon composites	1.6	2.1	152	30	2000
Titanium	4.5	0.9	103	12	127
Aluminum	2.7	0.5	69	180	4.3
Carbon steel	7.85	0.19-0.758	190-220	24.3-65.2	130-1250

1.1.3. Carbon nanotubes production methods

The three methods used for the synthesis of CNTs are arc discharge method, chemical vapor deposition (CVD) and laser ablation synthesis. Arc discharge was the first method used for producing MWCNTs by Ijima (Ijima 1991). In this method, a direct current is used to produce an arc between two high purity graphite electrodes. This process produces carbon nanotubes as soot on the cathode. The CVD method includes heating a catalytic substrate in a tube furnace till 1200 ˚C and passing a hydrocarbon gas through the whole length of the tube for a specific period of time. Amongst SWCNT production methods, this method gives highest yield (Wilson 2002).

The laser ablation method also uses a graphite source for carbon. Figure 1.2 shows a diagram of typical process of CNTs production with laser ablation technique (Braidy, El Khakani et al. 2002). SWCNTs are produced by using a laser beam which is pointed at a target made of a combination of graphite and metallic catalysts (Co, Pt, Cu, or a combination of them) in a furnace at 1100˚C in an Argon atmosphere. The nanotubes formed are collected on a cold finger downstream of the target. A graphite-Co-Ni mixture is typically used as a target to form SWCNTs. MWCNTs can be obtained by this method only if the metal catalysts are not added to the graphite target.

The main advantages of the SWCNTs produced by the laser ablation method are their excellent structural integrity and highest purity compared to other production methods. Using this method, a mixture of conductive and semiconductive nanotubes is produced which is suitable for use in transistor applications.

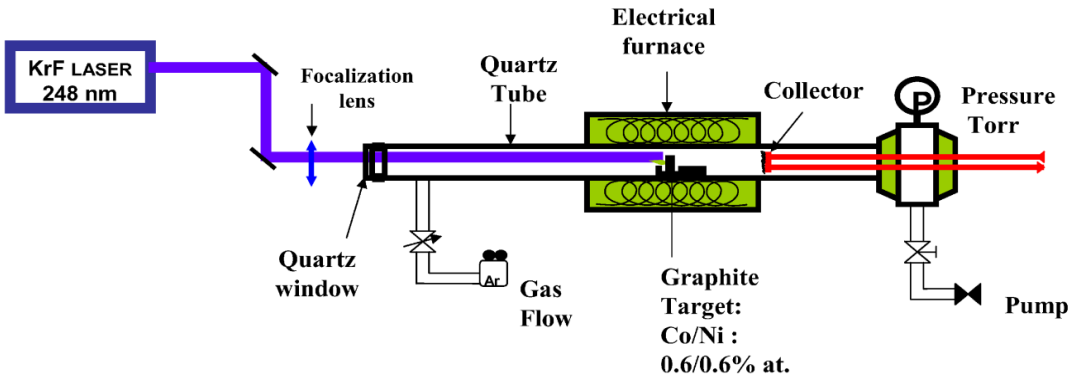

Figure 1.2 Schematic of the laser ablation method for the fabrication of SWCNTs using a laser beam which is pointed at a target of a graphite-Co-Ni mixture in a furnace at 1100˚C in an Argon atmosphere (Braidy, El Khakani et al. 2002)

1.2. Carbon nanotubes-polymer nanocomposites

Polymer nanocomposites are defined as multiphase materials that incorporate nanosized fillers (i.e., fillers have at least a dimension of less than100 nm) into a polymer matrix. The addition of nanofillers into polymer matrices results in a drastic improvement in properties that may include mechanical strength, toughness and electrical or thermal conductivity. Polymer nanocomposites are generally preferred over metals for moderate temperature applications in the field such as structural composites because of their light weight and cost-effective properties. Future aerospace and current developmental systems need to further enhance the mechanical, electrical and thermal properties of nanocomposite systems. For example, heat generated by spacecraft components often presents difficult thermal design problems due to the high and localized heat flux, the need for a large total power dissipation and the wide temperature changes over time. Moreover, many applications may require electrical conductivity of polymer-based composites. Carbon fiber-reinforced polymer composites cannot provide these requirements because of presence of insulating resin regions including the surface.

CNTs exhibit unique properties that make them an attractive material option for incorporation in a new generation of high-performance engineering composites. CNTs can introduce multifunctional capabilities to polymer matrices serving as an effective structural reinforcement, conductive elements as well as large-surface platform for sensing purposes. Understanding the nanocomposite structure-property relationship enables to find the proper processing and fabrication conditions in order to manufacture nanocomposite-based products representing the desired properties for a specific application.

1.2.1. Mechanical reinforcement

During the last decades, a great deal of interests has been directed toward maximizing the potential of SWCNTs as mechanical reinforcements in polymer matrix composites. Theoretical modeling results predict excellent enhancement of mechanical properties of the nanocomposites reinforced with SWCNTs compared to the neat polymers (Seidel and Lagoudas 2006; Giannopoulos, Georgantzinos et al. 2010). Despite many experimental efforts, the full potential of SWCNT-nanocomposites has not been fully realized because of processing challenges and the lack of load transfer from the matrix to the nanotubes.

1.2.1.1. Aspect ratio

Aspect ratio is defined as the length/diameter ratio of the reinforcement. To maximize the load transfer from the matrix to the nanotubes, the aspect ratio has to be large (i.e., >100). Nanotubes chemical treatment as well as mixing techniques may destroy the wall integrity, break the nanotubes and consequently reduce their aspect ratio. Although the length must be long, on the other hand, proper dispersion of long SWCNTs within the matrix would be very difficult.

Similarly, nanotubes with smaller diameters have larger surface area which helps to improve interfacial attraction, but small-diameter SWCNTs limits the maximum loading of SWCNTs due to order of typical polymers gyration radius (Khan et al. 2006). Hence, the length and diameter of CNTs needs to a trade-off and must be optimized to take the maximum efficiency of the reinforcement (Chiang, Brinson et al. 2001; Haddon, Sippel et al. 2004; Coleman, Khan et al. 2006). Since SWCNTs diameter varies in a narrow range of 1.1-1.6 nm, control of their length during the nanocomposite processing is important for mechanical and electrical points of view.

1.2.1.2. Dispersion

For effective reinforcement, SWCNTs need to be individually and uniformly dispersed in polymer matrices during the nanocomposite processing. The nanotube dispersion is imperative to maximize load transfer to the nanotubes and also helps to achieve a more uniform stress distribution (Nakashima and Fujigaya 2007). The main problem associated with SWCNTs is their agglomeration into bundles. With strong van der Waals attractions between the nanotubes as well as their high aspect ratio and high flexibility, they are typically held together as bundles and tend to exist as aggregates when mixed with a polymer matrix. The slippage of the inner nanotubes in bundles decreases the effectiveness of nanoreinforcements. Additionally, their effective aspect ratio is reduced when they are in the form of bundles compared to the individual SWCNTs (Thostenson and Chou 2006).

1.2.1.3. Alignment

The alignment of SWCNTs is necessary to maximize the strength and stiffness of nanocomposites (Sandler, Kirk et al. 2003; Du, Scogna et al. 2004; Coleman, Khan et al. 2006; Moisala, Li et al. 2006; Dumitrescu, Wilson et al. 2007). It has been reported that nanotubes

alignment led to five-fold increase of nanocomposite modulus in the direction of the nanotube alignment when compared to that of nanocomposite with random oriented state (Coleman, Khan et al. 2006). However, alignment is not always beneficial, since it leads to very anisotropic mechanical properties. Alignment is of importance when maximizing the mechanical properties of the nanocomposite in a desired direction. The anisotropy may need to be avoided in most nanocomposite products, however, it has no drawback in nanocomposite fibers. Hence, nanotubes alignment is an effective method to maximize their reinforcing effects in fibers and also in composite materials which require maximum reinforcing effect along a specific direction.

1.2.1.4. Interfacial interaction

Probably the most important parameter for reinforcing polymers using SWCNTs is the interfacial stress transfer (Coleman, Khan et al. 2006). If external loading can be efficiently transferred from the polymer matrix to the nanotubes, the strength and modulus of the composite should be increased. The transferred stress to the nanotubes is proportional to the shear stress in the polymer at the interface. The interfacial shear strength controls the maximum stress transfer to the nanotubes and is defined as a shear stress at which the interface fails. Three main mechanisms of load transfer from a matrix to a reinforcement are micromechanical interlocking, chemical bonding at the interface and van der Waals bonds between the filler and the matrix (Coleman, Khan et al. 2006). Micromechanical interlocking is unlikely due to the SWCNTs smooth surface. Due to their non-reactive surface, the lack of chemical bonding at the nanotube-matrix interface limits the load transfer capability (Sun, Warren et al. 2008). With poor adhesion between nanotubes and matrix, the nanotubes are typically pulled out of the matrix upon failure. For unfunctionalized carbon nanotubes, weak van der Waals attraction between the matrix and the nanotubes is mainly responsible for slightly higher nanotube-polymer interfacial shear stress

(Schadler, Giannaris et al. 1998). Chemical bonding between SWCNTs and polymer matrix increases significantly the effective load transfer at the interface leading to a better mechanical properties (Coleman, Khan et al. 2006).

1.2.2. Electrical conductivity

Polymers such as epoxy resins are electrical insulators because of their very low concentration of free charge carriers. Their electrical conductivity can be altered by adding conductive materials such as carbon nanotubes. Compared to the composites reinforced with carbon fibers, a desired electrical conductivity can be obtained in a carbon nanotube/polymer composite at extremely lower filler contents because of carbon nanotubes larger aspect ratio (Loos, Schulte et al. 2011). The electrical conductivity is based on percolated pathways of conductive nanotubes. The increase of the conductivity can be attributed to the formation of conductive pathways when the filler content exceeds a critical volume fraction as shown in Figure 1.3. This critical concentration of the conductive additive (e.g., SWCNTs) is named the percolation threshold (Moisala, Li et al. 2006; dos Santos, Leite et al. 2008). Typically, the percolation threshold is determined at conductivity $\geq 10^{-6}$ S/m. In general for additive concentrations below the percolation threshold, the electrons must travel through several large zones of insulating epoxy matrix between the neighboring conductive nanotubes defined as electron tunneling. Figure 1.3 represents the tunneling mechanism for a nanocomposite below or close to the percolation threshold. In this case, the tunneling effect is the dominant mechanism and responsible for an increase of nanocomposite electrical conductivity. When the percolation networks are formed (above the percolation threshold), electrons conduct predominantly along the conductive nanotubes and move directly from one nanotube to the next as shown in Figure

1.4. The importance of tunneling effect gradually decreases with increasing the nanotube loadings by providing more conductive paths.

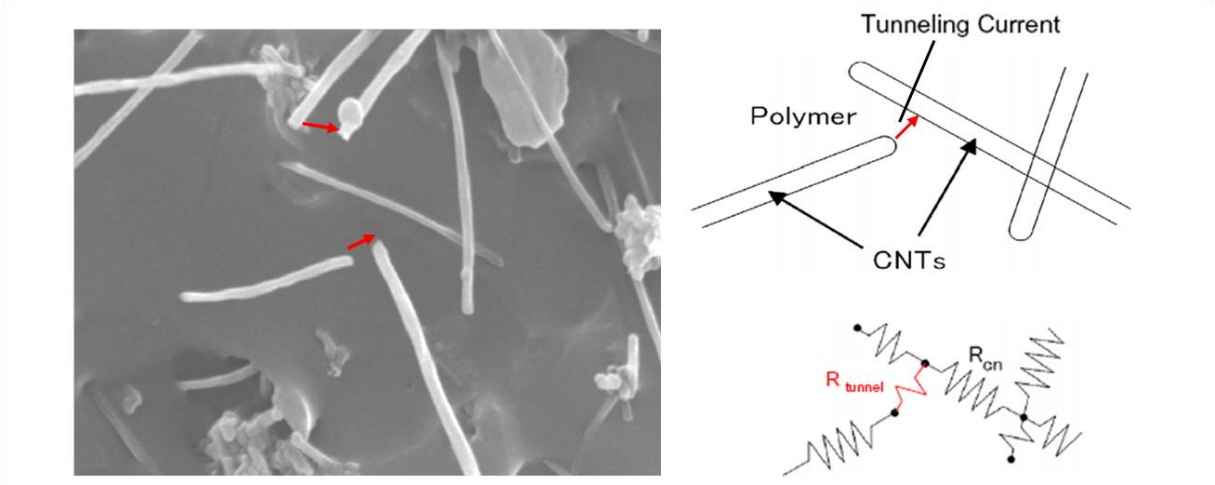

Figure 1.3 SEM image and schematic of possible tunnelling effect among CNTs in the nanocomposite (Hu, Karube et al. 2008)

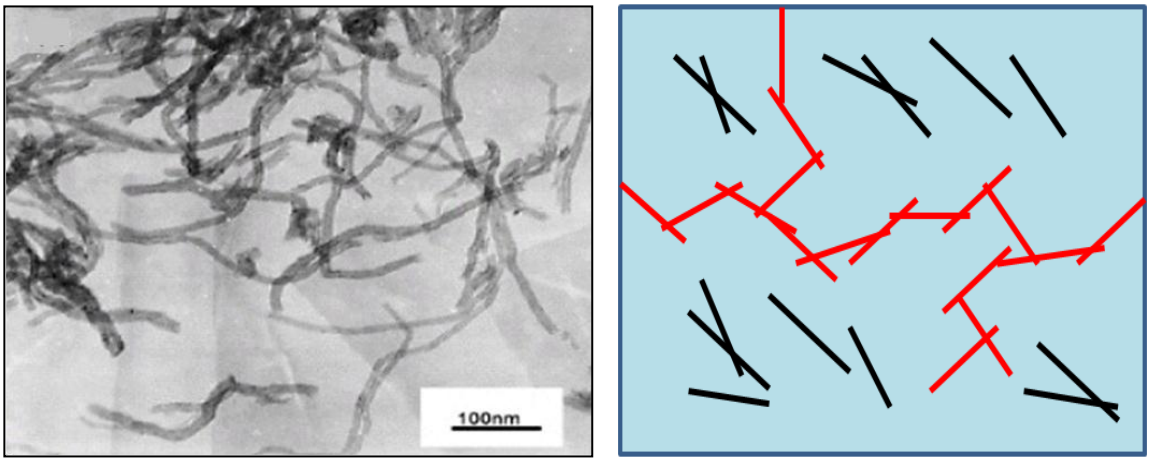

Figure 1.4 SEM image and schematic of CNTs percolation pathways in the nanocomposite (Li, Chen et al. 2008)

The percolation threshold for conductive particles embedded in an insulated polymer is very sensitive to the geometry of the fillers and their arrangements in the matrix. A decrease in electrical resistivity with an increase in filler content is attributed to the probability of the fillers

to contact each other. Electrical properties are sensitive to local statistical perturbations in the microstructure that create a conducting path for electrical transfer (Du, Fischer et al. 2005; Moisala, Li et al. 2006). The characteristics and properties of the carbon nanotubes themselves (e.g., aspect ratio, specific surface area, and surface conductivity), their dispersion and interfacial interaction between the nanotubes and polymer matrix are parameters influencing the composite conductivity. The percolation threshold can be achieved at lower SWCNTs concentrations by using high aspect ratio SWCNTs and by improving the dispersion of individual or small nanotube bundle through shear forces during the material processing. Any kind of treatment such as shear mixing, sonicating and functionalization can damage the SWCNTs and reduce the aspect ratio of the nanotubes which will lead to an increase of the percolation threshold (Gojny, Wichmann et al. 2006).

1.2.3. Nanocomposite preparation methods using thermosetting matrices

Thermosetting polymers are defined as polymer networks formed by chemical reaction of liquid monomers and transformed into a solid system (plastic or rubber) by a cross-linking process. Contrary to thermoplastic polymers which can soften or solidify with changing temperature, thermosetting polymers are irreversibly cured. Therefore, the polymerization (i.e., curing) of a thermosetting polymer and their processing are carried out at the same time to produce the final material with the desired shape. The curing process can be activated by heating at high temperatures, chemical reactions or irradiation.

Carbon nanotubes have been incorporated into a wide range of polymer matrices, both thermoplastics and thermosetting resins for various functional applications. A few steps of nanotube treatment have been applied for both polymer types before nanocomposite processing

to achieve a better dispersion that may involve nanotubes purification and surface functionalization. Dispersion of CNTs in thermoplastic matrices is well done by opposition to thermosetting matrices. High shear forces and complicated flow in twin-screw extruder and in-situ polymerization of polymers in presence of nanotubes produce a nanocomposite with excellent dispersion of nanotubes. Consequently, significant improvements of mechanical properties have been reported for the nanocomposite with thermoplastic matrices (Sun, Warren et al. 2008). However, reinforcement of thermosetting resins such as epoxy by SWCNTs has not been as successful.

1.2.3.1. Nanotube purification

SWCNTs production techniques usually generate impurities and undesirable structures (Chiang, Brinson et al. 2001; Haddon, Sippel et al. 2004). These undesirable materials are usually the metal catalysts used in the production process and other carbonaceous structures such as amorphous carbon (Laborde-Lahoz 2005). The proportion of impurities compared to carbon nanotubes depends on the production method. All purification techniques aim at removing the impurities without significantly affecting the SWCNTs structural integrity and their aspect ratio. The purification is difficult because the metal nanoparticles are typically covered by carbon layers which limit their solubility in an acid.

The purification methods are classified into four approaches such as acid oxidation, gas oxidation, filtration and chromatography. In acidic treatment, the nanotubes are refluxed in an acid like nitric acid or a mixture of different acids to oxidize impurities. A one acidic step has been done by Lebel et al. (Lebel 2008). In their work, the collected soot samples producied by the pulsed laser vaporization method was placed in a nitric acid solution. The suspension was filtered using a porous membrane and was washed with deionized water. The acidic treatment

could be preceded by other purification steps in order to enhance its efficiency. Lahoz et al. used a two-step reflux process (Laborde-Lahoz 2005). First, they have purified CNTs in H_2O_2 solution in order to remove the amorphous carbon. Then, they have refluxed the residual materials in a mixture of sulphuric acid and nitric acid for 24 h in order to eliminate the catalyst particles. This acidic treatment leads to different properties for chemically-treated carbon nanotubes compared to as-produced nanotubes (Laborde-Lahoz 2005).

1.2.3.2. Nanotube surface treatment

Surface treatment of SWCNTs improves both the dispersion of nanotubes and their adhesion to polymer matrix due to the creation of functional groups on the nanotube surface. If carbon atoms of the SWCNTs are bonded to the polymer, the interfacial adhesion and the shear strength would be significantly increased (Murakami 2003; Wang, Liang et al. 2006; Dumitrescu, Wilson et al. 2007). The main approaches for the surface treatment of SWCNTs are divided into covalent and non-covalent functionalization. The covalent functionalization involves grafting functional groups to the nanotube surface. For nanocomposites using epoxy matrix, several covalent functionalization methods with different functional groups such as amine groups (Sun, Warren et al. 2008), carboxylic groups (Moniruzzaman, Du et al. 2006), epoxide groups (Wang, Liang et al. 2008) and dicarboxylic acid peroxide groups (Barrera, Zhu et al. 2004) have been reported in the literature.

The acid treatment of nanotubes (e.g., in HCL and HNO_3) is common practice to not only purify but also functionalize SWCNTs by oxidation. Carboxylic groups are created on the nanotubes surface and the degree of functionalization depends on the duration of the acid treatment. The created carboxylic acid groups are able to adhere to the epoxy molecules via

covalent bonds and a strong bond between nanotube and epoxy matrix is formed (Gojny, Wichmann et al. 2005; Laborde-Lahoz 2005). Although refluxing CNTs in a concentrated acid or grafting functional groups to the nanotubes offer some advantages, they have some crucial disadvantages such as breakage, side wall damages and opening of the tube ends. Figure 1.5 shows AFM images of SWCNTs before and after HNO_3 reflux treatment. The breakage of SWCNTs is observed in Figure 1.5b and its inset. However, according to the application area of the CNTs and considering the defects created, the optimum degree of functionalization must be appropriately tailored.

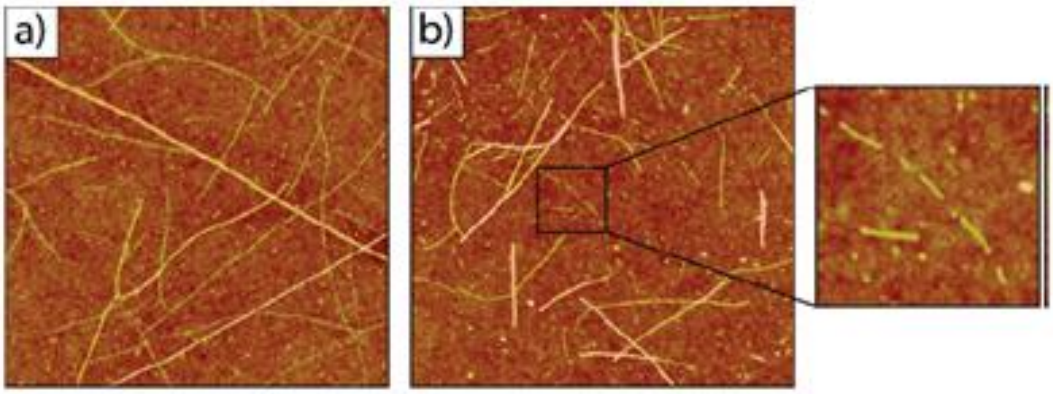

Figure 1.5 Topographic AFM images of SWCNT networks (a) before and (b) after 14 h of 3 M HNO_3 reflux treatment. The breakage of SWCNTs after HNO_3 reflux treatment is observed (Dumitrescu, Wilson et al. 2007).

The second approach is non-covalent functionalization of CNTs using surfactants which are expected to entangle the CNTs and to improve interfacial attraction as shown in Figure 1.6a (Lebel et al. 2010; Islam, Rojas et al. 2003; Moore, Strano et al. 2003; Murakami 2003; Li, Zhou et al. 2004; Nakashima and Fujigaya 2007). The surfactants are capable of causing the counterbalance of van der Waals attractions between individual nanotubes in order to prevent their re-aggregation and even match the polarity to the polymer matrix (Miyagawa, Mirsa et al. 2005). Aromatic hydrocarbons such as pyrene (Dai, Chen et al. 2001; Taeger, Xuang et al. 2005)

and porphyrin (Sun, Li et al. 2004; Kobuke, Satake et al. 2005) molecules derivatives are found to be useful for both deagglomeration and interfacial interaction through non-covalent bonds as shown in Figure 1.6. For example, SWCNTs aggregates were solubilized in an organic solvent like methanol in the presence of Zinc protoporphrin IX (ZnPP) (Nakashima and Fujigaya 2007). Nakashima et al. (Nakashima and Fujigaya 2007) reported that purified SWCNTs solely are insoluble in dimethylformamide (DMF) but after adding ZnPP as a surfactant, the nanotubes are soluble in the solution. They observed individual nanotubes in their solution after sonication and centrifugation.

Non-covalent functionalization is based on π-π stacking interaction between those molecules and carbon nanotube sidewall (Figure 1.6b). The other end of these surfactants like protoporphyrin has two carboxyl functional groups, which are capable of interacting with epoxy groups, forming a chemical bridge between nanotubes and epoxy matrix.

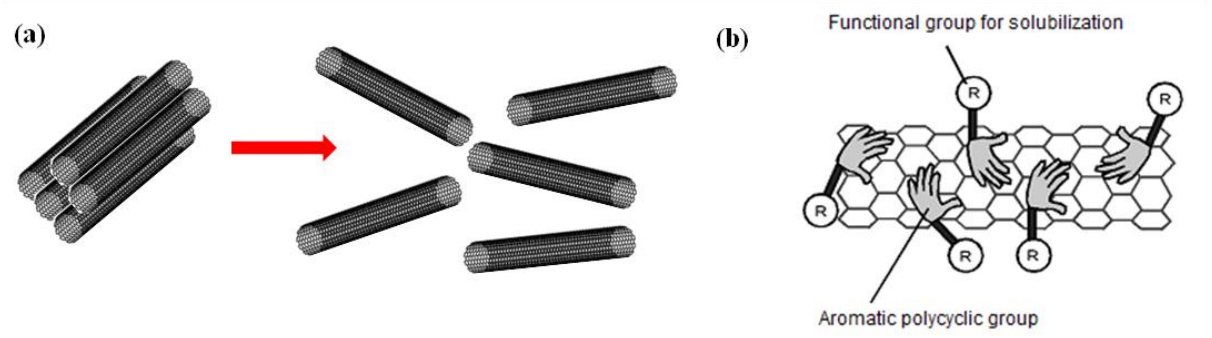

Figure 1.6 Schematic illustration of the procedure for solubilizing SWCNTs using porphyrins. The use of porphyrins as surfactants leads to (a) deagglomeration of nanotube bundles and (b) surface functionalization of CNTs due to carboxyl functional groups (R) (Nakashima and Fujigaya 2007).

The surfactants attraction towards metallic and semiconducting nanotubes depends on their reactivity. Li et al. (Li, Zhou et al. 2004) have reported the selectivity of a porphyrin derivative

toward semiconducting SWCNTs. They found that the selectivity leads to predominantly enriched semiconducting SWCNTs in the uniform suspension (solubilized sample) and significantly metallic SWCNTs in the precipitated sample. Therefore, the selection of the proper surfactant to interact with the major proportion of nanotubes, either conductive or semiconductive in their as-produced soot enables to non-covalently functionalize nanotubes more efficiently.

One of the main advantages of non-covalent functionalization of SWCNTs using surfactants is the conservation of the SWCNTs structural integrity and their aspect ratio (Murakami 2003; Nakashima and Fujigaya 2007; Zhao and Ding 2008). Additionally, there is considerable attention on the preparation of nanotube/polymer composite by solution method in order to form a composite as either a film or a suspension for the next steps of mixing (Breuer and Sundararaj 2004; Moniruzzaman, Du et al. 2006). Therefore, non-covalent functionalization of nanotubes and nanocomposite processing can be simultaneously carried out only if a suitable solvent and a proper surfactant are used. A covalent grafting of functional groups with a sufficient control of the degree of functionalization (e.g., acid treatment duration) combined with non-covalent functionalization could be the best possible option to enhance the interfacial interactions between nanotube and epoxy matrix without compromising the high aspect ratio and structural integrity of nanotubes.

1.2.3.3. Mixing in solution method

Solution processing of nanocomposites is the most common method to mix the CNTs in thermosetting polymers. All solution methods are almost carried out the same way in which nanotubes are dispersed in either a solvent or a polymer solution. The nanotubes and polymer are mixed in a solution by energetic agitation, followed by the evaporation of the solvent (Andrews

and Weisenberger 2004; Breuer and Sundararaj 2004; Moniruzzaman, Du et al. 2006). The commonly-used techniques to provide energetic agitation are magnetic stirring using magnetic mixers and sonication, either in a bath or using a tip. Although the sonication technique is usually used by researchers, the dispersion of the nanotubes is far from their fully individualization and distribution (Thostenson and Chou 2006).

The main advantage of the solution method is that both the debundling and the dispersion of the SWCNTs into polymer matrix take place by agitating the nanotubes in a solvent. On the other hand, the main drawback of this method is the toxicity of the solvents used such as Dimethylformamide (DMF) or acetone.

1.2.3.4. High shear mixing methods

High shear mixing is known as an efficient method toward the development of well-dispersed nanocomposites. For the nanocomposite using thermosetting resins, the three-roll mixer (Thostenson and Chou 2006) and the twin-screw batch mixer (Moniruzzaman, Du et al. 2006) have proven their efficiency to disperse nanotubes into the matrix. Figure 1.7 shows a schematic of the general configuration of the three-roll mixer. The mixer consists of three adjacent cylindrical rolls which turn at a different velocity and each two adjacent rolls rotate in different directions. The very small gap between rolls and their velocity difference result in high shear stresses. Figure 1.7b shows the area of intense shear mixing between two adjacent rolls. During this processing method, high shear forces break up and untangle nanotube bundles while the short residence time limits physical damage of nanotubes (Thostenson and Chou 2006). The main advantage of three-roll mixing method is the uniform application of shear forces over the whole composite between the rolls while the sonicating technique locally introduces the energy.

A significant increase of the viscosity of the composites during shear mixing has been reported and was attributed to the homogenous dispersion of the nanotubes (Moniruzzaman, Du et al. 2006; Lebel, Aissa et al. 2010). On the other hand, the increase of viscosity reduces the possibility of the composite degassing with voids remaining in the matrix. The initial failure of the nanocomposite can be caused by these voids leading to the reduced mechanical properties of the final product (Gojny, Wichmann et al. 2005).

A series of experiments under different processing conditions have been accomplished by Thostenson et al. (Thostenson and Chou 2006) in order to understand the influence of processing parameters on the dispersion of nanotubes in three-roll mixing method. They observed that after processing the nanotube/epoxy composite at a gap setting of 50 μm, the structure was highly agglomerated while after processing at smaller gap settings, there was a much larger quantity of nanotubes dispersed in the matrix with smaller agglomerate sizes. A highly dispersed nanocomposite with little agglomerates was obtained at the gap settings of 5 μm after several passing of the materials.

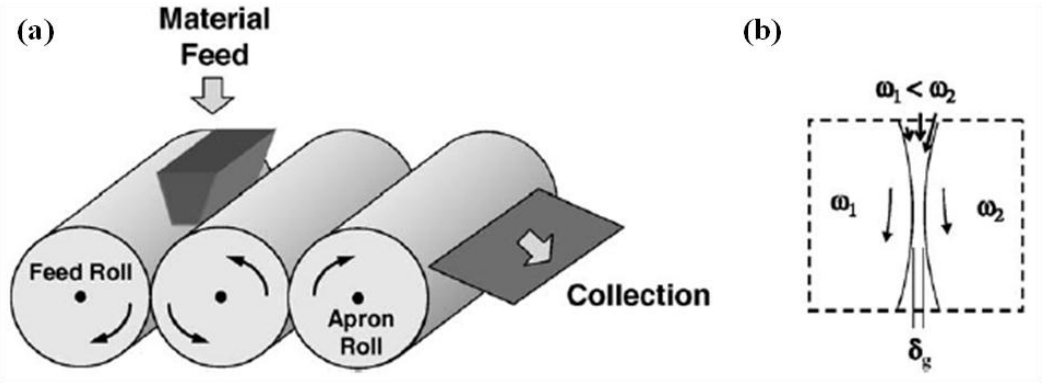

Figure 1.7 Schematic representation of (a) high shear mixing in three-roll mixer and (b) region of high shear mixing between the feed and center rolls. The materials must pass through the small gap between the cylinders closely located to each other. The rolls with different speeds and different rotating directions provide high shear forces which is able to disperse nanotubes into the matrix (Thostenson and Chou 2006).

1.2.4. Nanocomposite bulk properties

There is a strong relationship between the local structure at the micro and nano scales and the macroscale bulk properties of the composites. The overall mechanical and electrical properties of the final product depend on the type of nanotubes, their aspect ratio, their concentration, their orientation, surface treatment and the nanocomposites mixing processes. Therefore, a wide range of bulk properties have been reported in the literature depending on the preparation and mixing procedures of nanocomposites reinforced with SWCNTs. In this section, we will review some of the mechanical and electrical properties achieved in epoxy-nanotube composites.

1.2.4.1. Mechanical properties

Several experimental and theoretical efforts have been performed towards maximizing the potential of CNTs as reinforcing fillers in polymer matrix composites. Several mechanical characterization techniques such as tensile testing, indentation and static and dynamic three-point bending have been used to analyze their properties. The properties enhancement of nanocomposites when compared to the neat polymer was demonstrated even at very low nanotubes concentrations (Allaoui, Bai et al. 2002; Zhu, Kim et al. 2003; Gojny, Wichmann et al. 2004; Miyagawa and Drzal 2004; Xiaodong and M. 2004; Bai and Lijie 2006; Moniruzzaman, Du et al. 2006; Sun, Warren et al. 2008). Most of the works reported significant improvements of the Young's modulus (E) and the tensile strength (σ). Table 1.3 lists some of the results reported on tensile properties of the functionalized SWCNTs-epoxy nanocomposites prepared by different mixing methods. Although different carbon nanotubes with different

functionalization methods have been used, the best improvement of mechanical properties has been achieved for the nanocomposites prepared by sonication followed by shear mixing.

Table 1.3 Mechanical properties enhancement of the nanocomposites reinforced with functionalized SWCNTs

SWCNTs wt.%	Mixing method	E_{Matrix} (GPa)	E_{NC} (GPa)	ΔE %Increase	σ_{Matrix} (MPa)	σ_{NC} (MPa)	$\Delta\sigma$ %Increase	Ref.
0.1	Sonication	1.10	1.72	+56	---	---	---	(Valentini, 2008)
1	Stirring	2.76	3.49	+26	64.1	74.7	+17	(Sun, 2008)
1	Shear mix.	3.40	4.20	+24	---	---	---	(Hubert, 2009)
1	Sonication &shear mix.	2.0	3.20	+60	72.6	101.9	+40	(Wang, 2008)
1	Sonication &shear mix.	2.02	2.65	+31	83	104	+25	(Barrera, 2004)

The dynamic and quasi-static mechanical properties of the nanocomposites have also been characterized. The dynamic mechanical properties represent the viscoelastic properties as complex flexural modulus ($E^* = E' + iE''$) which is separated into storage E' and loss moduli E''. The storage modulus indicates the capacity of the nanocomposites to store and return energy (i.e., elastic energy), which is highly sensitive to the nanocomposite morphology, nanotube loading and the interfacial bonding strength between nanotubes and epoxy matrix. The loss modulus reveals the amount of energy dissipation due to the friction of polymer chains in their internal motion or at nanotube-polymer interface. This approach also enables to locate the glass transition temperature (T_g) of the nanocomposites that may vary with the addition of nanotubes and nanotube-matrix interface quality.

Table 1.4 lists some experimental results reported in the literature representing the effect of SWCNTs incorporation on the storage modulus of epoxy nanocomposites, with the improvements range between 20 to 44% at ambient temperature. The presence of functionalized

SWCNTs is reported to have a more pronounced enhancement effect (i.e., higher E' values) for temperature above the T_g of the resin where the epoxy resin is softer. At temperatures above T_g, the stiffening effect would be maximized when the well-bonded nanotubes are mobilized by the epoxy molecules (Sun, Warren et al. 2008).

The quasi-static three-point bending test is also performed to characterize the mechanical performance of the nanocomposites at ambient temperature under flexural solicitation. The flexural modulus (E_f) and flexural strength (σ_f) are calculated from the load-deflection curves (Moniruzzaman, Du et al. 2006). It has been reported that the incorporation of SWCNTs with the loading as low as 0.05 wt% significantly increased the E_f (17%) and σ_f (10%) of the epoxy matrix (Wachtman et al. 1996).

Table 1.4 Dynamic mechanical properties of epoxy-based nanocomposites reinforced with SWCNTs

SWCNTs wt.%	**Functionalization**	**Mixing method**	***E′* %Increase**	**Ref.**
1	Polyamido amine	Stirring	20	(Sun, 2008)
1	Epoxide	Sonication & Shear mix.	41	(Wang, 2008)
1	Alkyl carboxylic	Sonication & Shear mix.	44	(Barrera, 2004)
0.3	Carboxylic	Stirring & Sonication	33	(Miyagawa 2004)

The mechanical properties of the SWCNT-epoxy nanocomposites mentioned in this section are superior to the neat resin but the increase remains significantly lower than the theoretical predictions. The nanocomposite properties are still far from the traditional composites reinforced with continuous fibers (Haggenmueller, Du et al. 2006). This important difference is attributed to the imperfect dispersion, the incomplete alignment and the insufficient load transfer from matrix to the CNTs (Coleman, Khan et al. 2006).

1.2.4.2. Electrical conductivity

The two-probe and four-probe methods have been used to measure the electrical conductivity of SWCNT-based nanocomposites. Significant increase in electrical conductivity of nanotube-polymer composites have been reported at very low nanotube contents. The electrical percolation threshold occurs at much lower filler concentrations when compared to those reinforced with traditional fillers. Different values for percolation threshold have been reported starting from 5×10^{-5} wt.% in SWCNTs-epoxy composites as summarized in Table 1.5. This large range for the percolation concentration threshold primarily stems from the dispersion of the nanotubes. The aggregation of nanotubes, which typically reduces their effective aspect ratio, decreases the number of discrete conductive fillers (or increases the distance of adjacent fillers), and thereby increases the percolation threshold. Since better dispersion generally reduces the percolation threshold, numerous preparation methods have been developed that may involve nanotubes treatment and nanocomposite mixing strategies.

Table 1.5 Percolation concentration threshold achieved for some SWCNT-polymer composites

Processing method	Percolation threshold	Reference and year
Sonication	5.2×10^{-5}	(Bryning, Islam et al. 2005)
High shear mixing	0.05	(Moisala, Li et al. 2006)
Sonication	0.074	(Kim, Lee et al. 2003)
Stirring & Sonication	0.062	(Li, Huang et al. 2006)

It has been reported that covalent functionalization of nanotubes disrupts the extended π conjugation (i.e., electronic structure) of nanotubes and reduces their electrical conductivity. However, the improved dispersion enabled by chemical functionalization outweighs their drawbacks with respect to nanotube conductivity. Similarly, non-covalent functionalization using

surfactants improves nanotube dispersion and thereby generally improves the electrical conductivity of the nanocomposite. Although non-covalent functionalization do not destroy the nanotube wall integrity, remaining surfactant molecules between the nanotubes may increase the interfacial resistance (Hobbie, Obrzut et al. 2006).

Another parameter affecting the nanocomposite electrical conductivity is the nanotube alignment in the polymer matrix. It has been reported that the electrical conductivity of the nanocomposite decreases with increasing the nanotube orientation state (Abbasi, Carreau et al. 2010). The minimum conductivity is obtained for the nanocomposite with the nanotubes perfect alignment. This might be attributed to the decrease of the probability of nanotubes contact points and also the increase of distance between adjacent nanotubes (Du, Scogna et al. 2004; Kharchenko, Douglas et al. 2004; Abbasi, Carreau et al. 2010). However, the increase of electrical conductivity by aligning nanotubes also has been reported (Du, Fischer et al. 2005). It seems that a randomly orientation or partially alignments of nanotubes represents lower percolation concentration threshold compared to the perfectly aligned nanotubes in the nanocomposites (Hobbie, Obrzut et al. 2006).

1.2.5. Orientation of CNTs

Both mechanical and electrical properties of the nanocomposites reinforced with nanotubes are influenced by the nanotubes orientation state. Shear flow (Fan and Advani 2005; Abbasi, Carreau et al. 2010), electromagnetic fields (Kimura, Ago et al. 2002) and dimensional constraints have been used to address the CNTs alignment along a desired direction in a polymer matrix. Dimensional constraining effect on CNTs orientation in 1D and 2D has been employed in several nanocomposite processing techniques including fiber electrospinning (Chronakis

2005), compression molding (Abbasi, Carreau et al. 2010), extrusion (Zhou, Vavro et al. 2004) and film casting (Sandler, Pegel et al. 2004). Figure 1.8 shows TEM images of CNTs aligned at high shear rate in the direction of flow using a micro-injection technique (Abbasi, Carreau et al. 2010). The flow of nanocomposites under high shear condition causes the CNTs to align in the direction of the flow where the degree of orientation directly depends on the extent of the applied shear (Fan and Advani 2005; Abbasi, Carreau et al. 2010). The Brownian motion (i.e., random movement of particles suspended in a fluid) that may impose small disturbances can contribute to the rotational motion by increasing the frequency of Jeffery orbits (Hogberg and Lundstrom 2011). Advani et al. (Fan and Advani 2005) have investigated the orientation of CNTs in vinyl ester resin with the approach of shear flow. They found that the degree of orientation increases with the increase of the applied shear rate. The same results have been reported by Rahatekar et al. (Rahatekar, Koziol et al. 2006). They also believed nanotubes orientation depends on their concentration so that the degree of alignment decreases with an increase of nanotube content. They observed that nanotubes at 0.035 wt% were oriented at low shear rates as shown in Figure 1.9.

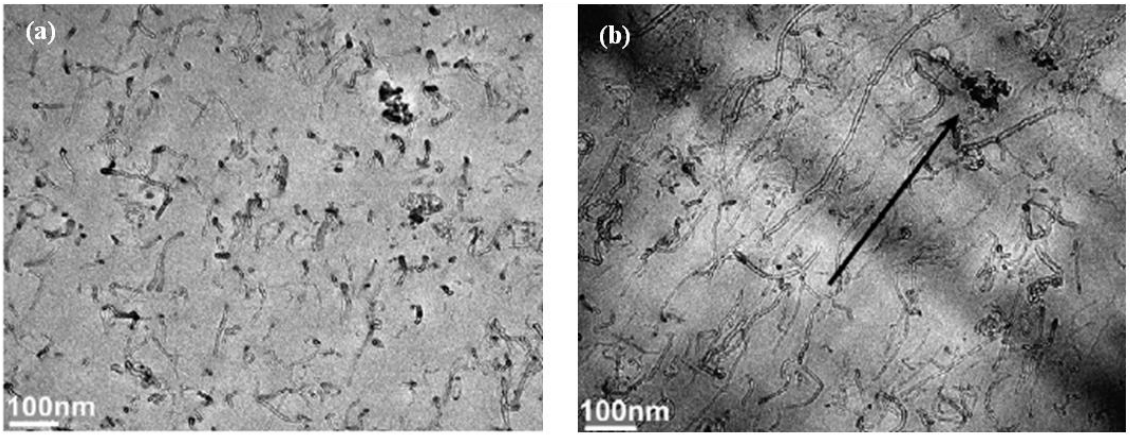

Figure 1.8 TEM micrographs of thin sections of PC/5 wt% MWCNT nanocomposites prepared along the flow direction (a) at low shear rate and (b) at high shear rate (Abbasi, Carreau et al. 2010)

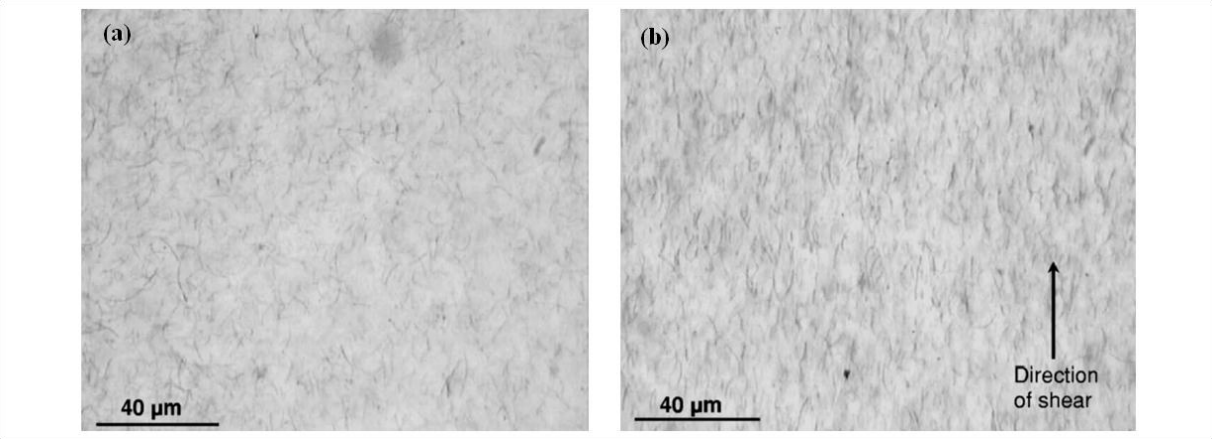

Figure 1.9 Microscopic images of CNTs nanocomposites (0.035 wt% MWNCT suspensions): a) random orientation of CNTs and b) shear alignment of at shear rate of 10 s^{-1} (CNTs at very low fraction, 0.035 wt%, were aligned even after a small amount of shear was applied) (Rahatekar, Koziol et al. 2006)

1.2.6. Rheological behavior of nanocomposites with thermosetting matrices

The rheological behavior and the microstructure of the materials significantly change during the different processing steps of the final product. Generally, the incorporation of CNTs into epoxy matrix increases its viscosity and also influences its Newtonian rheological behavior. An increase of the viscosity, especially at the low shear rate region and a high shear thinning behavior (i.e., a decrease of the viscosity with increasing shear rates) has been observed after adding carbon nanotube to epoxy resins as shown in Figure 1.10. The deviation from the viscosity of the pure epoxy is observed at very low nanotube loadings (i.e., ~ 0.15 wt.%). Higher apparent of viscosity and a stronger shear-thinning behavior were observed at nanotube loadings ranging from 0.15 wt.% to 0.5 wt.%. High aspect ratio of nanotubes, their alignment, nanotube functionalization and presence of interconnected aggregates at low shear rates are thought to be responsible of this behavior (Rahatekar, Koziol et al. 2006). Seyhan et al. (Seyhan, Gojny et al. 2007) reported that nanotubes functionalization improves the polymer-nanotube interaction and

consequently affect the polymer mobility in the presence of well-bonded nanotubes but on the other hand, may reduce the nanotube aspect ratio.

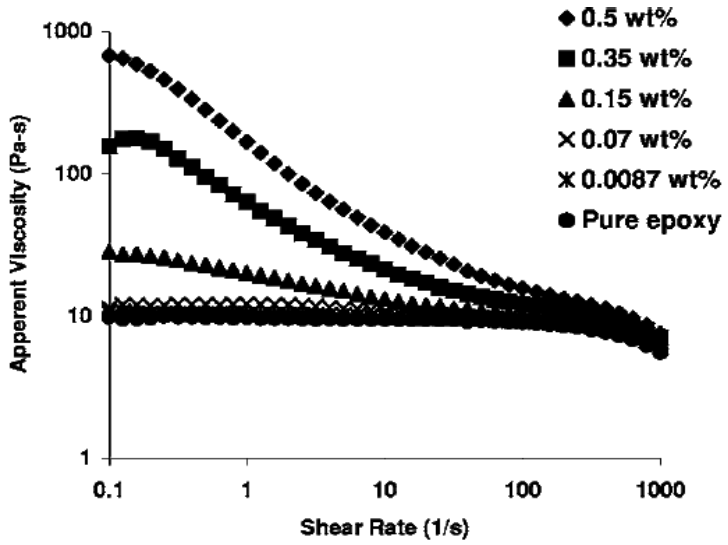

Figure 1.10 Variation of apparent viscosity as a function of shear rate for a pure epoxy matrix and epoxy suspensions containing different wt% of CNT (Rahatekar, Koziol et al. 2006)

1.3. Fabrication of 3D nanocomposite microstructures

Micro- and nanotechnological systems have rapidly progressed through the miniaturization of components and the fabrication of smaller functional devices. They have gained considerable attention in recent years in various fields such as micro electromechanical systems (MEMS), microelectronics, optoelectronics, biotechnology and microchemical systems. Despite this wide variety of applications, new manufacturing and materials advances to extend their performance efficiency while being more compact.

1.3.1. Microfabrication techniques

To fabricate two- and three-dimensional (2D/3D) microstructures for MEMS applications, several microfabrication techniques have been developed such as photolithographic techniques, laser micromachining and rapid prototyping (Tse, Hesketh et al. 2003, Meeusen, Clijnen et al., 2003). Material constraints and the limitation to fabricate relatively thin devices are the main drawbacks of these techniques. A few novel microfabrication techniques have emerged to fabricate three-dimensional structures including microstereolithography, electrochemical fabrication, microphotoforming, spatial forming and localized electrochemical deposition (Kawata, Sun et al. 2001). These conventional microfabrication methods may require expensive systems such as photomasks and long fabrication process. Depending on the technique, polymer, ceramic and metal can be used to fabricate relatively complex 3D microstructures with a feature size of few microns.

The main structural materials used in most of microfabrication methods of miniaturized systems components are silicon, glass or quartz materials. These materials are not able to satisfy largely divergent applications of microdevices. Therefore, depending on their applications, other structural materials may be required. For example, biocompatible materials are required in bio-MEMS while structural ceramic may be used for high temperature applications in fuel cells. The fabrication of actuators requires flexible materials due to the high strain and displacement imposes (Varadan 2001).

The utilization of polymeric materials and nanocomposites in microfabrication is a promising alternative due to their versatility, lightweight, and physical and mechanical properties. In addition, the properties of the polymer materials can be easily tailored by adding other polymers and/or reinforcing fillers to achieve the desired performance.

1.3.2. Direct-write (DW) techniques

A promising microfabrication method is the “direct-write” approach which consists of a computer-controlled robot that moves an extrusion nozzle in order to achieve the desired 3D microstructures layer-by-layer. This technique provides fast and flexible way for fabricating 3D microdevices in photonic, MEMS and biotechnology applications (Therriault, Shepherd et al. 2005). Extruded materials of moderate to high viscosities are necessary to create stable filaments in this method. Since high viscosity may limit flow through fine extrusion nozzles, an extruded materials shear-thinning behavior (i.e., a decrease of viscosity with an increase of shear forces inside the nozzle) is preferable. Therefore, several materials can be used in the DW method such as polyelectrolyte inks (Gratson, Xu et al. 2004), flocculated colloidal suspensions (Smay, Gratson et al. 2002), silver nanoparticle inks (Ahn, Duoss et al. 2009), and thermosetting resins (Lebel et al., 2010). A fugitive ink was used for the fabrication of 3D scaffolds of several layers with this method by Therriault et al. (Therriault, White et al. 2003; Therriault, Shepherd et al. 2005). A schematic illustration of the fabrication procedure is shown in Figure 1.11. In their work, a pressure dispensing-equipped robot was used to deposit the fugitive ink on a substrate, resulting into a 2D pattern (Figure 1.11a). The following layers were deposited by moving the dispensing nozzle in *z*-direction to yield a 3D scaffold (Figure 1.11b). After the encapsulation of the structure using an epoxy resin (Figure 1.11c) and removing the fugitive ink (Figure 1.11d), 3D microfluidic channels were created (Figure 1.11e) (Therriault, Shepherd et al. 2005). This kind of microfluidic networks could be used in different technological applications such as biotechnology (Stromberg, Karlsson et al. 2001) and microelectronics (Snyder, Lim et al. 2003).

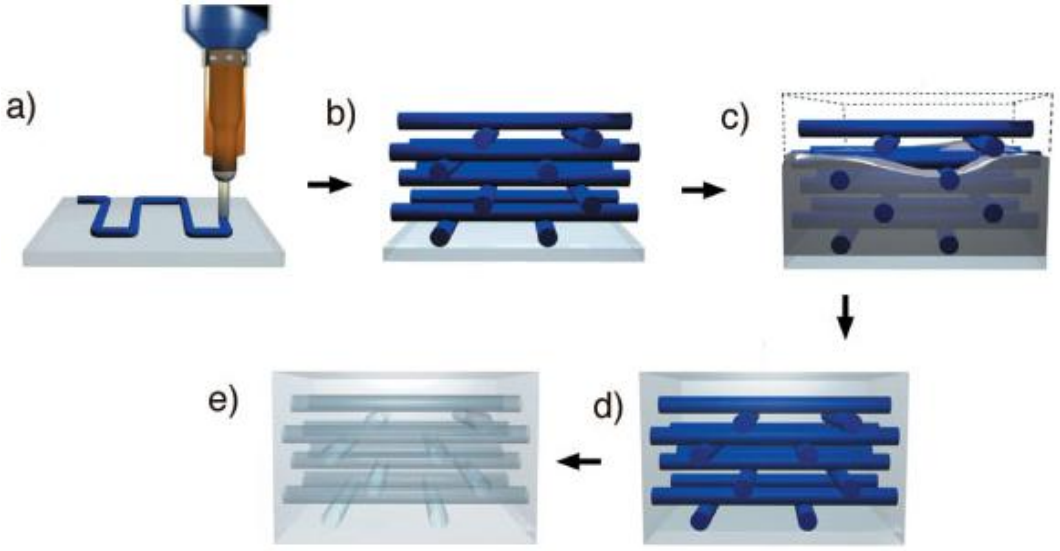

Figure 1.11 Schematic illustration of the fabrication of 3D scaffold by direct-write method: a) deposition of fugitive ink; b) ink layers after deposition; c) encapsulation with epoxy; d) resin solidification; and e) 3D microchannels after the ink removal (Therriault, Shepherd et al. 2005).

Lebel et al. has reported the fabrication of 3D-reinforced nanocomposite rectangular beams using similar microfluidic networks (Lebel, Aissa et al. 2009). The fabricated 3D-reinforced beams which consist of 3D skeleton structure of nanocomposite microfibers have been fabricated by infiltrating a polyurethane nanocomposite suspension into the empty channels made of epoxy. Figure 1.12 represents the schematic of their nanocomposite manufacturing approach (Laberge Lebel 2009). Due to relatively lower mechanical properties of the polyurethane nanocomposite used (modulus of ~ 0.1 GPa), the 3D-reinforced beams showed inferior mechanical properties when compared to the bulk epoxy (modulus of ~ 3.1GPa). The temperature-dependent mechanical properties of the 3D-reinforced microstructures revealed higher damping properties over their elastic properties with respect to the bulk epoxy beams. This characteristic might be useful in products where vibration absorption and management are important (Lebel, Aissa et al. 2009).

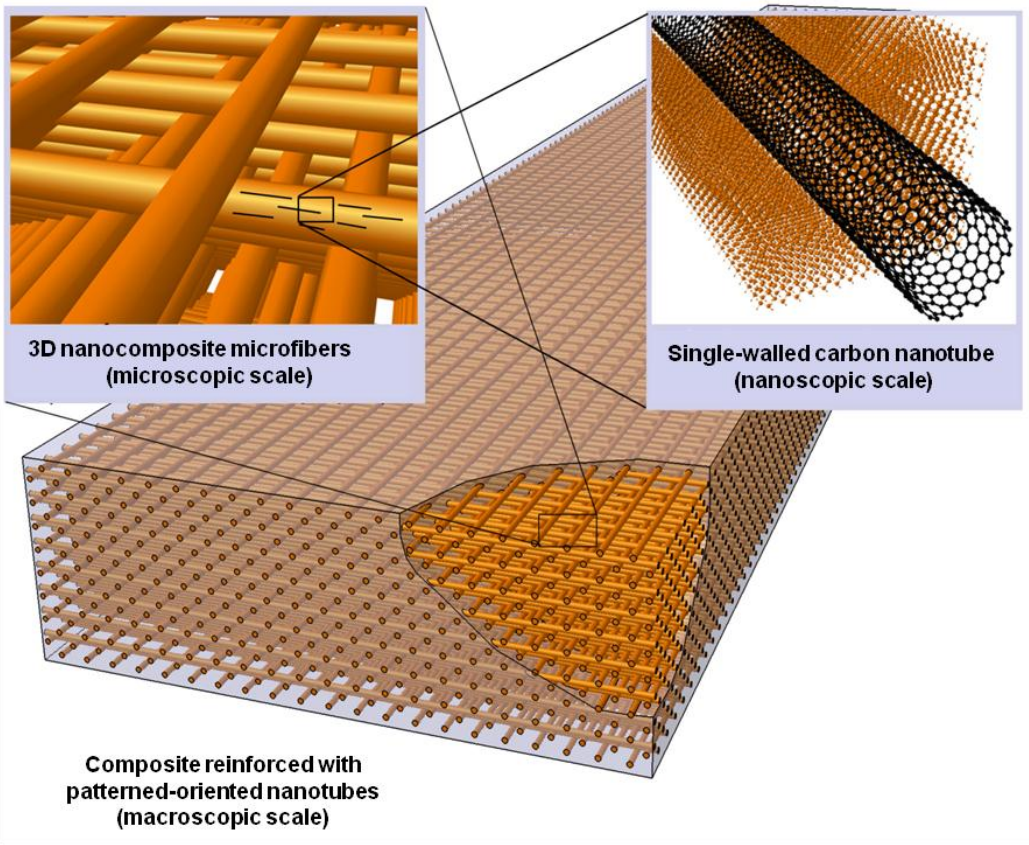

Figure 1.12 Schematic of a 3D-reinforced beam. An epoxy matrix is reinforced with nanotube nanocomposite microfibers located three-dimensionally using an infiltration technique (reproduced from (Laberge Lebel 2009).

1.3.3. Photopolymers in microfabrication

Many of the commercially available thermosetting polymers like epoxy consist of two components, the resin and the curing agent (i.e., hardener). The use of two component epoxy systems comes with some drawbacks such as limited work time, long curing time, high shrinkage and probable incomplete curing with slight deviation from their mix ratio (Fisher, Dean et al. 2001).

Ultraviolet curable resins obviate these drawbacks and have many benefits over its two component counterparts. The photoinitiated polymerization of monomers occurs in seconds to give highly cross-linked polymers. Solvent-free formulations, low energy consumption and room

temperature processing are amongst their advantages. Also, the curing takes place only in exposed regions to the radiations. Moreover, These types of materials are used in various applications such as MEMS, dental composites, coating, printing inks and adhesives (Decker 1996). However, the UV-curable epoxy systems exhibit lower mechanical properties in comparison to traditional epoxy systems and their synthesis is more expensive.

Photopolymers have been extensively used for the microfabrication of 2D and 3D microdevices. Stereolithographic techniques such as photopolymerization (Liska, Schuster et al. 2007) and two-photon absorption (Kawata, Sun et al. 2001) have proven their efficiency to fabricate 3D products using photopolymers. Figure 1.13 shows some microstructures fabricated by these techniques. Two-photon absorption technique is known as a precise and powerful technique to manufacture 3D microstructures with a very low resolution down to 120 nm. However, material requirements such as low viscosity and transparency limit the application of this technique for the fabrication of devices based on multifunctional polymer materials such as nanotube-based nanocomposites.

The incorporation of nanofillers confer functionality such as electrical conductivity and sensing capability to inherently insulating polymers, which make their nanocomposites suitable for use in a broad range of potential applications. Varadan et al. (Varadan 2001) have proposed a distributed MEMS phase shifter for communication systems. The system consists of MEMS conductive bridges which can be made of nanotube/polymer composites. In another work, they reported the fabrication of microsprings with nanotube-reinforced UV-curable polymer. The conductivity induced by the incorporation of nanotubes made the microsprings suitable for the use in the applications such as drag control in aircraft, beam focusing and steering, microsensing devices, and electromagnetic shielding and absorption (Varadan, Varadan et al. 1996).

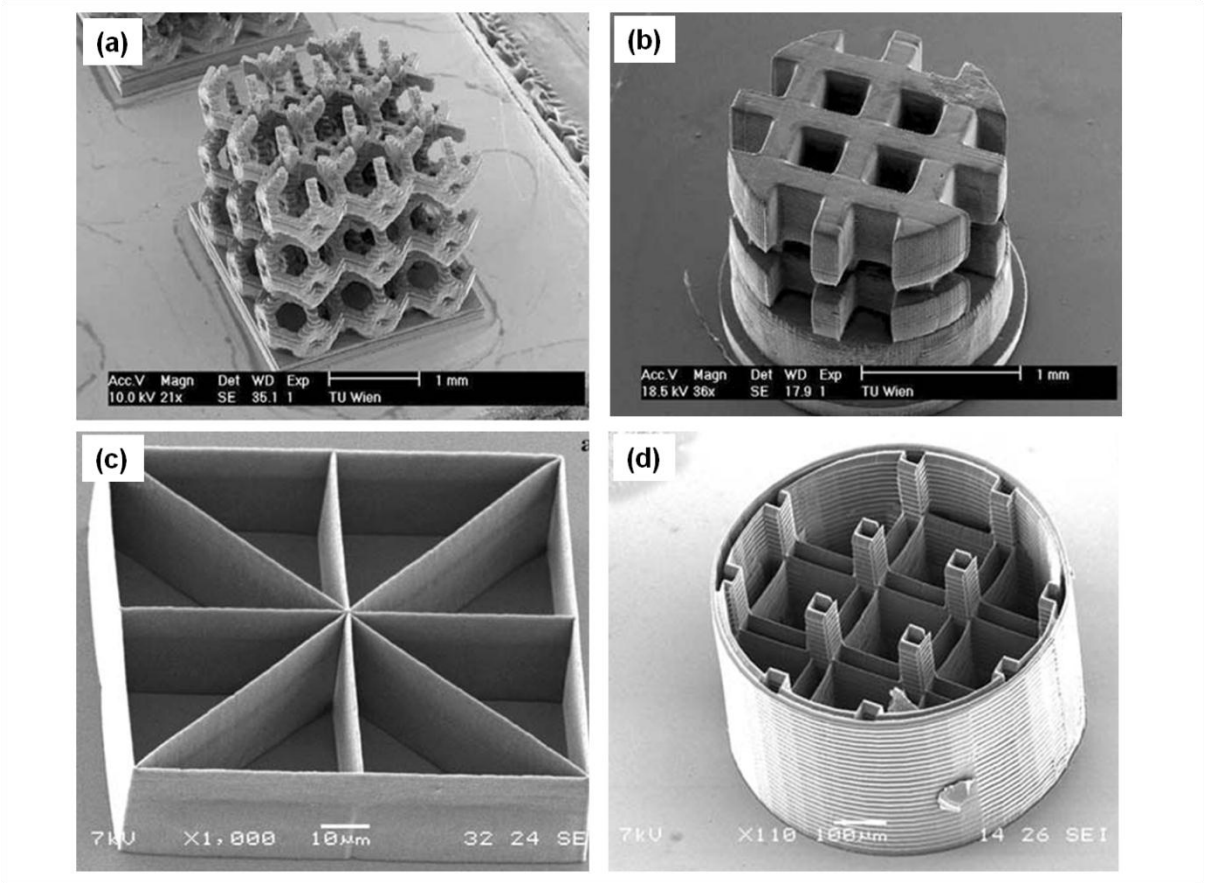

Figure 1.13 3D Microstructures made of photopolymers manufactured with (a) and (b) stereolithography photopolymerization) (Liska, Schuster et al. 2007) and (c) and (d) two-photon absorption and two-photon absorption (Kawata, Sun et al. 2001).

1.3.4. UV-assisted direct-write technique

The ultraviolet-assisted direct-write assembly (UV-DW) (Lebel, Aissa et al. 2010) is a technique to manufacture complex 2D and 3D microdevices using UV-curable polymers or their associated nanocomposites. A schematic illustration of the technique is shown in Figure 1.14. The UV-DW technique consists of the robotized deposition of extruded filaments. The materials are extruded through a capillary nozzle by an applied pressure and are simultaneously photopolymerized in seconds under UV exposure by a set of six optical fibers arranged in a circular pattern. The fast-curing of the nanocomposite materials enables the fabrication of

supported or freestanding 3D structures while the extrusion point is changed by the computer-controlled robot along the *x*, *y*, and *z* axes.

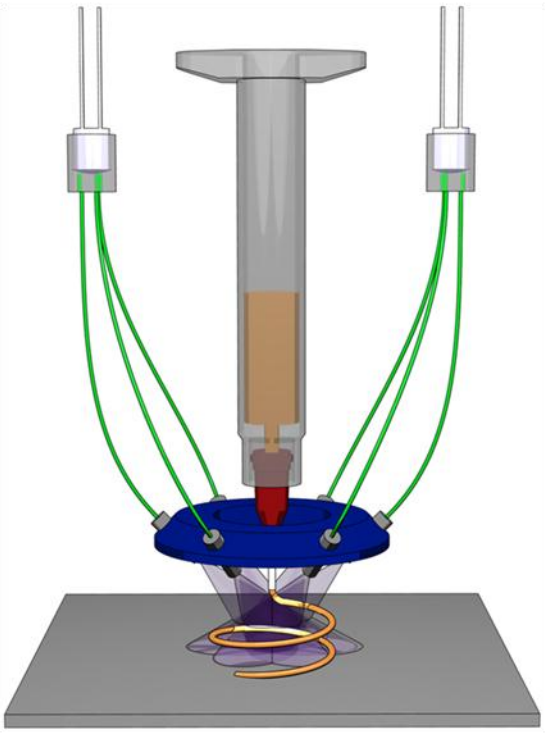

Figure 1.14 Schematic illustration of UV-assisted direct-write method for the fabrication of the nanocomposite micro-coils. The UV-curable nanocomposite was extruded using a controlled-robot through a needle (Lebel, Aissa et al. 2010)

Several parameters must be taken into account such as photo-curing rate, nanocomposite flow rate, UV-exposure region, nanocomposite rheological behavior and the dispensing robot speed for accurate microfabrication. An extruded material with moderate to high viscosity is necessary to maintain its filamentary form after being extruded during the UV-DW manufacturing (Lebel, Aissa et al. 2010; Lebel, Aissa et al. 2010). Thus, a shear-thinning behavior is preferable since high viscosity of the materials may limit their flow through the fine extrusion nozzle.

1.4. CNT-based nanocomposites for sensing applications

In general, the terms “micro electromechanical systems” (MEMS) refer to a collection of actuators and sensors which have the ability to react to changes in their environments with the use of microcircuit control. Due to their large aspect ratio and high electrical properties, carbon nanotubes are increasingly used in MEMS where they serve as large-surface sensing elements. Numerous works have reported the use of an individual CNT as well as nanotubes embedded within polymer matrices to sense temperature, toxic gases in the environment, biomolecules in the biomedical applications and mechanical strains in structural composite applications (Atashbar, bejcek et al. 2004; Liu, Chakrabartty et al. 2007; Hu, Yin et al. 2011).

CNT-based nanocomposites have been used to manufacture strain sensor films (Ji, Jung et al. 2007; Liu, Chakrabartty et al. 2007; Hu, Yin et al. 2011). The nanocomposite strain sensors are capable of monitoring strain, shape, pressure and load for applications that range from microsurgery to flexible artificial skins of robots (Hu, Yin et al. 2011). Figure 1.15 shows a schematic and a real image of a nanocomposite strain sensor. Nanocomposite films strain sensors might be preferred over conventional metal foil strain sensors in some applications due to their enhanced electromechanical sensitivity and their ability to accurately measure large strains. Here, the sensing mechanism is the nanocomposites electrical conductivity variation when the nanocomposite films undergo mechanical strains. This piezoresistive behavior is due to the rearrangement of percolating conducting network arising from physical contacts between neighboring CNTs (Hu, Yin et al. 2011). The nanocomposite electrical conductivity decreases with increasing mechanical strain under tension because the distances between neighboring nanotubes are increased (Hu, Karube et al. 2008). This leads to a significant decrease in the electron tunneling between neighboring nanotubes and consequently to a decrease in the overall

electrical properties of the nanocomposites. The mechanical strain may also decrease the contacting area between the neighboring nanotubes in their percolation pathways. Another possible contribution may arise from the intrinsic CNTs conductivity variation under mechanical strain as reported in literature (Stampfer, Helbling et al. 2006; Stampfer, Jungen et al. 2006; Singh, Rice et al. 2007).

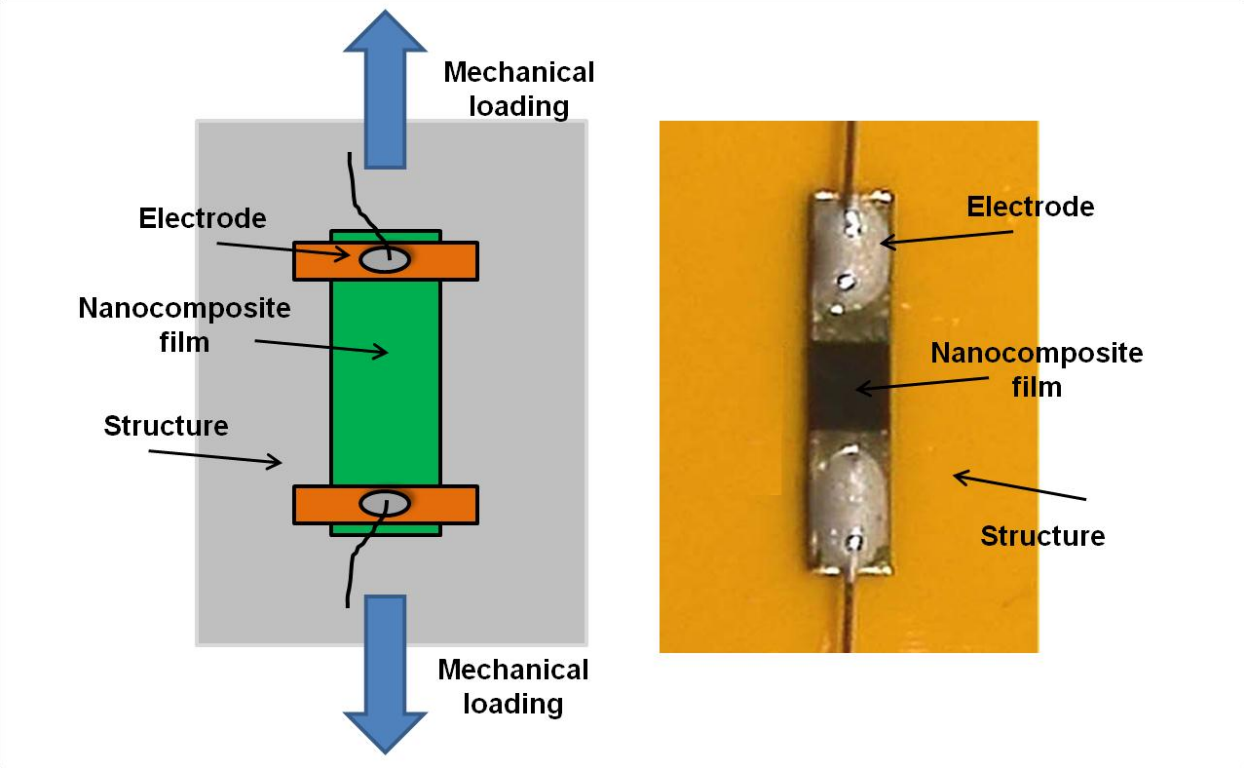

Figure 1.15 Schematic and real image of a nanocomposite strain sensor under tensile strain (Hu, Yin et al. 2011)

Higher electromechanical sensitivity has been observed in nanotube-reinforced polymer films in comparison to the conventional strain sensors as they exhibit relatively lower gauge factor (i.e., the ratio of relative resistance variation over strain variation) (Murugaraj and Mainwaring 2011). It has been found that nanotubes concentration, dispersion and manufacturing process used are the key parameters affecting the electromechanical sensitivity of such nanocomposite-based sensors. Higher nanotube loadings with a uniform dispersion enhance

the probability of contact points through where the electrons are transferred and also decrease the distance of adjacent nanotubes (Hu, Yin et al. 2011; Murugaraj and Mainwaring 2011).

Most of the nanocomposite strain sensors have been made of nanocomposite films so far (Stampfer, Helbling et al. 2006; Stampfer, Jungen et al. 2006; Ji, Jung et al. 2007; Singh, Rice et al. 2007; Park, Pham et al. 2008). Nanocomposite films with thermosetting polymers are fabricated by either spin coating on to substrates or slip casting (Murugaraj and Mainwaring 2011). Nanocomposite films are limited, by nature, to only provide in-plane strain measurements. In addition, they must be bonded over their whole area and might capture undesired parasitic perturbations (e.g., local cracks, plasticity, etc.) in applications where overall measurements are sought. The sensitivity of such sensors can be improved by decreasing their width and thickness (Murugaraj and Mainwaring, 2011). However, this potential tailoring is somewhat limited by fabrication and manipulation constraints. Finally, bulk nanocomposite films cannot be patterned as traditional strain sensors consisting of a long, thin conductive strip of patterned lines. This limits further the possibilities for improving their sensitivities.

CHAPTER 2: Scientific approach and coherence of articles

2.1. Scientific approach and organization of research work

The principal aim of this work was to manufacture three-dimensional (3D) microstructures with nanocomposite materials with desired mechanical and electrical properties for different applications. To reach the principal goal, different mixing strategies should be used to properly disperse nanotubes within the epoxy matrix. Then, two fabrication techniques (i.e., micro-infiltration and UV-assisted direct-write approaches), shown in Figure 2.1 should be employed to manufacture 3D microstructures. The micro-infiltration technique should confirm its capability to manufacture a 3D-reinforced nanocomposite with tailored mechanical properties by positioning the reinforcement and co-patterning of epoxy matrices (objective 1) and also by controlling nanotubes spatial orientation (objective 2). The UV-DW technique should be used to fabricate complex 3D freestanding microstructures using UV-curable nanocomposites for the applications such as micro electromechanical systems (objective 3 and objective 4). The research was therefore organized in two main parts: a) nanocomposite preparation and (b) microfabrication.

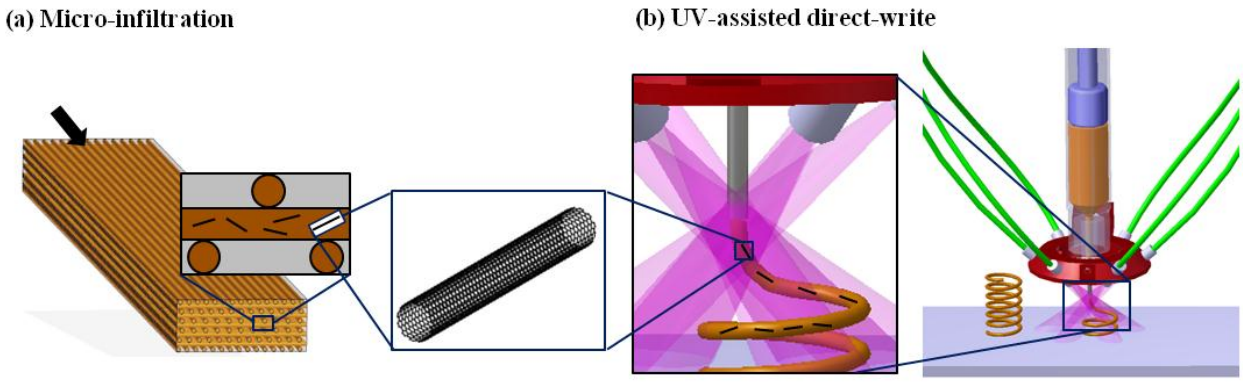

Figure 2.1 Schematic of two microfabrication approaches used to manufacture 3D nanocomposite microstructures

This research work was done with the collaboration of Professor Daniel Therriault and Professor Martin Lévesque from Ecole Polytechnique de Montreal and Professor My Ali El Khakani from Institut National de la Recherche Scientifique, INRS-Énergie, Matériaux et Télécommunications (INRS-EMT). This project was funded by the Fonds Québécois de la Recherche sur la Nature et les Technologies (FQRNT). Professor El Khakani and his students, Brahim Aissa, Vincent Le Borgne, Loick A. Gartier were responsible for the nanotube synthesis, the purification and the characterization. The nanocomposite preparation, microstructures fabrication and their characterization were accomplished in our group under the supervision of Professor Therriault and Professor Lévesque.

2.2. Article presentation and coherence with research objectives

Chapters 3 to 6 present the main scientific findings of this work and represent the core of the thesis. The work is presented in the form of four peer reviewed papers in archival journals (the article in Chapter 3 has already been published) and two peer reviewed proceeding papers (Proceeding paper, Appendix). The first two journal papers focused on the mechanical properties improvement by positioning and orientation of SWCNTs in 3D-reinforced nanocomposites manufactured using the micro-infiltration approach (objective 1 and objective 2). The second two journal papers focused on the fabrication of nanocomposite microstructures and their characterization for MEMS applications (objective 3 and objective 4). These six papers cover the objective of nanocomposite preparation and microstructures fabrication with 3D complex patterns (objective 1-4) as detailed in the following section.

2.2.1. Manufacturing 3D-reinforced beams with the micro-infiltration technique: Chapter 3-4 (Articles 1-2)

Epoxy composite beams reinforced with a complex three-dimensional (3D) skeleton structure of nanocomposite microfibers were fabricated via micro-infiltration of 3D porous microfluidic networks with carbon nanotube nanocomposites. A systematic experimental study of the manufacturing of composites beams with two different epoxy resins and also the influence of nanotube positioning at higher stress regions for optimal conditions were studied (objective 1). The microfibers 3D pattern was adapted to offer better performance under flexural solicitation by the positioning most of the reinforcing microfibers at higher stress regions. The main objective of the article is to show the flexibility of the manufacturing method which enables the utilization of different thermosetting materials and nanofillers in order to design multifunctional composites for a wide variety of applications such as structural composites and components for micro electromechanical systems. This work entitled "Micro-infiltration of three-dimensional porous networks with carbon nanotube-based nanocomposite for material design" was presented in the journal of *Composites Part A: Applied science and manufacturing* (chapter1).

An experimental and theoretical study on the nanotube spatial orientation and its effect on mechanical properties of the 3D-reinforced beams was presented in chapter 4 (objective 2). "Flow-induced orientation of functionalized single-walled carbon nanotubes embedded in epoxy using three-dimensional microfluidic networks" was submitted to the journal of *Polymer*. This journal was chosen because it publishes strong research works in the field of polymer manufacturing and polymer chemistry. This paper presents a study of shear conditions along with constraining effect on the nanotube orientation inside the microfluidic channels. To do this, the nanocomposite suspensions were injected into the empty networks under two different

controlled and constant pressures in order to subject the suspensions to different shear conditions in the microchannels. An experimental method based on capillary viscometry was performed to estimate the shear conditions inside the microchannels. Then, the effect of nanotube orientation on the mechanical properties of the manufactured composite beams was experimentally studied. Finally, the stiffness of the 3D-reinforced beams was compared with the theoretically predicted values obtained from a micromechanical model. The paper's main results are:

- The mechanical properties of the 3D-reinforced beams show different features which cannot be obtained for those of their individual components bulks;
- Higher nanotube orientation degree is obtained when higher nanocomposite injection pressure applied;
- Different orientation degree is achieved in longitudinal and perpendicular channels;
- The experimental mechanical results are in a fairly-good agreement with those obtaine from the homogenization model.

2.2.2. Manufacturing 3D freestanding nanocomposite microstructures with the UV-DW technique: Chapter 5-6 and appendix A and B (Articles 3-4 and proceeding papers, Appendices)

With the successful functionalization of nanotubes surfaces with biomolecules and carboxylic functional groups, the UV-DW technique was presented as a powerful tool for the fabrication of 3D freestanding microstructures for the applications such as high strength nanocomposites, biosensors (objective 3) and patterned strain sensors (objective 4). Chapter 5 reports on the preparation of nanocomposites consisting of biofunctionalized single-walled carbon nanotubes reinforcing an ultraviolet curable epoxy polymer by means of biotin-

streptavidin interactions. The corresponding paper entitled “Biotin-streptavidin interactions in functionalized carbon nanotube-epoxy composites” was submitted to the journal of *macromolecular Bioscience* (Article 3, chapter 5). This journal was chosen because it constitutes an important platform for publications on biopolymers and biosensors made of different sensing elements like nanotubes. The article focuses mainly on the influence of the nanotube functionalization on their dispersion as well as the mechanical and electrical properties of the resulting nanocomposite microfibers, manufactured by the UV-DW technique. Different mixing strategies were used to disperse nanotubes into the epoxy matrix and the results were presented a paper proceeding in *the second joint US-Canada on composites conference (Appendix A)*. The main results obtained are as following:

- The biomolecules grafted to the nanotubes surface not only facilitate the load transfer, but also improve the nanotube dispersion into the epoxy matrix;
- The nanotube biofunctionalization expands their utilization for a wide variety of applications;
- The nanotube biofunctionalization led to considerable enhancement in both strength (by 76%) and modulus (by 93%) with the addition of only 1 wt.% of BF-SWCNTs to the neat epoxy.
- The presence of biomolecules on the nanotube surface decreased the electrical conductivity of the resulting nanocomposites.

Finally, the work on the use of the nanocomposite to fabricate two freestanding 3D patterned strain sensors using the UV-DW technique (objective 4) was submitted to the journal of *Nanotechnology*. This journal publishes the research works on the use of nanomaterials in different technological applications. The sensors electromechanical sensitivity was evaluated

under mechanical strains in this paper. The present manufacturing method offers new prospective to manufacture freestanding microstructured MEMS sensors with a 3D designed pattern. The effect of nanotube orientation on mechanical properties of the microfibers fabricated with the UV-DW technique was also experimentally and theoretically studied. The results were presented in *the second joint US-Canada on composites conference (Appendix B)*. The main results of these two papers are as following:

- The manufactured sensors exhibited highly sensitive response to small mechanical disturbances, especially for lower nanotube loadings;
- A relatively higher sensors sensitivity were obtained for the geometry-controlled nanocomposite sensors when compared to traditional metallic or nanocomposite films;
- According to theoretical predictions, the beneficial orientation of nanotubes that could occur during the extrusion of the nanocomposites may contribute to the mechanical properties of the nanocomposite microfibers.

CHAPTER 3: Article 1: Micro-infiltration of three-dimensional porous networks with carbon nanotube-based nanocomposite for material design[1]

Rouhollah D. Farahani[a], Hamid Dalir[a], Brahim Aissa[b], My Ali El Khakani[b], Martin Lévesque[a], and Daniel Therriault[a,*]

[a] Center for Applied Research on Polymers and Composites (CREPEC), Mechanical Engineering Department, École Polytechnique de Montréal, C.P. 6079, Succ. Centre-Ville, Montreal (QC), Canada H3C 3A7

[b] Institut National de la Recherche Scientifique, INRS-Énergie, Matériaux et Télécommunications, 1650 Blvd. Lionel-Boulet, Varennes (QC), Canada J3X 1S2

Phone: 1-514-340-4711 x4419; Fax: 1-514-340-4176; E-mail: daniel.therriault@polymtl.ca

Abstract

Epoxy composite beams reinforced with a complex three-dimensional (3D) skeleton structure of nanocomposite microfibers were fabricated via micro-infiltration of 3D porous microfluidic networks with carbon nanotube nanocomposites. The effectiveness of this manufacturing approach to design composites microstructures was systematically studied by using different epoxy resins. The temperature-dependent mechanical properties of these multifunctional beams showed different features which cannot be obtained for those of their individual components bulks. The microfibers 3D pattern was adapted to offer better performance under flexural solicitation by the positioning most of the reinforcing microfibers at higher stress regions. This led to an increase of 49% in flexural modulus of a reinforced-epoxy

[1] This article is accepted in the journal of Composites Part A: Applied Science and Manufacturing

beam in comparison to that of the epoxy bulk. The flexibility of this method enables the utilization of different thermosetting materials and nanofillers in order to design multifunctional composites for a wide variety of applications such as structural composites and components for micro electromechanical systems.

Keywords: A. Theromosetting resin, B. Mechanical properties, B. Microstructures, E. Assembly, nanocomposite.

3.1. Introduction

Micro- and nano-fibers have been increasingly used as reinforcement in epoxy-based composites for structural applications in aerospace [1,2] and organic electronics [3]. Since epoxies are known to exhibit low toughness and impact resistance, several approaches have been employed to improve specific properties of fiber-reinforced epoxies [4]. Among these approaches, the selection of a suitable reinforcement which optimizes the composite properties [5], the improvement of the matrix toughness with other thermosetting resins or thermoplastics [6], and the critical optimization of the fiber-matrix interface to enhance the stress transfer properties [4] can be cited. More recently, multiscale approaches have been developed to design optimized microstructures using both nanoscale and microscale reinforcements [7].

Fibers produced from polymers such as polypropylene and nylon have been recently used as reinforcements for the fabrication of polymeric composites [8]. Various fiber parameters such as material nature, aspect ratio, fibers alignment, volume fraction, processing technique and fiber-matrix interface have been shown to influence the general performance of such composites. Main challenges with these polymeric fibers are their adhesion to the epoxy matrix and their lower mechanical properties with respect to traditional fibers [8,9]. However, fabrication of

nanocomposite microfibers by the addition of nano-particles having superior mechanical properties could further enhance the effectiveness of the polymeric fibers, which could lead to physical and mechanical properties improvement in these types of multiscale composites. Single-walled carbon nanotubes (SWCNTs) have been identified to be highly promising candidates for reinforcing polymer fibers not only for enhancing mechanical properties of the resulting nanocomposite [10-13], but also for improving their electrical [10,14] and thermal [15] properties, even for very low loadings. Hence, specific properties of an epoxy matrix could be tailored by taking the advantages of other polymers as fibers combined with excellent properties of SWCNTs. For specific loading conditions, positioning the nanocomposite microfibers at higher stress regions in these multifunctional composites could enhance their effectiveness compared to nanocomposites with randomly distributed fibers.

In this paper, we report on the use of a composite manufacturing approach inspired from an original microfluidic infiltration technique which was recently developed in our laboratory [16]. This approach is based on the micro-infiltration of a 3D microfluidic network with SWCNTs-based nanocomposite suspension for the fabrication of 3D-reinforced multiscale composites. After micro-infiltrating, the nanocomposite suspension was cured, resulting in a multiscale composite which consists of a complex 3D skeleton structure of nanocomposite microfibers. The micro-infiltration technique enables orienting the nanotubes along the fiber axis [17] and then positioning the nanocomposite fibers into a designed pattern for optimal conditions. Here, the most of nanocomposite microfibers were positioned at higher stress regions to offer better performance under flexural solicitation. Another focus is put here on the comparative study of three different epoxy resins with different properties (i.e., mechanical properties and glass transition temperatures) in order to point out the respective influences of both matrix and

nanocomposite fibers on the overall properties of resulting reinforced beams. The temperature-dependent mechanical and flexural properties of the fabricated multiscale nanocomposites were characterized with dynamic mechanical analyzer (DMA) and quasi-static three-point bending tests, respectively. These properties of the 3D-reinforced beams showed different features which usually cannot be obtained in their components bulks. The performance of the nanocomposite and 3D-reinforced beams were also characterized under tensile testing. The results provide sufficient evidence that the applied loads are effectively transferred to the 3D-patterned fibers (microscale) and subsequently to the SWCNTs in the nanocomposite-based fibers (nanoscale). The present manufacturing method opens new prospects for the design of multifunctional composite materials for optimal conditions.

3.2. Experimental

3.2.1. Nanocomposite preparation

The SWCNTs were produced by means of the pulsed laser ablation technique, using an excimer KrF laser (248 nm, 20 ns, 50 Hz, 300 mJ). The as-grown SWCNTs were chemically purified and functionalized by refluxing them in a 3M-HNO_3 (Sigma-Aldrich) solution for 5h (More details on the SWCNTs growth and purification can be found in earlier work [18]). The nanocomposites were prepared by blending purified-SWCNTs (at two loads of 0.5wt% and 1wt%), as reinforcement, and two different epoxy resins, either a special one-component dual cure (ultraviolet/heat curable) epoxy resin (UV-epoxy, UVE, UV15DC80, Master Bond Inc.) or two- component epoxy (EPON 862/ANCAMINE 2049), as matrices. The purified-SWCNTs were first dispersed in a solution of 0.1 mM of protoporphyrin IX (PP, Sigma-Aldrich) in acetone (Sigma-Aldrich) by bath ultrasonication (Ultrasonic cleaner 8891, Cole-Parmer) for 30

min. The resins were then mixed with the nanotube suspension in acetone over a magnetic stirring hot plate (model SP131825, Barnstead international) at 50°C for 4 h. The residual solvents were evaporated by heating the mixtures at 30°C for 12 h and at 50°C for 24 h in a vacuumed-oven (Cole Parmer). After evaporation of solvent, the nanocomposites were subjected to high shear mixing through a very small gap in a three-roll mill mixer (Exakt 80E, Exakt Technologies) for several times in progressing steps [19]. The gaps between rolls were adjusted at 25 µm for 5 passes and 10 µm for another 5 passes, followed by 10 passes at 5 µm while the speed of apron roll was 250 RPM. The final mixtures were then degassed under vacuum of 0.15 bar for 24 h. For the mixture prepared with the EPON 862 resin, the curing agent (resin:curing agent weight proportion = 3:1) was then mixed with the nanocomposite mixture and was passed in the three-roll mill mixer for 5 times with a gap of 15 µm and an speed of 250 RPM. The final mixture was degassed under vacuum of 0.15 bar for 2 h.

3.2.2. Fabrication of 3D microfluidic networks

Three-dimensional microfluidic networks were fabricated via the robotic deposition of a fugitive organic ink scaffold structure [20,21]. The fugitive ink was a 40 wt% binary mixture of a microcrystalline wax (SP18, Strahl & Pitstch) and a petroleum jelly (Lever Pond's). Figure 3.1(a) schematically illustrates the ink deposition process. The fabrication of the scaffold began with the deposition of the ink-based filaments on an epoxy substrate using a computer-controlled robot (I & J2200-4, I & J Fisnar) and a dispensing apparatus (HP-7X, EFD), leading to a two-dimensional pattern. The following layers were deposited by successively incrementing the *z*-position of the dispensing nozzle by the diameter of the filaments. The filaments' diameter was 150 µm for a deposition speed of 4.7 mm/s at an extrusion pressure of 1.9 MPa. The overall

dimensions of the 3D ink structure were 62 mm in length, 8 mm in width and 1.7 mm in thickness. The scaffold consisted of eleven layers of fugitive ink filaments, in which each layer was alternatively oriented along and perpendicular to the scaffold longitudinal, *x*, axis. The number of filaments deposited along the width direction, *y*, (even layers) was constant while the number of filaments along the longitudinal direction (odd layers) gradually decreased from the outer layers (1 and 11) to the center of structure in middle layers (5 and 7). Considering that the fugitive ink will be eventually replaced by the infiltrated-nanocomposite fibers, the reinforcing pattern can be tailored at will by using the flexible direct-write assembly method. In other words, depending on the final application of the microstructure, quantity and position of the reinforced filaments can be easily controlled for optimal properties. Axial stress distribution linearly increases from the neutral mid-plane to a maximum value at the outer surfaces during flexural mechanical solicitation. Thus, the number of axial reinforcing infiltrated microfibers was increased in higher stress regions to offer optimal performance under flexural solicitation.

After the deposition, the ink-based scaffolds were surrounded with two different epoxy resins: either EP1 (Epon 828/Epikure 3274, Miller-Stephenson Chemical Co.) or EP2 (Epon862/Ancamine 2049, Miller-Stephenson Chemical Co./Air Products Inc.), as shown in Figure 3.1(b). Prior to encapsulation, the epoxy systems were degassed under vacuum of 0.15 bar for 1 h to remove the bubbles trapped during mixing the epoxy components. For epoxy encapsulation, drops of epoxy were placed over the inclined (30°) scaffold structure at its upper end and let the epoxy to flow into the pore spaces between filaments through gravity and capillary forces. The quantity of the epoxy was controlled using a fine needle (7018225, EFD, internal diameter = 0.51mm) connected to a fluid dispenser (EFD800, EFD) in order to minimize the risk of bubble trapping [22-24]. When the epoxy resin reached the lower end of the scaffold,

the resin-encapsulated structure was placed under a vacuum of 0.4 bar for eliminating the remaining bubbles. The low viscosity of the epoxy system prior its full curing enhanced the degassing effect. The fiber displacement might be another issue that affects the encapsulation process. The rigidity of the fugitive ink used in this study enables both the scaffolds to retain their shape during the fabrication and subsequent epoxy encapsulation under ambient conditions [20]. After the pre-curing of the surrounding epoxy resin at room temperature for 48 h, the ink was removed by liquefaction at ~100°C in a vacuumed-oven for 30 min, as shown in Figure 3.1(c). Shortly after taking the samples out of the oven, the channel networks were washed with the suction of boiling distilled water for 5 min followed by hexane (Sigma Aldrich) for another 5 min.

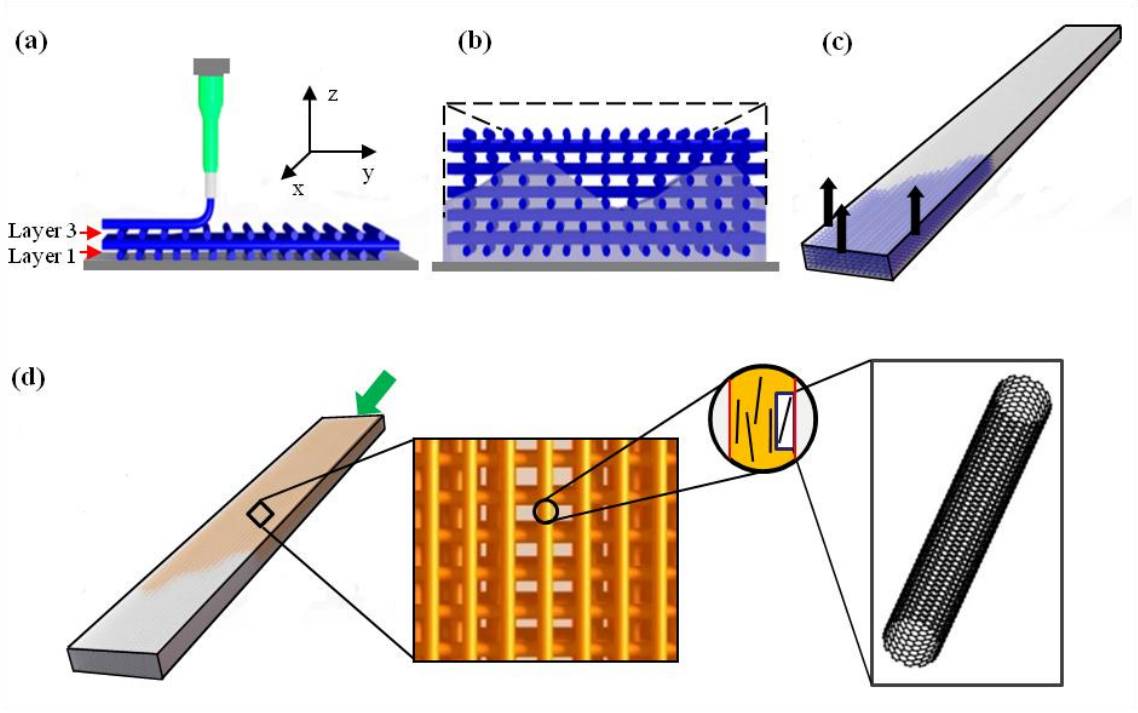

Figure 3.1 Schematic representation of the manufacturing process of a 3D-reinforced nanocomposite beam through micro-infiltration of 3D microfluidic network: (a) deposition of fugitive ink scaffold on an epoxy substrate, (b) encapsulation of the 3D ink-based scaffold using epoxy resin followed by resin solidification, (c) ink removal at 100 °C under vacuum, (d) micro-infiltration of the empty network by the nanocomposite followed by its curing.

3.2.3. Preparation of the 3D-reinforced beams via micro-infiltration technique

The 3D-reinforced beams were produced by micro-infiltrating the created tubular microfluidic networks with the pure epoxy resins (defined as resin-infiltrated beams) and their nanocomposites counterpart (defined as nanocomposite-infiltrated beams). The materials infiltrated behave like microscale fibers inside an epoxy matrix. Figure 3.1(d) schematically illustrates the micro-infiltration step for a nanocomposite-infiltrated beam at both micro- and nanoscales. The empty channels were infiltrated by the pure epoxy resins and their nanocomposites using the fluid dispenser via a plastic tube connected to the end of the beams and the fluid dispenser at both ends. The infiltration pressure was adjusted at 400 kPa, which led to an average infiltration speed of ~1 mm/s. In resin transfer molding (RTM) process, two major issues may arise when a liquid resin with nanoparticles is injected into the mold containing fibrous performs; void formation and nanoparticle deposition [23,25-28]. As in vacuum assisted resin transfer molding (VARTM) [29], a vacuum of 0.3 bar was applied to the other end (i.e., outlet side) of the microfluidic network in order to reduce the formation of voids. This not only contributed to provide the required pressure gradient for the infiltration of the nanocomposite, but also made less air available at the flow front to be entrapped [22]. The bubbles created during the infiltration process were moved with the material flow and gradually escaped by keeping the applied pressure for 30 sec after complete filling of the channels. Few holes were drilled in the length-thickness plane of the beams (each 20 mm on both sides) in order to remove the bubbles that might still existed in the width-channels as possible stationary points. Shortly after, the infiltration process was resumed for another 30 sec. Second, deposition of nanofillers potentially leading to a total blockage of the flow has been reported for RTM and VARTM processes [27,28,30]. This issue is of importance when large clusters are passed through smaller channels.

Considering the size of SWCNT aggregates in our study (~2 μm max.), it is thought that their deposition inside the channels of ~ 160 μm is unlikely. Other nanoparticle deposition mechanisms, like sedimentation of nanoparticles due to their gravity and non-Newtonian behavior, have also been reported [27]. Since the SWCNTs and the epoxies used in this study had similar densities, sedimentation of nanoparticles might be negligible. The effect of Non-Newtonian behavior is also unlikely since Newtonian behavior or slight shear thinning of the nanocomposites were observed (results for rheological behavior are not shown here).

After micro-infiltration step, the beams filled by the UV-epoxy- and its associated nanocomposite were put under illumination of a UV lamp with an intensity of 21mW/cm² (Cole-Parmer) for 30 min for pre-curing. The beams were then post-cured in the oven at 80 °C for 1 h followed by 130°C for another 1 h. The cure schedule for the second type of beams that were filled by EPON 862 resin and its associated nanocomposites was 90 °C for 2 h followed by 130°C for another 2 h. All the beams were cut and polished to the desired dimensions (i.e., ~60 mm in length, ~7.5 mm in width and ~1.7 mm in thickness). Figures 3.2(a) and 3.2(b) show an isometric and cross-sectional view of a nanocomposite-infiltrated beam, respectively. To verify presence of trapped bubbles, the cross-sections of few representative beams were observed under optical microscope for different locations along both longitudinal and width directions. No voids were seen, indicating the proper filling of the microfluidic channels. This also suggests that the filling speed did not affect the infiltration process since it reduces gradually towards the other end of the beams. Figures 3.2(c)-(e) show schematics of the cross-section of porous, resin-infiltrated and nanocomposite-infiltrated beams, respectively. Table 3.1 lists the different types of beams manufactured along with their components. For each type of beams, nine samples were prepared for mechanical testing. Three bulk specimens (molded samples) for each epoxy (i.e.,

EP1, EP2 and UVE) having the same dimensions as the beams were also prepared for comparison purposes.

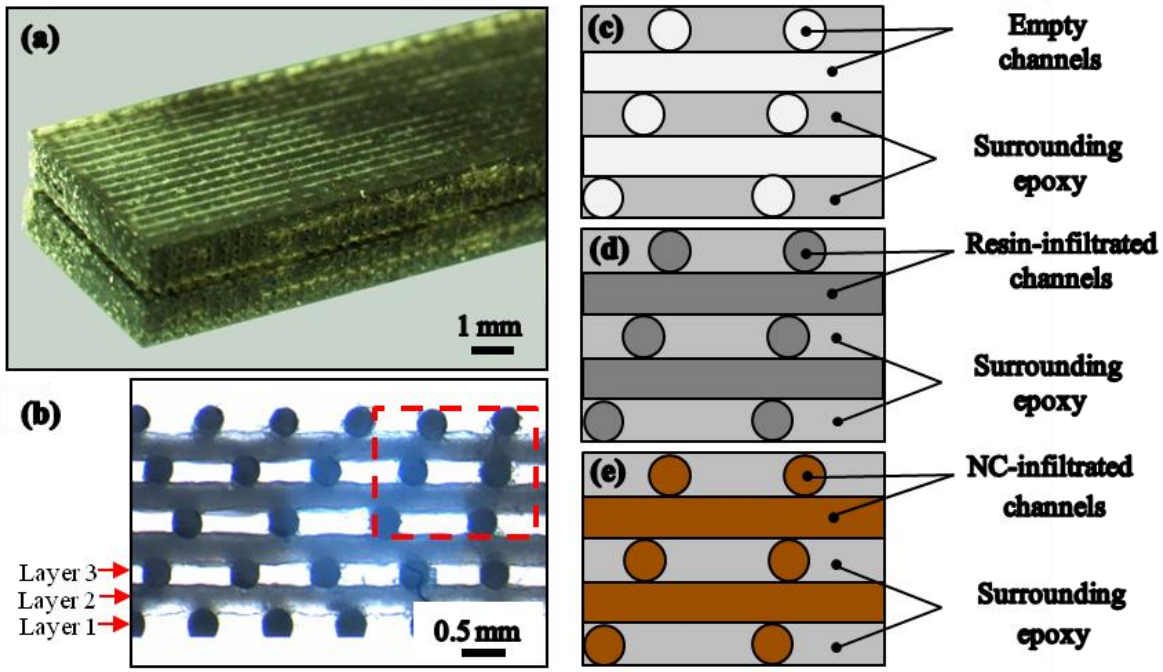

Figure 3.2 (a) Isometric image of a EP2-beam/NC-UVE-infiltrated containing 0.5 wt% SWCNT/UV-epoxy nanocomposite, (b) typical cross-section of a nanocomposite-infiltrated beam, (c)-(e) schematic illustration of the fabricated beams: porous (empty microfluidic network), resin-infiltrated and nanocomposite-infiltrated beams, respectively.

Table 3.1 Different types of 3D-reinforced beams, prepared in this study, and their components.

Type of sample		Components	
		Matrix (material-surrounded)	Microfiber (material-infiltrated)
Resin-infiltrated beams	EP1-beam/UVE-infiltrated	EPON 828	UV-epoxy
	EP2-beam/UVE-infiltrated	EPON 862	UV-epoxy
	EP1-beam/EP2-infiltrated	EPON 828	EPON 862
Nanocomposite-infiltrated beams	EP1-beam/NC-UVE-infiltrated	EPON 828	UV-epoxy/SWCNT nanocomposite
	EP2-beam/NC-UVE-infiltrated	EPON 862	UV-epoxy/SWCNT nanocomposite
	EP1-beam/NC-EP2-infiltrated	EPON 828	EPON 862/SWCNT nanocomposite

3.2.4. Morphological and mechanical characterization

The purified SWCNTs were observed by transmission electron microscopy (TEM) using a Jeol JEM-2100F (FEG-TEM, 200 kV) microscope in order to characterize the nanotube structure. Raman spectra were acquired at room temperature in the 100-2000 cm^{-1} spectral region under ambient conditions using a back-scattering geometry on a microRaman spectrometer (Renishaw Imaging Microscope Wire TM) with a 50× objective to focus the laser beam on the sample. The sample excitation was performed by using a 514.5 nm (2.41 eV) line from an air cooled Ar+ laser.

For optical imaging purposes, a ~20 μm-thick film of the nanocomposite was fabricated via its direct deposition on a glass substrate by means of the pressure dispensing-equipped robot. The quality of the mixing was observed for the cured nanocomposite film using an optical microscope (BX-61, Olympus) and image analysis software (Image-Pro Plus6, Media Cybernetics). Gold-coated fracture surfaces of the resin-infiltrated and the nanocomposite-infiltrated beams were observed using field emission scanning electron microscopy (FESEM) (JEOL, JEM-2100F) at 2 kV in order to observe the failure mode.

Temperature-dependent mechanical properties (complex modulus, $E^* = E' + iE''$, where E' is the storage modulus and E'' is the loss modulus) of the beams were measured in a DMA (DMA 2980, TA instruments) with a three-point bending mode at a ramp rate of 3°C/min and at a frequency of 1 Hz over the temperature range of 25 - 160°C. Quasi-static three-point bending tests were conducted on a DMA (DMA^+ 450, 01 DB-MetraviB) with a maximum load of 450 N and a crosshead speed of 0.5 mm/min for a support span of 35 mm according to the standard ASTM D790. Tensile properties (i.e., tensile modulus and strength) of the reinforced beams were also measured in a tensile testing machine (Instron 4400R) with a load cell of 5 kN according to

the ASTM D638 standard. The crosshead speed was set to 1 mm/min. Typical dimensions of the infiltrated- and bulk-beams were 60 mm × 7.5 mm × 1.7 mm.

3.3. Results and discussion

3.3.1. Carbon nanotube structural characterization

Figure 3.3(a) shows typical TEM micrographs of the laser-synthesized SWCNTs after their purification and functionalization. The nanotubes are seen to self-organize into bundles of few nanotubes and occasionally as individual SWCNTs. These SWCNTs feature a high aspect ratio since their length can reach up to several microns and their diameter is in the nanometer range. The inset of Figure 3.3(a) shows a bundle of SWCNTs where a carbon nanotube with a diameter of ~1.2 nm is clearly distinguished. Structural information on the diameter of nanotubes in a given sample can be directly obtained by analyzing Raman spectra, particularly in the low frequency region where the radial breathing mode (RBM) bands occur. Figure 3.3(b) shows a typical spectrum of the purified SWCNTs with a narrow radial breathing mode (RBM) band centered around 185 cm^{-1}. The frequency positions of the RBM vibrational mode can be used to determine the nanotubes diameters by means of the relationship reported by Bandow *et al* [31]:

$$d(nm) = 223.75 / \omega(cm^{-1}) \qquad (3.1)$$

where d and ω are the diameter of nanotubes and the frequency of the RBM vibrational mode. According to the equation (4.1), our SWCNTs are found to have a narrow diameter distribution centered around 1.2 nm, in accordance with the direct measurement of TEM (inset of Figure 3.3(a)).

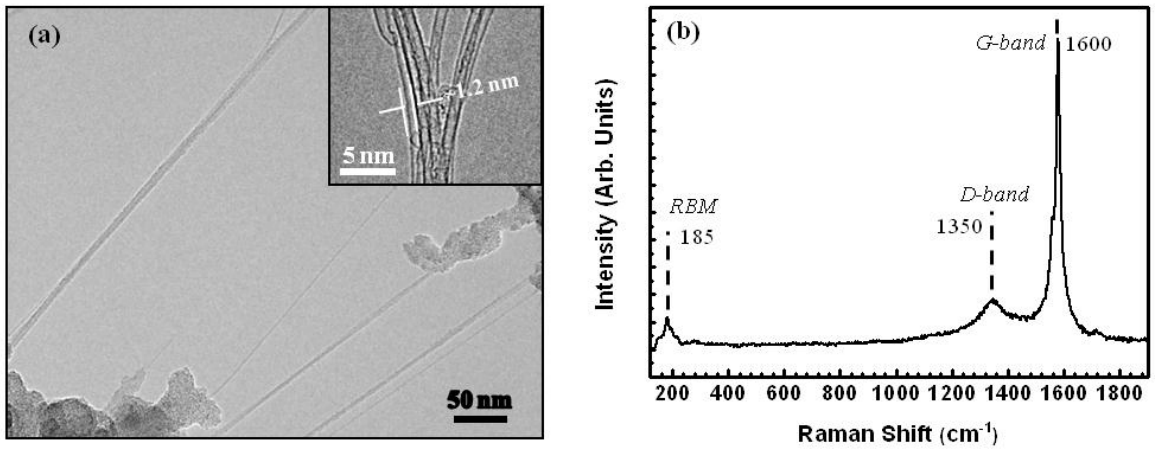

Figure 3.3 (a) TEM image of the purified SWCNTs soot material which are either in bundles or as individual entities. (b) typical Raman spectrum of the nanotubes featuring three peaks: the radial breathing modes (RBM) at around 185 cm^{-1}, the *G*-band around 1600 cm^{-1} and the *D*-band around 1350 cm^{-1}.

3.3.2. Morphological characterization

Figure 3.4 shows an optical micrograph of a representative UVE nanocomposite film with 0.5 wt% of nanotube. The observed dark spots are thought to be nanotubes aggregates, the majority of which has a size in the sub-micron range (Although some micron-size aggregates of up to ~1 μm-diam. are also present). The fairly uniform dispersion of the nanotube aggregates might be attributed to the effectiveness of the nanocomposite mixing procedure combining ultrasonication and three-roll mill mixing and also the presence of chemical groups at nanotube-matrix interface [32]. The chemical groups were grafted to the SWCNTs surfaces either in the nanotube purification process as confirmed by the *X*-ray photoelectron spectroscopy (XPS) results (these results can be found elsewhere [16]) or by non-covalent functionalization of the nanotubes with protoporphyrin IX as surfactant [33].

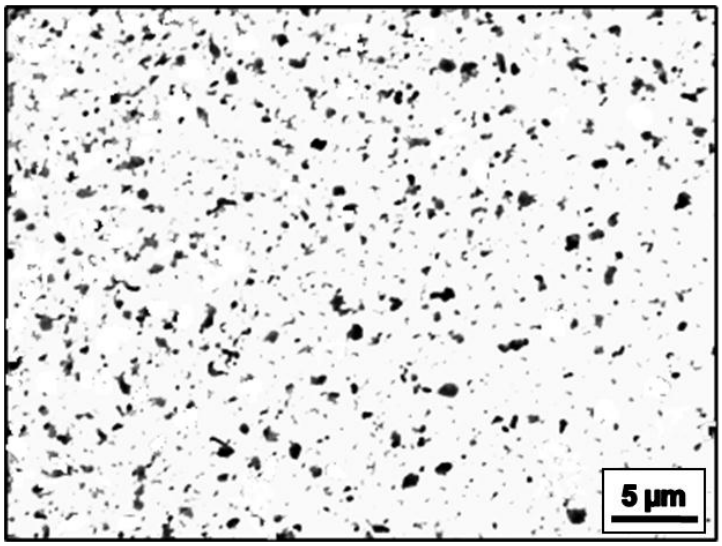

Figure 3.4 Optical microscopic image of a 20-µm thick film of SWCNT/UV-epoxy nanocomposites where both submicron- and micron-size aggregates are observed.

To examine the matrix-fiber interface and the composite structure, the fracture surface of two representative (one resin-infiltrated and one nanocomposite-infiltrated) beams broken during a three-point bending test were observed under SEM. Figure 3.5(a) and 3.5(c) show typical SEM images of the fracture surface of the EP2-beam/UVE-infiltrated and the EP2-beam/UVE-NC-infiltrated, respectively. No debonding and no pull-out of the embedded microfibers are observed, suggesting that the fibers were strongly adhered by the surrounding EP2 matrix at fiber-matrix interfaces. This confirms the effectiveness of the cleaning procedure used for the complete removal of the sacrificial ink during the microfluidic network fabrication.

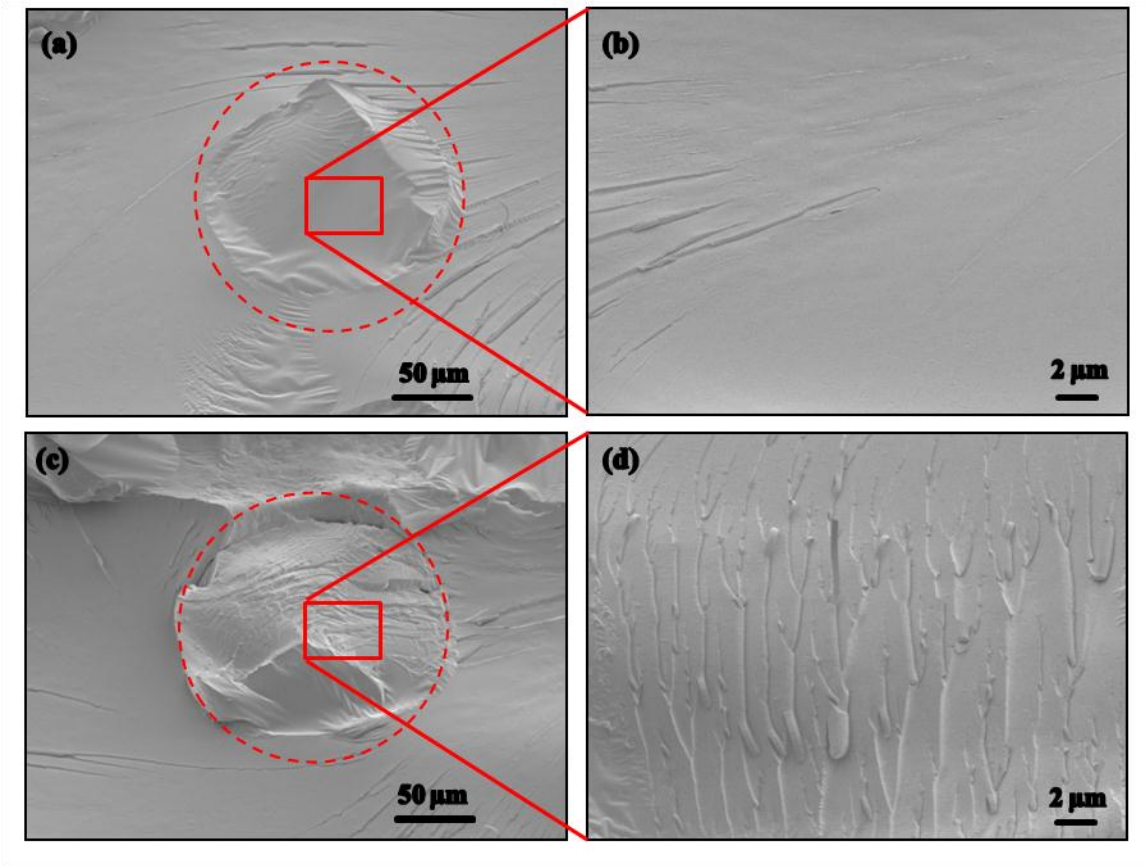

Figure 3.5 SEM images of the fracture surface of the 3D-reinforced beams in three-point bending test. (a) Typical fracture surface of a representative EP2-beam/UVE-infiltrated and (b) enlarged region on the fiber surface, (c) typical fracture surface of a representative EP2-beam/NC-UVE-infiltrated and (d) enlarged region on the fiber surface. The dashed lines show the microfibers.

Figures 3.5(b) and 3.5(d) are close-up view of the fracture surface of the UVE- and NC-UVE-microfibers, respectively. Comparison of these fracture surfaces allows to gain insights in the different fracture mechanisms and to eventually point out the effect of the SWCNTs on the failure behavior of the microfibers. The fracture surface of the UVE-fiber is relatively smooth compared to that of NC-UVE-fiber which is seen to contain more layered features. The larger roughness of the fracture surface of the NC-UVE-fiber is thought to be due to possible toughening effect induced by the presence of carbon nanotubes as reported in literature [34].

3.3.3. Mechanical characterizations

3.3.3.1. Temperature-dependent mechanical properties

Figure 3.6 shows the storage modulus, E', and the loss modulus, E'', of the 3D-reinforced beams and the molded bulk epoxy samples. The T_g of the bulk-epoxies which is observed as a peak in the E'' curves (Figures 3.6(b), (d) and (f)), were measured as ~ 60°C, ~ 125°C and ~ 115°C for the bulk-EP1, bulk-EP2 and bulk-UVE, respectively. The E' and the E'' curves of the resin- and nanocomposite-infiltrated beams, in all cases, show a combination of the bulk properties of their components. For the EP1-beam/UVE-infiltrated (Figure 4.6(a)), a major drop of the storage modulus is observed at ~ 65°C which is near the T_g of EP1 followed by a less pronounced decrease between 80°C to 115°C, close to the T_g of the UVE. Similar mechanism is observed for the EP1 beams filled by EP2 resin and its nanocomposite (Figure 3.6(e) and (f)). For the beams with EP1 as surrounding matrix (i.e., EP1-beam/UVE-infiltrated and EP1-beam/EP2-infiltrated), above 60°C, the T_g of EP1, the E' is completely controlled by the fibers, where the E' of the bulk-EP1 approaches to zero. The EP2-beam/UVE- and NC-UVE-infiltrated storage modulus exhibit a constant decreasing trend until a temperature of ~110°C (near the T_g of the UVE), followed by a slower decrease between 110°C to 125°C (the latter temperature is the T_g of the EP2). Based on Figure 3.6, the E' of the 3D-reinforced beams are influenced by the properties of the microfibers and the surrounding matrices for the range of temperature studied, depending on the T_g of their components. In other words, the temperature-dependent mechanical properties of the epoxy matrices could be tailored by the presence of the microfibers, prepared by the other epoxy resins. Hence, 3D co-patterning of thermosetting polymers like epoxies led to make the whole epoxy composite materials with different temperature-dependent feature which usually cannot be obtained in a single material.

Table 3.2 summarizes the measured values of the T_g and the E' of the 3D-reinforced beams and the bulk epoxies at 25°C. The variation of the E' of nanocomposite-infiltrated beams from their corresponding neat epoxy-infiltrated beams (i.e., the effect of SWCNTs addition) is presented in the last column. At 25°C, the E' of the bulk-EP1 and the bulk-EP2 are 2.95 GPa and 3.05 GPa, which are almost twice that of bulk-UVE. Regardless of the type of surrounding epoxies, the nanocomposite-infiltrated beams (i.e., multiscale composite beams) demonstrated a reasonable increase (above average compared to those reported in literature as listed in Table 3.3) in the E' compared to the resin-infiltrated beams. At 25°C, the E' of the EP1-beam/UVE-infiltrated was measured 2.51 GPa and is found to increase to 2.91 GPa (about 16% of improvement) with the addition of nanotubes for the EP1-beam/NC-infiltrated. For the EP2-beam/NC-UVE-infiltrated, the E' showed an increase of 18% compared to EP2-beam/UVE-infiltrated. The EP1-beam/NC-EP2-infiltrated resulted in a E' as 3.46 GPa, about a 16% increase in comparison to the EP1-beam/EP2-infiltrated. Interestingly, the presence of SWCNTs was found to have a more pronounced enhancement effect (higher E' values), particularly in the high temperature range where the UVE resin is softer. This is thought to be due to SWCNTs fair dispersion and adhesion with the matrices. At temperatures above T_g, the stiffening effect would be maximized when the well-bonded nanotubes are mobilized by the epoxy molecules [36]. Given the very low amount of SWCNT added (estimated to be ~ 0.18 wt% in the whole beam), the considerable improvements of the E', over the whole range of temperatures and for all the nanocomposite-infiltrated beams, suggests an extremely efficient load transfer in the 3D-reinforced beams. This stems from the fair dispersion and adhesion of our SWCNTs with the UVE matrix.

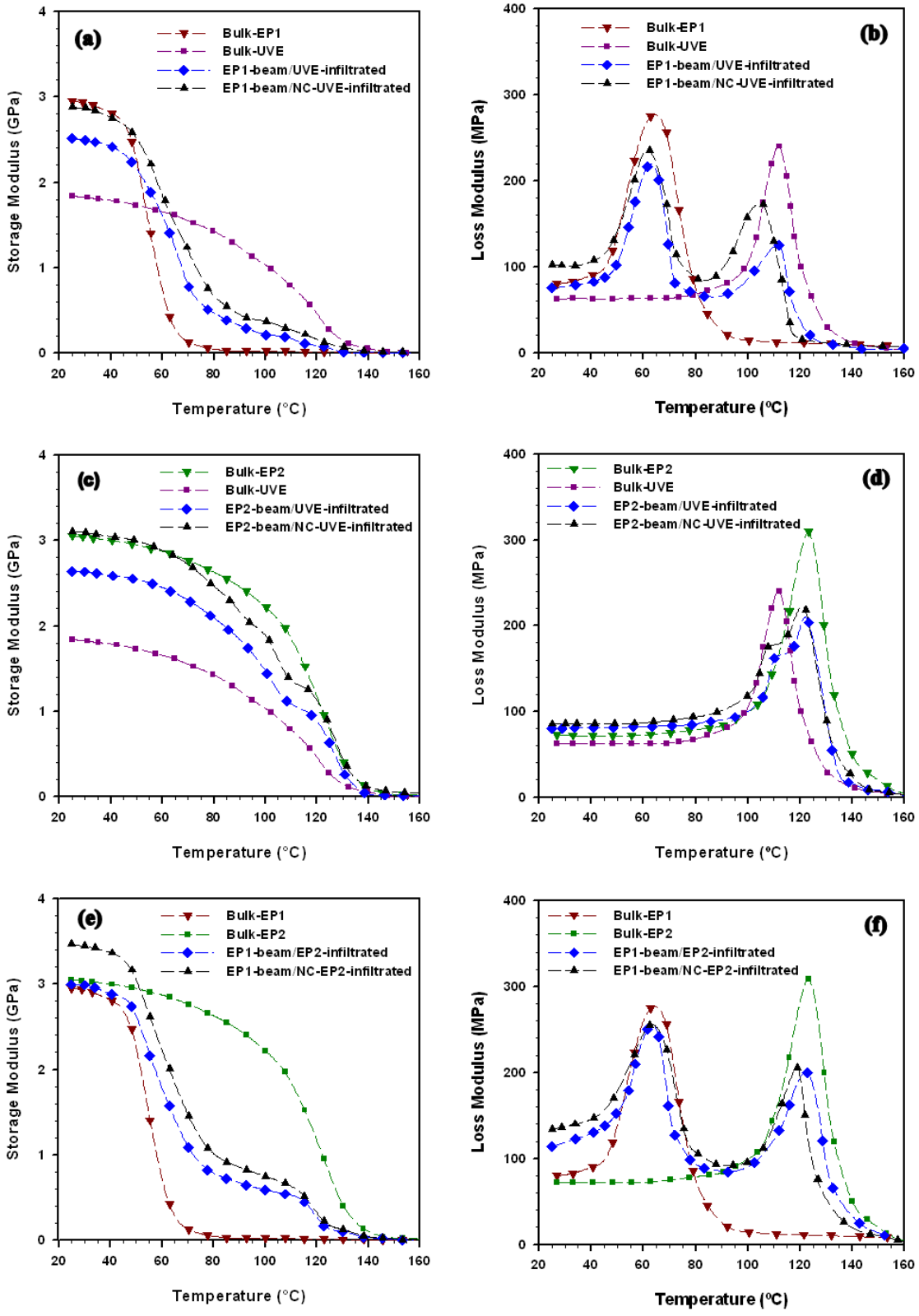

Figure 3.6 Dynamic mechanical properties of : (a) and (b) EP1-beam/UVE-infiltrated and NC-UVE-infiltrated, bulk-UVE and bulk-EP1, (c) and (d) EP2-beam/UVE-infiltrated and NC-UVE-infiltrated, bulk-UVE and bulk-EP2, and (e) and (f) EP1-beam/EP2-infiltrated and NC-EP2-infiltrated, bulk-EP2 and bulk-EP1.

Table 3.2 Glass transition temperature (T_g) and storage modulus at 25°C for the 3D-reinforced beams and the bulk epoxies. The E' variation for the three different types of nanocomposite-infiltrated beams compared to their corresponding neat epoxy-infiltrated beams is presented in the last column.

Type of sample	Glass transition temperature, Tg (°C)	Storage modulus at 25°C (GPa)	Storage modulus at 25°C Var. (%)
Bulk-UVE	~115	1.84	---
Bulk-EP1	~60	2.95	---
Bulk-EP2	~125	3.05	---
EP1-beam/UVE-infiltrated	~60 and ~115	2.51	0
EP1-beam/NC-UVE-infiltrated	~60 and ~110	2.88	15
EP2-beam/UVE-infiltrated	~125 and ~115	2.64	0
EP2-beam/NC-UVE-infiltrated	~125 and ~109	3.11	18
EP1-beam/EP2-infiltrated	~60 and ~125	2.99	0
EP1-beam/NC-EP2-infiltrated	~60 and ~121	3.46	16

Table 3.3 Comparison of increase of storage modulus at 25°C by adding SWCNTs to epoxy matrices achieved in our work with those reported in literature.

Researcher		SWCNTs wt.%	Increase of Storage Modulus at 25°C (%)	Normalized (Increase of Storage Modulus/wt.%) (%)
Barrera et al. [35]		1.0	44	44
Sun et al. [32]		1.0	20	20
Wang et al. [36]		1.0	41	41
Our results	EP1-beam/NC-UVE-infiltrated	0.18 (in whole beam)	15	83
	EP2-beam/NC-UVE-infiltrated	0.18 (in whole beam)	17	94
	EP1-beam/NC-EP2-infiltrated	0.18 (in whole beam)	16	88

3.3.3.2. Quasi-static three-point bending

Quasi-static three-point bending tests were performed to evaluate the effect of the microfibers and SWCNTs positioning on the mechanical properties of the 3D-reinforced beams. Figure 3.7 shows the averaged flexural stress-flexural strain curves in the quasi-static three-point bending tests, performed on three specimens for each beam type. The flexural modulus, E_f and

flexural strength, σ_f, were calculated from the load-deflection curves according to the ASTM D790 standard for flexural testing [37].

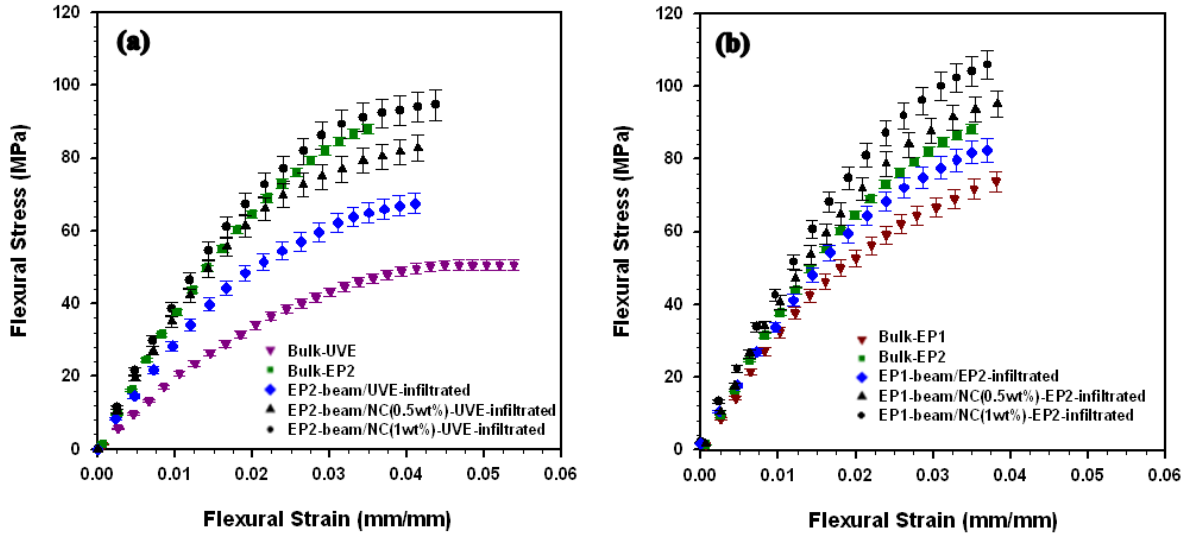

Figure 3.7 The averaged curves of the flexural stress with respect to the flexural strain for 3D-reinforced beams and bulk-epoxies: (a) bulk-UVE, bulk-EP2 and EP2-beam/UVE-infiltrated and EP2-beam/NC-UVE-infiltrated with the nanocomposite fibers containing two different loading of SWCNT (0.5 wt% and 1wt%) and (b) bulk-EP1, bulk-EP2 and EP1-beam/EP2-infiltrated and EP1-beam/NC-EP2-infiltrated with the nanocomposite fibers containing two different loading of SWCNT (0.5 wt% and 1wt%).

Table 3.4 lists the E_f and the σ_f of the bulk epoxies, the EP2-beam/UVE-infiltrated, EP2-beam/NC-UVE-infiltrated, EP1-beam/EP2-infiltrated and EP1-beam/NC-EP2-infiltrated and also the increase of the properties of neat epoxy-infiltrated beams when SWCNTs added. The E_f of the bulk-EP1 and bulk-EP2 are almost twice the value of the UVE. The addition of SWCNTs in EP2-beam/NC-UVE-infiltrated led to an increase of flexural properties of the EP2-beam/UVE-infiltrated. The EP2-beam/NC-UVE-infiltrated with 0.5wt% SWCNTs in microfibers (i.e., 0.18wt% in the whole beam) showed an increase of 27% for the E_f and an increase of 18% for the σ_f when compared to the EP2-beam/UVE-infiltrated. Further improvement is achieved for

EP2-beam/NC-UVE-infiltrated with 1wt% SWCNTs (i.e., 0.33wt% in the whole beam) (39% increase in modulus and 31% increase in strength). For the EP1-beam/EP2-infiltrated, the average flexural properties slightly increased when compared to the bulk-EP1 due to higher value of the material (EP2) used for the infiltration. The addition of 0.5wt% SWCNTs improved the E_f and the σ_f of the EP1-beam/NC-EP2-infiltrated by 22% and 16%, respectively. An increase of 34% in E_f is observed for the EP1-beam/NC-EP2-infiltrated with 1wt% SWCNTs compared to the EP1-beam/EP2-infiltrated while their σ_f showed an increase of 28%. Considering the very low fraction of the SWCNTs loading (i.e., ~ 0.18wt% and 0.33wt%), these improvements in flexural properties are among the largest improvements reported so far [38].

Contrary to typical nanocomposite manufacturing methods by which the reinforcements are randomly distributed throughout the matrix, the 3D-patterning of the microfibers in the 3D-reinforced beams enabled positioning the microfibers and SWCNTs at higher stress region to offer optimal performance under flexural solicitation. The interface is more solicitated during the quasi-static three-point bending test when compared to the small deformation in dynamic mechanical analyzing test. Therefore, higher flexural strain for the 3D-reinforced beams compared to those of the bulk-EP1 and the bulk-EP2 and strong bonding at the interface of the fibers and surrounding matrices suggest a proper load transfer at their interface (microscale), as observed by SEM images. The reasonable improvement of flexural properties for the NC-infiltrated beams compared to the resin-infiltrated beams might be attributed to subsequent stress transfer to the SWCNTs at nanotube/UV-epoxy interface (nanoscale) in the fibers and also to the positioning the nanotubes at higher stress regions.

Table 3.4 Flexural properties in three-point bending test for the 3D-reinforced beams and the bulk epoxies. The variation of the properties for the two different types of nanocomposite-infiltrated beams from their corresponding neat epoxy-infiltrated beams is also presented.

Type of sample	Flexural modulus (GPa)	Flexural modulus Var. (%)	Flexural strength (MPa)	Flexural strength Var. (%)
Bulk UVE	1.63	---	50.6	---
Bulk EP1	2.54	---	73.8	---
Bulk EP2	3.15	---	88.1	---
EP2-beam/UVE-infiltrated	2.41	0	69.8	0
EP2-beam/NC(0.5wt%)-UVE-infiltrated	3.06	+27	82.2	+18
EP2-beam/NC(1wt%)-UVE-infiltrated	3.36	+39	92.1	+31
EP1-beam/EP2-infiltrated	2.82	0	82.4	0
EP1-beam/NC(0.5wt%)-EP2-infiltrated	3.43	+22	95.2	+16
EP1-beam/NC(1wt%)-EP2-infiltrated	3.78	+34	105.2	+28

3.3.3.3. Tensile testing

The influence of SWCNTs on mechanical properties of the 3D-reinforced beams was also studied under tensile loadings. Table 3.5 lists the results obtained for the 3D-reinforced beams and the bulk epoxies. The second and forth columns present the increase of properties of neat epoxy-infiltrated beams by adding SWCNTs. The incorporation of SWCNTs into the reinforced beams led to an increase of Young's modulus and strength when compared to values for resin-infiltrated beams. Comparing the Young's modulus results with rules of mixtures predictions (see Table 3.5) showed that the SWCNTs reinforcement is close to its theoretical potential. For the calculations, the Young's modulus of the nanotube bundles was assumed to be 200 GPa [39] and the volume fractions of 0.18 and 0.33 since the densities of SWCNT and the epoxies used were similar. The volume fraction of the nanocomposites in the whole beam was 35%. It is worth noting that the elastic modulus of the reinforced beams could be maximized by aligning SWCNTs inside the channels along the longitudinal direction [17,40]. The orientation state of SWCNTs in these multiscale composites could be controlled by considering the channels size-

dependent mechanisms governing nanotube orientation. For example, applying higher pressure gradient will cause the SWCNTs to align with the flow and frequently rotate by 180° in Jeffery orbits. The Brownian motion that may impose small disturbances can contribute to the rotational motion by increasing the frequency of Jeffery orbits [27]. The experimental and theoretical studies on nanotube orientation inside the channels and its effect on mechanical properties of the final product will be presented in another paper.

Table 3.5 Tensile properties of the 3D-reinforced beams and the bulk epoxies. The second and forth columns present the variation of the tensile properties of the two different nanocomposite-infiltrated beams from their corresponding neat epoxy-infiltrated beams. The last column lists the results obtained from rules of mixtures for each type of the infiltrated beams.

Type of sample	Tensile Strength (MPa)	Tensile Strength Var. (%)	Young's Modulus (GPa)	Young's Modulus Var. (%)	Young's Modulus-Rules of Mixtures (GPa)
Bulk UVE	50.4	---	1.32	---	---
Bulk EP1	71.3	---	2.83	---	---
Bulk EP2	79.8	---	3.10	---	---
EP2-beam/UVE-infiltrated	64.7	0	2.34	0	2.47
EP2-beam/NC(0.5wt%)-UVE-infiltrated	68.9	+7	2.64	+11	2.83
EP2-beam/NC(1wt%)-UVE-infiltrated	72.4	+12	2.82	+17	3.13
EP1-beam/EP2-infiltrated	74.3	0	2.81	0	2.92
EP1-beam/NC(0.5wt%)-EP2-infiltrated	78.8	+6	3.06	+9	3.28
EP1-beam/NC(1wt%)-EP2-infiltrated	81.7	+10	3.26	+16	3.58

3.4. Conclusion

A method based on polymer micro-infiltration of a microfluidic network was used for the fabrication of multifunctional 3D-reinforced composite beams with a designed pattern of reinforcement. The temperature-dependent mechanical and flexural properties of the 3D-reinforced beams showed different features depending on the individual properties of the

microfibers and surrounding epoxies. Higher mechanical properties were achieved by the incorporation of SWCNTs to the 3D microstructured beams even at a very low nanotube nominal load of 0.5wt% (0.18wt% in whole beam). The improvement of mechanical properties and SEM observations at the fiber-matrix interface indicated that the load has been effectively transferred to the fibers (microscale) and subsequently to the SWCNTs in the nanocomposite-based fibers (nanoscale). This new fabrication method may enable also to align SWCNTs in the 3D microfluidic network by using a higher infiltration speed under shear flow. Due to the flexibility of this manufacturing method, various thermosetting polymer and their nanocomposites reinforced by other nanofillers such as nanoclay and nanosilver (in a wide range of viscosities) could be used either as microfibers or as a host matrix, depending on the composite final application. This manufacturing method opens new prospects for the design of thermosetting multifunctional composite materials for a wide variety of applications such as internal damage detection and embedded organic flexible electronics. Highly conductive nanofillers with a proper dispersion and required loadings could be used to tailor the conductivity of resulting nanocomposite for these applications. The internal damage of composite containing conductive fillers could be detected by mapping the electrical conductivity (or impedance) information.

3. Acknowledgments

The authors acknowledge financial support from FQRNT (Le Fonds Québécois de la Recherche sur la Nature et les Technologies). Prof. El Kahakani acknowledges also the finanial support from NSERC (National Science Engineering Research Council of Canada) and Plasma-Québec (le Réseau Stratégique du FQRNT sur la Science et Technologies des Plasmas). The authors would like to thank the technical support of Dr. Nadir Kchit and Mr. Matthieu Sola for

the mechanical characterizations and also Dr. Louis Laberge Lebel and Mr. Charles Tremblay for sample preparation.

3. References

[1] Ear Y, Silverman E. Challenges and opportunities in multifunctional nanocomposite structures for aerospace applications. MRS Bulletin. 2007;32(4):328-34.

[2] Zhou G, Movva S, Lee LJ. Nanoclay and long-fiber-reinforced composites based on epoxy and phenolic resins. Journal of Applied Polymer Science. 2008;108(6):3720-6.

[3] Bo XZ, Lee CY, Strano MS, Goldfinger M, Nuckolls C, Blanchet GB. Carbon nanotubes-semiconductor networks for organic electronics: The pickup stick transistor. Applied Physics Letters. 2005;86(18):182102, 1-3.

[4] Luo XF, Ou RQ, Eberly DE, Singhal A, Viratyaporn W, Mather PT. A Thermoplastic/Thermoset Blend Exhibiting Thermal Mending and Reversible Adhesion. Acs Applied Materials & Interfaces. 2009;1(3):612-20.

[5] Sgriccia N, Hawley M. Thermal, morphological, and electrical characterization of microwave processed natural fiber composites. Compos Sci Technol. 2007;67(9):1986-91.

[6] Park J, Park S, Lee S. Thermal and mechanical properties of carbon fiber reinforced epoxy composites modified with CTBN and hydroxyl terminated polyester. Adv Polym Emerg Technol 2007:568–72.

[7] Chen W, Shen H, Auad M, Huang C, Nutt S. Basalt fiber–epoxy laminates with functionalized multi-walled carbon nanotubes. Composites: Part A. 2009;40:1082-9.

[8] Huang ZM, Zhang YZ, Kotaki M, Ramakrishna S. A review on polymer nanofibers by electrospinning and their applications in nanocomposites. Composites Science and Technology. 2003;63(15):2223-53.

[9] Chronakis IS. Novel nanocomposites and nanoceramics based on polymer nanofibers using electrospinning process - A review. Journal of Materials Processing Technology. 2005;167(2-3):283-93.

[10] Allaoui A, Bai S, Cheng HM, Bai JB. Mechanical and electrical properties of a MWNT/epoxy composite. Composites Science and Technology. 2002;62(15):1993-8.

[11] Andrews R, Weisenberger MC. Carbon nanotube polymer composites. Current Opinion in Solid State & Materials Science. 2004;8(1):31-7.

[12] Coleman JN, Khan U, Gun'ko YK. Mechanical reinforcement of polymers using carbon nanotubes. Advanced Materials. 2006;18(6):689-706.

[13] Meyyappan M. Carbon nanotubes: science and applications. Boca Raton, Fl: CRC Press; 2005.

[14] Sandler JKW, Kirk JE, Kinloch IA, Shaffer MSP, Windle AH. Ultra-low electrical percolation threshold in carbon-nanotube-epoxy composites. Polymer. 2003;44(19):5893-9.

[15] Moisala A, Li Q, Kinloch IA, Windle AH. Thermal and electrical conductivity of single- and multi-walled carbon nanotube-epoxy composites. Composites Science and Technology. 2006;66(10):1285-8.

[16] Lebel LL, Aissa B, Paez OA, El Khakani MA, Therriault D. Three-dimensional micro structured nanocomposite beams by microfluidic infiltration. Journal of Micromechanics and Microengineering. 2009;19(12):155009, 1-7.

[17] Fan ZH, Advani SG. Characterization of orientation state of carbon nanotubes in shear flow. Polymer. 2005;46(14):5232-40.

[18] Lebel LL, Aissa B, El Khakani MA, Therriault D. Preparation and mechanical characterization of laser ablated single-walled carbon-nanotubes/polyurethane nanocomposite microbeams. Composites Science and Technology. 2010;70(3):518-24.

[19] Thostenson ET, Chou TW. Processing-structure-multi-functional property relationship in carbon nanotube/epoxy composites. Carbon. 2006;44(14):3022-9.

[20] Therriault D, Shepherd RF, White SR, Lewis JA. Fugitive inks for direct-write assembly of three-dimensional microvascular networks. Advanced Materials. 2005;17(4):395-99.

[21] Therriault D, White SR, Lewis JA. Chaotic mixing in three-dimensional microvascular networks fabricated by direct-write assembly. Nature Materials. 2003;2(4):265-71.

[22] Frishfeld V, Lundstrom TS, Jakovics A. Bubble motion through non-crimp fabrics during composites manufacturing. Composites Part a-Applied Science and Manufacturing. 2008;39(2):243-51.

[23] Lundstrom TS. Measurement of void collapse during resin transfer moulding. Composites Part a-Applied Science and Manufacturing. 1997;28(3):201-14.

[24] Nordlund M, Fernberg SP, Lundstrom TS. Particle deposition mechanisms during processing of advanced composite materials. Composites Part a-Applied Science and Manufacturing. 2007;38(10):2182-93.

[25] Advani SG, Chohra M, Yarlagadda S. Filtration of particles through a single layer of dual scale fibrous porous media. Advanced Composites Letters. 2007;16(6):205-21.

[26] Advani SG, Steggall-Murphy C, Simacek P, Barthelemy A, Yarlagadda S, Walsh S. A Model for Particle Deposition during Impregnation of Fibrous Porous Media. Journal of Porous Media. 2011;14(5):383-94.

[27] Hogberg SM, Lundstrom TS. Motion of dispersed carbon nanotubes during impregnation of fabrics. Plastics Rubber and Composites. 2011;40(2):70-9.

[28] Lundstrom TS, Frishfelds V. Modelling of particle deposition during impregnation of dual scale fabrics. Plastics Rubber and Composites. 2011;40(2):65-9.

[29] Lundstrom TS, Gebart BR, Lundemo CY. Void Formation in Rtm. Journal of Reinforced Plastics and Composites. 1993;12(12):1339-49.

[30] Advani SG, Chohra M, Gokce A, Yarlagadda S. Modeling of filtration through multiple layers of dual scale fibrous porous media. Polymer Composites. 2006;27(5):570-81.

[31] Bandow S, Asaka S, Saito Y, Rao AM, Grigorian L, Richter E, et al. Effect of the growth temperature on the diameter distribution and chirality of single-wall carbon nanotubes. Physical Review Letters. 1998;80(17):3779-82.

[32] Wang S, Liang R, Wang B, Zhang C. Reinforcing polymer composites with epoxide-grafted carbon nanotubes. Nanotechnology. 2008;19(8) :085710, 1-7.

[33] Nakashima N, Fujigaya T. Fundamentals and applications of soluble carbon nanotubes. Chemistry Letters. 2007;36(6):692-7.

[34] Gojny FH, Wichmann MHG, Fiedler B, Schulte K. Influence of different carbon nanotubes on the mechanical properties of epoxy matrix composites - A comparative study. Composites Science and Technology. 2005;65(15-16):2300-13.

[35] Barrera EV, Zhu J, Peng HQ, Rodriguez-Macias F, Margrave JL, Khabashesku VN, et al. Reinforcing epoxy polymer composites through covalent integration of functionalized nanotubes. Advanced Functional Materials. 2004;14(7):643-8.

[36] Sun L, Warren GL, O'Reilly JY, Everett WN, Lee SM, Davis D, et al. Mechanical properties of surface-functionalized SWCNT/epoxy composites. Carbon. 2008;46(2):320-8.

[37] Wachtman J. Mechanical properties of ceramics. New York: Wiley; 1996.

[38] Moniruzzaman M, Du FM, Romero N, Winey KI. Increased flexural modulus and strength in SWNT/epoxy composites by a new fabrication method. Polymer. 2006;47(1):293-8.

[39] Wang LF, Zheng QS. Extreme anisotropy of graphite and single-walled carbon nanotube bundles. Applied Physics Letters. 2007;90(15):153113, 1-3.

[40] Carreau PJ, Abbasi S, Derdouri A. Flow induced orientation of multiwalled carbon nanotubes in polycarbonate nanocomposites: Rheology, conductivity and mechanical properties. Polymer. 2010;51(4):922-35.

CHAPTER 4: Article 2: Flow-induced orientation of functionalized single-walled carbon nanotubes embedded in epoxy using three-dimensional microfluidic networks[2]

Rouhollah D. Farahani[a], Maryam Pahlavan pour[a], Hamid Dalir[a], Brahim Aissa[b], My Ali El Khakani[b], Martin Lévesque[a], Daniel Therriault[a,*]

[a] Center for Applied Research on Polymers and Composites (CREPEC), Mechanical Engineering Department, École Polytechnique de Montréal, C.P. 6079, Succ. Centre-Ville, Montreal (QC), Canada H3C 3A7

[b] Institut National de la Recherche Scientifique, INRS-Énergie, Matériaux et Télécommunications, 1650 Blvd. Lionel-Boulet, Varennes (QC), Canada J3X 1S2

Abstract

Functionalized single-walled carbon nanotubes (SWCNTs)-epoxy nanocomposite suspensions were prepared and injected into three-dimensional (3D) interconnected microfluidic networks in order to fabricate composite beams reinforced with patterned-oriented nanotubes. The microfluidic networks were fabricated by the robotized direct deposition of fugitive ink filaments in a layer-by-layer sequence onto substrates, followed by their epoxy encapsulation and the ink removal. Then, the nanocomposite suspensions prepared by ultrasonication and three-roll mill mixing methods were injected into the empty networks under two different controlled and constant pressures in order to subject the suspensions to different shear conditions in the microchannels. Morphological studies revealed that the SWCNTs were preferentially aligned in the microchannels along the flow direction at the higher injection pressure. The

[2] This article was submitted to the journal of Polymer

improvement of Young's modulus of the manufactured 3D-reinforced rectangular beams prepared at the high injection pressure was almost doubled when compared to that of beams prepared at the low injection pressure. Finally, the stiffness of the 3D-reinforced beams was compared with the theoretically predicted values obtained from a micromechanical model. The analytical predictions give a close estimation of the stiffness at different micro-injection conditions. Based on the experimental and theoretical results, the present manufacturing technique enables the spatial orientation of nanotube in the final product by taking advantage of shear flow combined with dimensional constraining inside the microfluidic channels.

Keywords: Nanocomposites, Nanotube orientation, Analytical modeling

4.1. Introduction

Single-walled carbon nanotubes (SWCNTs) reinforced polymer nanocomposites have attracted considerable attention for a wide variety of applications such as high-performance polymer composites [1], actuators and sensors [2], shape memory polymers [3], electrostatic microvalves [4] and communication systems [5]. Production of high quality carbon nanotubes (CNTs) having large aspect ratio, their proper dispersion and orientation in polymer matrices as well as the improvement of interfacial bonding are the main parameters affecting nanocomposites mechanical performance [6]. Grafting chemical groups to the surface of CNTs is the usual approach to minimize nanotubes agglomeration and also to enhance their interfacial interactions with the polymer matrix [7-9]. Carboxylic groups grafted during the acid purification process of the CNTs [10], as well as the non-covalent functionalization using surfactants like porphyrins [11], can significantly improve interfacial stress transfer [12,13].

To address the CNTs alignment along a desired direction in a polymer matrix, shear flow [14, 15] and electromagnetic fields [16] along with dimensional constraints have been used. The

injection of nanocomposites under high shear flow causes the CNTs to be aligned in the direction of the flow where the degree of orientation directly depends on the extent of applied shear [14,15]. However, depending on the type of flow, most of the nanotubes remain randomly oriented and shear-induced orientation of CNTs takes place only at higher shear zones. Dimensional constraining effect on CNTs orientation in 1D and 2D has been employed in several nanocomposite processing techniques including fiber spinning and electrospinning [17], compression molding [15], extrusion [18] and film casting [19]. None of these techniques enable manufacturing a final product with sufficient control on the three-dimensional (3D) orientation of the reinforcement. More recently, an approach based on the micro-infiltration of microfluidic networks with nanocomposite suspensions has been developed to manufacture 3D-reinforced microstructure beams [20]. This approach typically attempts to design optimized microstructures using different thermosetting matrices and nanofillers. However, these studies have not addressed the influence of manufacturing process conditions such as channels diameter, injection pressures or shear rates on CNTs orientation and its resulting influence on the mechanical properties of 3D-reinforced beams.

In this paper, 3D-reinforced microstructure beams were manufactured via micro-injection of 3D microfluidic networks with purified-SWCNTs/epoxy nanocomposite suspensions at different injection pressures. After curing the nanocomposite suspension, the final product was a rectangular beam reinforced with a complex 3D nanocomposite microfiber scaffold. The main goal is the fabrication of nanocomposite beams reinforced with three-dimensionally oriented SWCNTs by taking the advantages of high shear flow and also dimensional constraining in small-diameter interconnected microfluidic channels. In addition to dimensional constraining, the microchannels present large shear surfaces, involved in the shear-induced orientation of

CNTs. The effective process-related apparent shear rates inside the microfluidic channels in micro-injection process were estimated from capillary viscometry. The morphology of the nanocomposite and 3D-reinforced beams were characterized under scanning electron microscopy (SEM) and transmission electron microscopy (TEM) and their mechanical properties were measured under tensile testing. Furthermore, a micromechanical model is used to predict the effective stiffness of the manufactured 3D-reinforced beams in order to estimate if the manufactured samples reached their full potential. Our results provide sufficient evidence for the effectiveness of the present manufacturing approach to enhance the stiffness of the nanocomposite materials caused by homogenously aligning CNTs throughout the final product.

4.2. Experimental

4.2.1. Materials

The SWCNTs were produced by means of the pulsed laser ablation technique, using an excimer KrF laser (248 nm, 20 ns, 50 Hz, 300 mJ) with a graphite target and Co/Ni catalyst in a furnace at 1100˚C in an Argon atmosphere [21]. The as-produced SWCNTs were chemically purified and functionalized by refluxing them in a 3M-HNO_3 (Sigma-Aldrich) solution for 5 h (more details on the SWCNTs purification can be found in an earlier work [10]). Zinc Protoporphyrin IX (ZnPP), obtained from Sigma Aldrich was used as the surfactant. The two epoxy systems used in this study were a special one-component dual cure (ultraviolet/heat curable) epoxy resin (UV-epoxy, UV15DC80, Master Bond Inc.) and a two-component epoxy system composed of EPON resin 862 (Miller-Stephenson Chemical Company Inc.) and ANCAMINE 2049 (Air Products Inc.) as the hardener. The UV-epoxy used here contains a UV photo-initiator having an optimal absorption at 365 nm and a heat-initiator active in the 60 - 80°C range.

4.2.2. Preparation of nanocomposites

The nanocomposites were prepared by blending the UV-epoxy and purified-SWCNTs at two loads of 0.5wt% and 1wt%. The desired amount of purified-SWCNTs was added to a solution of 0.1 mM of zinc protoporphyrin IX in acetone (Sigma-Aldrich). The suspension was sonicated in an ultrasonic bath (Ultrasonic cleaner 8891, Cole-Parmer) for 30 min. The UV-epoxy was then slowly mixed with the nanotube suspension in acetone over a magnetic stirring hot plate (Model SP131825, Barnstead international) at 50°C for 4 h. After stirring, the nanocomposite mixture was simultaneously sonicated and heated in the ultrasonication bath at 50°C for 1 h. The residual trace of solvent was evaporated by heating the nanocomposite mixture at 30°C for 12 h and at 50°C for 24 h in a vacuumed-oven (Cole Parmer). After the evaporation of the solvent, the nanocomposites were passed through a three-roll mill mixer (Exakt 80E, Exakt Technologies) for final high shear mixing. The gaps between the rolls varied in three batch-wise processing steps including 5 passes at 25 µm, 5 passes at 10 µm and 10 passes at 5 µm, respectively. The speed of the apron roll was set to 250 RPM. The final mixture was then degassed under vacuum for 24 h.

4.2.3. Micro-injection of 3D microfluidic networks

Three-dimensional microscaffolds were fabricated using a computer-controlled robot (I & J2200-4, I & J Fisnar) that moves a dispensing apparatus (HP-7X, EFD) along the *x*, *y* and *z* axes [22, 23]. The fabrication of the microscaffold began with the deposition of the ink-based filaments on an epoxy substrate, leading to a two-dimensional pattern. The fugitive ink was a 40 wt% binary mixture of a microcrystalline wax (SP18, Strahl & Pitstch) and a petroleum jelly (Lever Pond's). The following layers were deposited by successively incrementing the *z*-position of the dispensing nozzle by the diameter of the filaments. The 3D microscaffold consisted of

eleven layers of fugitive ink filaments, deposited alternatively along and perpendicular to the scaffold longitudinal, *x,* axis. The filament diameter was 150 μm for a deposition speed of 4.7 mm/s at an extrusion pressure of 1.9 MPa. The overall dimensions of the 3D ink structure were 62 mm in length, 8 mm in width and 1.7 mm in thickness with 0.25 mm spacing between filaments. The empty space between the scaffold filaments was filled with the same epoxy resin used for the substrate fabrication. Upon the curing of the epoxy, the fugitive ink was removed from the structure by the liquefaction at 100°C and applying vacuum, yielding an interconnected 3D microfluidic network. Figure 4.1a shows a schematic of a typical rectangular beam which consists of a microfluidic network embedded in the epoxy resin with its overall dimensions.

The created tubular microfluidic network was filled by nanocomposite suspension, through a plastic tube attached to the opened channels using the fluid dispenser as shown in Figure 4.1b. The micro-injection process led to the fabrication of 3D-reinforced nanocomposite rectangular beam (i.e., nanocomposite-injected beams). The injection pressure was set either to 0.7 MPa (defined as low injection pressure), or 4.2 MPa (defined as high injection pressure). For comparison purposes, beams filled with pure UV-epoxy (defined as resin-injected beams) were also prepared. Shortly after the injection, the beams filled by the UV-epoxy- and its nanocomposites were put under illumination of a UV lamp (RK-97600-00, Cole-Parmer) for 30 min for pre-curing in order to avoid effect of Brownian motion on the CNTs orientation. Resin- and nanocomposite (NC)-injected beams were then post-cured in the oven at 80 °C for 1 h followed by 130°C for another 1 h. The beams were cut and polished to the desired dimensions (i.e., ~60 mm in length, ~6.8 mm in width and ~1.6 mm in thickness) for mechanical and morphological characterizations. Figure 4.1c shows an isometric view of a NC-injected beam,

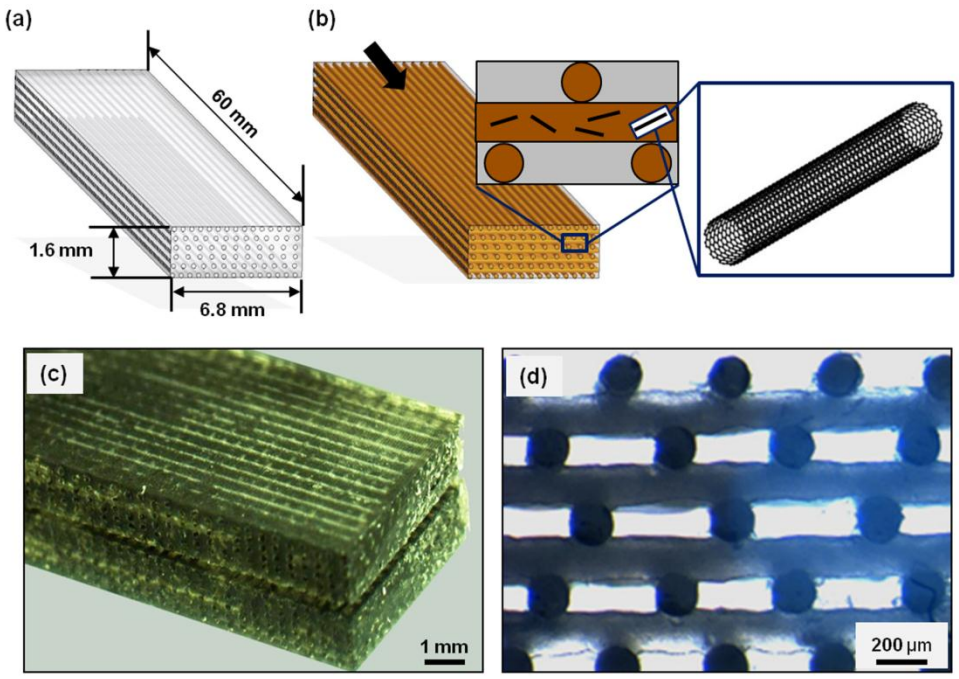

Figure 4.1 Illustration of the manufacturing process of a 3D beam reinforced with aligned and localized SWCNTs through micro-injection of 3D microfluidic network: (a) overall dimensions of the microfluidic network beams, fabricated by the direct-writing of the fugitive ink upon epoxy encapsulation and ink removal, (b) micro-injection of the empty network with nanocomposite suspension which led to the fabrication of 3D-reinforced beams (the arrow shows the direction of micro-injection flow), (c) isometric image of a 3D-reinforced beam, (d) typical cross-section of a nanocomposite-injected beam, showing the configuration of microchannels filled with nanocomposites.

prepared by the nanocomposite suspension with the nanotube load of 0.5wt% and Figure 4.1d shows the cross-section of the beam (microscale).

4.2.4. Nanotube and nanocomposites morphological characterizations

The purified SWCNTs were observed by transmission electron microscopy (TEM) using a Jeol JEM-2100F (FEG-TEM, 200 kV) microscope. The nanotubes Raman spectra were acquired at room temperature in the 100 - 2000 cm^{-1} spectral region under ambient conditions using a back-scattering geometry on a microRaman spectrometer (Renishaw Imaging Microscope Wire TM) with a 50× objective to focus the laser beam on the sample. Sample excitation was performed using a 514.5 nm (2.41 eV) line from an air cooled Ar+ laser. In addition, the

SWCNTs were characterized by X-ray photoelectron spectroscopy (XPS, Escalab 220i-XL system, VG instruments) using the monochromatic Al Ka radiation as the excitation source (1486.6 eV, full width at half-maximum of the Ag 3d5/2 line = 1 eV at 20 eV pass energy). Fracture surface of the 3D-reinforced and the bulk nanocomposite beams were observed using field emission scanning electron microscopy (FESEM JEOL, JSM-7600TFE) at 2 kV in order to observe the failure modes. The orientation state of the CNTs in the NC-injected beams was studied under TEM (JEOL, JEM-2100F). Prior to observation, the samples were prepared by ultramicrotoming of the NC-injected beams surfaces using a diamond knife at room temperature.

4.2.5. Viscosity characterization

Since the degree of CNTs orientation depends on the shear rate (or applied injection pressure) of nanocomposite flow, the shear conditions through the micro-injection of 3D microfluidic networks were studied at the two different injection pressures. The complexity of the nanocomposite flow pattern inside the complex 3D interconnected microfluidic network prevents accurate shear conditions to be characterized. Since the accurate modeling of the nanocomposite flow is not the main focus of this study, a simple assumption was made to estimate the process-related shear rates encountered in the micro-injection process. The microfluidic network was assumed as a bundle of similar disconnected parallel channels in which the flow pattern is corresponding to a simple Poiseuille flow. This flow mechanism may also occur in pressure-constant capillary viscometry. Therefore, the process-related apparent shear rate and apparent viscosity of the pure UV-epoxy and its nanocomposite in the microfluidic network were estimated from an experimental method based on capillary viscometry [10, 24]. For the purpose of similarity (i.e., similar flow conditions in micro-injection process and capillary viscometry), the materials were extruded through a micro-nozzle (5132-0.25-B,

Precision Stainless Steel Tips, EFD, *L* = ~20 mm and *ID* = 100 µm) under the same applied pressures used for the micro-injection of empty microchannels with nanocomposites (i.e., 0.7 MPa and 4.2 MPa). To obtain the materials flow rate, ten continuous filaments of materials were deposited over a glass substrate using the computer-controlled robot and the fluid dispenser. Shortly after the deposition, the filaments were cured under illumination of the UV lamp for 5 min. The flow rates of the materials were calculated from the cross-section of the filaments and the deposition speed controlled by dispensing apparatus. The cross-section area of the filaments was measured using an optical microscope (BX-61, Olympus) and image analysis software (Image-Pro Plus v5, Media Cybernetics). Considering the very low shrinkage of the UV-epoxy, it is fair to neglect its effect on the filaments cross-section. The process-related apparent shear rate and the process-related apparent viscosity were calculated based on capillary viscometry equations including Rabinowitsch correction [24]. The process-related wall shear stress was calculated as:

$$\tau_W = \frac{P_{mi} - P_a}{2(L/R)} \tag{4.1}$$

where P_{mi} is the pressures applied, corresponding to the micro-injection pressures. The wall shear rate was determined from the flow rate Q, by firstly calculating the Newtonian shear rate using:

$$\dot{\gamma}_{Nt} = \frac{4Q}{\pi R^3} \tag{4.2}$$

and using the Rabinowitch correction for non-Newtonian effects as:

$$\dot{\gamma}_W = \dot{\gamma}_{Nt}\left(\frac{3+b}{4}\right) \tag{4.3}$$

where b is obtained from the log-log plot of τ_W with respect to $\dot{\gamma}_{Nt}$. Finally the process-related apparent viscosity was calculated using:

$$\eta_{app} = \frac{\tau_W}{\dot{\gamma}_W} \tag{4.4}$$

4.2.6. Mechanical properties

Mechanical properties (i.e., tensile modulus, strength and elongation at break) of the beams were measured in a tensile testing machine (Instron 4400R) with a load cell of 5 kN according to the ASTM D638 standard. The crosshead speed was set to 1 mm/min and typical dimensions of the sample beams were 60 mm × 6.8 mm × 1.6 mm.

4.3. Mechanical modeling

A three-step analytical homogenization model was developed to estimate the effective mechanical properties of the resin- or NC-injected beams (Figure 4.2). The first homogenization step was used to estimate the mechanical properties of NC-based fibers. In the second homogenization step the mechanical properties of different layers in the beam were calculated. The third step was used to derive the effective properties of the injected beam. The different phases (i.e., the UV-epoxy matrix in the microfibers, EPON 862 matrix around the microfibers and the carbon nanotubes) were assumed to be linearly elastic and perfectly bonded. The Mori-Tanaka method [25] was used in the first and second homogenization steps while the Classical Lamination Theory was used at the last step. According to the Mori-Tanaka scheme, the effective stiffness tensor, $\tilde{\mathbf{C}}_{MT}$, for a two-phase material is given by:

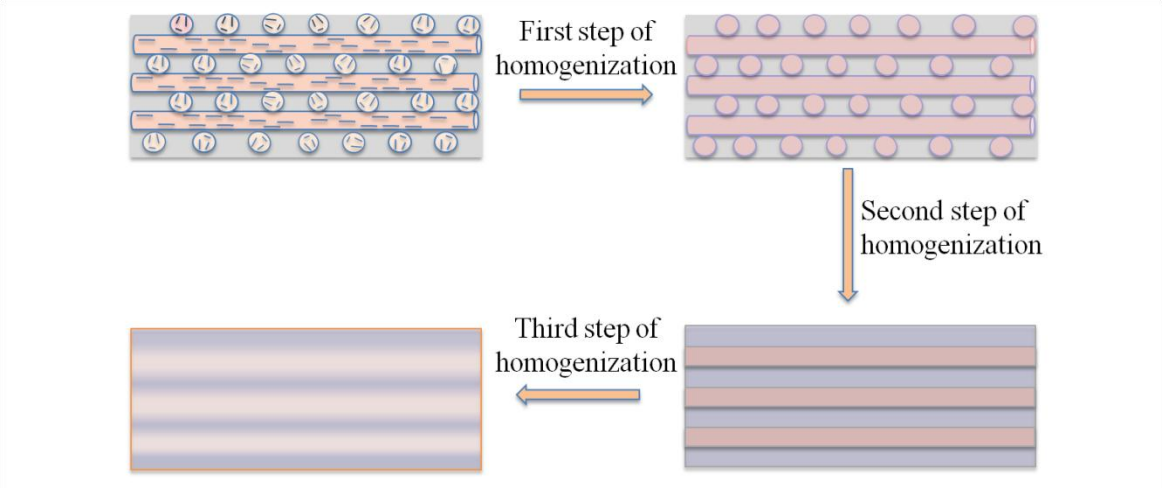

Figure 4.2 Schematic of homogenization steps

$$\tilde{\mathbf{C}}_{MT} = \mathbf{C_m} + c_i[(\mathbf{C_i} - \mathbf{C_m}) : \mathbf{T}][(1-c_i)\mathbf{I} + c_i\mathbf{T}]^{-1}, \qquad (4.5)$$

where $\mathbf{C}_m$ and $\mathbf{C}_i$ refer respectively to stiffness tensor of the matrix and the reinforcements and c_i is the reinforcements volume fraction. $\mathbf{T}$ is given by:

$$\mathbf{T} = [\mathbf{I} + \mathbf{S} : \mathbf{C_m^{-1}} : (\mathbf{C_i} - \mathbf{C_m})]^{-1}, \qquad (4.6)$$

where $\mathbf{S}$ is the fourth-order Eshelby's tensor [26] that depends on the reinforcement shape as well as the matrix properties (the detailed expressions for Eshelby tensor can be found in Appendix 4.A).

Nanotubes orientations can be characterized by Euler angles (Figure 4.3a). For the specific case that all the nanotubes have their long axis oriented along X_2, equation (4.5) leads to a transversely isotropic material whose axis of transverse isotropy is X_2. Considering that the

nanotubes are oriented arbitrarily, a weighted orientation averaging was used to obtain the effective elasticity tensor, $\langle \tilde{\mathbf{C}} \rangle$, as:

$$\langle \tilde{\mathbf{C}} \rangle = \frac{\int_0^{2\pi}\int_0^{\pi}\int_0^{\pi/2} g(\theta,\varphi,\beta)\mathbf{C}^{Tr}(\theta,\varphi,\beta)\sin\theta\, d\theta d\varphi d\beta}{\int_0^{2\pi}\int_0^{\pi}\int_0^{\pi/2} g(\theta,\varphi,\beta)\sin\theta\, d\theta d\varphi d\beta}, \qquad (4.7)$$

where $g(\theta,\varphi,\beta)$ is the Orientation Probability Density Function (OPDF) [27] and

$$\mathbf{C}^{Tr}(\theta,\varphi,\beta) = \mathbf{R}(\theta,\varphi,\beta)\cdot\tilde{\mathbf{C}}_{MT}.\mathbf{R}(\theta,\varphi,\beta)^{T}, \qquad (4.8)$$

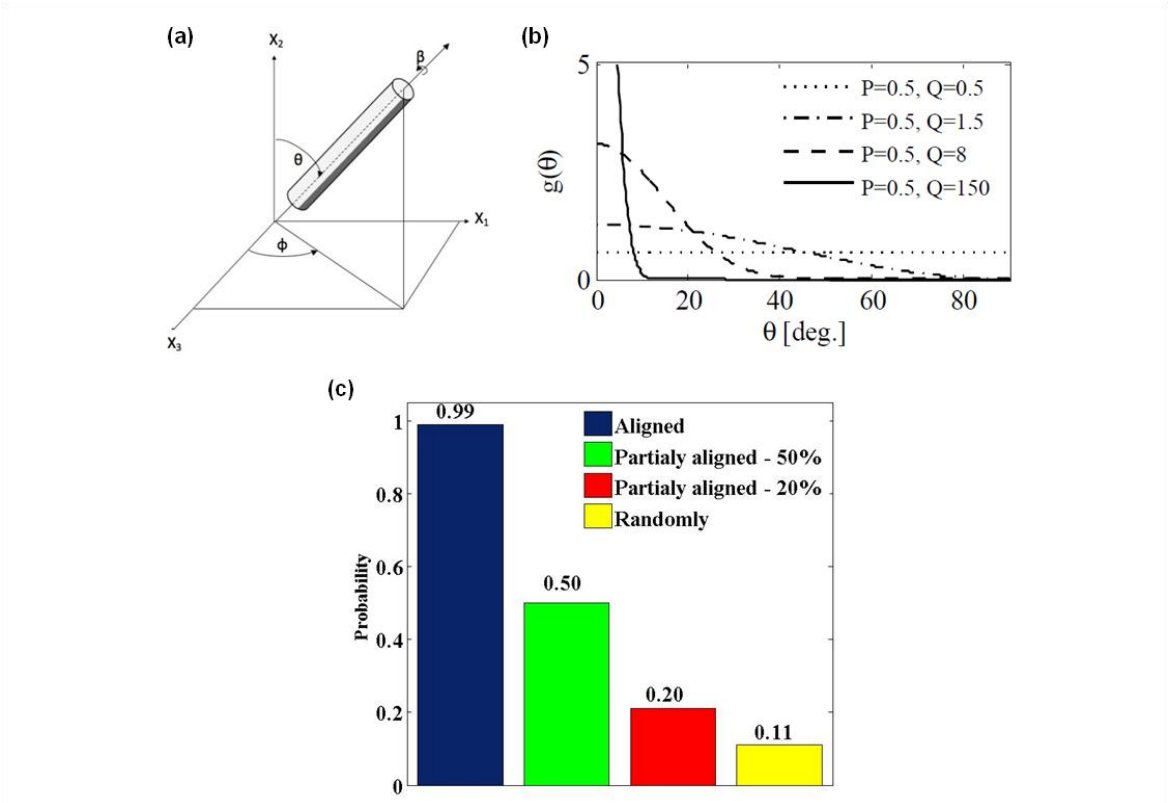

Figure 4.3 (a) Euler angles, (b) Orientation Probability Density Function (OPDF) and (c) probability of finding a CNT oriented at $\pm 10^{\circ}$ from X_2.

where $\mathbf{R}$ and $\mathbf{R}^T$ are the corresponding rotation matrix and its transpose, θ, φ and β as shown in Figure 4.3a are the Euler angles (details on $\mathbf{R}$ can be found in [27]). The ODPF can be interpreted as the probability of having a CNT oriented according to specific values of θ, φ and β. Note that $\sin(\theta)$ in equation (4.8) is due to the transformation to the spherical coordinate system. During the injection process, the shearing forces are axisymmetric with respect to the flow axis. As a result, it was assumed that the CNT orientation distribution was also axisymmetric with respect to the fiber axis, X_2. Therefore, $g(\theta,\phi,\beta)$ was simplified to $g(\theta)$ [27]. In this study, the OPDF introduced by Maekawa et al. [28]

$$g(\theta) = \frac{(\sin\theta)^{2P-1}(\cos\theta)^{2Q-1}}{\int_0^{\frac{\pi}{2}} (\sin\theta)^{2P-1}(\cos\theta)^{2Q-1} d\theta}, \qquad (4.9)$$

where P and Q are parameters accounting for the degree of reinforcement alignment, was used. Table 4.1 lists different values of P and Q and the corresponding orientations. Plots of OPDF for four different values of P and Q are illustrated in Figure 4.3b. Figure 4.3c shows the probability of finding a CNT oriented at $\pm 10^\circ$ from X_2.

Table 4.1 Values of P and Q and the corresponding orientations.

Orientation	P	Q
Random	0.5	0.5
Partially aligned (20%)	0.5	1.5
Partially aligned (50%)	0.5	8
Aligned (99%)	0.5	150

Since nanotubes tend to form bundles, the elastic properties of SWCNT bundles reported in [29] were used as the reinforcement properties in the model:

$$\mathbf{C}_{Nanotube} = \begin{bmatrix} 40.68 & 12.40 & 39.32 & 0 & 0 & 0 \\ 12.40 & 625.72 & 12.40 & 0 & 0 & 0 \\ 39.32 & 12.40 & 40.68 & 0 & 0 & 0 \\ 0 & 0 & 0 & 2.44 & 0 & 0 \\ 0 & 0 & 0 & 0 & 1.36 & 0 \\ 0 & 0 & 0 & 0 & 0 & 2.44 \end{bmatrix}. \qquad (4.10)$$

Equations (4.5) to (4.10) were used for the first homogenization step where $\mathbf{C}_i$ should be taken equal to $\mathbf{C}_{Nanotube}$. The UV-epoxy was assumed to be isotropic with a Young's modulus of 1.32 GPa and a Poisson's ratio of 0.3. Nanotube bundles were considered as high aspect ratio ellipsoids. Their aspect ratio was set to 200 with two different volume fractions (V. F.), 0.5 and 1% (equal to weight fraction since CNTs and epoxy matrix have similar densities).

For the second homogenization step, each layer was considered as a unidirectional ply (i.e. composites with completely aligned fibers). Equation (4.5) was used with $\mathbf{C}_i$ equal to $\langle \tilde{\mathbf{C}} \rangle$ obtained in the first step. The EPON 862 matrix was assumed to be isotropic with Young's modulus and Poisson's ratio of 3.1 GPa and 0.3, respectively. The aspect ratio of the fibers (the ratio of their length over their diameter) was set to 400 (i.e., long fibers).

The composite beam consists of two parts; longitudinal layers and transverse layers. The volume fraction of fibers in each layer was 34.67%, based on the number and dimension of fibers in each layers. Therefore, the beams stiffness tensor, $\mathbf{C}_{Total}$, was obtained according to the classical lamination theory as:

$$\mathbf{C}_{Total} = \frac{N_l \mathbf{C}_l + N_t \mathbf{R}_t \cdot \mathbf{C}_t \cdot \mathbf{R}_t^T}{N_l + N_t}, \qquad (4.11)$$

where *l* and *t* correspond to longitudinal and transverse directions, respectively. $\mathbf{C}_l$ and $\mathbf{C}_t$ are obtained from the second step and correspond to the $\langle \tilde{\mathbf{C}} \rangle$ of the longitudinal and transverse layers, respectively. In our case of study, $\mathbf{C}_l$ and $\mathbf{C}_t$ were equal. *N* denotes the number of longitudinal and transverse layers that are 6 and 5, respectively. $\mathbf{R}$ is the rotation matrix corresponding to the 90° rotation of the transverse layers.

4.4. Results and discussion

4.4.1. Nanotube and nanocomposite morphological characterizations

Figure 4.4 shows typical TEM micrographs of the laser-synthesized SWCNTs before and after their chemical purification. The nanotubes are observed to self-organize most often into bundles, featuring a high aspect ratio since their length can reach up to several microns and their diameter is in the nanometer range. Figure 4.4a shows the TEM image of as-produced SWCNTs. In conjunction with the SWCNTs, other carbonaceous structures and impurities such as graphite and/or metal catalyst nanoparticles (dark spots in the TEM image) are observed. The nanotube chemical purification enabled to remove residual catalyst particles and other carbonaceous impurities as observed in Figure 4.4b.

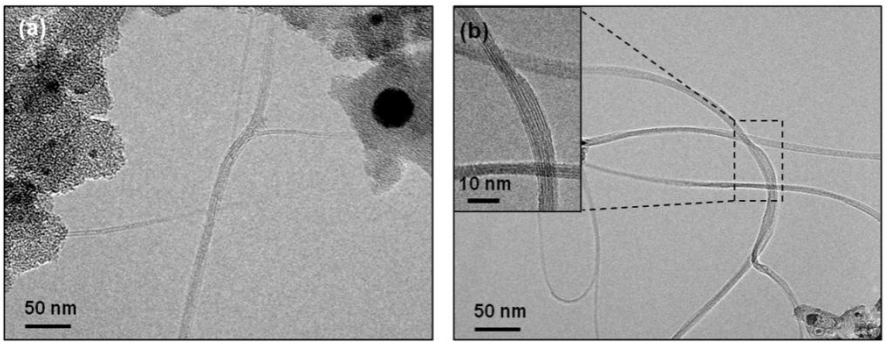

Figure 4.4 Typical TEM images of (a) the as-produced and (b) purified SWCNTs soot material

Figure 4.5a shows typical Raman spectra of the as-produced and purified SWCNTs. The spectra represents three typical peaks for the nanotubes including a narrow radial breathing mode (RBM) band centered around 185 cm^{-1}, the D-band centered around 1350 cm^{-1} and the G-band around 1600 cm^{-1}. The RBM band provides relevant information in terms of SWCNTs diameters [30]. Our SWCNTs are found to have a narrow diameter distribution centered around 1.2 nm. The G-band corresponds to the symmetric E_{2g} vibrational tangential mode in graphite-like materials and the D-band is as a signature of disorder and/or defects in these structures. The G/D intensity ratio is generally used to assess the degree of purity of the nanotubes. After subjecting the nanotubes to the purification process, their G/D peak intensity ratio is seen to decrease significantly in comparison to that of the as-produced mats. This indicates that the nitric acid oxidization based purification process inherently creates additional structural defects in the nanotubes. This is also confirmed by the XPS analysis shown in Figure 4.5b. The XPS results show that the C1s core level peak of purified SWCNTs is consisting of three clear components while that of as-produced samples exhibits only a relatively narrow C=C peak. The main peaks for both curves centered around 284.5 eV are due to the sp^2 bonding for the bulk structure of nanotubes. For the purified nanotubes, the two extra shoulders appearing clearly at ~ 286 eV and ~288 eV are attributed to C-O and/or C-NHx bonds, and to the COO group of carboxylic acid

groups [31, 32]. Based on the XPS results, the purification process has led to carboxylic groups grafting onto the SWCNTs surfaces (i.e., covalent functionalization).

Figures 4.6a and 4.6b show the SEM images of the fracture surface of the bulk pure UV-epoxy and its associated nanocomposite with the SWCNT loading of 0.5wt%, respectively. The fracture surface of the pure epoxy resin is smooth while the nanocomposite shows a layered fracture surface. The larger roughness of the fracture surface of the nanocomposite sample might be attributed to possible toughening effect induced by the presence of carbon nanotubes as reported in literature [33]. Figures 4.6c and 4.6d show higher magnification images of their fracture surface. Based on Figure 4.6d, the absence of micron-size aggregates of CNTs suggests a fairly uniform dispersion of the nanotube at least in microscale. The surface modification of CNTs interface [34] and the effective mixing procedure including ultrasonication and three-roll mill mixing [11] are believed to be responsible for achieving the fairly good dispersion of CNTs.

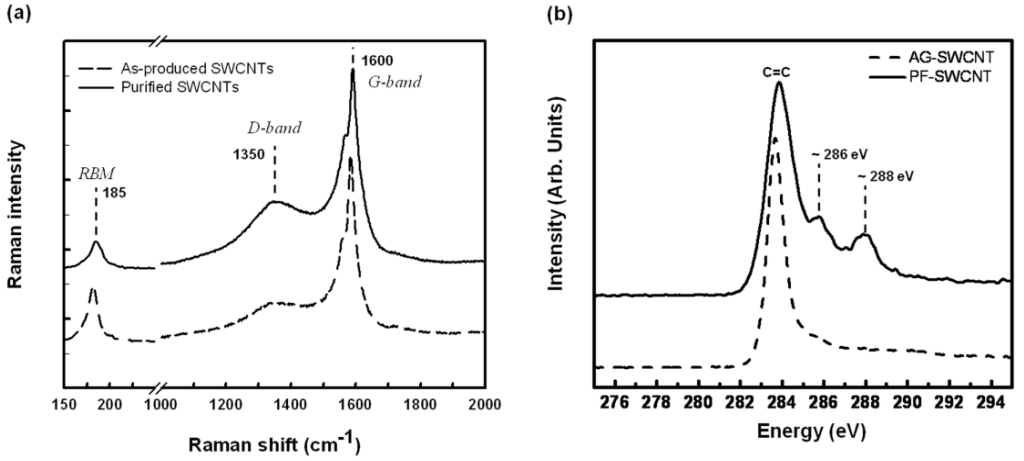

Figure 4.5 (a) Raman spectra and (b) photoelectron spectra of the nanotubes before and after their chemical purification (acidic treatment)

4.4.2. Shear rate estimation and viscosity characterization

Figure 4.7 shows the process-related apparent viscosity (η_{app}) with respect to the process-related apparent shear rates $(\dot{\gamma}_{app})$ induced by the extrusion of the pure UV-epoxy and its nanocomposites for five different extrusion pressures including the two extrusion pressures, corresponding to the low (shown as P_1) and high (shown as P_2) micro-injection pressures and also three additional middle pressures. The error bars are based on the standard deviations from the mean value obtained from the measurements. Although the estimation of shear conditions were needed only for two pressures (i.e., P_1 and P_2) corresponding to two micro-injection pressures, the viscosity-shear rate values were also obtained for the three additional pressures in order to study the rheological behavior of the materials for the pressures between P_1 and P_2. However, since the present viscometry is pressure-constant, different combinations of viscosity-shear rate were obtained for the neat epoxy and its nanocomposites for each extrusion pressure. Therefore, lower $\dot{\gamma}_{app}$ were obtained for the nanocomposites compared to the neat UV-epoxy at the same extrusion pressures due to the increase of viscosity with the addition of SWCNTs. Since the viscosity of nanocomposite is a good indicator of the quality of nanotube dispersion, the reasonable increase of the nanocomposite viscosity compared to the pure resin could support the effectiveness of nanocomposite mixing processes.

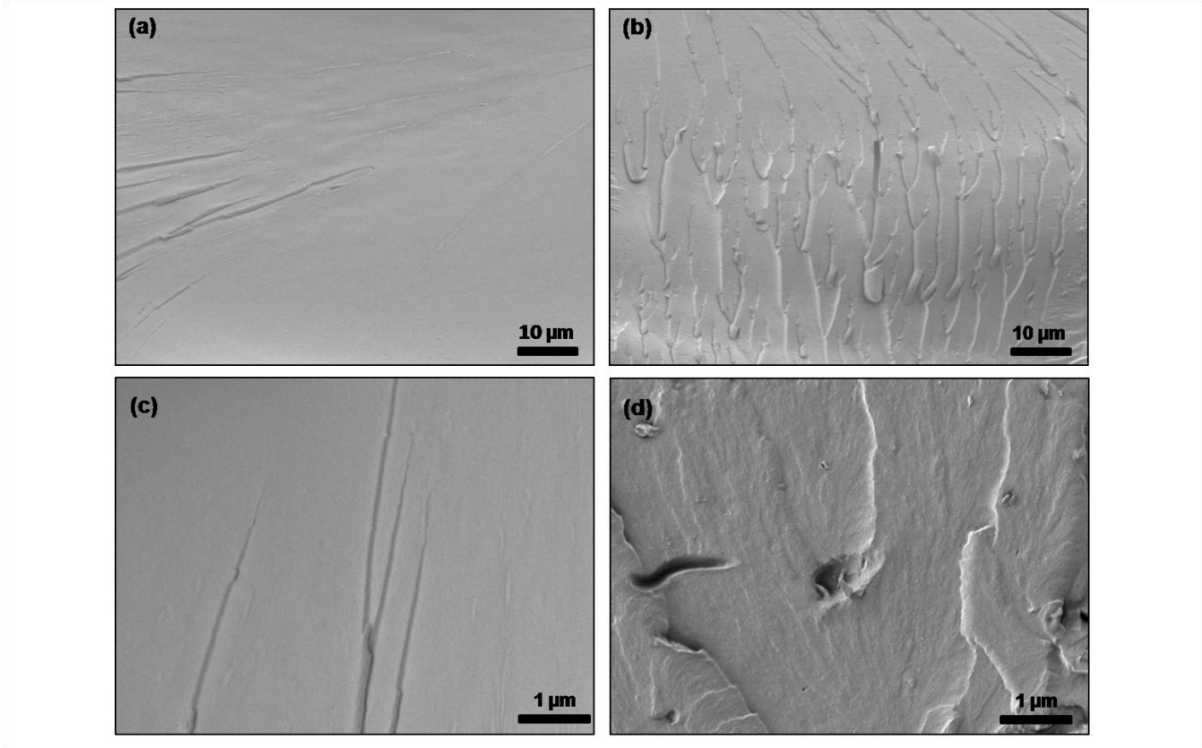

Figure 4.6 SEM images of the fracture surface of the bulk (a) UV-epoxy and (b) its nanocomposite containing 0.5wt% purified-SWCNTs after ultrasonication and three-roll mill mixing. (c) and (d) higher magnification images of (a) and (b), respectively.

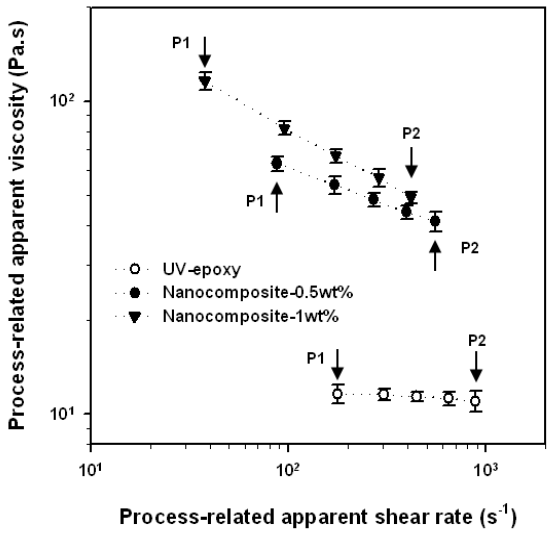

Figure 4.7 Viscosity-shear rate estimation of the pure UV-epoxy and its nanocomposites in microchannels using a method based on capillary viscometry.

Table 4.2 Estimation of the process-related apparent viscosity and the process-related apparent shear rate in microfluidic network.

Injected material	Injection pressure (MPa)	Process-related apparent shear rate (s^{-1})	Process-related apparent viscosity (Pa.s)
Pure UV-epoxy	0.7	177	11.6±1.5
	4.2	879	10.9±1.6
Nanocomposite-0.5wt%	0.7	87	61.2±3.5
	4.2	554	41.3±4.4
Nanocomposite-1wt%	0.7	38	115.8±7.6
	4.2	414	49.1±5.2

The incorporation of SWCNTs into the epoxy led to the apparition of shear-thinning behavior (i.e., negative slope, decrease of viscosity with increase of shear rate). This slight shear-thinning behavior might be attributed to high aspect ratio of nanotubes and their orientation along the flow direction at higher shear rates. Table 4.2 lists the values estimated for η_{app} and $\dot{\gamma}_{app}$ of the materials only for the two pressures (i.e., P_1 and P_2). According to the equations (5.1) and (5.2), applying higher pressure gradient will lead to higher shear rates. Depending on the viscosity of matrix and the aspect ratio (i.e., length/diameter) of the fillers, the extent of the shear forces to induce an orientation could be different [35]. In general, higher shear rates consequently causes the SWCNTs to align with the flow and frequently rotate by 180° in Jeffery orbits. The Brownian motion that may impose small disturbances can contribute to the rotational motion by increasing the frequency of Jeffery orbits [36]. Therefore, higher $\dot{\gamma}_{app}$ corresponding to the high micro-injection pressure (i.e., P_2) is expected to increase the degree of orientation of nanotubes.

4.4.3. Morphological characterization of the 3D-reinforced beams

The fracture surface of a few representative 3D-reinforced (resin- and NC-injected) beams in tensile testing was observed under SEM in order to examine the matrix-microfiber interface. Figure 4.8a shows a SEM image of typical fracture surface of a resin-injected beam prepared at 0.7 MPa and Figure 4.8b is close-up view of the surface of a microfiber. No perpendicular microfibers (i.e., microfibers in transverse layers) are seen and the fracture surface is extensively embedded with the surrounding matrix. This suggests that the cohesive failure took place in the region filled with the surrounding resin. Similar failure mechanism was observed for the fracture surface of the nanocomposite-injected beams. In addition, no debonding and no pull-out of the embedded microfibers were observed, indicating that the microfibers were strongly bonded to the surrounding matrix. This confirms that the very low shrinkage of the UV-epoxy used in this study prevented the probable shrinkage-induced detachment of the microfiber surface from the microfluidic channel walls.

Figures 4.8c and 4.8d show TEM images of the nanocomposite (0.5wt% SWCNTs) microfibers (i.e., the nanocomposite filled the microfluidic channels) along the longitudinal direction for the nanocomposite-injected beams prepared at the low and high injection pressures, respectively. Figure 4.8e and 4.8f show TEM images of the nanocomposite containing 1wt% for similar processing conditions. The arrows show the direction of flow inside the microfluidic channels along the longitudinal direction of the beams. For the beams prepared at low injection pressure (i.e., corresponding to the low shear rate), the TEM image of embedded microfiber (Figure 4.8c and 4.8e) do not indicate any preferential orientation and the nanotube aggregates are randomly oriented in the matrix. A clear change in the orientation of SWCNTs in the microfibers along the longitudinal direction is observed for the microfluidic channels filled at

high injection pressure (i.e., corresponding to the higher shear rate) (Figure 4.8d and 4.8f). The higher pressure-induced shear rate caused the nanotube aggregates to be aligned in the longitudinal channels along the direction of flow. Considering the fact that the nanotubes typically tend to exist as entangled agglomerates when mixed into a polymer matrix, some nanotubes remained randomly oriented in their aggregates. However, most of nanotube aggregates were well stretched along their lengths. Although the degree of orientation increased with the increase of shear rate by applying higher micro-injection pressure, it is still far from a perfect alignment. Comparing the TEM images for two different injection pressures suggests that higher shear rate not only contributes to the CNTs alignment but also enables their further dispersion within the matrix. Note that no preferential orientation of SWCNTs aggregates was observed in the microfluidic channels along the width direction of 3D-reinforced beams for both micro-injection cases.

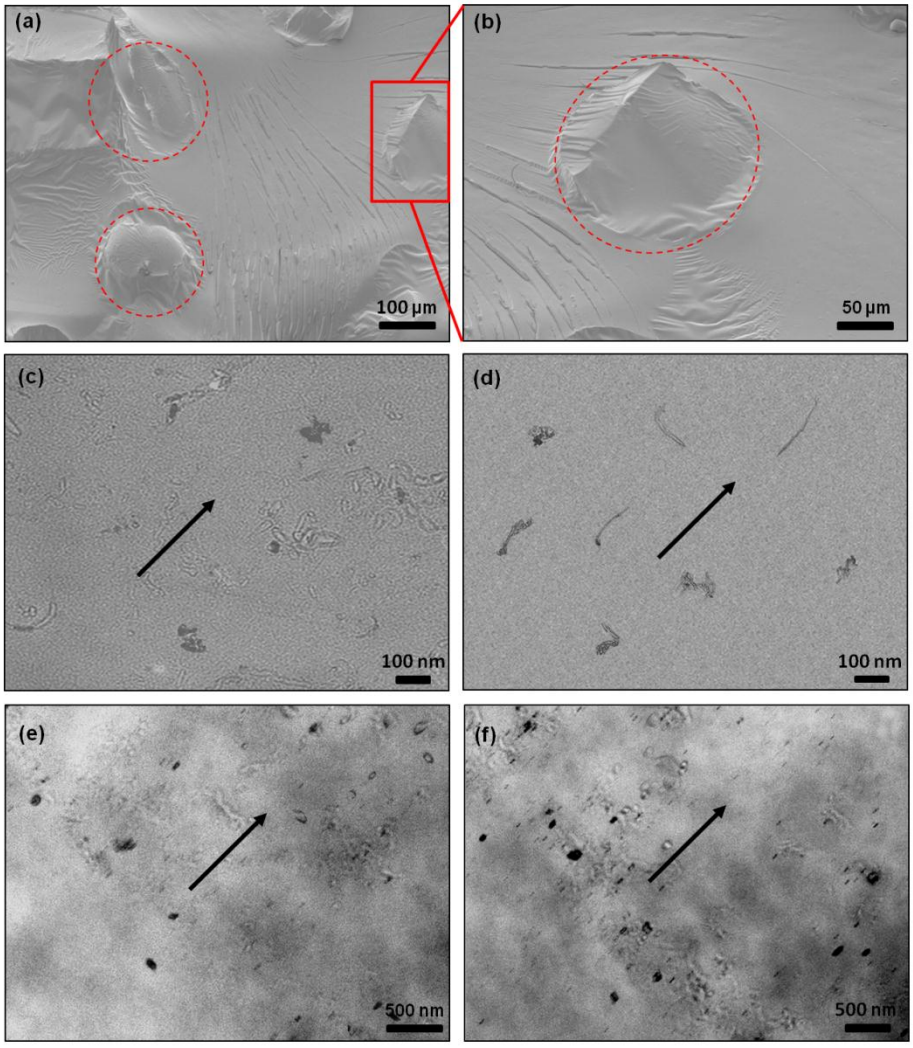

Figure 4.8 SEM images of typical fracture surface of (a) a representative injected beam filled at 0.7 MPa and (b) a close-up view of an embedded microfiber. The pointed-dashed circles highlight the microfibers; and TEM images of SWCNT orientation state inside the microfiber along the longitudinal direction for the nanocomposite (0.5wt%)-injected beams filled at (c) low injection pressure and (d) high injection pressure and for the nanocomposite (1wt%)-injected filled at (e) low injection pressure and (f) high injection pressure (The arrows show the direction of flow in longitudinal direction of the beam).

4.4.4. Mechanical properties

The influence of CNTs and their orientation on mechanical properties of the 3D-reinforced beams is studied under tensile loadings. Figure 4.9 shows stress-strain curves of the pure resin- and nanocomposite-injected beams for the low and the high injection pressures. The error bars were calculated from the 95% confidence intervals on the mean value obtained from the

measurements. The stress-strain curves of the resin-and NC-injected beams show a linear behavior followed by a short plastic response of the stress under strain before rupture. This is a typical behavior of brittle polymers like epoxies. The failure behavior of the 3D-reinforced beams were slightly influenced with the addition of the SWCNTs due to their small loadings, estimated to be ~0.18wt% (0.5wt% in nanocomposite microfibers) and ~0.35wt% (1wt% in nanocomposite microfibers) in the overall beam volume. Table 4.3 summarizes the mechanical properties of the 3D-reinforced beams, the bulk epoxies and their deviations. The Young's modulus and the tensile strength of the resin-injected beams were measured to be 2.34 GPa and 64.7 MPa, respectively. For the NC-injected beams containing 0.18wt% of nanotubes, prepared at low injection pressure, the average Young's modulus increased to 2.51 GPa, about a 7% enhancement. Their failure strengths increased by 6% to a value of 68.6 MPa. The incorporation of 0.35wt% SWCNTs further increased the Young's modulus (by 14%) and the tensile strength (by 13%) of the 3D-reinforced beams. A fairly good dispersion of SWCNTs within the UV-epoxy matrix and also a proper stress transfer between the host polymer matrix (the UV-epoxy) and the carbon nanotubes are believed to be responsible for the reasonable increase in the mechanical properties (stiffness and strength) of the NC-injected beams. The interfacial bonding between SWCNTs and epoxy molecules through the functional groups are thought to facilitate load transfer. Figure 4.10 represents two proposed interaction mechanisms in this study. Covalent grafting of carboxylic groups at the nanotube surfaces offers interaction possibility with the epoxy groups [37]. Non-covalent functionalization of SWCNTs using ZnPP affords the opportunity for additional interaction with epoxy matrix [10]. The ZnPP molecules can interact with the nanotube walls through π-π interactions. The carboxylic groups provided by both

covalent and non-covalent functionalizations of the SWCNTs are capable to interact with epoxy groups, potentially leading to an enhanced stress transfer.

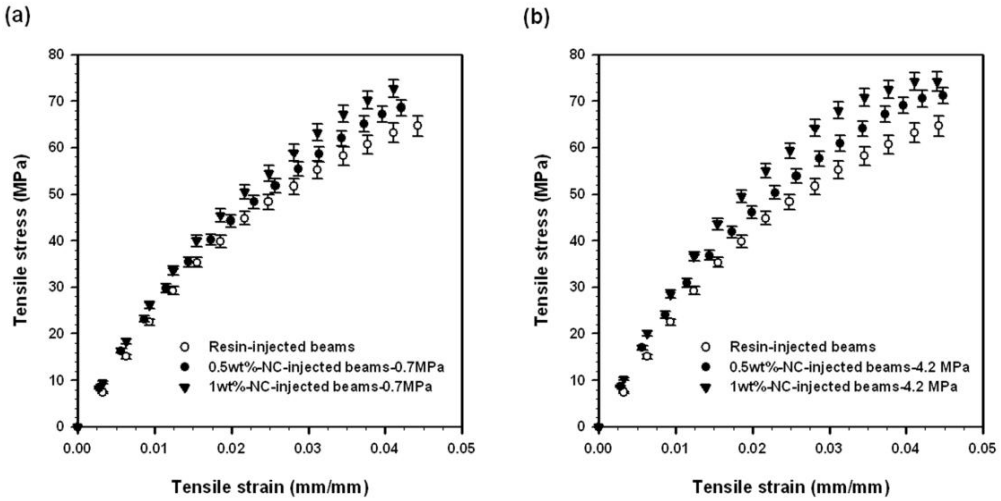

Figure 4.9 Tensile properties of the 3D-reinforced beams: Averaged stress-strain curves of the resin- and NC-injected beams filled (a) at 0.7 MPa and (b) 4.2 MPa micro-injection pressure.

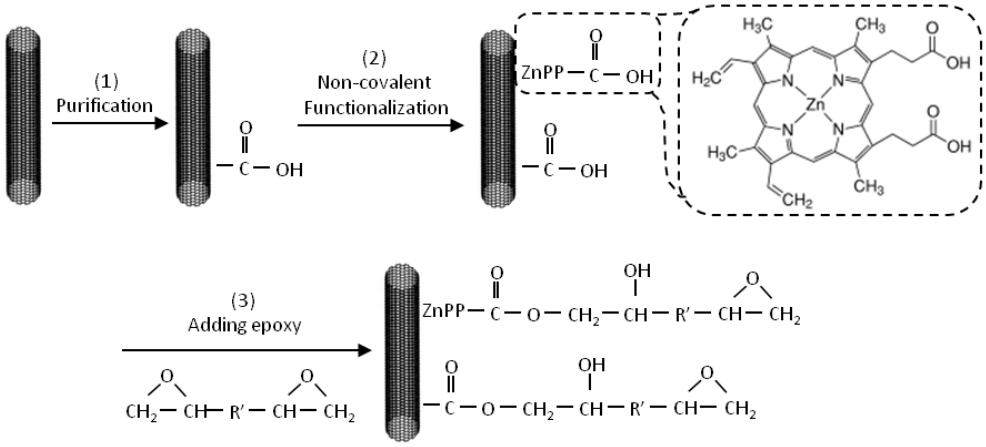

Figure 4.10 Schematic of proposed interaction mechanisms between SWCNTs and epoxy matrix through both carboxylic group grafting [31] and non-covalent functionalization of SWCNTs [9].

The higher micro-injection pressure led to further improvement in mechanical properties of the 3D-reinforced beams for the same nanotube loadings. The average Young's modulus increased by 13% for 3D-reinforced beams containing 0.18wt% nanotubes and 25% for the

beams with 0.35wt% nanotubes compared to the resin-injected beams. For both nanotube loadings, the average improvements of the Young's modulus of the beams, prepared at the high injection pressure, were doubled when compared to the beams prepared at the low injection pressure. These considerable improvements (above average compared to those reported in literature as listed in Table 4.4) in mechanical properties could be attributed to shear-induced orientation of the SWCNTs, caused by higher injection pressure, in the small diameter microfluidic channels (dimensional constraining effect) along the longitudinal direction (i.e., in the direction of material injection). Another contribution may come from probable better dispersion caused by breakage of aggregates at higher shear rate [10]. Given the amount of SWCNTs added, the considerable improvement in Young's modulus of the beams compared to those reported in literature (Table 4.4) indicates the effectiveness of the present manufacturing method to take the advantage of nanotube orientation in microfluidic network.

Table 4.3 Mechanical properties of the resin-injected and the nanocomposite-injected beams prepared by micro-injection of the materials at two different shear rates and bulk epoxies.

Type of beams	Young's Modulus (GPa)	Young's Modulus Var. (%)	Tensile Strength (MPa)	Tensile Strength Var. (%)	Elongation at break (%)	Elongation at break Var. (%)
Bulk UV-epoxy	1.32±0.02	---	50.4±1.1	---	14.6±0.4	---
Bulk-EPON862	3.10±0.05	---	79.8±1.6	---	3.2±0.1	---
Resin-injected	2.34±0.03	0	64.7±0.7	0	4.4±0.1	0
0.5wt%-NC-injected-0.7 MPa	2.51±0.05	+7	68.6±1.4	+6	4.2±0.2	-4
1wt%-NC-injected-0.7 MPa	2.67±0.03	+14	72.7±2.1	+13	4.1±0.1	-7
0.5wt%-NC-injected-4.2 MPa	2.65±0.04	+13	71.1±1.4	+10	4.5±0.1	+2
1wt%-NC-injected-4.2 MPa	2.93±0.07	+25	74.3±1.8	+15	4.4±0.1	0

4.4.5. Stiffness prediction with homogenization model

Table 4.5 lists the computed Young's modulus of the resin- and nanocomposite-based microfibers for aligned, partially aligned and randomly oriented cases. The predictions of the Young's modulus of the UV-epoxy microfibers increased about 70% by the addition of 1wt% randomly oriented CNTs while this value for the aligned CNTs showed an increase of 405% in comparison with UV-epoxy fibers. Table 4.6 lists the final analytical predictions of the resin- and NC-injected beams for the different cases studied. The NC-injected beams with the CNTs alignment along the longitudinal direction and random orientation in transverse direction showed the highest value of the Young's modulus. Although the stiffness of a layer in longitudinal direction increases with the nanotube alignment in the channels, this factor decreases the longitudinal stiffness in transverse layers. In the resin-injected beams, there are only small differences between the analytical and experimental results (4%). This confirms that the microfibers are strongly bonded to the surrounding matrix, as observed by SEM. Assuming that there is the same initial difference between the analytical and experimental estimations for the NC-injected beams as for the resin-injected beams, along with the TEM observations, the 50% aligned CNTs in the longitudinal and randomly oriented in the transverse layers appears to be the most appropriate assumption for the structural state of CNTs in NC-injected beams prepared at high injection pressure. On the other hand, applying the same logic to keep the initial difference between the analytical and experimental estimations for the NC-injected beams and the resin injected beams under low pressure supports TEM observations: low pressure of injection results in randomly oriented CNTs in both longitudinal and transverse layers.

Table 4.4 Comparison of increase of storage modulus at 25°C by adding SWCNTs to epoxy matrices achieved in our work with those reported in literature.

Researcher		SWCNTs wt.%	Increase of property (%)	Normalized (Increase of property/wt.%) (%)
Barrera et al. [7]		1.0	31	31
Sun et al. [12]		1.0	26	26
Wang et al. [8]		0.5	30	60
Our results	0.5wt% – 0.7 MPa	0.18 (whole beam)	7	39
	1wt% – 0.7 MPa	0.33 (whole beam)	14	42
	0.5wt% – 4.2 MPa	0.18 (whole beam)	13	72
	1wt% – 4.2 MPa	0.33 (whole beam)	25	75

The reasonable consistency of the analytical estimations to those obtained from the tensile experiments indicates that the CNTs reinforcement is not far from achieving their theoretical potential. The differences might be attributed to the following phenomena: 1. The probable presence of impurities produced along with CNTs like amorphous carbon which was not considered in modeling, may affect the mechanical properties. 2. The curvature of the flexible CNTs bundles may reduce their effective aspect ratio as observed by TEM images [38]. In addition, the slippage of the inner nanotubes in bundles may also decrease the effectiveness of nanoreinforcements. 3. A homogeneous orientation state is assumed in whole cross-section area of the microfluidic channels. However, the shear rate maximum at the channel wall gradually reduces towards the channel center at which the shear rate becomes zero. In other words, the carbon nanotubes near the microfluidic channel center were subjected to very low shear rates and consequently might be randomly oriented. This effect could be reduced through the injection of even smaller microchannels. 4. The Mori-Tanaka model has an intrinsic precision but, for the volume fraction considered, it should be quite precise.

Table 4.5 Analytical Young's modulus of the resin- and NC-based microfibers with aligned, partially aligned and randomly oriented CNTs.

Type of microfiber	Young's modulus (GPa)		Young's modulus Var.(%)	
Non-reinforced	1.32		0	
	V.F. 0.5%	**V.F. 1%**	**V.F. 0.5%**	**V.F. 1%**
Random oriented CNTs	1.78	2.24	35%	70%
Partially aligned CNTs (20%)	2.25	3.26	79%	147%
Partially aligned CNTs (50%)	3.35	5.36	153%	306%
Aligned CNTs	4	6.67	203%	405%

Table 4.6 Analytical and experimental Young's modulus of the resin- and NC-injected beams with aligned, partially aligned and randomly oriented CNTs.

CNTs orientation state in		Longitudinal Young's modulus (GPa)					
		Experimental Injection pressure				Analytical	
Longitudinal Fibers	Transverse Fibers	0.7 MPa		4.2 MPa		V.F. 0.5%	V.F. 1%
		V.F. 0.5%	V.F. 1%	V.F. 0.5%	V.F. 1%		
Resin-injected beams		2.34±0.03				2.4	
Aligned	Aligned					2.97	3.54
Partially Aligned	Partially Aligned					2.62	2.89
Random	Random	**2.51±0.05**	**2.67±0.03**			**2.59**	**2.78**
Aligned	Random					3.01	3.62
Aligned	Partially Aligned					2.95	3.5
Partially Aligned (20%)	Random					2.69	2.96
Partially Aligned (50%)	Random			**2.65±0.04**	**2.93±0.07**	**2.89**	**3.37**

4.5. Conclusion

Three-dimensional microstructured beams reinforced with SWCNT/epoxy nanocomposite with spatial localization and orientation of the nanotubes were fabricated via the nanocomposite

micro-injection of a microfluidic network. The nanotube orientation was performed by taking the advantages of shear flow and dimensional constraining of small-diameter channels. The SEM observations revealed a fair dispersion of SWCNTs aggregates in UV-epoxy matrix after the ultrasonication and three-roll mill mixing. The morphological analysis using TEM showed a random orientation of SWCNT aggregates at the lower shear rate, caused by the lower injection pressure, while the nanotubes were partially aligned along the direction of flow at higher shear rate, caused by the higher injection pressure. For the beams reinforced with the partially aligned nanotube aggregates, the improvement of Young's modulus was doubled compared to the beams with randomly oriented nanotubes. The stiffness values of the beams predicted by the micromechanical model for the case of partial orientation of nanotubes were close to the experimental data, indicating the efficiency of the present manufacturing method in orientation and localization of CNTs within a polymer matrix. To further align the nanotubes, higher injection pressures (i.e., higher shear rate) and smaller-diameter microfluidic channels (i.e., higher constraining effect) could be employed. The flexibility of this manufacturing method enables the design of functional 3D-reinforced nanocomposite macroscopic products for a wide variety of applications such as structural composite applications and components for micro electromechanical systems. It is worth noting that the nanomaterials incorporated inside the 3D microfluidic network can be used to enhance the structure properties other than mechanical such as electrical or thermal conductivity.

4. Acknowledgments

The authors acknowledge the financial support from FQRNT (Le Fonds Québécois de la Recherche sur la Nature et les Technologies). Prof. El Khakani also acknowledges the finanial

support from NSERC (National Science Engineering Research Council of Canada) and Plasma-Québec (le Réseau Stratégique du FQRNT sur la Science et Technologies des Plasmas). The authors would like to thank the technical support of Mr. Charles Tremblay for the beam grinding, Dr. Hesameddin Tabatabayi for the tensile testing and Mr. Nima Nateghi for the TEM characterization.

4. Appendix 4.A

"The components of Eshelby tensor for a fibrous reinforcement are [27]:

$$S_{2222} = \frac{1}{2(1-\nu_m)}(1-2\nu_m + \frac{3a^2-1}{a^2-1} - (1-2\nu_m + \frac{3a^2}{a^2-1})g),$$

$$S_{1111} = S_{3333} = \frac{3}{8(1-\nu_m)}\frac{a^2}{a^2-1} + \frac{1}{4(1-\nu_m)}(1-2\nu_m - \frac{9}{4(a^2-1)})g,$$

$$S_{1133} = S_{3311} = \frac{1}{4(1-\nu_m)}\frac{a^2}{2(a^2-1)} - (1-2\nu_m + \frac{3}{4(a^2-1)})g,$$

$$S_{1122} = S_{3322} = -\frac{1}{2(1-\nu_m)}\frac{a^2}{a^2-1} + \frac{1}{4(1-\nu_m)}(\frac{3a^2}{(a^2-1)} - (1-2\nu_m))g,$$

$$S_{2211} = S_{2233} = -\frac{1}{2(1-\nu_m)}(1-2\nu_m + \frac{1}{a^2-1}) + \frac{1}{2(1-\nu_m)}(\frac{3}{2(a^2-1)} + 1 - 2\nu_m)g,$$

$$S_{3131} = \frac{1}{4(1-\nu_m)}(\frac{a^2}{2(a^2-1)}) + (\frac{3}{4(a^2-1)} + 1 - 2\nu_m)g,$$

$$S_{1212} = S_{3232} = \frac{1}{4(1-\nu_m)}(1-2\nu_m - \frac{a^2+1}{2(a^2-1)}) - \frac{1}{2}(\frac{3(a^2+1)}{4(a^2-1)} + 1 - 2\nu_m)g,$$

where a is the aspect ratio of the reinforcement defined as the ratio of its length to its diameter and g for fiber reinforcement is given by:

$$g = \frac{a}{(a^2-1)^{3/2}}\left[a(a^2-1)^{1/2} - \cosh^{-1} a\right]$$

Then, the Eshelby tensor, **S**, has the following matrix form:

$$\mathbf{S} = \begin{bmatrix} S_{1111} & S_{1122} & S_{1133} & 0 & 0 & 0 \\ S_{2211} & S_{2222} & S_{22333} & 0 & 0 & 0 \\ S_{3311} & S_{3322} & S_{3333} & 0 & 0 & 0 \\ 0 & 0 & 0 & 2S_{3232} & 0 & 0 \\ 0 & 0 & 0 & 0 & 2S_{3131} & 0 \\ 0 & 0 & 0 & 0 & 0 & 2S_{1212} \end{bmatrix},,$$

4. References

1. Ear Y and Silverman E. MRS Bulletin 2007;32(4):328-334.
2. Mirfakhrai T, Krishna-Prasad R, Nojeh A, and Madden JDW. Nanotechnology 2008;19(31) :315706, 1-8.
3. Sahoo NG, Jung YC, Yoo HJ, and Cho JW. Composites Science and Technology 2007;67(9):1920-1929.
4. Varadan VK, Varadan VV, and Motojima S. Three-dimensional polymeric and ceramic MEMS and their applications. Smart Structures and Materials 1996: Smart Electronics and MEMS. San Diego, CA, 1996.
5. Varadan VK, Xie, J., Ji, T. BioMEMS and Smart Nanostructures, Proceeding of SPIE 2001;4590:131-141.
6. Coleman JN, Khan U, and Gun'ko YK. Advanced Materials 2006;18(6):689-706.
7. Barrera EV, Zhu J, Peng HQ, Rodriguez-Macias F, Margrave JL, Khabashesku VN, Imam AM, and Lozano K. Advanced Functional Materials 2004;14(7):643-648.

8. Wang S, Liang R, Wang B, and Zhang C. Nanotechnology 2008;19(8):085710, 1-7.

9. Wang SR, Liang ZY, Liu T, Wang B, and Zhang C. Nanotechnology 2006;17(6):1551-1557.

10. Lebel LL, Aissa B, El Khakani MA, and Therriault D. Composites Science and Technology 2010;70(3):518-524.

11. Nakashima N and Fujigaya T. Chemistry Letters 2007;36(6):692-697.

12. Sun L, Warren GL, O'Reilly JY, Everett WN, Lee SM, Davis D, Lagoudas D, and Sue HJ. Carbon 2008;46(2):320-328.

13. Zhu J, Kim JD, Peng HQ, Margrave JL, Khabashesku VN, and Barrera EV. Nano Letters 2003;3(8):1107-1113.

14. Fan ZH and Advani SG. Polymer 2005;46(14):5232-5240.

15. Abbasi S, Carreau PJ, and Derdouri A. Polymer 2010;51(4):922-935.

16. Kimura T, Ago H, Tobita M, Ohshima S, Kyotani M, and Yumura M. Advanced Materials 2002;14(19):1380-1383.

17. Chronakis IS. Journal of Materials Processing Technology 2005;167(2-3):283-293.

18. Zhou W, Vavro J, Guthy C, Winey KI, Fischer JE, Ericson LM, Ramesh S, Saini R, Davis VA, Kittrell C, Pasquali M, Hauge RH, and Smalley RE. Journal of Applied Physics 2004;95(2):649-655.

19. Sandler JKW, Pegel S, Cadek M, Gojny F, van Es M, Lohmar J, Blau WJ, Schulte K, Windle AH, and Shaffer MSP. Polymer 2004;45(6):2001-2015.

20. Lebel LL, Aissa B, Paez OA, El Khakani MA, and Therriault D. Journal of Micromechanics and Microengineering 2009;19(12):125009, 1-7.

21. Braidy N, El Khakani MA, and Botton GA. Chemical Physics Letters 2002;354(1-2):88-92.

22. Therriault D, Shepherd RF, White SR, and Lewis JA. Advanced Materials 2005;17(4):395-399.

23. Therriault D, White SR, and Lewis JA. Nature Materials 2003;2(4):265-271.

24. Bruneaux J, Therriault D, and Heuzey MC. Journal of Micromechanics and Microengineering 2008;18(11):115020,1-11.

25. Mori T, Tanaka K. Acta metallurgica 1973;21:571-574.

26. Eshelby JD. Proceedings of the Royal Society of London A 1957;241(1226):376-396.

27. Schjodt-Thomsen J and Pyrz R. Mechanics of Materials 2001;33(10):531-544.

28. Maekawa Z, Hamada H, and Yokoyama A. Composite Structures 5 1989:701-714.

29. Wang LF and Zheng QS. Applied Physics Letters 2007;90(15):153113, 1-3.

30. Bandow S, Asaka S, Saito Y, Rao AM, Grigorian L, Richter E, and Eklund PC. Physical Review Letters 1998;80(17):3779-3782.

31. Baker SE, Cai W, Lasseter TL, Weidkamp KP, and Hamers RJ. Nano Letters 2002;2(12):1413-1417.

32. Okpalugo TIT, Papakonstantinou P, Murphy H, McLaughlin J, and Brown NMD. Carbon 2005;43(1):153-161.

33. Gojny FH, Wichmann MHG, Fiedler B, and Schulte K. Composites Science and Technology 2005;65(15-16):2300-2313.

34. Thostenson ET and Chou TW. Carbon 2006;44(14):3022-3029.

35. Hobbie EK, Wang H, Kim H, Lin-Gibson S, and Grulke EA. Physics of Fluids 2003;15(5):1196-1202.

36. Hogberg SM and Lundstrom TS. Plastics Rubber and Composites 2011;40(2):70-79.

37. Moniruzzaman M, Du FM, Romero N, and Winey KI. Polymer 2006;47(1):293-298.

38. Li XD, Gao HS, Scrivens WA, Fei DL, Xu XY, Sutton MA, Reynolds AP, and Myrick ML. Journal of Nanoscience and Nanotechnology 2007;7(7):2309-2317.

CHAPTER 5: Article 3: Biotin-streptavidin interactions in functionalized carbon nanotube-epoxy composites[3]

Rouhollah Dermanaki Farahani[a], Hamid Dalir[a], Vincent Le Borgne[b], Loick. A. Gautier[b], My Ali El Khakani[b], Martin Lévesque[a], and Daniel Therriault[a]*

[a]Laboratory of Multiscale Mechanics, Center for applied research on polymers (CREPEC), École Polytechnique de Montreal, C.P. 6079, succ. Centre-Ville, Montreal (QC), H3C 3A7 (Canada)

[b]Institut National de la Recherche Scientifique, INRS-Énergie, Matériaux et Télécommunications, 1650 Blvd. Lionel-Boulet, Varennes (QC), J3X 1S2 (Canada)

* Corresponding author:

Phone: 1-514-340-4711 x4419

Fax: 1-514-340-4176

E-mail: daniel.therriault@polymtl.ca

Keywords: Carbon nanotubes, surface modification, micro electromechanical systems, UV-assisted direct-write assembly

Abstract

We report on the preparation of nanocomposites consisting of biofunctionalized single-walled carbon nanotubes (BF-SWCNTs) reinforcing an ultraviolet curable epoxy polymer by means of biotin-streptavidin interactions. The as-produced laser ablation SWCNTs are

[3] This article was submitted to the journal of Macromolecular Bioscience

biofunctionalized via acid oxidization based purification process and non-covalent functionalization using surfactant, followed by grafting the resulting nanotubes with biomolecules. The biotin-grafted nanotubes are capable of interacting with epoxy groups in presence of streptavidin molecules by which chemical bridges between BF-SWCNTs and epoxy matrix are formed. The biomolecules grafted to the nanotubes surface not only facilitate the load transfer, but also improve the nanotube dispersion into the epoxy matrix, as observed by optical imaging and scanning electron microscopy. Mechanical characterization on the nanocomposite microfibers demonstrates considerable enhancement in both strength (by 76%) and modulus (by 93%) with the addition of only 1 wt.% of BF-SWCNTs. The electrical measurements reveal a clear change in electrical conductivity of nanocomposite microfibers reinforced with 1 wt.% of BF-SWCNTs in comparison to the microfibers containing solely purified carbon nanotubes. These multifunctional nanocomposite materials could be used to fabricate macro and microstructures for a wide variety of applications such as high strength polymer nanocomposite and potential easy-manipulating biosensors.

5.1. Introduction

Nanomaterials, such as single-walled carbon nanotubes (SWCNTs), are increasingly used to achieve multifunctional capabilities where they serve as an effective structural reinforcement, as well as large-surface platform for sensing purposes [1,2]. Owing to their high mechanical [3] and electrical [4] properties, SWCNTs show a strong potential for reinforcing polymers for a wide variety of applications such as high-performance structural composites [5,6], electromechanical actuators and sensors [7], non-destructive life prediction technology and shape memory polymers [8]. When compared to other polymer nanocomposites, nanotube-reinforced epoxy systems

could exhibit high strength and multifunctional features for aircrafts and electronic products [6,9]. However, several fundamental challenges still have to be addressed in order to take full advantage of the excellent properties of the nanotubes. In particular, the ability to manipulate these entangled structures with their structurally smooth surface is required for their effective use in the development of nanodevices based on an individual nanotube or bulk nanotubes [10,11], as well as nanotube-reinforced nanocomposites [12-16].

The chemical treatment of carbon nanotubes surface significantly extends their potential for various applications. The surface functionalization of carbon nanotubes not only leads to their debundling, but also enables the design of an efficient interface to bond them to other active groups, like epoxy groups in nanocomposite materials. In particular, the purification induced covalent grafting of carboxylic groups at the surface of the nanotubes [17] as well as their non-covalent functionalization using surfactants like porphyrins [18] can be used to improve the reinforcing effect when compared to as-produced nanotubes. However, nanotube reinforcement is still far from achieving its theoretical potential and new advances are needed for an efficient load transfer.

Functionalized nanotubes have been used for the immobilization of various biomolecules for biosensor applications [10]. Biomolecules bonded to functionalized nanotubes through functional groups are capable of interacting with other active biomolecules via reversible chemical bonding. Among these biomolecules, biotin-streptavidin bonding is known as one of the strongest interactions in nature. Therefore, biotin-functionalized nanotubes could be used as a support to immobilize streptavidin molecules in biosensor applications. However, until now, most of the researches undertaken on using nanotubes in microelectronics have been limited to the use of an individual nanotube or bulk nanotubes. Due to the size order of an individual

nanotube or their bulk physical state (i.e., powder of entangled structures), manufacturing and manipulation of these materials is quite challenging [10,11]. To address these difficulties, nanotubes have been added to a solution or a polymer matrix, suitable for use in electrospinning [19] and direct-write techniques [20]. Since fibers fabricated by electrospining need additional patterning processes, the ultraviolet (UV)-assisted direct-write assembly [21] could be an alternative to manufacture complex microstructures with desired patterns when an UV-curable epoxy resin is used as a matrix.

Here, we report on the use of biotin-streptavidin interactions for further development of a multifunctional nanotube/epoxy composite system. This nanocomposite material was used for the fabrication of nanocomposite microfibers as an example of patterned microstructures for potential micro electromechanical systems (MEMS). Figure 5.1 shows the schematic of the fabrication process of nanocomposite microfibers suspended between two rectangular pads of nanocomposite by means of UV-assisted direct-write technique. To fabricate the nanocomposites, the SWCNTs were biofunctionalized via acidic treatment and non-covalent functionalization using surfactant, followed by grafting of biomolecules to chemically bridge SWCNTs and epoxy matrix. The different steps of nanotubes functionalization were assessed using various structural characterization techniques. Finally, the effects of SWCNTs biofunctionalization and their dispersion on mechanical and electrical properties of the fabricated epoxy nanocomposite microfibers were studied to understand the nanocomposite structure-property relationship.

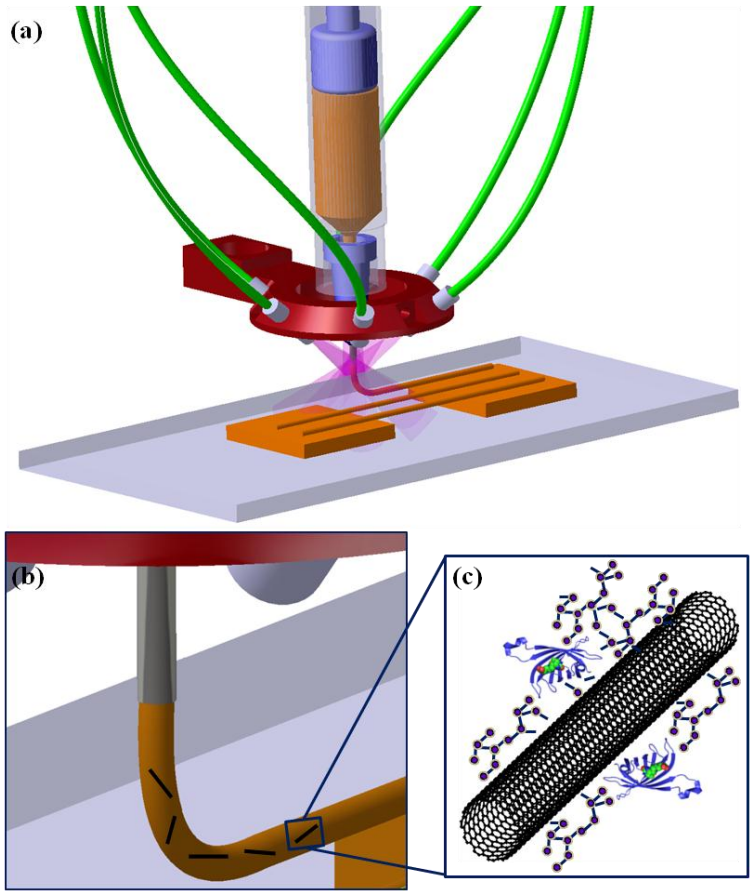

Figure 5.1 Schematic representation of the UV-assisted direct-writing of nanocomposite microfibers: (a) nanocomposite extrusion through a capillary micronozzle by an applied pressure; fibers are partially cured shortly after extrusion under UV illumination, (b) close-up view of the microfibers, and (c) interfacial bonding between SWCNTs and epoxy matrix through biotin-streptavidin interactions.

5.2. Experimental details

5.2.1. SWCNTs synthesis, purification and biofunctionalization

Single-walled carbon nanotubes were synthesized by using UV-laser ablation (248 nm, 20 ns, 400 mJ) of a Co/Ni-doped (1.2 at. %) graphite target pellet. The KrF-laser ablation was performed under a controlled argon atmosphere at a temperature of 1150°C through a 45° quartz window (more experimental details on the KrF-laser synthesis and effects of key growth parameters can be found elsewhere [22,23]). The as-produced SWCNTs condensed on a water-cooled collector, located outside of the hot zone of the furnace, onto which they formed a thick

rubbery-like film. This SWCNTs mat was peeled off and subjected to subsequent chemical purification treatment. The chemical purification treatment consisted of three main successive steps, each of which is targeted a specific purification. First, the Soxhlet extraction in toluene (for 1h) was conducted on the as-produced SWCNTs to remove residual fullerenes and some disordered carbon nanostructures in the deposit. Second, the SWCNTs were treated by hydrogen peroxide (10%) at room temperature (for 24 h) in order to crack the graphitic shells surrounding the residual catalyst nanoparticles. Finally, HNO3 (3M) oxidation was conducted to remove metal catalyst particles and covalently functionalize the SWCNTs by the attachment of carboxylic groups at their surface. These chemically P-SWCNTs were collected by vacuum filtration on alumina filters (pore size 20 nm) and after successive rinsing cycles.

The desired amounts of P-SWCNTs and 1,3-diaminopropane 99% (D23602, Sigma-Aldrich), with a proportion of 1g P-SWCNTs/5 mL 1,3-diaminopropane 99%, were added to a solution of 0.1 mM of zinc protoporphyrin IX (ZnPP, Sigma-Aldrich) in methanol. The suspension was sonicated in an ultrasonic bath (Ultrasonic cleaner 8891, Cole-Parmer) for 1 h. After ultrasonication, the mixture was shaken using a mixer/shaker (Spex CertiPrep 8000M Mixer/Mill) for 12 h at room temperature. The Soxhlet extraction for 2 h with methanol was performed on the aminated P-SWCNTs to remove any unreacted amine. The aminated P-SWCNTs were then added into a solution of 30 mL methanol containing desired amounts of biotin and N,N’-diisopropylcarbodiimide 99% (DIC, D125407, Sigma-Aldrich) with a proportion of 1g biotin/5 mL DIC. Biotinylation of the aminated P-SWCNTs were subsequently performed by shaking the resulting mixture using the mixer/shaker for 12 h at room temperature. Finally, these biotinylated nanotubes were washed with methanol twice, followed by rinsing with distilled water several times to remove any unreacted biotin.

5.2.2. SWCNTs characterization

The KrF-laser synthesized SWCNTs were systematically characterized by various techniques before and after their chemical purification and functionalization. Their Raman spectra were acquired at room temperature in the 100 - 2000 cm-1 spectral region under ambient conditions using a back-scattering geometry on a microRaman microscope (Renishaw Imaging Microscope Wire TM) with a 50× objective. A 514.5 nm (2.41 eV) line from an air cooled Ar+ laser was used for excitation radiation. The chemical bonding states of the SWCNTs (before and after chemical purification) were analyzed by means of X-ray photoelectron spectroscopy (XPS) using the Cu K_α monochromatic radiation (1486.6 eV) of an ESCALAB 200I-XL spectrophotometer. The purified, aminated and biotinylated SWCNTs were characterized by FT-IR (Digilab FTS7000) in order to characterize the chemical components attached to the surface of the nanotubes and assess the biofunctionalization procedure. Finally, the nanostructural characteristics of as-produced, P-SWCNTs and BF-SWCNTs were directly examined by transmission electron microscopy (TEM) using a Jeol JEM-2100F (FEG-TEM, 200 kV) microscope.

5.2.3. Nanocomposite preparation

The nanocomposite materials were prepared by mixing an Ultraviolet curable epoxy (UV-epoxy, UVE, UV15DC80, Master Bond Inc.) and either P-SWCNTs or BF-SWCNTs (at two loads of 0.5 wt.% and 1 wt.%). The UV-epoxy used in this study was a special one-component dual cure (ultraviolet/heat curable) epoxy resin which contains a UV photo-initiator having a maximum absorption at 365 nm and a heat-initiator active in the 60 – 80℃ range. Biotin and 1,3-diaminopropane 99% (1g biotin/5 mL 1,3-diaminopropane 99%) were stored in 30 mL acetone

and ultrasonicated for 30 min. The desired amount of functionalized nanotubes was subsequently added to the solution. Then, the UV-epoxy was slowly mixed with the resulting solution over a magnetic stirring hot plate (Model SP131825, Barnstead international) at 50℃ for 4 h. Finally, the streptavidin solution (1 mL 10 μg/mL, S4762, from streptomyces avidinii, Sigma-Aldrich) was slowly added to the nanocomposite mixture and stirred for 1 h. After stirring, the nanocomposite mixture was simultaneously sonicated and heated in the ultrasonication bath at 50℃ for 2 h. The residual trace of solvent was evaporated by heating the nanocomposite mixture at 30℃ for 12 h and at 50℃ for 24 h in a vacuumed-oven (RK-52402, Cole Parmer). After evaporation of the solvent, the nanocomposites were passed through a very small gap in a three-roll mill mixer (Exakt 80E, Exakt Technologies) for final high shear mixing [24]. The gaps between the rolls varied in three batch-wise progressing steps (10 passes each) with three different gaps at 25 μm, 10 μm and 5 μm, respectively. The speed of the apron roll was adjusted to 250 RPM. The final mixture was then degassed under vacuum for 12 h. For comparison purposes, the nanocomposites with P-SWCNTs were also prepared using the same mixing procedure.

5.2.4. Nanocomposite morphological characterization

For optical imaging purposes, ~20 μm-thick films of the nanocomposites were fabricated by direct deposition on a glass substrate by means of a computer-controlled robot (I & J2200-4, I & J Fisnar) that moves a dispensing apparatus (HP-7X, EFD) along the x, y and z axes [20,25]. The quality of the mixing was observed for the cured nanocomposite films using an optical microscope (BX-61, Olympus) and image analysis software (Image-Pro Plus V5, Media Cybernetics). Microtomed surface of the bulk nanocomposite samples were also observed using

field emission scanning electron microscopy (FESEM JEOL, JSM-7600TFE) in order to observe the nanotube dispersion.

5.2.5. Nanocomposite electrical and mechanical characterizations

The ultraviolet-assisted direct-write technique [21] was used to fabricate nanocomposites microfibers in order to assess the reinforcing effects of P-SWCNTs and BF-SWCNTs in the epoxy matrix. Two parallel thick square pads of the nanocomposites with 6 mm gap were first fabricated by extruding the nanocomposites suspensions through a micro-nozzle (5127-0.25-B, Precision Stainless Steel Tips, EFD, internal diameter (ID) = 150 μm) over a glass substrate. Right after, the pads were in situ cured using the optical fibers collected the light from two high-intensity UV light-emitting diodes (LED, NCSU033A, Nichia). Three suspended microfibers were then fabricated between two pads made of the same material. The microfibers were cured using UV exposure while being extruded (Figure 5.1). The electrical properties of the nanocomposite microfibers were characterized using a Keithley 4200 semiconductor parametric analyzer with silver electrodes sputtered on the pads. Mechanical properties (tensile modulus, strength and elongation at break) of the nanocomposites microfibers were measured in a dynamic mechanical analyzer (DMA, DMA2980, TA instruments) using a film tension clamp. The microfibers were tested with a constant loading rate adjusted to reach failure within 20 ± 3 s according to the ASTM D2256 standard. A minimum of five specimens from each nanocomposite sample were tested.

5.3. Results and Discussion

5.3.1. Nanotube structural characterization

Figure 5.2(a) shows typical Raman spectra of the KrF-laser synthesized SWCNTs before and after their chemical purification. The peaks located in the 100-300 cm-1 and the 1500-1600 cm-1 ranges are typical fingerprints of SWCNTs. The first peak is due to the radial breathing mode (RBM) of the SWCNTs while the second is associated with the tangential vibrations of the C atoms forming the nanotube surface (G band). The RBM peak centred around 182 cm-1 arises from SWCNTs with a diameter of 1.26 nm [26]. The D band (1340 cm-1) is generally attributed to the presence of amorphous carbon (a-C) and/or disordered carbon (d-C). The G/D ratio is generally used to qualify the degree of purity of the nanotubes. Here, the G/D ratio of the as-produced SWCNTs is already quite high, indicating that the starting material is of high quality. However, the G/D ratio is found to decrease for the purified SWCNTs (P-SWCNTs). This is in fact a consequence of the creation of defects on SWCNTs' surface by the nitric acid oxidation step in the purification process. This is further supported by XPS measurements shown in Figure 5.2(b). The main C 1s core level peak that arises from the C=C bonds is narrow in both samples at 284.5 keV. However, for P-SWCNTs, a shoulder appearing at 288 keV is also present in the spectrum. This component is attributed to the C-O-O carboxylic groups resulting from the covalent functionalization of the nanotubes by the nitric acid treatment [27]. Based on the XPS results, it is fair to assume that the purification process led to carboxylic groups grafting onto the SWCNTs surfaces.

Figure 5.2(c) shows a typical TEM micrograph of the as-produced SWCNTs where the nanotubes are found to self assemble, most often into bundles with a diameter in the 5-20 nm range and lengths reaching up to few microns. Other structures, such as carbon-surrounded

catalyst nanoparticles and/or graphitic nanostructures (i.e., dark spots in the micrograph) are also present. The various steps of purification are intended to remove residual metal catalyst nanoparticles and most of the undesired carbon forms (e.g., a-C, d-C, fullerenes). Figure 5.2(d) shows a typical TEM image of the P-SWCNTs. Nevertheless, one can still notice the presence of few dark spots that line the bundles. These are likely some residual catalyst nanoparticles, which were not entirely digested during the nitric acid oxidation treatment. Thermogravimetry analysis (TGA) measurements (not shown here) have demonstrated a substantial decrease (by more than 60%) in the concentration of residual catalyst in the P-SWCNTs samples, when compared to the as-produced SWCNTs.

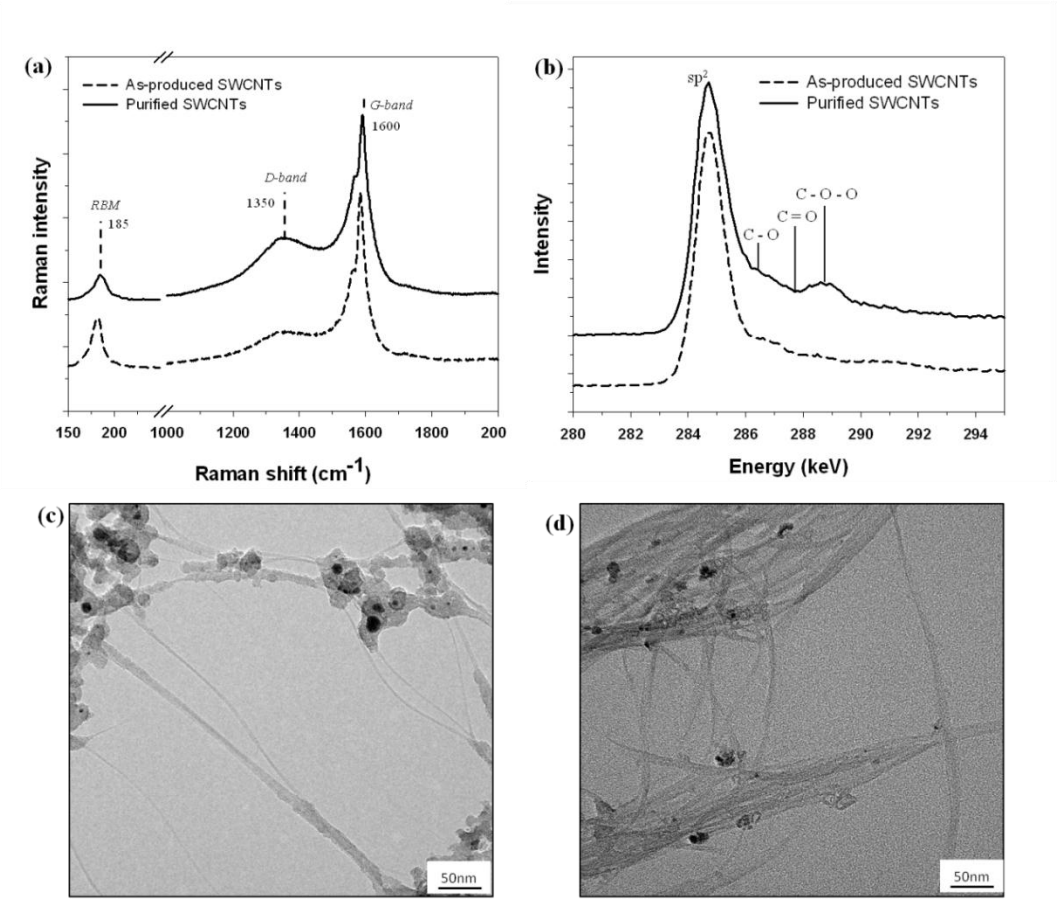

Figure 5.2 (a) Raman spectra, (b) X-ray photoelectron spectra of as-produced (bottom) and purified (top) SWCNTs, (c) typical TEM image of as-produced SWCNTs, and (b) TEM image of P-SWCNTs.

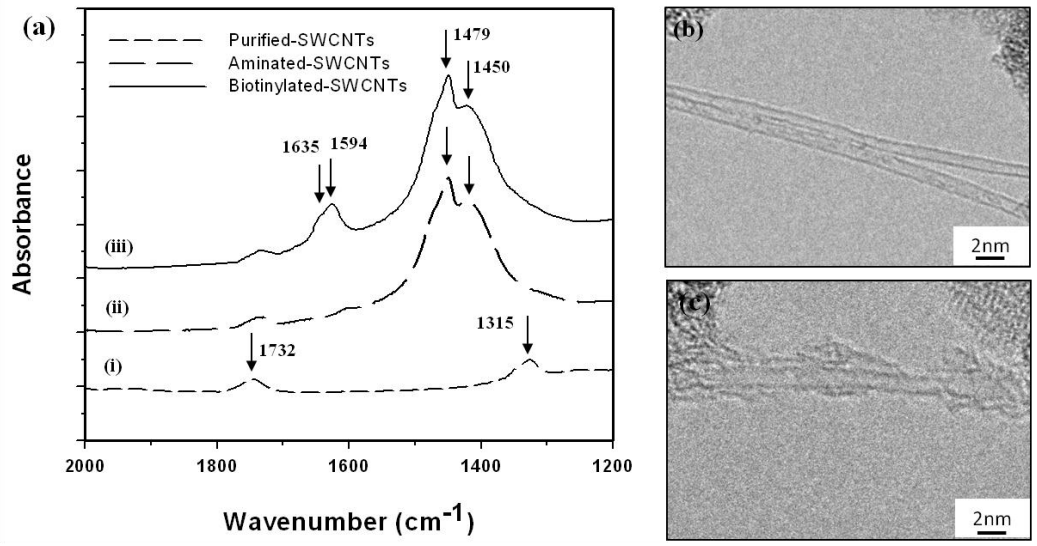

Figure 5.3 (a) FT-IR spectra of (i) P-SWCNTs (bottom), (ii) aminated SWCNTs (middle), and (iii) biotinylated SWCNTs (BF-SWCNTs) (top), (b) high-resolution TEM image of a P-SWCNTs, and (c) high-resolution TEM image of a BF-SWCNTs.

FT-IR spectroscopy was also used to characterize the chemical components attached to the surface of SWCNTs. Figure 5.3(a) shows the FT-IR spectra of the functionalized SWCNTs at each step of the biofunctionalization process. The FT-IR spectrum of P-SWCNTs shows two specific bands at 1315 cm^{-1} and 1732 cm^{-1}, associated with carboxylic groups [28]. The aminated and biotinylated SWCNTs revealed an appearance of two new strong bands centered at 1450 cm^{-1} and 1479 cm^{-1}, confirming reactions between carboxylic and amino groups [29]. The FT-IR spectrum of biofunctionalized carbon nanotubes (i.e., biotinylated SWCNTs) shows appearance of two new broad peaks centered around at 1594 cm^{-1} and 1635 cm^{-1}, which are assigned to 2° amide I and amide II, respectively [29]. The original amide groups of biotin as well as the amide bonds formed between amino groups on the aminated SWCNTs and carboxylic groups on the biotin are believed to be responsible for the two new peaks. The appearance of these peaks in the spectrum of biofunctionalized SWCNTs (BF-SWCNTs) proves the grafting of the active biotin groups on the nanotubes surfaces through covalent bonds [29]. A high resolution TEM image

(Figure 5.3(b)) shows individual P-SWCNTs with a very clean surface. This figure permits the direct measurement of the nanotube diameters (1.1-1.3 nm). Finally, Figure 5.3(c) shows a high-resolution TEM image of a SWCNT covered with a rough-looking material, most likely biomolecules or a mixture of carbonaceous residue and biomolecules, suggesting the effective presence of the grafted biomolecules on the SWCNTs surface [13].

5.3.2. Morphology characterization

Figures 5.4(a) and 5.4(b) show optical micrographs of two representative nanocomposites films with 1 wt.% loading of P-SWCNTs and BF-SWCNTs, respectively. The observed dark spots are thought to be nanotubes aggregates or nanotubes entangled around other carbonaceous materials. For the P-SWCNTs (Figure 5.4(a)), the majority of the nanotube aggregates are in the sub-micron range but some micron-size aggregates with a diameter of up to ~1 μm are also present. A drastic change of the size of the aggregates was observed for the nanocomposite film with the BF-SWCNTs (Figure 5.4(b)). The larger spots observed for the P-SWCNTs-reinforced nanocomposite film became smaller, to 0.7 μm diameter (in average) when the BF-SWCNTs were used. To further support the optical observations, the cross-section of the nanocomposites microfibers was also observed under scanning electron microscopy (SEM). Figures 5.4(c) and 5.4(d) show typical SEM images of the surface of nanocomposites with 1 wt.% loading of P-SWCNTs and BF-SWCNTs, respectively. In the purified SWCNT-reinforced nanocomposite, the nanotubes formed clusters and large aggregates (i.e., the bright spots). When the biofunctionalized SWCNTs were used, the large aggregates disappeared and it was difficult to spot clusters of SWCNTs. Based on all the above observations, the fairly uniform dispersion of the nanotubes and their associated aggregates for both cases might be attributed to the

effectiveness of the nanocomposite mixing procedure combining ultrasonication and three-roll mill mixing methods. Comparing the nanocomposites dispersion suggests that the presence of biomolecules at the nanotube-matrix interface prevented re-aggregation of nanotubes and improved the SWCNTs dispersion.

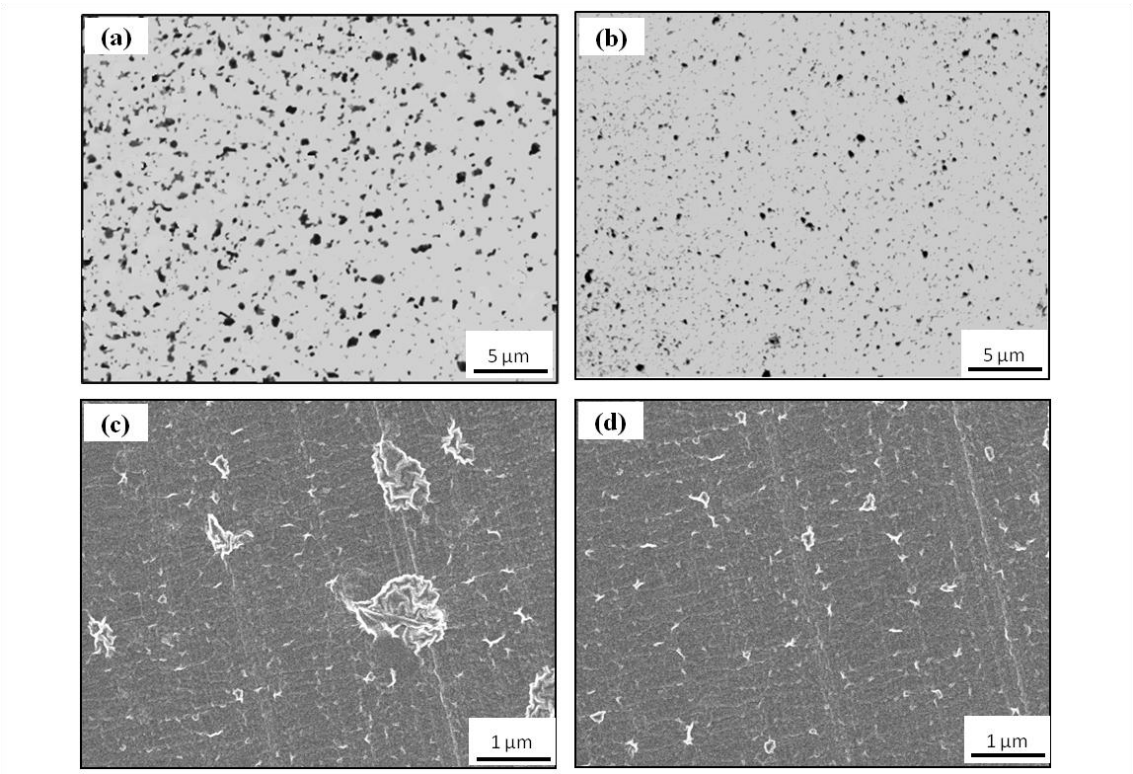

Figure 5.4 Optical microscope images of a 20-µm thick film of the nanocomposite containing (a) 1 wt% P-SWCNTs and (b) 1 wt% BF-SWCNTs, (c) and (d) typical SEM images of the cross-section surface of the bulk nanocomposites containing 1 wt% P-SWCNTs and 1 wt% BF-SWCNTs, respectively.

5.3.3. Mechanical properties

The effect of biofunctionalization of SWCNTs on the mechanical properties was assessed by tensile testing. Figure 5.5 shows the stress-strain curves along with their resulting histograms of the neat UV-curable epoxy (UV-epoxy) and its associated nanotube-reinforced nanocomposites, prepared either with the P-SWCNTs or BF-SWCNTs. Figure 5.5(a) shows an

optical image of typical microfibers used in the tensile experiments and Figure 5.5(b) is a representative SEM image of a fiber cross-section after its fracture under tensile loading. The error bars on the histograms were calculated from the 95% confidence intervals on the mean value obtained from the measurements. When the BF-SWCNTs were added to the composite with 0.5 wt.% loading, the average modulus showed an increase of 59% compared to that of the neat resin and an increase of 19% when compared to that of the nanocomposite reinforced with the same nanotube loading of P-SWCNTs. The improvement of modulus for the composites with 1 wt.% BF-SWCNTs loading were found to be 93% and 16% when compared to those of the neat resin and the P-SWCNTs-reinforced composites, respectively. The increased stiffness, from the neat epoxy resin to the nanocomposites, might be attributed to the proper dispersion as well as beneficial orientation of the nanotubes that may occur during the extrusion of the nanocomposite through the micronozzle. For both nanotube loadings, BF-SWCNTs led to nanocomposites ~20% stiffer than that obtained with P-SWCNTs. This is most likely attributed to the increased effective aspect ratio of the BF-SWCNTs as a consequence of their better dispersion.

The average failure strength of the P-SWCNTs- and BF-SWCNTs-reinforced nanocomposite was also improved with the addition of nanotubes. The incorporation of 0.5 wt.% BF-SWCNTs to the epoxy matrix increased its strength by approximately 50%. The nanocomposite with 1 wt.% BF-SWCNTs showed further enhancement (by 75%). For both nanotube loadings, higher failure strength (up to 24%) was achieved for the composites reinforced with BF-SWCNTs when compared to the P-SWCNTs-reinforced composites. More interestingly, the strength of the nanocomposite microfibers containing 0.5 wt.% BF-SWCNTs was found to be very close to that of the 1 wt.% P-SWCNTs-reinforced nanocomposite

microfibers. This relatively higher improvement could be attributed to a possible strong nanotube/matrix interfacial interaction and to a good dispersion of nanotubes with the presence of the biomolecules. Considering the quantity of the SWCNTs added, these improvements of both modulus and strength are among the highest improvements for epoxy composites reported so far, as compared in Table 5.1 [9,12,13].

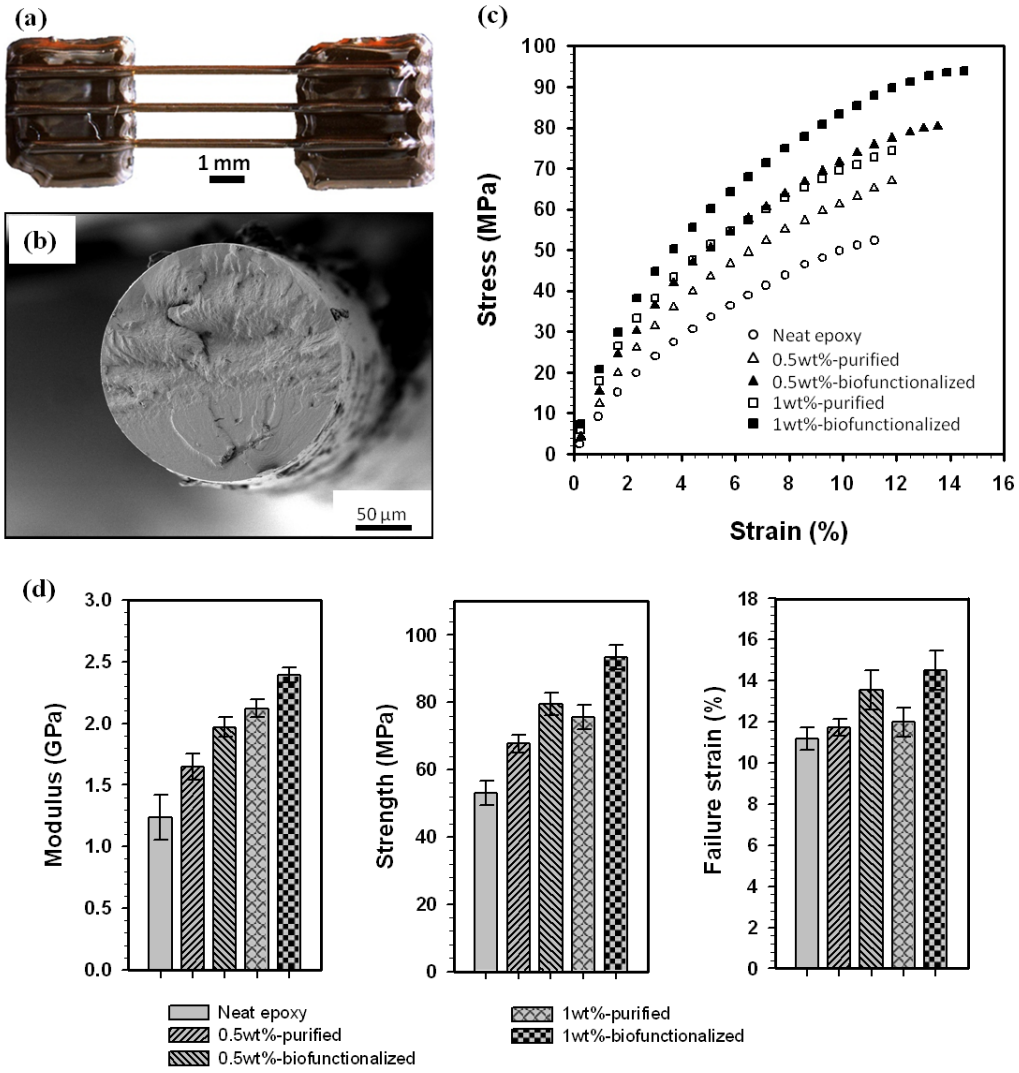

Figure 5.5 Mechanical characterization of the nanocomposite materials: (a) optical image of a typical fabricated specimen consisting of three suspended fibers between two rectangular pads, (b) SEM image of fracture surface of a nanocomposite fiber, (c) typical stress–strain curves and (d) histograms of modulus, strength and failure strain of the pure UV-epoxy and its associated nanocomposites.

Table 5.1 Comparison of the mechanical properties improvements in our work with those reported in literature.

SWCNTs wt.%	Increase of Modulus (%)	Increase of Strength (%)	Ref.
1.0	31	25	[9]
1.0	26	16	[12]
1.0	60	40	[13]
1.0	93	75	Present work

5.3.4. Governing interaction mechanisms

The possible governing interaction mechanisms between nanotubes and epoxy matrix with the presence of biomolecules are schematized in Figure 5.6. The nanotube biofunctionalization begins with grafting (covalently and non-covalently) carboxylic and amine groups to the surface of SWCNTs (more details on the synthesis procedure are found in experimental section). Grafting biomolecules on the nanotubes surface relies on the carboxylic groups created during the nanotube purification and on the use of Zinc protoporphyrin IX (ZnPP) molecules. ZnPP molecules can non-covalently interact with the nanotubes wall through $\pi - \pi$ interactions [18,20]. It should be mentioned that the functionalization procedure used in this study is non-destructive to the sidewall by attaching functional groups to the nanotubes. Since the long acidic treatment can destroy the wall integrity and consequently affect the mechanical properties of the resulting nanocomposite, the duration of acidic treatment was effectively controlled in our purification process. The carboxylic groups are capable of interacting with the amine groups and could contribute to further grafting of biomolecules to the surface of nanotubes. Streptavidin molecules offer four active sites which are equally capable of binding with biotin. A very strong nanotube-epoxy cross-linked network could be obtained by the action of still-active streptavidin that binds to other biotin molecules, which are attached to either epoxy groups or BF-SWCNTs. The formation of such chemical bonding is believed to be responsible for the reasonable increase

of failure strength obtained for the BF-SWCNTs-reinforced nanocomposites. It is worth noting that the average failure strain of 1 wt.% BF-SWCNTs-reinforced nanocomposite microfibers showed a slight increase (by 19%) in comparison to that of neat epoxy microfibers. Considering the flexibility of SWCNTs, the improvement of failure strain might be another proof of strong interfacial interaction [9]. Another contribution might come from stretching the curved and entangled nanotubes during the mechanical solicitation [9]. Therefore, the BF-SWCNTs could be used not only as a strong reinforcement but also to slightly improve toughening properties of intrinsically brittle epoxies.

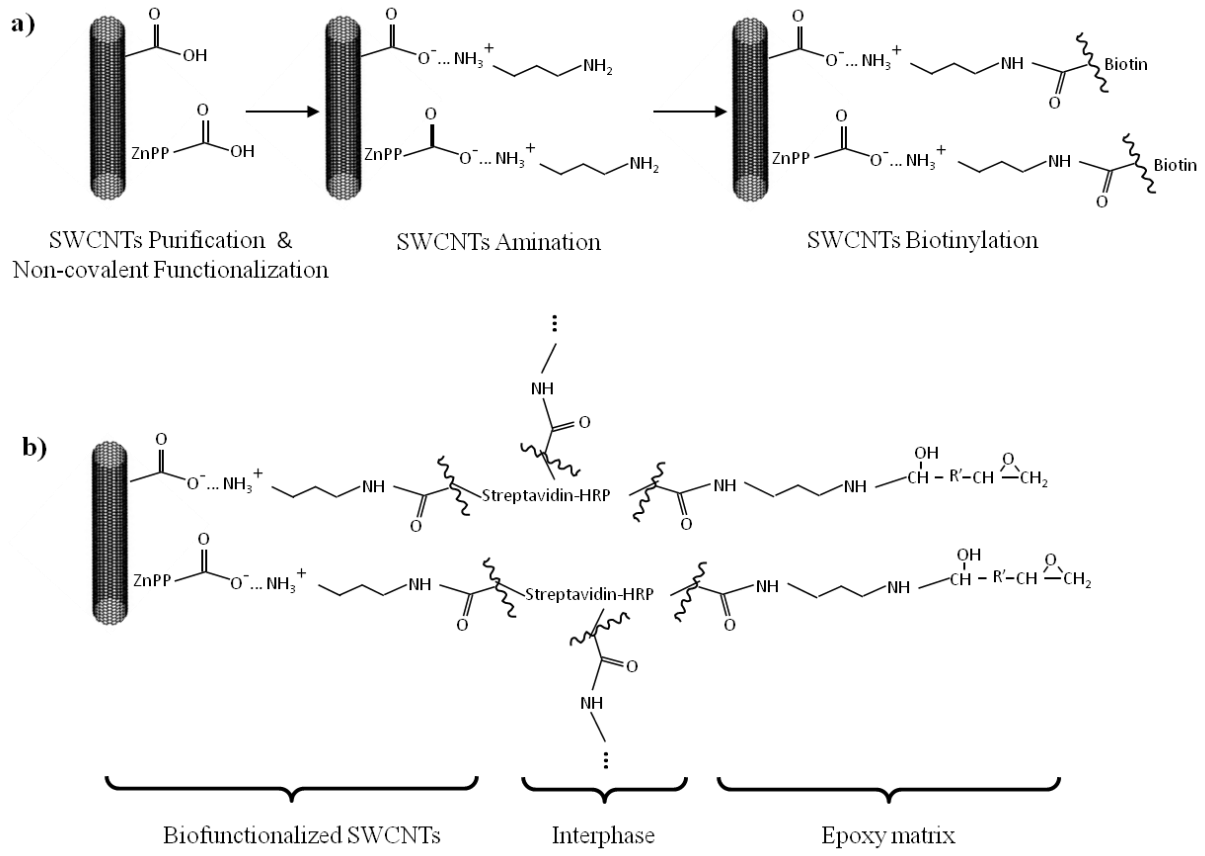

Figure 5.6 Schematics of (a) synthesis procedure of the BF-SWCNTs and (b) proposed interaction mechanisms governing the interaction of the BF-SWCNTs and the epoxy matrix by bridge formation through biotin-streptavidin interactions.

5.3.5. Electrical conductivity

The effect of biofunctionalization of the nanotubes on electrical conductivity was studied. The electrical conductivity of the P-SWCNTs and BF-SWCNTs-reinforced composite microfibers was characterized upon voltage application between two silver-coated pads. Figure 5.7 shows the measured current with respect to applied voltage (I-V) curve of the nanocomposite microfibers for two different nanotubes loadings. Linear responses, with different slopes (R), of the currents versus the applied voltage were observed for all nanocomposite microfibers. For the microfibers with nanotube loading of 0.5 wt.%, the BF-SWCNTs were found to lead to slightly lower conductivities (by 19%), but this remains within the uncertainty of the measurements. At nanotube loading of 1 wt.%, the nanocomposite microfibers with BF-SWCNTs showed a decrease of 129% in electrical conductance (i.e., 1/R) when compared to that of P-SWCNTs-reinforced nanocomposite. The decrease of electrical conductivity might be attributed to the presence of streptavidin molecules that possibly act as a less-conductive layer surrounding the SWCNTs. The measured resistivity was decreased with the addition of more nanotubes (1 wt.%) through which more electrical percolation pathways should be formed. At the nanotube loading of 0.5 wt.%, electrons must travel through larger amounts of insulating epoxy matrix between the conductive nanotubes. When the percolation networks are formed (at higher nanotube loadings), electrons conduct predominantly along the conductive nanotubes and move directly from one nanotube to the next [30]. Therefore, it is thought that the presence of biomolecules is more significant at higher nanotube concentrations and responsible for a clear change in the electrical conductivity of the nanocomposite microfibers containing 1 wt.% of SWCNTs. This phenomenon might be used for potential biosensor applications where streptavidin molecules are detected by their attachment to the surface of biotin-functionalized nanotubes in porous

nanocomposite patterned fibers [29,31]. These patterned microfibers could be manufactured by adding a fugitive material, being able to be extracted later to the nanocomposite reinforced with biofunctionalized nanotubes. The available active biotin molecules in nanoscale pore spaces could still be capable of interacting with streptavidin molecules and to detect them in their solution.

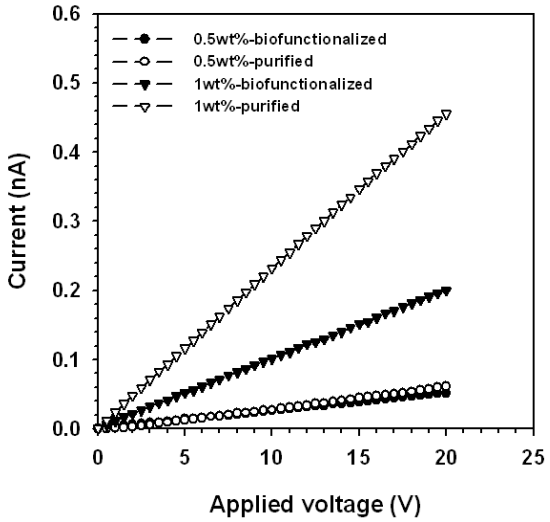

Figure 5.7 Measured current upon voltage application for the nanocomposite microfibers.

5.4. Conclusions

Surface biofunctionalization of SWCNTs, along with an efficient mixing procedure consisting of ultrasonication and three-roll mill mixing has been found to be an effective method towards the full integration of nanotubes within an epoxy matrix. Although the nanotube dispersion and mechanical properties of the nanocomposite reinforced with P-SWCNTs were reasonably improved in comparison to the neat epoxy, subsequent grafting of biotin molecules to the P-SWCNTs led to a fairly good dispersion and further enhancement in their reinforcing effect. The failure strength of nanocomposite microfibers reinforced with 1 wt.% of BF-SWCNTs showed an increase of 76% when compared to that of pure resin and an increase of

25% when compared to that of the nanocomposite reinforced with P-SWCNTs, indicating the effectiveness of biofunctionalization to facilitate load transfer. The process-induced orientation of SWCNTs during the fabrication of microfibers combined with high strength provided by the biomolecules interactions make these multifunctional nanocomposites a good choice for the fabrication of high-performance nanocomposite-based devices in micro electromechanical systems and microelectronics. Considering the ability to change the electrical conductivity of the microfibers under mechanical disturbances and also by capturing biomolecules, the utilization of these multifunctional nanocomposite materials enables the fabrication of easily-manipulated strain sensors and porous microfibers or 3D complex patterns as solid support materials for potential biosensor applications.

5. Acknowledgements

The authors acknowledge the financial support from FQRNT (Le Fonds Québécois de la Recherche sur la Nature et les Technologies). Prof. El Khakani acknowledges also the financial support from NSERC (National Science Engineering Research Council of Canada) and Plasma-Québec (le Réseau Stratégique du FQRNT sur la Science et Technologies des Plasmas). The authors would like to thank the technical support of Dr. K. Laaziri from Laboratoire de recherche sur les nanostructures et interfaces conductrices for the electrical measurements.

5. References

[1] P. Dharap, Z. L. Li, S. Nagarajaiah, E. V. Barrera, *Nanotechnology* **2004**, *15*, 379.

[2] P. G. Su, S. C. Huang, *Sensors Actuators B:Chem.* **2006**, *113*, 142.

[3] D. Qian, G. J. Wagner, W. K. Liu, M.-F. Yu, R. S. Ruoff, *Appl. Mech. Rev.* **2002**, *55*, 495.

[4] S. J. Tans, M. H. Devoret, H. J. Dai, A. Thess, R. E. Smalley, L. J. Geerligs, C. Dekker, *Nature* **1997**, *386*, 474.

[5] J. N. Coleman, U. Khan, Y. K. Gun'ko, *Adv. Mater.* **2006**, *18*, 689.

[6] Y. Ear, E. Silverman, *MRS Bull.* **2007**, *32*, 328.

[7] T. Mirfakhrai, R. Krishna-Prasad, A. Nojeh, J. D. W. Madden, *Nanotechnology* **2008**, *19, 31*.

[8] N. G. Sahoo, Y. C. Jung, H. J. Yoo, J. W. Cho, *Compos. Sci. Technol.* **2007**, *67*, 1920.

[9] J. Zhu, H. Q. Peng, F. Rodriguez-Macias, J. L. Margrave, V. N. Khabashesku, A. M. Imam, K. Lozano, E. V. Barrera, *Adv. Funct. Mater.* **2004**, *14*, 643.

[10] M. Z. Atashbar, B. Bejcek, S. Singamaneni, S. Santucci, *Proceedings of the IEEE Sensors 1-3* **2004**, 1048.

[11] J. Kong, N. R. Franklin, C. W. Zhou, M. G. Chapline, S. Peng, K. J. Cho, H. J. Dai, *Science* **2000**, *287*, 622.

[12] L. Sun, G. L. Warren, J. Y. O'Reilly, W. N. Everett, S. M. Lee, D. Davis, D. Lagoudas, H. J. Sue, *Carbon* **2008**, *46*, 320.

[13] S. Wang, R. Liang, B. Wang, C. Zhang, *Nanotechnology* **2008**, *19, 8.*

[14] S. R. Wang, Z. Y. Liang, T. Liu, B. Wang, C. Zhang, *Nanotechnology* **2006**, *17*, 6.

[15] J. X. Zhao, Y. H. Ding, *J. Phys. Chem. C* **2008**, *112*, 11.

[16] J. Zhu, J. D. Kim, H. Q. Peng, J. L. Margrave, V. N. Khabashesku, E. V. Barrera, *Nano Lett.* **2003**, *3*, 1107.

[17] J. Chen, M. A. Hamon, H. Hu, Y. S. Chen, A. M. Rao, P. C. Eklund, R. C. Haddon, *Science* **1998**, *282*, 95.

[18] N. Nakashima, T. Fujigaya, *Chem. Lett.* **2007**, *36*, 692.

[19] A. C. Patel, S. X. Li, J. M. Yuan, Y. Wei, *Nano Lett.* **2006**, *6*, 1042.

[20] L. L. Lebel, B. Aissa, M. A. El Khakani, D. Therriault, *Compos. Sci. Technol.* **2010**, *70*, 518.

[21] L. L. Lebel, B. Aissa, M. A. El Khakani, D. Therriault, *Adv. Mater.* **2010**, *22*, 592.

[22] N. Braidy, M. A. El Khakani, G. A. Botton, *Carbon* **2002**, *40*, 2835.

[23] V. Le Borgne, B. Aissa, M. Mohamedi, Y. A. Kim, M. Endo and M. A. El Khakani 2011 *J. Nanopart. Res.*DOI: 10.1007/s11051-011-0409-9.

[24] E. T. Thostenson, T. W. Chou, *Carbon* **2006**, *44*, 3022.

[25] D. Therriault, R. F. Shepherd, S. R. White, J. A. Lewis, *Adv. Mater.* **2005**, *17*, 395.

[26] S. M. Bachilo, M. S. Strano, C. Kittrell, R. H. Hauge, R. E. Smalley, R. B. Weisman, *Science* **2002**, *298*, 2361.

[27] T. I. T. Okpalugo, P. Papakonstantinou, H. Murphy, J. McLaughlin, N. M. D. Brown, *Carbon* **2005**, *43*, 153.

[28] J. Bruneaux, D. Therriault and M. C. Heuzey 2008 *J. Micromech. Microeng.* **18**, 11.

[29] D. Wang, G. Sun, B. Xiang, B. S. Chiou, *Eur. Polym. J.* **2008**, *44*, 2032.

[30] K. I. Winey, T. Kashiwagi, M. F. Mu, *MRS Bull.* **2007**, *32*, 348.

[31] S. Sotiropoulou, N. A. Chaniotakis, *Anal. Bioanal Chem.* **2003**, *375*, 103.

5. Table of contents entry:

Microelectronic devices with desired patterns are manufactured by UV-assisted direct-write assembly of a multifunctional UV-curable nanocomposite material. The nanocomposite consists of biofunctionalized single-walled carbon nanotubes reinforcing an ultraviolet curable epoxy polymer by means of biotin-streptavidin interactions. The biotin-grafted nanotubes are used as reinforcement as well as sensing elements to detect streptavidin biomolecules in its solution for potential biosensor applications.

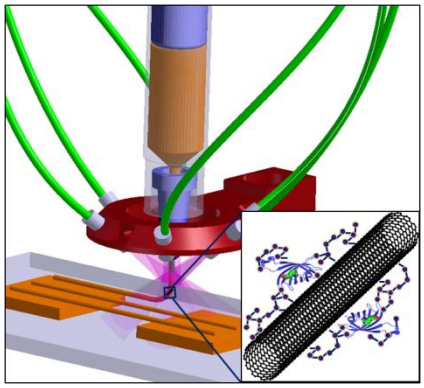

CHAPTER 6: Article 4: Direct-write fabrication of freestanding nanocomposite strain sensors[4]

Rouhollah Dermanaki Farahani[1], Hamid Dalir[1], Vincent Le Borgne[2], Loick. A. Gautier[2], My Ali El Khakani[2], Martin Lévesque[1], and Daniel Therriault[1]*

[1]Laboratory for Multiscale Mechanics, Center for applied research on polymers (CREPEC), École Polytechnique de Montreal, C.P. 6079, succ. Centre-Ville, Montreal (QC), H3C 3A7 (Canada)

[2]Institut National de la Recherche Scientifique, INRS-Énergie, Matériaux et Télécommunications, 1650 Blvd. Lionel-Boulet, Varennes (QC), J3X 1S2 (Canada)

Abstract

This paper deals with the design and microfabrication of two three-dimensional (3D) freestanding patterned strain sensors made of single-walled carbon nanotubes (SWCNTs) nanocomposites with the ultraviolet-assisted direct-write (UV-DW) technique. The first sensor consisted of three nanocomposite microfibers suspended between two rectangular epoxy pads. The flexibility of the UV-DW technique enables manufacturing the sensor and its housing in one monolithic structure. The second sensor was composed of a nanocomposite network consisting of four parallel microsprings, which demonstrates the high capability of the technique when compared to the conventional photolithographic technologies. The performances of the sensors were assessed under tension and compression, respectively. The sensors sensitivities were evaluated by correlating their measured resistivities to the applied displacements/strains.

[4] This article was submitted to the journal of Nanotechnology.

Electrical conductivity measurements revealed that the manufactured sensors are highly sensitive to small mechanical disturbances, especially for lower nanotube loadings when compared to traditional metallic or nanocomposite films. The present manufacturing method offers a new perspective for manufacturing highly sensitive 3D freestanding microstructured sensors.

6.1. Introduction

There has been a growing interest over the past decade for the development of carbon nanotubes (CNTs)-reinforced polymer nanocomposites, considered as realistic alternatives to conventional smart materials [1-11]. CNTs high aspect ratio [12] and excellent electrical properties [13] confer electrical conductivity and sensing capability to inherently insulating polymers, which make their nanocomposites suitable for use in a broad range of potential applications such as electrostatic charge protection for aircrafts [14], sensors [2,8,10,11], actuators [1,15] and electromagnetic interference shielding [10,14].

Among these applications, CNTs-reinforced polymer nanocomposite films have been extensively used for structural health monitoring for industrial and national infrastructures [4,5,8]. Nanocomposite films strain sensors might be preferred over conventional metal foil strain sensors in some applications due to their enhanced electromechanical sensitivity and their ability to accurately measure large strains [16]. Nanocomposite sensors' electromechanical sensitivity stems from the rearrangement of percolating conducting pathways induced by an external mechanical disturbance. In particular, the nanocomposite films electrical conductivity decreases with increasing mechanical strain under tension because the distances between non-contacting neighboring nanotubes are increased and/or the contact area between the nanotubes in their percolation pathways are influenced [3]. Another possible contribution may arise from the

intrinsic CNTs conductivity variation due to mechanical strain, as reported in the literature [17-19]. It has been found that nanotubes concentration, dispersion and manufacturing process are the key parameters affecting the electromechanical sensitivity of such nanocomposite-based sensors. In general, the highest sensitivity is achieved when the nanotubes contents approaches the percolation concentration threshold where the electron tunneling between the neighboring nanotubes at sufficiently close proximity is the dominant mechanism [3].

Most of the researches have been limited to the use of nanocomposite films to manufacture strain sensors [5,10,17-19]. Nanocomposite films are limited, by nature, to only provide in-plane strain measurements. In addition, they must be bonded over their whole area and might capture undesired parasitic perturbations (local cracks, plasticity, etc.) in applications where overall measurements are sought. The sensitivity of such sensors can be improved by decreasing their width and thickness [20]. However, this potential tailoring is somewhat limited by fabrication and manipulation constraints. Finally, bulk nanocomposite films cannot be patterned as traditional strain sensors consisting of a long, thin conductive strip of patterned lines. This limits further the possibilities for improving their sensitivities. Photolithography techniques (resolution down to 120 nm [21]) could be used for manufacturing patterned nanocomposite strain sensors. This technique could also enable to fabricate sensing elements directly on structures surfaces [22]. However, this technique is far from being cost-effective. Therefore, new advances on the fabrication processes are still needed to easily and cost-effectively manufacture a supported or freestanding nanocomposite strain sensor with desired 2D and 3D patterns.

This paper focuses on the use of the ultraviolet-assisted direct-write (UV-DW) technique recently developed in our group [23] for the fabrication of freestanding nanocomposite patterned strain sensors. The flexibility of this fabrication method enabled to tailor and cost-effectively

pattern deposited nanocomposite 2D lines like traditional strain gauges and also to fabricate two freestanding 3D-patterned strain sensors. The first manufactured freestanding strain sensor consisted of three nanocomposite microfibers suspended between two rectangular epoxy pads. The electromechanical sensitivity of the structure was evaluated under tensile loading in a dynamic mechanical analyzer (DMA) with a film tension clamp. The second sensor was composed of a square network of four parallel microsprings enclosed by two circular pads at its top and bottom. The sensitivity of this sensor was characterized in DMA with a compression clamp. The manufacturing technique presented here opens new prospects for the achievement of cost-effective geometry-optimized nanocomposite microdevices for microelectronics applications.

The paper is organized as follows: Section 2 deals with all the experimental details including nanotube characterization with a few methods, nanocomposites preparation procedure and their viscosity characterization. This is followed by the fabrication of two freestanding nanocomposite patterned strain sensors with the UV-DW technique. All the results obtained from the experiments are discussed in section 3. This section begins with the CNTs and their epoxy nanocomposites viscosity characterization. Finally, the nanocomposite sensors electromechanical sensitivities are presented and discussed.

6.2. Experimental Details

6.2.1. Nanocomposite preparation and characterization

The SWCNTs were synthesized by the UV-laser ablation (248 nm, 20 ns, 400 mJ) method using a Co/Ni-doped graphite target in an argon atmosphere at a temperature of 1150°C. The as-produced SWCNTs were then subjected to a three-step chemical purification treatment (details

can be found in [24,25]) to remove the impurities like metal catalyst particles and other carbonaceous structures.

The purified SWCNTs were then used to prepare nanocomposites at different nanotube loadings by mixing them with an ultraviolet/heat curable epoxy (UV-epoxy, UV15DC80, Master Bond Inc.). The UV-epoxy used here contains a UV photo-initiator with an optimal absorption at 365 nm and a heat-initiator active in the 60 - 80°C range. Nanotubes non-covalent functionalization using surfactant was applied to the nanotube aggregates solubilization. The desired amount of purified SWCNTs was added to a solution of 0.1 mM of Zinc protoporphyrin IX (Sigma-Aldrich) in acetone. The suspension was sonicated in an ultrasonic bath (Ultrasonic cleaner 8891, Cole-Parmer) for 90 min. The UV-epoxy was then slowly mixed with the nanotube suspension in acetone over a magnetic stirring hot plate (Model SP131825, Barnstead international) at 50°C for 4 h. The solvent was evaporated by placing the nanocomposite under hood at room temperature for 24 h, followed vacuumed-oven (RK-52402, Cole Parmer) curing at 30°C for 12 h and at 50°C for 24 h. The nanocomposites were passed through a three-roll mill mixer (Exakt 80E, Exakt Technologies) for final high shear mixing upon solvent evaporation. The gaps between the rolls varied in three batch-wise processing steps including 5 passes at 25 µm, 5 passes at 10 µm and 10 passes at 5 µm, respectively. The rotation speed of the apron roll was set to 250 RPM. The final mixture was then degassed under a vacuum of 0.15 bar for 24 h.

The purified SWCNTs were observed by transmission electron microscopy (TEM) using a Jeol JEM-2100F (FEG-TEM, 200 kV) microscope. Their Raman spectra were acquired at room temperature in the 100 - 2000 cm^{-1} spectral region under ambient conditions using a back-scattering geometry on a microRaman microscope (Renishaw Imaging Microscope Wire TM)

with a 50× objective. A 514.5 nm (2.41 eV) line from an air cooled Ar+ laser was used for excitation radiation.

The process-related apparent viscosity of the pure UV-epoxy and its associated nanocomposites were measured from an experimental method based on capillary viscometry [26,27]. To obtain different shear conditions, ten continuous filaments of materials were extruded through a micro-nozzle (5132-0.25-B, Precision Stainless Steel Tips, EFD, L = ~20 mm and Internal Diameter (ID) = 100 μm) at five different pressures over glass substrates. The filaments were deposited using a computer-controlled robot (I & J2200-4, I & J Fisnar) and a fluid dispenser (HP-7X, EFD) with a calibrated deposition speed. Shortly after the deposition, the filaments were cured under a UV lamp (RK-97600, Cole-Parmer) illumination for 5 min. The materials flow rates were calculated from the filaments cross-section and the extrusion speed was controlled by the dispensing apparatus. The cross-section area of the filaments was measured with an optical microscope (BX-61, Olympus) and image analysis software (Image-Pro Plus V5, Media Cybernetics). The process-related apparent viscosity and the process-related apparent shear rate were calculated from capillary viscometry equations including Rabinowitsch correction.

6.2.2. Fabrication of the sensors and their characterizations

UV-DW technique was used to fabricate nanocomposite-based strain sensors. The UV-DW technique relies on a computer-controlled robot (I & J2200-4, I & J Fisnar) that moves a dispensing apparatus (HP-7X, EFD) and a UV light-emission set-up along the x, y and z axes. Figure 6.1a schematically represents the fabrication of different microstructures using UV-curable nanocomposite materials. The materials are photopolymerized under the illumination of UV light using two high-intensity UV light-emitting diodes (LED, NCSU033A, Nichia) while

being extruded. The fast-curing of nanocomposite materials enables the fabrication of supported or freestanding 3D structures when the extrusion position spatially changes in three dimensions. Figures 6.1b and 6.1c show optical images of two deposited nanocomposite microstructures with a sufficient control of the resolution and patterns manufactured with this flexible, efficient and cost-effective method. In particular, the network shown in Figure 1b was fabricated in only 20 seconds.

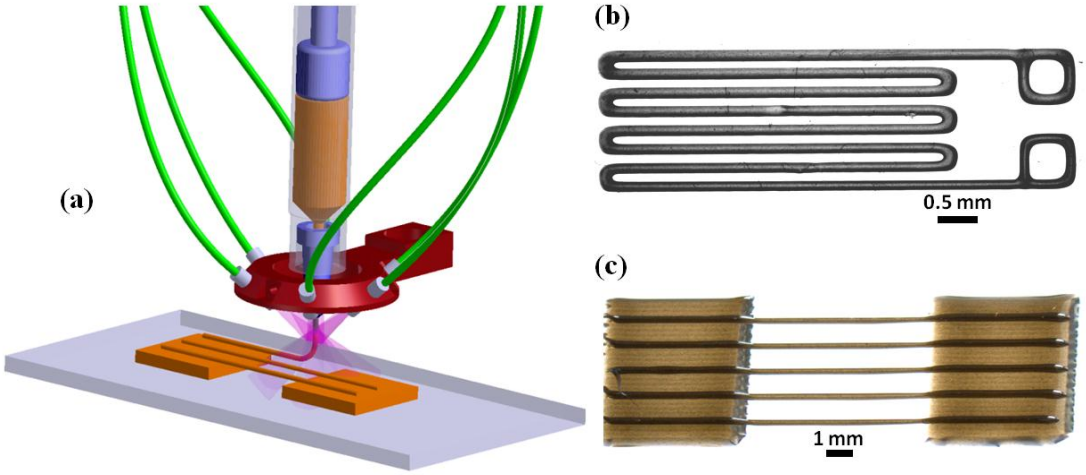

Figure 6.1 (a) Schematic representation of the UV-assisted direct-writing of nanocomposite microstructures, (b) a deposited line network similar to traditional strain gauges and (c) a microfibers coupon. To fabricate these microstructures using the UV-DW technique, the nanocomposite is extruded through a capillary micronozzle by an applied pressure and is partially cured shortly after extrusion under UV illumination.

The UV-DW technique was also used to fabricate two 3D-patternned freestanding nanocomposite strain sensors. In the first sensor, three 100μm-diameter nanocomposite microfibers suspended over a 8 mm gap between two rectangular epoxy pads were fabricated by extruding the nanocomposites suspension through a micro-nozzle (Precision Stainless Steel Tips, EFD, internal diameter = 100 μm). The two epoxy pads were silver-coated for ensuring proper electrical contact and served as electrodes. Another layer of epoxy was subsequently deposited

over the two pads using the UV-DW technique. This insulated electrically the fibers in order to reduce the parasitic effects.

The second type of sensors was composed of a square network of four identical 1mm-diameter microsprings. The microsprings were fabricated on a small circular aluminum plate in a rectangular layout having an inter-coil distance of 2 mm. Another aluminum plate was subsequently attached to the top of the springs. Electrical measurement probes were attached to the aluminum plates which served as conductive electrodes. Finally, the microfibers and the microspring networks were post-cured at 120°C for 1 h.

The sensors electromechanical sensitivity was evaluated by relating both their measured electrical conductivity and strains (or displacements) as the sensors underwent mechanical loading. The nanocomposite-based sensors electrical conductivities were measured with a Keithley 4200 semiconductor parametric analyzer (MM 2000 probe station). The strain sensors mechanical response (i.e., force–displacement) was measured in a dynamic mechanical analyzer (DMA, DMA2980, TA instruments). The microfibers were tested using a film tension clamp with a constant loading rate of 0.5 N/min^{-2} to reach a maximum displacement of 1 mm. The microsprings network mechanical response under compression was characterized with a compression fixture at a load rate of 5 mN/min^{-2} for a maximum displacement of 3 mm.

6.3. Results and discussions

6.3.1. Carbon nanotube characterization

Figure 6.2a shows a typical laser-synthesized SWCNTs TEM micrograph after their chemical purification. The nanotubes are observed to self-organize into high aspect ratio (i.e., length/diameter) bundles (length: up to 10 μm; diameter: ~1.24 nm). The nanotube chemical

purification removed any residual catalyst particles and other carbonaceous structures. However, few dark spots are still observed. These are most probably residual catalyst nanoparticles that were not entirely digested during the nitric acid oxidation treatment.

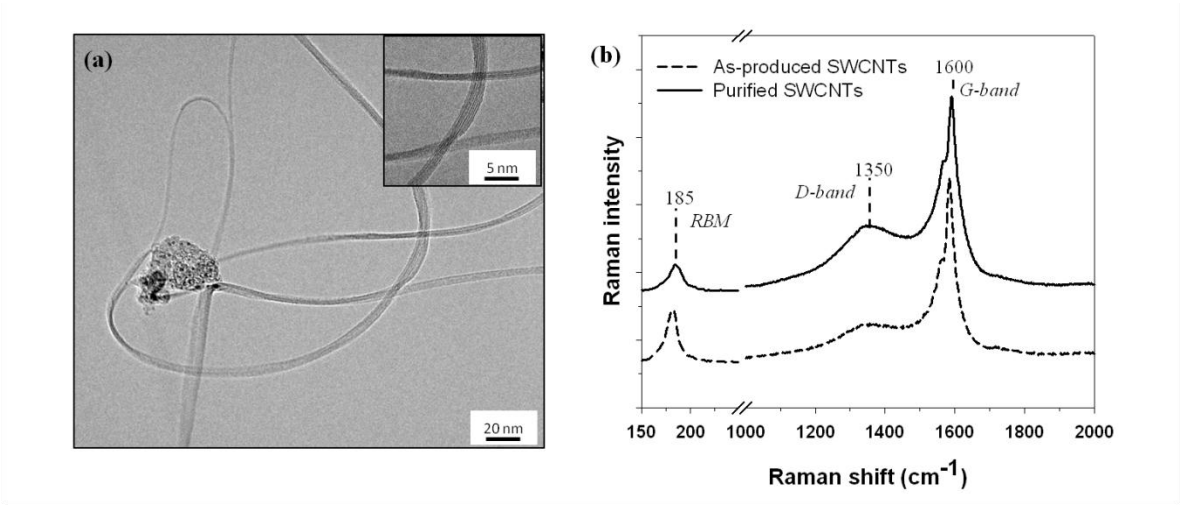

Figure 6.2 (a) Typical TEM images of purified SWCNTs and (b) Raman spectra as-produced (bottom) and purified (top) SWCNTs.

The structure of as-produced and purified SWCNTs was characterized using Raman spectroscopy. Figure 6.2b shows typical Raman spectra of the as-produced and purified SWCNTs, representing three typical peaks for the carbon nanotubes. The spectra includes a narrow radial breathing mode (*RBM*) band centered around 185 cm^{-1}, the *D*-band centered around 1350 cm^{-1} and the *G*-band around 1600 cm^{-1}. The RBM peak is attributed to the presence of SWCNTs with a mean diameter of 1.2 nm, in accordance with the measurements from direct TEM observations. The *G*-band corresponds to the symmetric vibrational tangential mode in graphite-like materials and the *D*-band is as a signature of disorder and/or defects in these structures. The high *G/D* intensity ratio is generally used to qualify the nanotubes purity. When the nanotubes were subjected to the purification process, their *G/D* intensity ratio significantly decreased in comparison to that of the as-produced mats. This is a consequence of the creation of additional structural defects in the nanotubes surface during the nitric acid oxidation based

purification process. However, the improved dispersion enabled by the creation of functional groups during the purification process outweighs their drawbacks with respect to nanotube conductivity [28].

6.3.2. Nanocomposite viscosity characterizations

Materials viscosity is a critical parameter in the UV-DW technique. Extruded materials of moderate to high viscosities are necessary to create stable filaments [23, 27]. Since high viscosity may limit flow through fine extrusion nozzles, an extruded materials shear-thinning behavior (i.e., a decrease of viscosity with an increase of shear forces inside the nozzle) is preferable. Figure 6.3 shows the process-related apparent viscosity (η_{app}) with respect to the process-related apparent shear rates ($\dot{\gamma}_{app}$) induced by the extrusion of the neat UV-epoxy and its associated nanocomposites for five extrusion pressures. A nearly constant η_{app} of ~12 Pa.s is observed for the neat UV-epoxy, indicating a Newtonian behavior in the range of shear rates studied. The incorporation of purified SWCNTs to the neat resin resulted in a considerable increase (12-fold increase by adding 1 wt% SWCNTs) for η_{app} at low $\dot{\gamma}_{app}$ and the apparition of a shear-thinning behavior. The carbon nanotubes high aspect ratio which possibly enabled the formation of a rheological percolation network and also their possible orientation during extrusion is thought to be responsible for the observed shear thinning behavior [29]. The nanocomposites viscosity and shear thinning behavior enabled the fabrication of microfibers coupons as well as the microsprings networks with the UV-DW technique.

The nanocomposites viscosity increase is also a good indicator for the nanotubes dispersion quality [30]. This is also supported by optical and SEM observation [31]. The achieved

dispersion is the result of nanocomposite mixture ultrasonication combined with important shear forces induced in the three-roll mixer.

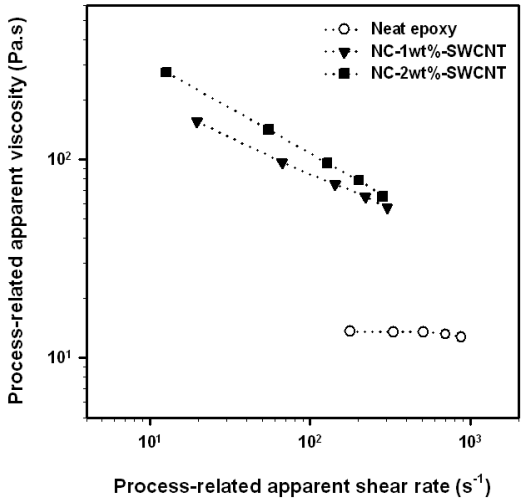

Figure 6.3 Process Process-related apparent viscosity of the neat UV-epoxy and its nanocomposites with respect to apparent shear rate using a method based on capillary viscometry

6.3.3. Sensors electromechanical sensitivity

6.3.3.1. Microfibers coupon

Figure 6.4 presents various aspects related to the nanocomposite microfibers coupons electromechanical testing. Figure 6.4a shows a typical microfibers optical image. Figure 6.4b shows that the freestanding microfibers circular cross-section with a diameter of ~ 120 µm. To avoid the microfibers failure during the electromechanical testing, the displacement at break was measured that is found to be ~ 1.5 mm (corresponds to ~ 0.19 of tensile strain). Therefore, the tensile testing was stopped when the displacement reached to a maximum of 1 mm. Figure 4c shows the force–displacement curves obtained for the nanocomposite microfibers for the range of displacements studied (average on five specimens for each fiber type). The nanocomposite microfibers for both nanotube loadings exhibit a non-linear response. This behavior might be due to the possible toughening effect of the nanotubes [32] since the response of neat epoxy resins is

linearly elastic. The rigidity (i.e., tangent of curves in their linear parts) of the nanocomposite microfibers containing 1 wt% SWCNTs was found to be ~ 4.7 N mm^{-1}, and increased to ~ 6.3 N mm^{-1} (about 34% increase) for the fibers reinforced with 2 wt% SWCNTs. This might be attributed to the potentially high elasticity of SWCNTs, their proper dispersion and their possible beneficial orientation that may occur during the extrusion of the nanocomposite through the micronozzle.

Figures 6.4d and 6.4e show the current with respect to applied voltage (I-V) curves for the nanocomposite microfibers measured at three different strains and for nanotube loadings of 1 wt.% and 2 wt.%, respectively. Table 6.1 lists the microfibers electrical conductivities for five different strains. Nearly linear responses were observed for all nanocomposite microfibers within the voltage range investigated. The increase of nanotube contents increased the electrical conductivity of the microfibers and also decreased their electromechanical sensitivity, as listed in Table 6.1. Electromechanical sensitivity is usually represented as gauge factor defined as the ratio of relative resistance variation over strain variation. Higher nanotube loadings enhance the probability of contact points through which electrons are transferred and also decrease the distance of adjacent nanotubes [4,16]. As a result, electrical conductivity is less susceptible to strain at higher nanotube loadings. A large value of the gauge factor was obtained despite the relatively high nanotube concentrations when compared to that of percolation concentration threshold. This might be attributed to the proper nanotubes dispersion of and also the small microfibers diameters since gauge factor is strongly influenced by the nanocomposite geometry. Finally, Figure 6.4f shows the microfibers resistivity variation as a function of the applied tensile strains. The curves non-linearity might be due to neighboring nanotubes separation through which electron tunneling is compromised [3].

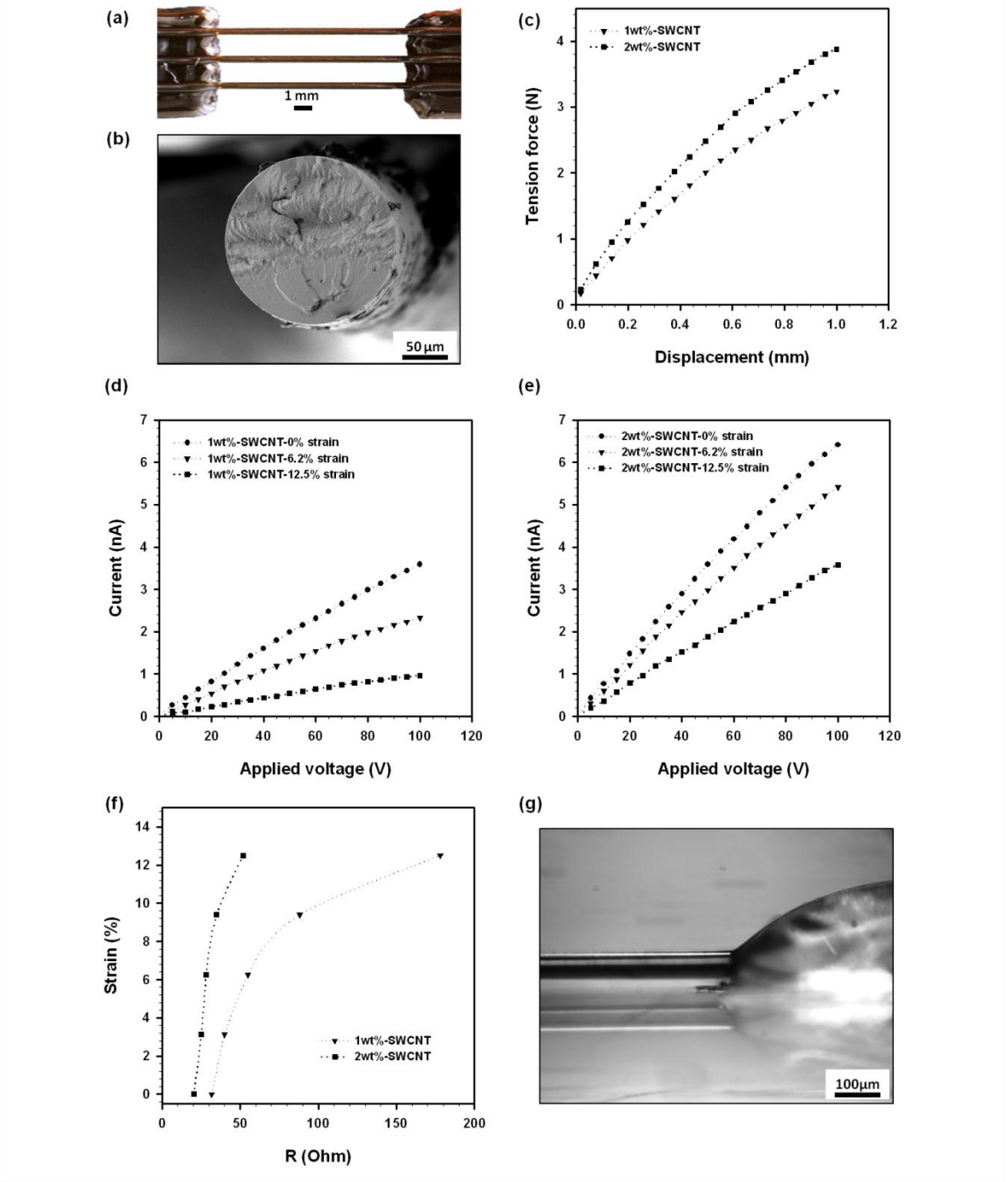

Figure 6.4 Electromechanical characterization of the nanocomposite microfibers under tensile strains: (a) optical image of a typical fabricated specimen consisting of three suspended fibers between two rectangular pads, (b) SEM image of fracture surface of a nanocomposite fiber, (c) typical force–displacement curves, (d) and (e) measured current upon voltage application between two pads for the nanocomposite microfibers respectively at 1wt% and 2wt% SWCNTs loadings, (f) strain-resistivity correlated curves based on electrical resistivity changes and (g) an optical image of a microfibers coupon adhered to a structure from the pads.

Table 6.1 Electrical conductivity changes for the microfibers under applied strains.

Electrical conductivity at different strain ($S.cm^{-1}$)						Gauge factor
Strain (%)	0	3.1	6.2	9.4	12.5	
1 wt.% SWCNTs	1.1×10^{-6}	9.4×10^{-7}	7.1×10^{-7}	4.8×10^{-7}	2.8×10^{-7}	~ 22
2 wt.% SWCNTs	2.0×10^{-6}	1.9×10^{-6}	1.7×10^{-6}	1.4×10^{-6}	1.0×10^{-6}	~ 7

The microfibers coupons could be used as real tensile strain sensors. The epoxy adhesive pads enable to attach the sensor to a structure (Figure 6.4g) while the freestanding geometry eludes any parasitic effects (local buckling) between the two ends. The geometry of the sensor can be easily tailored, depending on the applications to either sense tensile local strains (e.g., short microfibers) or overall strains (e.g., long microfibers like neurons). Diameter and number of the microfibers also can be controlled by the extrusion nozzle and the deposition robot. Interestingly, the sensor can be fabricated directly on the structure using the flexible UV-DW technique. However, the direct deposition of the sensor elements is possible only if the thickness of structures is smaller than 50 mm (i.e., maximum distance between the extrusion nozzle and the deposition platform of the deposition robot). It is worth noting that the microfibers sensor may find other applications such as a force sensor to measure small tension loads.

6.3.3.2. Microsprings network

Microsprings networks were manufactured with the aim of fabricating a freestanding strain sensor capable of sensing out-of-plane strains. Figure 6.5 presents various aspects related to the electromechanical testing of the nanocomposite microsprings networks. Figure 6.5a shows a SEM image of a typical network consisting of four identical springs with five coils. The first and last coils were flat in order to attach the aluminum pads for electromechanical testing. The final sensor geometry is shown in Figure 6.5b. The springs were arranged in rectangular array for

structural stability. The manufactured springs geometry matched the programmed robot's paths, which shows the high fidelity of the UV-DW fabrication technique. Figure 6.5c is a representative SEM image of the nanocomposite filament surface. The filament's diameter was ~ 130 μm, which is larger than that of the extrusion nozzle due to material swelling.

Figure 6.5d shows force–displacement curves achieved for the microsprings networks under compression. The specific rigidity of the networks was increased (by 28%) with the increase of SWCNTs loading to 2 wt%. Similar to the microfibers tensile experiments, the current was measured under applied voltage between two aluminum pads (top and bottom of the network) at seven different displacements as shown in Figures 6.5e and 6.5f (only the curves for three displacements are shown) for different nanotube loadings used. Table 6.2 summarizes the electrical conductivity of the springs for different displacements under compressive loads. As for microfibers, a linear relationship is obtained. The microsprings network electrical conductivity increased under compressive displacements. This might be due to the increased probability for SWCNTs to be in contact, facilitating electron transfer.

Figure 6.5g shows the microsprings networks electromechanical sensitivity. The results show that gauge factors of 3.1 and 2.2 were obtained for the sensor with 1 wt.% and 2 wt.% nanotube loadings, respectively. These values could be improved by optimizing the number and diameter of coils and the filaments diameter as well as the nanotube concentration. The desired spring geometry could be easily programmed and fabricated using the UV-DW technique. Although this technique enables to fabricate longer springs, this type of sensor cannot be used for large structures because of fabrication limitations. The microsprings network sensor could be used as a potential accurate scale to measure very small weights and find other applications in micro electromechanical systems.

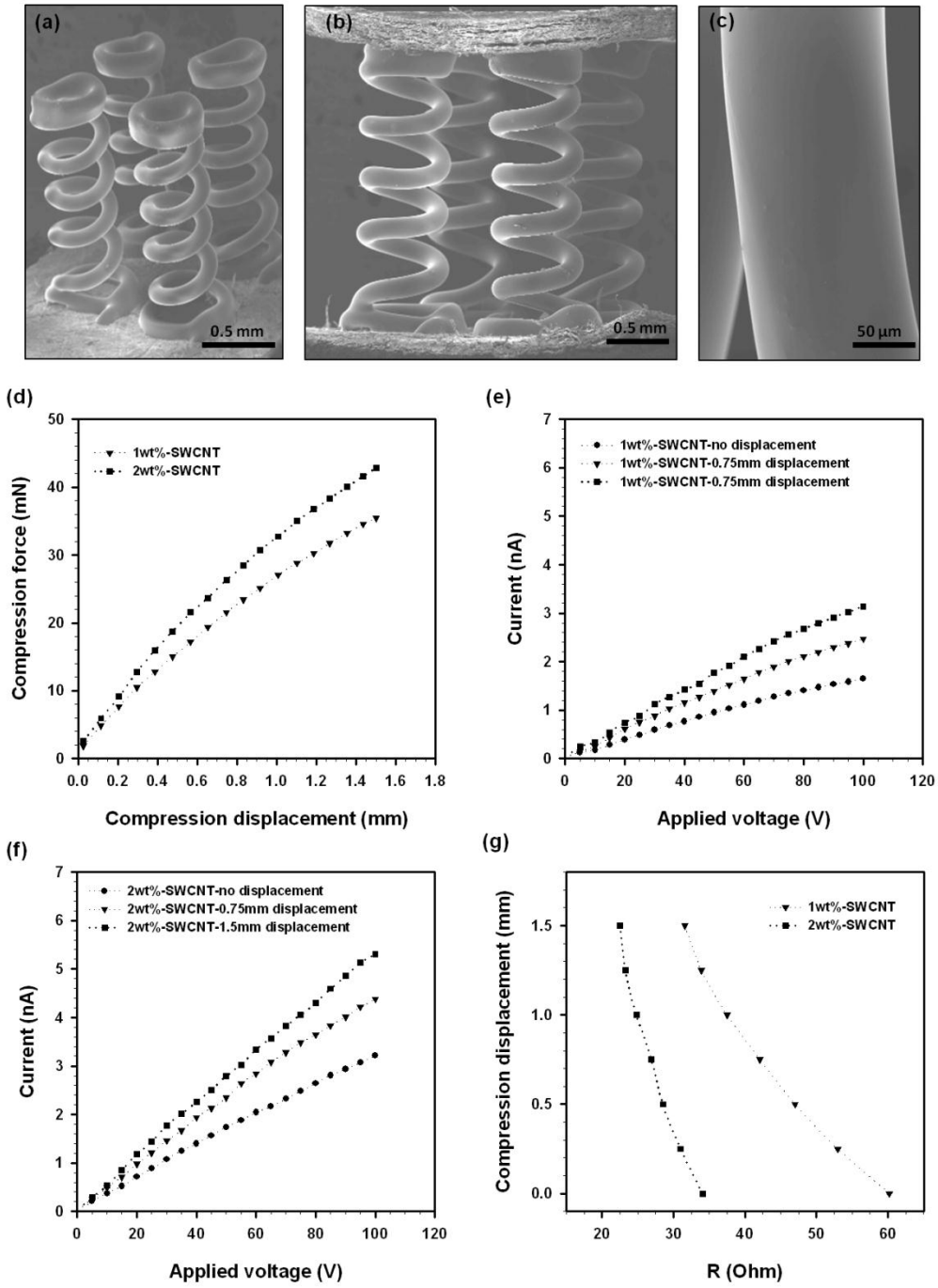

Figure 6.5 Nanocomposite microsprings electromechanical characterization: (a) SEM image of a typical fabricated specimen consisting of four freestanding microsprings, (b) SEM image of the final configuration of the sensor (a circular pad on the top), (c) filament surface SEM image, (d) typical force–displacement curves, and (e) and (f) measured current upon voltage application between two aluminum pads for the nanocomposite microfibers respectively at 1wt% and 2wt% SWCNTs loadings and (g) displacement-resistivity correlated curves based on electrical resistivity changes for the microsprings network.

Table 6.2 Electrical conductivity changes for the microsprings network under applied displacements.

Electrical conductivity at different displacements ($S.cm^{-1}$)							
Displacement (mm)	0	0.25	0.5	0.75	1	1.25	1.5
1 wt.% SWCNTs	9.9×10^{-7}	1.0×10^{-6}	1.2×10^{-6}	1.5×10^{-6}	1.6×10^{-7}	1.8×10^{-6}	2.0×10^{-6}
2 wt.% SWCNTs	1.9×10^{-6}	2.0×10^{-6}	2.3×10^{-6}	2.6×10^{-6}	2.8×10^{-6}	3.0×10^{-6}	3.2×10^{-6}

6.4. Conclusions

Two 3D-patterned freestanding nanocomposite strain sensors were manufactured with UV-DW technique. The nanocomposite-based sensors electromechanical sensitivities were evaluated under tension and compression. A sufficient control of the sensors geometries provided by patterning small-diameter nanocomposite microfibers enabled to reach a fairly-high electromechanical sensitivity (i.e., gauge factor: ~22). Additionally, the results are thought to be more reliable since the freestanding geometry of the sensors may reduce the effect of undesirable stimulus on the results. Higher sensitivity might be achieved at lower nanotube loadings close to their percolation threshold. The contribution of the geometry such as smaller diameter could be easily maximized using the flexible UV-DW technique. Since the strain sensors manufactured here are as examples of 3D MEMS sensors, any other complex pattern for sensing components or other applications in microelectronics such as electromagnetic shielding could be manufactured using this technique.

6. Acknowledgements

The authors acknowledge the financial support from FQRNT (Le Fonds Québécois de la Recherche sur la Nature et les Technologies). Prof. El Khakani acknowledges also the financial support from NSERC (National Science Engineering Research Council of Canada) and Plasma-Québec (le Réseau Stratégique du FQRNT sur la Science et Technologies des Plasmas). The

authors would like to thank the technical support of Dr. B. Aissa from INRS and also Dr. K. Laaziri from Laboratoire de recherche sur les nanostructures et interfaces conductrices for the electrical measurements.

6. References

[1] Chou TW, Li C and Thostenson E T 2008 *Compos. Sci. Technol.* **68**, 1227.

[2] Culpepper M L and Cullinan M A 2010 *Phys. Rev. B.* 82, 11.

[3] Hu N, Karube Y, Yan C, Masuda Z and Fukunaga H 2008 *Acta Materialia* **56**, 2929.

[4] Hu N, Yin G, Karube Y, Liu Y L, Li Y and Fukunaga H. 2011 *J. Compos. Mat.* **45**, 1315.

[5] Ji T S, Jung S Y, Xie J N and Varadan V K. 2007 *7th IEEE Conference on Nanotechnology*, **1-3**, 375.

[6] Kchit N and Bossis G. 2009 *J. Phys. D*. **42**.

[7] Kchit N, Lancon P and Bossis G. 2009 *J. Phys. D*. **42**.

[8] Liu Y, Chakrabartty S, Gkinosatis D S, Mohanty A K and Lajnef N. *2007 IEEE Biomedical Circuits and Systems Conference* **119**, 22.

[9] Liu Z M, An G M, Na N, Zhang X R, Miao Z J and Miao S D 2007, *Nanotechnology*, **18**, 435307.

[10] Park Y B, Pham G T, Liang Z, Zhang C, Wang B. 2008, *Composite Part B*, **39**, 209.

[11] Schulte K, Schueler R and Joshi S P. 2001, *Compos. Sci. Technol.* **61**, 921.

[12] Bethune D S, Kiang C H, Devries M S, Gorman G, Savoy R and Vazquez J 1993, *Nature*, **363**, 605.

[13] Tans S J, Devoret M H, Dai H J, Thess A, Smalley R E and Geerligs L J. 1997, *Nature*, **386**, 474.

[14] Baughman R H, Zakhidov A A and de Heer W A. 2002, *Science*, **297**, 787.

[15] Ashrafi B, Hubert P and Vengallatore S. 2006, *Nanotechnology*, **17**, 4895.

[16] Murugaraj P and Mainwaring D. 2011, *Electronic Functionality of Nanocomposites*, **23**, 549.

[17] Singh G, Rice P, Mahajan R L. 2007, *Nanotechnology*, **18**, 47.

[18] Stampfer C, Helbling T, Obergfell D, Schoberle B, Tripp M K and Jungen A. 2006, *Nano Lett.* **6**, 233.

[19] Stampfer C, Jungen A and Hierold C. 2006, *IEEE Sens. J.,* **6**, 613.

[20] Murugaraj P, Mainwaring D E and Mora-Huertas N. 2009, *Compos. Sci. Technol.* **69**, 2454.

[21] Kawata S, Sun H B, Tanaka T and Takada K. 2001, *Nature*, **412**, 697.

[22] Meeusen W, Clijnen J, Reynaerts D, Van Brussel H and Puers R. 2003, *IEEE Sens. J.*, **3**, 632.

[23] Lebel L L, Aissa B, El Khakani M A and Therriault D. 2010, *Adv. Mat.* **22**, 592.

[24] Braidy N, El Khakani M A and Botton G A. 2002, *Carbon*, **40**, 2835.

[25] Le Borgne V, Aissa B, Mohamedi M, Kim Y A, Endo M and El Khakani M A. *J. Nanopart. Res.*DOI: 10.1007/s11051-011-0409-9.

[26] Bruneaux J, Therriault D and Heuzey M C. 2008, *J. Micromech. Microeng.* **18**, 11.

Moniruzzaman M, Du F M, Romero N and Winey K I. 2006, *Polymer*, **47**, 293.

[27] Lebel L L, Aissa B, El Khakani M A and Therriault D. 2010, *Compos. Sci. Technol.* **70**, 518.

[28] Hobbie E K, Obrzut J, Kharchenko S B, Grulke E A. 2006, *J. Chem. Phys.* **125**, 4.

[29] Rahatekar S S, Koziol K K K, Butler S A, Elliott J A, Shaffer M S P, Mackley M R. 2006, *J. Rheol*. **50**, 599.

[30] Thostenson E T, Chou T W. 2006, *Carbon*. **44**, 3022.

[31] Farahani D R, Dalir H, Aissa B, El Khakani M A, Levesque M, Therriault D. 2011, *Composites: Part A.* DOI: 10.1016/j.compositesa.2011.08.016.

[32] Gojny F H, Wichmann M H G, Fiedler B, Schulte K. 2005, *Compos. Sci. Technol.* **65**, 2300.

CHAPTER 7: General Discussion

The general discussion is divided into three sections. First, the different procedures used for the nanocomposite preparation is discussed. Then, two different approaches used to manufacture 3D nanocomposite microstructures and their applications are discussed.

7.1. Incorporation of CNT into the epoxy matrix

One of the main objectives of the thesis was to homogeneously disperse CNTs into an epoxy matrix. With strong van der Waals attractions between the nanotubes, they are typically held together as bundles. Moreover, they have very low solubility in most of solvents. In addition, their high aspect ratio and high flexibility increase their tendency to exist as aggregates when mixed with a polymer matrix. All nanocomposite processing strategies aim at dispersing CNTs individually into the matrix in order to improve resulting nanocomposite properties. Although nanotube covalent functionalization improves their dispersion and their interfacial interaction with the matrix, it may damage nanotubes structural integrity and decrease nanotubes electrical conductivity.

Here an efficient mixing procedure was applied to disperse SWCNTs into an epoxy matrix and was described in chapters 4-7. A nanotube functionalization method was used for improving nanotube dispersion without significant damaging of CNTs. This method consists of a controlled acid purification (i.e., treatment duration) and a non-covalent functionalization with a surfactant. First, high-quality SWCNTs were produced by the UV-laser ablation method and were then subjected to a chemical purification treatment to remove the impurities. The duration of acidic treatment was effectively controlled in our purification process. The Raman spectroscopy and X-ray photoelectron spectroscopy (XPS) proved the creation of carboxylic functional groups on the

surface of nanotubes. Meanwhile, non-covalent functionalization of SWCNTs using Zinc protoporphyrin IX as a surfactant was performed for additional interaction with the epoxy matrix. Subsequent functionalization using biomolecules was applied on the nanotubes surface. The biotin-grafted nanotubes are capable of interacting with epoxy groups in presence of streptavidin molecules by which chemical bridges between biofunctionalized-SWCNTs and epoxy matrix are formed (Chapter 5). Different mixing strategies including stirring, ultrasonication and high shear mixing were used to properly disperse nanotubes within the epoxy matrix. Morphological characterization on the nanocomposites revealed that the best dispersion is achieved when the biofunctionalized-SWCNTs are mixed with the epoxy using ultrasonication followed by three-roll mixing techniques. Superior mechanical improvement was also observed for the biofunctionalized-SWCNT nanocomposites when compared to those prepared with the purified-SWCNTs. The strong interfacial bonding between SWCNTs and epoxy molecules through the functional groups are thought to facilitate load transfer. However, remaining biomolecules between nanotubes may increase the interfacial electrical resistance (Hobbie, Obrzut et al. 2006). This may limits the utilization of these nanocomposites for some applications where higher electrical conductivity is required.

The presence of nanotube aggregates have been reported more or less in all works dealing with SWCNTs and epoxy matrices. Low viscosity of epoxy resins limits the application of huge shear forces to break nanotubes aggregates in the shear mixing methods. Since the viscosity of the resins varies with temperature, the temperature of the rotating rolls in three-roll mixer reduced using its cooling system by circulating cold water behind the rolls. Unfortunately, the nanotube aggregates are still observed and consequently the nanotube reinforcement is still far from its potential. It is believed that future works should focus mainly on nanotube debundling

before their incorporation into an epoxy matrix. An ultracentrifugation technique would be helpful to remove the larger aggregates before mixing with the matrix.

7.2. 3D-reinforced composites fabricated by micro-infiltration technique

Another objective of this work was to tailor overall nanocomposite properties by taking advantage of reinforcement patterning and orienting with a powerful and flexible micro-infiltration (injection) approach. This technique was shown to be a suitable technique for designing overall mechanical properties of a manufactured nanocomposite product for optimal conditions. To this end, epoxy composite beams reinforced with a complex 3D skeleton structure of nanocomposite microfibers were fabricated via micro-infiltration of carbon nanotube nanocomposites into a 3D porous microfluidic network as described in Chapter 4. In typical nanocomposite manufacturing methods, the reinforcements are randomly distributed throughout the matrix. Here, the microfibers 3D pattern was adapted to offer better performance under flexural solicitation by the positioning most of the reinforcing microfibers (i.e., nanotubes) at higher stress regions. This technique also enable to tailor temperature-dependent mechanical properties of these beams by co-patterning two epoxy resins with different mechanical properties and glass transition temperatures.

Several challenges were faced for the fabrication of these nanocomposite beams. Residual traces of fugitive ink (that acts as a lubricant) after removing it to build an empty microfluidic network led to a poor mechanical shear stress at the microfluidic channels wall. A suction of boiling distilled water followed by hexane was found an efficient method to completely remove the residual ink. Another issue was the creation of air bubbles during the micro-infiltration

process. A vacuum-assisted micro-infiltration technique was used in order to minimize the risk of bubble trapping.

In general, nanotube orientation increases their reinforcing effect in direction of their alignment. The present micro-injection method enabled also to align SWCNTs in the 3D microfluidic network by taking advantage of high shear flow combined with constraining effect in microfluidic channels as described in details in Chapter 5. The flow of nanocomposites under high shear condition caused the CNTs to be aligned in the direction of the flow where the degree of orientation directly depends on the extent of applied shear. Morphological studies revealed that the SWCNTs were preferentially aligned in the microchannels along the flow direction at the higher injection pressure. To further align the nanotubes, higher injection pressures (i.e., higher shear rate) and smaller-diameter microfluidic channels (i.e., higher constraining effect) could be employed. However, the fabrication of microchannels with smaller diameters (less than 50 μm) is quite challenging due to the ink instability during the fabrication of microfluidic networks.

The flexibility of this micro-injection method enables the utilization of different thermosetting materials and nanofillers in order to design functional composites for a wide variety of applications such as structural composites, internal damage detection and embedded organic flexible electronics. Highly conductive nanofillers with a proper dispersion and required loadings could be used to tailor the conductivity of resulting nanocomposite for these applications. The internal damage of composite containing conductive fillers could be detected by mapping the electrical conductivity (or impedance) information.

7.3. 3D nanocomposite microstructures fabricated by UV-DW

The fabrication of 3D nanocomposite microstructures implies several fabrication challenges. Standard microfabrication techniques such as photolithography method possess sufficient resolution to manufacture complex 3D nanocomposite microstructures for the application such as micro electromechanical systems. However, materials constraint such as transparency and low viscosity limits their applications for the fabrication of nanotube-based nanocomposites structures. The UV-DW is found to be a flexible, fast and cost-effective method for the fabrication of complex 3D nanocomposite microstructures. The UV-DW technique consists of the robotized deposition of extruded filaments. The nanocomposite was photo-polymerized within seconds after extrusion under UV exposure while the extrusion point was changed in three directions using a computer-controlled robot. UV-radiation intensity, extrusion pressure, photopolymerization kinetics and material viscosity are the main parameters that should be taken into account in order to build a desirable geometry. Extruded materials of moderate to high viscosities are necessary to create stable filaments. Interestingly, the incorporation of CNTs into low viscosity epoxy resins increases their viscosity and makes them suitable for use in this technique. High aspect ratio of nanotubes causes an increase of nanocomposite viscosity by forming a rheological percolation network at a specific nanotube concentration. However, the addition of high nanotube loadings decreases resin transparency and consequently photopolymerization rate (or the fabrication speed).

CNTs have generated considerable interest during the past few decades due to their sensing ability for sensors applications. Due to the size order of an individual nanotube or their bulk physical state (i.e., powder of entangled structures), manufacturing and manipulation of these materials is quite challenging. The incorporation of CNTs into UV-curable epoxy resins expands

their utilization in these applications (Chou et al. 2008; Culpepper et al. 2010). The manufacturing technique presented here opens new prospects for the achievement of cost-effective geometry-optimized nanocomposite microdevices for microelectronics applications (Chapters 5 and 6).

CHAPTER 8 - Conclusion and recommendations

SWCNTs are increasingly used to achieve multifunctional capabilities where they serve as an effective structural reinforcement, as well as large-surface platform for sensing purposes. The incorporation of SWCNTs into polymer matrices extends their utilization for a broad range of application such as high strength composite materials and microsensors. The resulting nanocomposite materials can be engineered to deliver optimal properties in micro- and macro-devices for a targeted application. However, device miniaturization and three-dimensional (3D) shape optimization have not reached their full potential, partly because of the lack of suitable manufacturing techniques.

In this thesis, different nanocomposite mixing strategies were used to address the nanocomposite processing challenges that involved nanotubes purification, surface functionalization and dispersion. A nanocomposite preparation procedure consisting of nanotube purification, their surface functionalization using biomolecules and nanocomposite mixing with ultrasonication and three-roll mixing was found to be an efficient mixing strategy to properly disperse nanotubes into an epoxy matrix. In addition, two manufacturing approaches; micro-infiltration and UV-assisted direct-write (UV-DW) were used for the fabrication of 3D nanocomposite-based microstructures with tailored overall properties. In the first method, SWCNTs-epoxy nanocomposite suspensions were injected into 3D interconnected microfluidic networks in order to fabricate composite beams reinforced with patterned-oriented nanotubes. The effectiveness of this manufacturing approach to design composites microstructures was systematically studied by using different epoxy resins. The temperature-dependent mechanical and flexural properties of the 3D-reinforced beams showed different features depending on the individual properties of the microfibers and surrounding epoxies. The technique enabled

nanotubes positioning at higher stress regions for optimal conditions. In addition, the nanotube orientation inside the microfluidic networks under shear flow was systematically studied at different shear conditions by applying different micro-infiltration pressures. A micromechanical model was used to evaluate the stiffness of the manufactured composite beams with different states of nanotubes orientation. The technique enabled to partially align nanotubes inside the channels by applying high micro-infiltration pressure. The stiffness values of the beams predicted by the micromechanical model for the case of partial orientation of nanotubes were close to the experimental data, indicating the efficiency of the present manufacturing method in orientation of CNTs within a polymer matrix. Due to the flexibility of the micro-infiltration method, various thermosetting polymer and their nanocomposites reinforced by other nanofillers such as nanoclay and nanosilver (in a wide range of viscosities) could be used either as microfibers or as a host matrix, depending on the composite final application. This manufacturing method opens new prospects for the design of thermosetting multifunctional composite materials for a wide variety of applications such as internal damage detection and embedded organic flexible electronics.

The UV-DW technique was used to fabricate 3D freestanding microstructures using UV-curable nanocomposites. The viscosity characterization revealed that the addition of CNTs with a proper dispersion tailored the rheological behavior of resulting nanocomposite, suitable for the use in the UV-DW technique. Two 3D-patterned freestanding nanocomposite strain sensors were manufactured with this technique. A sufficient control of the sensors geometries enabled to reach a fairly-high electromechanical sensitivity, especially for lower nanotube loadings when compared to traditional metallic or nanocomposite films. The contribution of the geometry such as smaller diameter could be easily maximized using the flexible UV-DW technique. Since the

strain sensors manufactured here are as examples of 3D MEMS sensors, other complex pattern for sensing components or other applications in microelectronics such as electromagnetic shielding could be manufactured using this technique.

The obtained results on both nanocomposite preparation and fabrication of 3D nanocomposite structures constitute an important step forward to extend the utilization of nanocomposite materials in a broad range of technological applications. At the same time they also point out the necessity for future works. Future nanocomposite mixing strategies should concentrate on nanotubes debundling before mixing with an epoxy matrix in order to achieve a fully dispersed state. A centrifugation technique would be helpful to remove the larger aggregates before mixing the SWCNTs with the polymer. In addition, since the attraction of metallic and semiconductive nanotubes toward different surfactants is selective, using a proper co-surfactant being able to separate the remaining aggregates would help to properly disperse nanotubes in the matrix.

Regarding the nanotubes biofunctionalization, biofunctionalized-SWCNTs are capable of capturing other biomolecules such as streptavidin molecules. The incorporation of the biofunctionalized-SWCNTs into a UV-curable epoxy enables to easily manipulate these functional nanotubes for potential biosensor applications. However, when the nanotubes embedded with the epoxy, the streptavidin molecules do not have access to the biotin molecules. Probably adding a fugitive material being able to be extracted later as a third phase to the nanocomposite might be a solution. The material extraction may lead to the creation of nanopores where the available active biotin molecules could still be capable of interacting with streptavidin molecules and to detect them in their environment.

Regarding the fabrication of 3D freestanding nanocomposite strain sensors, their sensitivities would be improved by controlling the nanocomposite mixing process, nanotube loading and geometry of the sensors. It would be interesting to understand the influence of the surfactant (ZnPP) on the electrical conductivity and consequently on the sensors performance, since the presence of surfactant molecules between the nanotubes may increase the interfacial resistance.

REFERENCES

Abbasi, S., P. J. Carreau, et al. (2010). "Flow induced orientation of multiwalled carbon nanotubes in polycarbonate nanocomposites: Rheology, conductivity and mechanical properties." Polymer **51**(4): 922-935.

Advani, S. G., M. Chohra, et al. (2006). "Modeling of filtration through multiple layers of dual scale fibrous porous media." Polymer Composites **27**(5): 570-581.

Advani, S. G., M. Chohra, et al. (2007). "Filtration of particles through a single layer of dual scale fibrous porous media." Advanced Composites Letters **16**(6): 205-221.

Advani, S. G., C. Steggall-Murphy, et al. (2011). "A Model for Particle Deposition during Impregnation of Fibrous Porous Media." Journal of Porous Media **14**(5): 383-394.

Allaoui, A., S. Bai, et al. (2002). "Mechanical and electrical properties of a MWNT/epoxy composite." Composites Science and Technology **62**(15): 1993-1998.

Andrews, R. and M. C. Weisenberger (2004). "Carbon nanotube polymer composites." Current Opinion in Solid State & Materials Science **8**(1): 31-37.

Ashrafi, B., P. Hubert, et al. (2006). "Carbon nanotube-reinforced composites as structural materials for microactuators in microelectromechanical systems." Nanotechnology **17**(19): 4895-4903.

Atashbar, M. Z., B. Bejcek, et al. (2004). "Carbon nanotube based biosensors." Proceedings of the Ieee Sensors 2004, Vols 1-3: 1048-1051.

Bachilo, S. M., M. S. Strano, et al. (2002). "Structure-assigned optical spectra of single-walled carbon nanotubes." Science **298**(5602): 2361-2366.

Bai, J. and C. Lijie (2006). "The reinforcement role of carbon nanotubes in epoxy composites with different matrix stiffness." Composites Science and Technology **66**(3-4): 599-603.

Baker, S. E., W. Cai, et al. (2002). "Covalently bonded adducts of deoxyribonucleic acid (DNA) oligonucleotides with single-wall carbon nanotubes: Synthesis and hybridization." Nano Letters **2**(12): 1413-1417.

Bandow, S., S. Asaka, et al. (1998). "Effect of the growth temperature on the diameter distribution and chirality of single-wall carbon nanotubes." Physical Review Letters **80**(17): 3779-3782.

Barrera, E. V., J. Zhu, et al. (2004). "Reinforcing epoxy polymer composites through covalent integration of functionalized nanotubes." Advanced Functional Materials **14**(7): 643-648.

Baughman, R. H., A. A. Zakhidov, et al. (2002). "Carbon nanotubes - the route toward applications." Science **297**(5582): 787-792.

Bethune, D. S., C. H. Kiang, et al. (1993). "Cobalt-Catalyzed Growth of Carbon Nanotubes with Single-Atomic-Layerwalls." Nature **363**(6430): 605-607.

Bo, X. Z., C. Y. Lee, et al. (2005). "Carbon nanotubes-semiconductor networks for organic electronics: The pickup stick transistor." Applied Physics Letters **86**(18):182102.

Braidy, N., M. A. El Khakani, et al. (2002). "Carbon nanotubular structures synthesis by means of ultraviolet laser ablation." Journal of Materials Research **17**(9): 2189-2192.

Braidy, N., M. A. El Khakani, et al. (2002). "Effect of laser intensity on yield and physical characteristics of single wall carbon nanotubes produced by the Nd : YAG laser vaporization method." Carbon **40**(15): 2835-2842.

Braidy, N., M. A. El Khakani, et al. (2002). "Single-wall carbon nanotubes synthesis by means of UV laser vaporization." Chemical Physics Letters **354**(1-2): 88-92.

Breuer, O. and U. Sundararaj (2004). "Big returns from small fibers: A review of polymer/carbon nanotube composites." Polymer Composites **25**(6): 630-645.

Bruneaux, J., D. Therriault, et al. (2008). "Micro-extrusion of organic inks for direct-write assembly." Journal of Micromechanics and Microengineering **18**(11): 115020.

Bryning, M. B., M. F. Islam, et al. (2005). "Very low conductivity threshold in bulk isotropic single-walled carbon nanotube-epoxy composites." Advanced Materials **17**(9): 1186-89.

Carreau, P. J., S. Abbasi, et al. (2010). "Flow induced orientation of multiwalled carbon nanotubes in polycarbonate nanocomposites: Rheology, conductivity and mechanical properties." Polymer **51**(4): 922-935.

Chae, H. G. and S. Kumar (2006). "Rigid-rod polymeric fibers." Journal of Applied Polymer Science **100**(1): 791-802.

Che, J. F., W. Yuan, et al. (2009). "Epoxy Composite Fibers Reinforced with Aligned Single-Walled Carbon Nanotubes Functionalized with Generation 0-2 Dendritic Poly(amidoamine)." Chemistry of Materials **21**(8): 1471-1479.

Chen, J., M. A. Hamon, et al. (1998). "Solution properties of single-walled carbon nanotubes." Science **282**(5386): 95-98.

Chen, W., H. Shen, et al. (2009). "Basalt fiber–epoxy laminates with functionalized multi-walled carbon nanotubes." Composites: Part A **40**: 1082-1089.

Chen, X. L. and Y. J. Liu (2004). "Square representative volume elements for evaluating the effective material properties of carbon nanotube-based composites." Computational Materials Science **29**(1): 1-11.

Chiang, I. W., B. E. Brinson, et al. (2001). "Purification and characterization of single-wall carbon nanotubes." Journal of Physical Chemistry B **105**(6): 1157-1161.

Chou, T. W., C. Li, et al. (2008). "Sensors and actuators based on carbon nanotubes and their composites: A review." Composites Science and Technology **68**(6): 1227-1249.

Chronakis, I. S. (2005). "Novel nanocomposites and nanoceramics based on polymer nanofibers using electrospinning process - A review." Journal of Materials Processing Technology **167**(2-3): 283-293.

Coleman, J. N., U. Khan, et al. (2006). "Small but strong: A review of the mechanical properties of carbon nanotube-polymer composites." Carbon **44**(9): 1624-1652.

Coleman, J. N., U. Khan, et al. (2006). "Mechanical reinforcement of polymers using carbon nanotubes." Advanced Materials **18**(6): 689-706.

Culpepper, M. L. and M. A. Cullinan (2010). "Carbon nanotubes as piezoresistive microelectromechanical sensors: Theory and experiment." Physical Review B **82**(11).

Dai, H. J., R. J. Chen, et al. (2001). "Noncovalent sidewall functionalization of single-walled carbon nanotubes for protein immobilization." Journal of the American Chemical Society **123**(16): 3838-3839.

Decker, C. (1996). "Photoinitiated crosslinking polymerisation." Progress in Polymer Science **21**(4): 593-650.

Dharap, P., Z. L. Li, et al. (2004). "Nanotube film based on single-wall carbon nanotubes for strain sensing." Nanotechnology **15**(3): 379-382.

dos Santos, A. S., T. D. N. Leite, et al. (2008). "Morphology, thermal expansion, and electrical conductivity of multiwalled carbon nanotube/epoxy composites." Journal of Applied Polymer Science **108**(2): 979-986.

Du, F. M., J. E. Fischer, et al. (2005). "Effect of nanotube alignment on percolation conductivity in carbon nanotube/polymer composites." Physical Review B **72**(12):121404.

Du, F. M., R. C. Scogna, et al. (2004). "Nanotube networks in polymer nanocomposites: Rheology and electrical conductivity." Macromolecules **37**(24): 9048-9055.

Dumitrescu, L., N. R. Wilson, et al. (2007). "Functionalizing single-walled carbon nanotube networks: Effect on electrical and electrochemical properties." Journal of Physical Chemistry C **111**(35): 12944-12953.

Ear, Y. and E. Silverman (2007). "Challenges and opportunities in multifunctional nanocomposite structures for aerospace applications." Mrs Bulletin **32**(4): 328-334.

Eshelby, J. D. (1957). "The determination of the elastic field of an ellipsoidal inclusion." Proceedings of the Royal Society of London A **241**(1226): 376-396.

Fan, Z. H. and S. G. Advani (2005). "Characterization of orientation state of carbon nanotubes in shear flow." Polymer **46**(14): 5232-5240.

Fisher, J. P., D. Dean, et al. (2001). "Photoinitiated polymerization of biomaterials." Annual Review of Materials Research **31**: 171-181.

Frishfeld, V., T. S. Lundstrom, et al. (2008). "Bubble motion through non-crimp fabrics during composites manufacturing." Composites Part a-Applied Science and Manufacturing **39**(2): 243-251.

Gojny, F. H., M. H. G. Wichmann, et al. (2006). "Evaluation and identification of electrical and thermal conduction mechanisms in carbon nanotube/epoxy composites." **47**(6): 2036-45.

Gojny, F. H., M. H. G. Wichmann, et al. (2005). "Influence of different carbon nanotubes on the mechanical properties of epoxy matrix composites - A comparative study." Composites Science and Technology **65**(15-16): 2300-2313.

Gojny, F. H., M. H. G. Wichmann, et al. (2004). "Carbon nanotube-reinforced epoxy-compo sites: enhanced stiffness and fracture toughness at low nanotube content." Composites Science and Technology **64**(15): 2363-2371.

Haddon, R. C., J. Sippel, et al. (2004). "Purification and separation of carbon nanotubes." Mrs Bulletin **29**(4): 252-259.

Haggenmueller, R., F. M. Du, et al. (2006). "Interfacial in situ polymerization of single wall carbon nanotube/nylon 6,6 nanocomposites." Polymer **47**(7): 2381-2388.

Hobbie, E. K., J. Obrzut, et al. (2006). "Charge transport in melt-dispersed carbon nanotubes." Journal of Chemical Physics **125**(4): 44712.

Hobbie, E. K., H. Wang, et al. (2003). "Orientation of carbon nanotubes in a sheared polymer melt." Physics of Fluids **15**(5): 1196-1202.

Hogberg, S. M. and T. S. Lundstrom (2011). "Motion of dispersed carbon nanotubes during impregnation of fabrics." Plastics Rubber and Composites **40**(2): 70-79.

Hu, N., Y. Karube, et al. (2008). "Tunneling effect in a polymer/carbon nanotube nanocomposite strain sensor." Acta Materialia **56**(13): 2929-2936.

Hu, N., G. Yin, et al. (2011). "A carbon nanotube/polymer strain sensor with linear and anti-symmetric piezoresistivity." Journal of Composite Materials **45**(12): 1315-1323.

Huang, Z. M., Y. Z. Zhang, et al. (2003). "A review on polymer nanofibers by electrospinning and their applications in nanocomposites." Composites Science and Technology **63**(15): 2223-2253.

Hubert, P., B. Ashrafi, et al. (2009). "Synthesis and characterization of carbon nanotube-reinforced epoxy: Correlation between viscosity and elastic modulus." Composites Science and Technology **69**(14): 2274-2280.

Hui, D., M. Chipara, et al. (2004). "Mechanical Properties of Carbon Nanotubes Composites." Journal of Computational and Theoretical Nanoscience **1**(2): 204-215.

Ijima, S. (1991). "Helical microtubules of graphitic carbon." Nature **354**: 56-58.

Ijima, S. (1991). "Helical microtubules of graphitic carbon." Nature **354**: 56-58.

Islam, M. F., E. Rojas, et al. (2003). "High weight fraction surfactant solubilization of single-wall carbon nanotubes in water." Nano Letters **3**(2): 269-273.

Ji, T. S., S. Y. Jung, et al. (2007). "Flexible Strain Sensors Based On Pentacene-Carbon Nanotube Composite Thin Films." 2007 7th Ieee Conference on Nanotechnology, Vol 1-3: 375-378.

Kchit, N. and G. Bossis (2009). "Electrical resistivity mechanism in magnetorheological elastomer." Journal of Physics D-Applied Physics **42**(10):105505.

Kchit, N., P. Lancon, et al. (2009). "Thermoresistance and giant magnetoresistance of magnetorheological elastomers." Journal of Physics D-Applied Physics **42**(10):105506.

Kharchenko, S. B., J. F. Douglas, et al. (2004). "Flow-induced properties of nanotube-filled polymer materials." Nature Materials **3**(8): 564-568.

Kim, B., J. Lee, et al. (2003). "Electrical properties of single-wall carbon nanotube and epoxy composites." Journal of Applied Physics **94**(10): 6724-6728.

Kim, W. J., M. L. Usrey, et al. (2007). "Selective functionalization and free solution electrophoresis of single-walled carbon nanotubes: Separate enrichment of metallic and semiconducting SWNT." Chemistry of Materials **19**(7): 1571-1576.

Kimura, T., H. Ago, et al. (2002). "Polymer composites of carbon nanotubes aligned by a magnetic field." Advanced Materials **14**(19): 1380-1383.

Kobuke, Y., A. Satake, et al. (2005). "Porphyrin - Carbon nanotube composites formed by noncovalent polymer wrapping." Chemistry of Materials **17**(4): 716-724.

Kong, J., N. R. Franklin, et al. (2000). "Nanotube molecular wires as chemical sensors." Science **287**(5453): 622-625.

Laberge Lebel, L. (2009). Fabrication de structures tridimensionnelles de nanocomposites polymeres charges de nanotubes de carbone a simple paroi. Mechanical Engineering. Montreal, Ecole Polytechnique **Docotor of philosoply**.

Laborde-Lahoz, P., Maser, W., Cano, P., Guzman de Villoria, R., Miravete, A. (2005). "Mechanical characterization of carbon nanotube composite materials. ." Mechanics of advanced materials and structures **12**(5): 13-19.

Le Borgne, V., B. Aissa, Mohamedi M., Kim Y. A., Endo M. and El Khakani M. A. (2010) "Pulsed KrF-laser synthesis of single-wall-carbon-nanotubes: effects of catalyst content and furnace temperature on their nanostructure and photoluminescence properties" Journal of Nanoparticle Research, **10**(04): 9.

Lebel, L., Aissa, B., El Khakani, M., Therriault, D. (2008). "Tridimensional Microstructures of C-SWNT Reinforced Polymer Nanocomposite by Means of a Microfluidic Infiltration Approach." Materials Research Society **1056**.

Lebel, L. L., B. Aissa, et al. (2010). "Preparation and mechanical characterization of laser ablated single-walled carbon-nanotubes/polyurethane nanocomposite microbeams." Composites Science and Technology **70**(3): 518-524.

Lebel, L. L., B. Aissa, et al. (2010). "Ultraviolet-Assisted Direct-Write Fabrication of Carbon Nanotube/Polymer Nanocomposite Microcoils." Advanced Materials **22**(5): 592-596.

Lebel, L. L., B. Aissa, et al. (2009). "Three-dimensional micro structured nanocomposite beams by microfluidic infiltration." Journal of Micromechanics and Microengineering **19**(12): 125009.

Li, H. P., B. Zhou, et al. (2004). "Selective interactions of porphyrins with semiconducting single-walled carbon nanotubes." Journal of the American Chemical Society **126**(4): 1014-1015.

Li, N., Y. Huang, et al. (2006). "Electromagnetic interference (EMI) shielding of single-walled carbon nanotube epoxy composites." Nano Letters **6**(6): 1141-1145.

Li, X., H. Gao, et al. (2007). "Reinforcing mechanisms of single-walled carbon nanotube-reinforced polymer composites." Journal of Nanoscience and Nanotechnology **7**(7): 2309-2317.

Li, X. D., H. S. Gao, et al. (2007). "Reinforcing mechanisms of single-walled carbon nanotube-reinforced polymer composites." Journal of Nanoscience and Nanotechnology **7**(7): 2309-2317.

Li, Y., C. X. Chen, et al. (2008). "Electrical conductivity and electromagnetic interference shielding characteristics of multiwalled carbon nanotube filled polyacrylate composite films." Applied Surface Science **254**(18): 5766-5771.

Liska, R., M. Schuster, et al. (2007). "Photopolymers for rapid prototyping." Journal of Coatings Technology and Research **4**(4): 505-510.

Liu, J. Z., Q. S. Zheng, et al. (2005). "Mechanical properties of single-walled carbon nanotube bundles as bulk materials." Journal of the Mechanics and Physics of Solids **53**(1): 123-142.

Liu, Y., S. Chakrabartty, et al. (2007). "Multi-walled carbon nanotubes/poly(L-lactide) nanocomposite strain sensor for biomechanical implants." 2007 Ieee Biomedical Circuits and Systems Conference: 119-122.

Liu, Z. M., G. M. An, et al. (2007). "SnO2/carbon nanotube nanocomposites synthesized in supercritical fluids: highly efficient materials for use as a chemical sensor and as the anode of a lithium-ion battery." Nanotechnology **18**(43): 435707.

Lundstrom, T. S. (1997). "Measurement of void collapse during resin transfer moulding." Composites Part a-Applied Science and Manufacturing **28**(3): 201-214.

Lundstrom, T. S. and V. Frishfelds (2011). "Modelling of particle deposition during impregnation of dual scale fabrics." Plastics Rubber and Composites **40**(2): 65-69.

Lundstrom, T. S., B. R. Gebart, et al. (1993). "Void Formation in Rtm." Journal of Reinforced Plastics and Composites **12**(12): 1339-1349.

Luo, X. F., R. Q. Ou, et al. (2009). "A Thermoplastic/Thermoset Blend Exhibiting Thermal Mending and Reversible Adhesion." Acs Applied Materials & Interfaces **1**(3): 612-620.

Ma, A. W. K., F. Chinesta, et al. (2009). "The rheology and modeling of chemically treated carbon nanotubes suspensions." Journal of Rheology **53**(3): 547-573.

Maekawa, Z., H. Hamada, et al. (1989). "Lamination Theory of Composite-Material with Complex Fiber Orientation Distribution." Composite Structures 5: 701-714.

Meyyappan, M. (2005). Carbon nanotubes : science and applications. Boca Raton, Fl, CRC Press.

Mirfakhrai, T., R. Krishna-Prasad, et al. (2008). "Electromechanical actuation of single-walled carbon nanotubes: an ab initio study." Nanotechnology **19**(31): 315706.

Miyagawa, H. and L. T. Drzal (2004). "Thermo-physical and impact properties of epoxy nanocomposites reinforced by single-wall carbon nanotubes." Polymer **45**(15): 5163-5170.

Moisala, A., Q. Li, et al. (2006). "Thermal and electrical conductivity of single- and multi-walled carbon nanotube-epoxy composites." Composites Science and Technology **66**(10): 1285-1288.

Moniruzzaman, M., F. M. Du, et al. (2006). "Increased flexural modulus and strength in SWNT/epoxy composites by a new fabrication method." Polymer **47**(1): 293-298.

Montazeri, A., M. Sadeghi, et al. (2010). "Computational modeling of the transverse-isotropic elastic properties of single-walled carbon nanotubes." Computational Materials Science **49**(04): 544-551.

Moore, V. C., M. S. Strano, et al. (2003). "Individually suspended single-walled carbon nanotubes in various surfactants." Nano Letters **3**(10): 1379-1382.

Mori, T. and K. Tanaka (1973). "Average stress in matrix and average elastic energy of materials with misfitting inclusions." Acta Metallurgica **21**(5): 571-4.

Mura, T. (1982). Micromechanics of defects in solids, Springer.

Murakami, H., Nomura, T., Nakashima N. (2003). "Noncovalent porphyrin-functionalized single-walled carbon nanotubes in solution and the formation of porphyrin–nanotube nanocomposites." Chemical Physical Letters **378**: 481-485.

Murugaraj, P. and D. Mainwaring (2011). "Electronic Functionality of Nanocomposites." Advances in Diverse Industrial Applications of Nanocomposites, **23**: 549-578.

Nakashima, N. and T. Fujigaya (2007). "Fundamentals and applications of soluble carbon nanotubes." Chemistry Letters **36**(6): 692-697.

Nordlund, M., S. P. Fernberg, et al. (2007). "Particle deposition mechanisms during processing of advanced composite materials." Composites Part a-Applied Science and Manufacturing **38**(10): 2182-2193.

Odegard, G. M., T. S. Gates, et al. (2003). "Constitutive modeling of nanotube-reinforced polymer composites." Composites Science and Technology **63**(11): 1671-1687.

Okpalugo, T. I. T., P. Papakonstantinou, et al. (2005). "High resolution XPS characterization of chemical functionalised MWCNTs and SWCNTs." Carbon **43**(1): 153-161.

Park, J., S. Park, et al. (2007). "Thermal and mechanical properties of carbon fiber reinforced epoxy composites modified with CTBN and hydroxyl terminated polyester." Adv Polym Emerg Technol 568–72.

Park, Y. B., G. T. Pham, et al. (2008). "Processing and modeling of conductive thermoplastic/carbon nanotube films for strain sensing." Composites Part B-Engineering **39**(1): 209-216.

Patel, A. C., S. X. Li, et al. (2006). "In situ encapsulation of horseradish peroxidase in electrospun porous silica fibers for potential biosensor applications." Nano Letters **6**(5): 1042-1046.

Qian, D., G. J. Wagner, et al. (2002). "Mechanics of carbon nanotubes", in Handbook of nanoscience, engineering and technology". **55**(6): 495-532.

Rahatekar, S. S., K. K. K. Koziol, et al. (2006). "Optical microstructure and viscosity enhancement for an epoxy resin matrix containing multiwall carbon nanotubes." Journal of Rheology **50**(5): 599-610.

Ruther, M. G., F. Frehill, et al. (2004). "Characterization of covalent functionalized carbon nanotubes." Journal of Physical Chemistry B **108**(28): 9665-9668.

Sahoo, N. G., Y. C. Jung, et al. (2007). "Influence of carbon nanotubes and polypyrrole on the thermal, mechanical and electroactive shape-memory properties of polyurethane nanocomposites." Composites Science and Technology **67**(9): 1920-1929.

Salvetat, J. P., J. M. Bonard, et al. (1999). "Mechanical properties of carbon nanotubes." Applied Physics a-Materials Science & Processing **69**(3): 255-260.

Sandler, J. K. W., J. E. Kirk, et al. (2003). "Ultra-low electrical percolation threshold in carbon-nanotube-epoxy composites." Polymer **44**(19): 5893-5899.

Sandler, J. K. W., S. Pegel, et al. (2004). "A comparative study of melt spun polyamide-12 fibres reinforced with carbon nanotubes and nanofibres." Polymer **45**(6): 2001-2015.

Schadler, L. S., S. C. Giannaris, et al. (1998). "Load transfer in carbon nanotube epoxy composites." Applied Physics Letters **73**(26): 3842-3844.

Schjdt-Thomsen, J. and R. Pyrz (2001). "The Mori-Tanaka stiffness tensor: Diagonal symmetry, complex fibre orientations and non-dilute volume fractions." Mechanics of Materials **33**(10): 531-544.

Schjodt-Thomsen, J. and R. Pyrz (2001). "The Mori-Tanaka stiffness tensor: diagonal symmetry, complex fibre orientations and non-dilute volume fractions." Mechanics of Materials **33**(10): 531-544.

Schulte, K., R. Schueler, et al. (2001). "Damage detection in CFRP by electrical conductivity mapping." Composites Science and Technology **61**(6): 921-930.

Seyhan, A. T., F. H. Gojny, et al. (2007). "Rheological and dynamic-mechanical behavior of carbon nanotube/vinyl ester-polyester suspensions and their nanocomposites." European Polymer Journal **43**(7): 2836-2847.

Sgriccia, N. and M. Hawley (2007). "Thermal, morphological, and electrical characterization of microwave processed natural fiber composites." Compos Sci Technol **67**(9): 1986-1991.

Singh, G., P. Rice, et al. (2007). "Fabrication and mechanical characterization of a force sensor based on an individual carbon nanotube." Nanotechnology **18**(47): 475501.

Sinnott, S. B. and R. Andrews (2001). "Carbon nanotubes: Synthesis, properties, and applications." Critical Reviews in Solid State and Materials Sciences **26**(3): 145-249.

Snyder, G. J., J. R. Lim, et al. (2003). "Thermoelectric microdevice fabricated by a MEMS-like electrochemical process." Nature Materials **2**(8): 528-531.

Sotiropoulou, S. and N. A. Chaniotakis (2003). "Carbon nanotube array-based biosensor." Analytical and Bioanalytical Chemistry **375**(1): 103-105.

Stampfer, C., T. Helbling, et al. (2006). "Fabrication of single-walled carbon-nanotube-based pressure sensors." Nano Letters **6**(2): 233-237.

Stampfer, C., A. Jungen, et al. (2006). "Fabrication of discrete nanoscaled force sensors based on single-walled carbon nanotubes." Ieee Sensors Journal **6**(3): 613-617.

Stromberg, A., A. Karlsson, et al. (2001). "Microfluidic device for combinatorial fusion of liposomes and cells." Analytical Chemistry **73**(1): 126-130.

Su, P. G. and S. C. Huang (2006). "Electrical and humidity sensing properties of carbon nanotubes-SiO2-poly (2-acrylamido-2-methylpropane sulfonate) composite material." Sensors and Actuators B-Chemical **113**(1): 142-149.

Sun, L., G. L. Warren, et al. (2008). "Mechanical properties of surface-functionalized SWCNT/epoxy composites." Carbon **46**(2): 320-328.

Sun, Y. P., H. P. Li, et al. (2004). "Selective interactions of porphyrins with semiconducting single-walled carbon nanotubes." Journal of the American Chemical Society **126**(4): 1014-1015.

Taeger, S., L. Y. Xuang, et al. (2005). "Noncovalent sidewall functionalization of carbon nanotubes by biomolecules: Single-stranded DNA and hydrophobin." Electronic Properties of Novel Nanostructures **786**: 262-265.

Tanaka, T. M. a. K. (1973). "Average elastic energy of materials with misfitting inclusions." Acta metallurgica.

Tans, S. J., M. H. Devoret, et al. (1997). "Individual single-wall carbon nanotubes as quantum wires." Nature **386**(6624): 474-477.

Therriault, D., R. F. Shepherd, et al. (2005). "Fugitive inks for direct-write assembly of three-dimensional microvascular networks." Advanced Materials **17**(4): 395-399.

Therriault, D., S. R. White, et al. (2003). "Chaotic mixing in three-dimensional microvascular networks fabricated by direct-write assembly." Nature Materials **2**(4): 265-271.

Thostenson, E. T. and T. W. Chou (2006). "Processing-structure-multi-functional property relationship in carbon nanotube/epoxy composites." Carbon **44**(14): 3022-3029.

Valentini, L., D. Puglia, et al. (2008). "Use of plasma fluorinated single-walled carbon nanotubes for the preparation of nanocomposites with epoxy matrix." Composites Science and Technology **68**(3-4): 1008-1014.

Varadan, V. K., V. V. Varadan, et al. (1996). Three-dimensional polymeric and ceramic MEMS and their applications. Smart Structures and Materials 1996: Smart Electronics and MEMS, San Diego, CA.

Varadan, V. K., Xie, J., Ji, T. (2001). "Three dimensional MEMS devices with functionalized carbon nanotubes." BioMEMS and Smart Nanostructures, Proceeding of SPIE **4590**: 131-141.

Wachtman, J. "Mechanical properties of ceramics. New York: Wiley;1996 ".

Wang, D., G. Sun, et al. (2008). "Controllable biotinylated polyethylene-co-glycidyl methacrylate) (PE-co-GMA) nanofibers to bind streptavidin-horseradish peroxidase

(HRP) for potential biosensor applications." European Polymer Journal **44**(7): 2032-2039.

Wang, L. F. and Q. S. Zheng (2007). "Extreme anisotropy of graphite and single-walled carbon nanotube bundles." Applied Physics Letters **90**(15): 153113.

Wang, S., R. Liang, et al. (2008). "Reinforcing polymer composites with epoxide-grafted carbon nanotubes." Nanotechnology **19**(8): 085710.

Wang, S. R., Z. Y. Liang, et al. (2006). "Effective amino-functionalization of carbon nanotubes for reinforcing epoxy polymer composites." Nanotechnology **17**(6): 1551-1557.

Wescott, J. T., P. Kung, et al. (2007). "Conductivity of carbon nanotube polymer composites." Applied Physics Letters **90**(3): 033116.

Wilson, M., Kamali, K., Geoff, S., Michelle, S., Burkhard, R. (2002). NANOTECHNOLOGY: Basic Science and Emerging Technologies.

Winey, K. I., T. Kashiwagi, et al. (2007). "Improving electrical conductivity and thermal properties of polymers by the addition of carbon nanotubes as fillers." Mrs Bulletin **32**(4): 348-353.

Xiaodong, L., Hongsheng, G., Scrivens, W., Dongling, F., Xiaoyou, X., Sutton, M., Reynolds, A., Myrick, M. and M. M. (2004). "Nanomechanical characterization of single-walled carbon nanotubes reinforced epoxy composites." Nanotechnology **15**: 1416-1423.

Yu, M. F., O. Lourie, et al. (2000). "Strength and breaking mechanism of multiwalled carbon nanotubes under tensile load." Science **287**(5453): 637-640.

Zhao, J. X. and Y. H. Ding (2008). "Functionalization of single-walled carbon nanotubes with metalloporphyrin complexes: A theoretical study." Journal of Physical Chemistry C **112**(30): 11130-11134.

Zhou, G., S. Movva, et al. (2008). "Nanoclay and long-fiber-reinforced composites based on epoxy and phenolic resins." Journal of Applied Polymer Science **108**(6): 3720-3726.

Zhou, W., J. Vavro, et al. (2004). "Single wall carbon nanotube fibers extruded from super-acid suspensions: Preferred orientation, electrical, and thermal transport." Journal of Applied Physics **95**(2): 649-655.

Zhu, J., J. D. Kim, et al. (2003). "Improving the dispersion and integration of single-walled carbon nanotubes in epoxy composites through functionalization." Nano Letters **3**(8): 1107-1113.

Zhu, J., H. Q. Peng, et al. (2004). "Reinforcing epoxy polymer composites through covalent integration of functionalized nanotubes." Advanced Functional Materials **14**(7): 643-648.

APPENDIX

Appendix A

Carbon nanotubes/epoxy nanocomposites for UV-assisted direct-write fabrication of microstructures: mechanical and rheological studies

Rouhollah Dermanaki Farahani[1], Hamid Dalir[1], Vincent Le Borgne[2], Loick. A. Gautier[2], My Ali El Khakani[2], Martin Lévesque[1], and Daniel Therriault[1]*

[1]Laboratory of Multiscale Mechanics, Center for applied research on polymers (CREPEC), École Polytechnique de Montreal, C.P. 6079, succ. Centre-Ville, Montreal (QC), H3C 3A7 (Canada)

[2]Institut National de la Recherche Scientifique, INRS-Énergie, Matériaux et Télécommunications, 1650 Blvd. Lionel-Boulet, Varennes (QC), J3X 1S2 (Canada)

ABSRACT

We report on the preparation of biofunctionalized single-walled carbon nanotube (BF-SWCNT)/epoxy nanocomposites with different mixing strategies. The SWCNTs were first purified by acidic treatment and then functionalized by grafting biomaterials onto the SWCNTs surface. The BF-SWCNTs were dispersed within an epoxy resin by means of ultrasonication and/or three-roll mixing methods. It is found that the mixing procedure consisting of ultrasonication and three-roll mixing is an effective method to disperse nanotubes within epoxy matrix. The biomaterial-grafting of SWCNTs surfaces along with their fair dispersion led to a significant increase of viscosity of the nanocomposite suspensions which enabled the UV-assisted direct-write fabrication of microfibers suspended between two pads and 3D freeform

helicoidal microsprings. Mechanical characterization of the slender microfibers (150 μm diameter) at a nanotube load of 1wt%, under tension revealed considerable increase in both modulus (by ~93%) and strength (by 75%) compared to the values for pure epoxy resin. These mechanical improvements are believed to be a consequence of the biomaterial-grafting of the nanotubes surfaces which facilitate load transfer and their fairly-dispersion into the epoxy matrix. The manufactured nanocomposite microstructures containing BF-SWCNT could find applications in biosensors, where other biomaterials and hazardous gaseous can be detected by affecting the electrical conductivity of nanotube-reinforced nanocomposite microstructures.

INTRODUCTION

New materials as well as new methods for materials fabrication are increasingly being developed to achieve advances at the micro- and nanoscale for wide variety of technological applications such as micro electromechanical systems (MEMS) and organic electronics. In these applications, photopolymer nanocomposites reinforced with carbon nanotubes are among the highly promising materials compared to neat polymers for their enhanced mechanical [1] and electrical properties [2]. However, several fundamental challenges have still to be addressed in order to fabricate high-performance nanocomposite microdevices with the desired two-dimensional (2D) and three-dimensional (3D) patterns [3]. Most of the microfabrication techniques such as stereolithography and two-photon absorption have been limited by material constraints and/or confined to relatively thin device layouts [4].

Ultraviolet-assisted direct-write (UV-DW) [5] is an alternative technique to manufacture nanocomposite-based microdevices with a desired 3D patterned structure. The UV-DW technique consists of the robotized deposition of extruded filaments. The materials are photopolymerized under UV exposure while being extruded. The fast-curing of nanocomposite

materials enables the fabrication of 3D structures when the computer-controlled robot moves the dispensing apparatus along the x, y, and z axes. In this method, the moderate or high viscosity of the extruded material is necessary to maintain its filamentary form after being extruded [5,6]. Since high viscosity of the materials may constraint their flow through the fine extrusion nozzle, a shear-thinning behavior (i.e., a decrease of viscosity with an increase of shear forces inside the nozzle) is preferable. In addition to other interesting effects like improvements of mechanical properties, carbon nanotubes are capable of tailoring rheology of low viscosity thermosetting resins [7]. High aspect ratio of nanotubes causes an increase of nanocomposite viscosity by forming a rheological percolation network at a specific nanotube concentration. In addition, a homogeneous dispersion of nanotubes throughout the polymer matrix can considerably increase the viscosity of the nanocomposites as well as their mechanical properties [8]. For epoxy nanocomposites, various mixing methods such as sonication [9], high shear mixing in a three-roll mill mixer [10] or a twin-screw batch mixer [8] and their combinations have been used to disperse intrinsically entangled nanotubes within the polymer matrix. However, new progresses are needed to achieve the individual dispersion of the nanotubes.

In this paper, different mixing strategies were used to prepare UV-curable epoxy nanocomposites reinforced with biofunctionalized single-walled carbon nanotubes (BF-SWCNTs). The SWCNTs were first purified by acidic treatment and then functionalized by grafting biomaterials onto the SWCNTs surface. The BF-SWCNTs were then dispersed within the epoxy resin by means of three-roll mixing and/or ultrasonication methods. The nanotubes dispersion was characterized using an optical microscope. The increase of viscosity of the nanocomposites due to the proper dispersion of BF-SWCNTs enabled to fabricate microstructures using UV-DW fabrication technique. The mechanical performance of the

nanocomposite microstructures under tension or compression loadings was characterized in order to assess the reinforcing effect of BF-SWCNTs.

EXPERIMENTAL DETAILS

SWCNTs Functionalization and Nanocomposite Preparation

SWCNTs were synthesized by the UV-laser ablation (248 nm, 20 ns, 400 mJ) method using a Co/Ni-doped graphite target in an argon atmosphere at a temperature of 1150°C. The as-produced SWCNTs were then subjected to chemical purification treatment to remove the impurities like metal catalyst particles and covalently functionalize the SWCNTs by the attachment of carboxylic groups at their surface (more experimental details on the KrF-laser synthesis and effects of key growth parameters can be found elsewhere [11,12]). The SWCNTs biofunctionalization procedure relies on these carboxylic groups based on a method which inspired from the work done by Wang et al. [13]. The desired amounts of purified SWCNTs and 1,3-diaminopropane 99% (D23602, Sigma-Aldrich) were added to a solution of 0.1 mM of zinc protoporphyrin IX (ZnPP, Sigma-Aldrich) in acetone. The suspension was sonicated in an ultrasonic bath (Ultrasonic cleaner 8891, Cole-Parmer) for 1 h at room temperature, followed by shaking using a mixer/shaker (Spex CertiPrep 8000M Mixer/Mill) for 12 h at room temperature. The resulting aminated purified SWCNTs solution were then added into a solution of 30 mL acetone containing desired amounts of biotin and N,N’-diisopropylcarbodiimide 99% (DIC, D125407, Sigma-Aldrich). Biotinylation of the aminated SWCNTs were subsequently performed by shaking the resulting mixture using the mixer/shaker for 12 h at room temperature.

The nanocomposite materials were prepared by mixing an Ultraviolet curable epoxy (UV-epoxy, UVE, UV15DC80, Master Bond Inc.) and BF-SWCNTs at a load of 1 wt%). The desired amount of the streptavidin solution (1 mL 10 μg/mL, S4762, from streptomyces avidinii, Sigma-

Aldrich) and the epoxy were mixed with the nanotube solution over a magnetic stirring hot plate (Model SP131825, Barnstead international) at 50°C for 4 h. After stirring, the nanocomposite mixture was sonicated for 2 h. The mixture was let at room temperature 24 h to evaporate the solvent. The residual trace of solvent was evaporated by heating the nanocomposite mixture at 30°C for 12 h and at 50°C for 24 h in a vacuumed-oven (Cole Parmer). The nanocomposites were subsequently subjected to final high shear mixing through a very small gap in a three-roll mixer (Exakt 80E, Exakt Technologies) for several times [10]. The gaps between the rolls varied in three batch-wise progressing steps (10 passes each) with three different gaps at 25 µm, 10 µm and 5 µm, respectively. The speed of the apron roll was set at 250 RPM. The final mixture was then degassed under vacuum for 12 h. The sonicated nanocomposite suspensions (without three-roll mixing) were also prepared in order to assess the effect of high shear mixing on the nanotube dispersion.

UV-DW Technique for Characterization and Fabrication

The UV-DW technique was used for viscosity characterization, microstructures fabrication and sample preparation for morphological characterization. The UV-DW technique consists of a computer-controlled robot (I & J2200-4, I & J Fisnar) that moves a dispensing apparatus (HP-7X, EFD) along the x, y and z axes. Figure 1 schematically represents the UV-DW fabrication of microfibers. The extruded materials are photopolymerized under UV exposure using two high-intensity UV light-emitting diodes (LED, NCSU033A, Nichia) while being deposited.

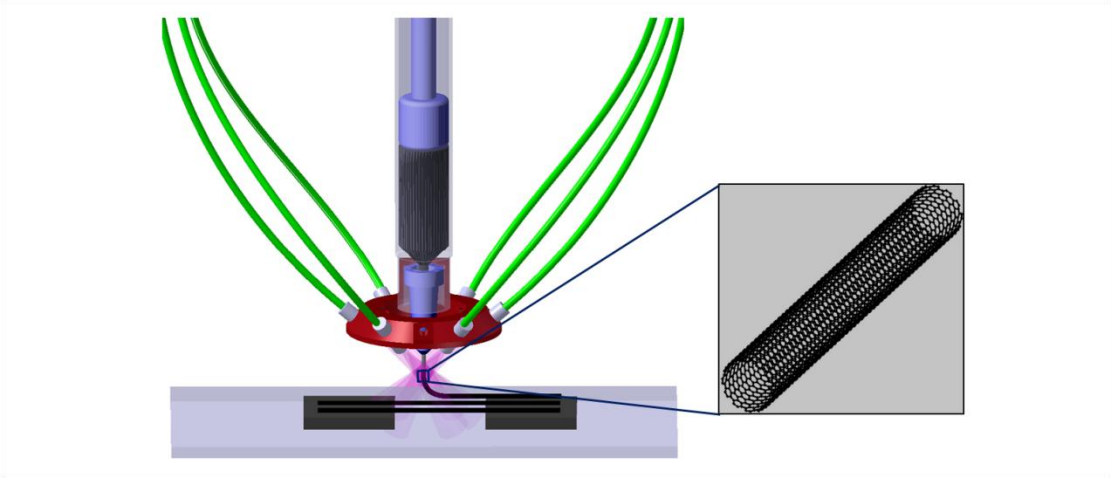

Figure 1. Schematic representation of the UV-assisted direct-writing of nanocomposite microfibers.

For optical imaging purposes, ~20 μm-thick films of the nanocomposites were fabricated via their direct deposition on a glass substrate. The optical images were captured using an optical microscope (BX-61, Olympus) and image analysis software (Image-Pro Plus V5, Media Cybernetics).

The process-related apparent viscosity of the pure UV-epoxy and its associated nanocomposites were measured from an experimental method based on capillary viscometry [6,14]. To obtain different shear conditions, ten continuous filaments of materials were extruded through a micro-nozzle (5132-0.25-B, Precision Stainless Steel Tips, EFD, Length = ~20 mm and internal diameter = 100 μm) at five different pressures over a glass substrate with a calibrated deposition speed. The flow rates of the materials were calculated from the cross-section of the filaments and the deposition speed controlled by the dispensing apparatus. The cross-section area of the filaments was measured using the optical microscope and the image analysis software. The process-related apparent viscosity and the process-related apparent shear rate were calculated from capillary viscometry equations including Rabinowitsch correction.

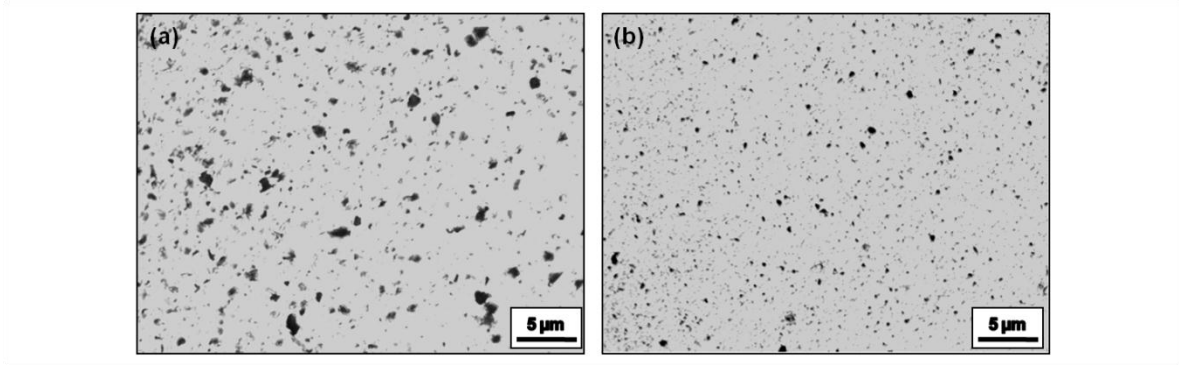

Figure 2. Optical microscopic image of a 20-µm thick film of nanocomposites containing 1 wt% BF-SWCNT prepared by (a) sonication and (b) sonication and three-roll mill mixing.

Nanocomposite microfibers with a diameter of 150 µm were fabricated over a 6 mm gap between two rectangular nanocomposite pads as shown in Figure 1. Moreover, a network consisting of four parallel microsprings was fabricated. The micro-coils with a filament diameter of 150 µm comprised 7 turns for a total height of 6 mm with the middle coils having a pitch of 1mm. The first and last turns were designed to be flat to provide support for mechanical solicitation. Mechanical properties (i.e., tensile modulus, strength and elongation at break) of the nanocomposites microfibers were characterized in a dynamic mechanical analyzer (DMA, DMA2980, TA instruments) using a film tension clamp. The microfibers were tested with a constant loading rate adjusted to reach failure within 20 ± 3 s according to the ASTM D2256 standard. The mechanical response of the nanocomposite microsprings under compression were also characterized in the DMA using a compression fixture at a load rate of 5 mN/min^{-2}.

Nanocomposite Characterization

The presence of functional groups on the surface of SWCNTs was assessed using different characterization methods including Raman spectroscopy, photoelectron spectroscopy (XPS) and TEM observation (results are not shown here). The nanotube dispersion was assessed by optical

imaging of nanocomposite films using the optical microscope. Figure 2a shows a representative optical image of the nanocomposites prepared by sonication technique. The dark spots are believed to be nanotube aggregates and/or carbonaceous materials. A combination of sub-micron and micron-size aggregates of up to ~5μm-diameter is observed. This indicates that the sonication was not an efficient method to obtain a well-dispersed nanocomposite. Figure 2b shows the optical image of nanocomposite prepared by sonication upon subsequent three-roll mixing. The size of large aggregates diminished when the nanocomposite suspension subjected to the high shear mixing and a relatively uniform dispersion was obtained. The relatively better dispersion of nanotubes after high shear mixing could be attributed to the enormous shear forces caused by the rotation of rolls with different speeds and also the small gaps between rolls in three-roll mixer.

The viscosity of materials is a critical factor in UV-DW technique and also is a good indicator of the quality of nanotube dispersion. Figure 3 shows the process-related apparent viscosity (η_{app}) with respect to the process-related apparent shear rates $(\dot{\gamma}_{app})$ induced by the extrusion of the pure UV-epoxy and its associated nanocomposites for five extrusion pressures. A constant η_{app} of ~12 Pa.s is observed for the UV-epoxy, indicating Newtonian behavior in range of the shear rates studied. For the sonicated nanocomposite, the incorporation of 1 wt% BF-SWCNTs to the pure resin resulted in a nine times increase in the η_{app} of the UV-epoxy at low $\dot{\gamma}_{app}$ and the apparition of a shear-thinning behavior. High shear mixing led to further increase (by 17 times) of the viscosity of the nanocomposites. High aspect ratio of our carbon nanotubes and their proper dispersion within the matrix are thought to be responsible of the significant increase of viscosity of the nanocomposites.

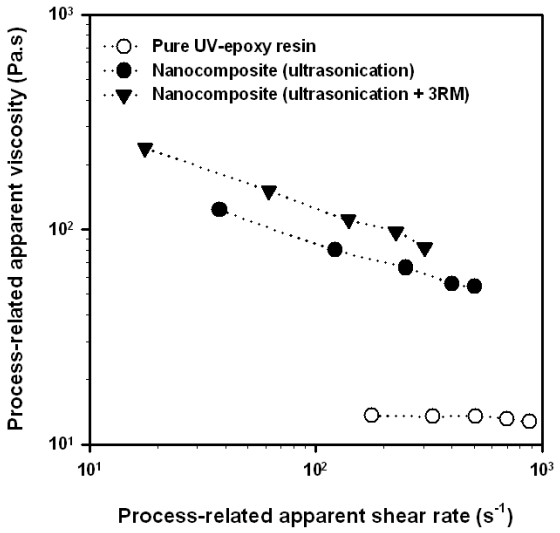

Figure 3. Viscosity characterization of the pure UV-epoxy and its nanocomposites using a method based on capillary viscometry.

The increase of viscosity enabled the fabrication of freeform 3D microstructures with nanocomposites using UV-DW technique. A microspring network consisting of four parallel microsprings were fabricated on aluminum thin pad and mechanically characterized under a compressive loading. The four springs with a rectangular fashion enabled to put another aluminum pad on the top of network for mechanical solicitation. Figure 4a shows force-displacement curves of networks of sonicated and high shear-mixed nanocomposites and a SEM image of the microspring network. The specific rigidity of the spring network made of sonicated nanocomposite was found to be ~ 28 mN mm^{-1} that increased to ~ 35 mN mm^{-1} for the high shear-mixed nanocomposite microspring networks. The stiffness of the nanocomposite structures could be improved by adding more nanotubes, changing the coil geometry and building more springs.

The reinforcing effect of BF-SWCNTs was also assessed by the measurement of the modulus and failure strength. Figure 4b shows the stress-strain curves of the neat epoxy and its

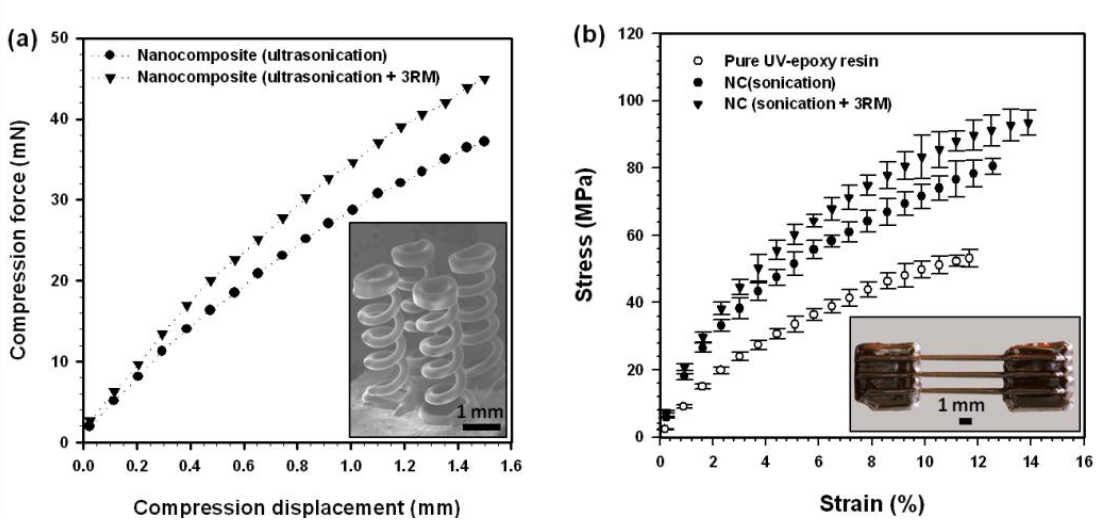

Figure 4. (a) Mechanical response of rectangular microspring networks made of nanocomposites under compressive force, and (b) typical stress–strain curves of the neat epoxy and the nanocomposites fibers**.**

associated nanotube-reinforced nanocomposites microfibers. For the neat epoxy, the average modulus and strength were found to be 1.24 GPa and 53.1 MPa, respectively. For the sonicated nanocomposite microfibers, the average modulus was enhanced to 2.18 GPa, about a 75% improvement, while the strength was increased to 80.5 MPa, about a 51% enhancement. When the nanocomposite subjected to the final high shear mixing, the mechanical properties showed higher increase in both modulus (by 93% to 2.39 GPa) and strength (by 75% to 93.5 MPa). The considerable improvement in mechanical properties of the nanocomposites prepared by three-roll mixing method might be attributed to the nanotube fair-dispersion, strong interfacial attraction between BF-SWCNTs and epoxy matrix as well as beneficial orientation of the nanotubes that may occur during the extrusion of the nanocomposite through the micronozzle.

CONCLUSIONS

UV-curable nanocomposite materials reinforced with BF-SWCNTs were prepared to fabricate nanocomposite 3D microstructures using UV-DW fabrication technique. Surface

biofunctionalization of SWCNTs along with an efficient mixing procedure consisting of ultrasonication and three-roll mill mixing methods led to a considerable enhancement in mechanical properties of the epoxy composites as well as their rheological behaviors. The beneficial orientation of nanotubes that could occur during the extrusion of the nanocomposites may contribute to the achieved improvement of the modulus of the nanocomposites. The significant increase of viscosity, with the addition of only 1 wt%, enabled the UV-DW fabrication of 3D freeform microstructures using nanocomposite materials. The flexible direct-write method enables the utilization of UV-curable nanocomposite materials containing BF-SWCNTs for the fabrication of porous microstructures having 3D complex patterns as solid support materials for potential easy-manipulating biosensor applications.

ACKNOWLEDGEMENTS

The authors acknowledge the financial support from FQRNT (Le Fonds Québécois de la Recherche sur la Nature et les Technologies). The authors would like to thank the technical support of Dr. Hamid Dalir and Mr. Vincent Le Borgne for the nanotube functionalization and characterization.

REFERENCES

1. Qian D, Wagner GJ, Liu WK, Yu M-F, Ruoff RS. 2002. “Mechanics of Carbon Nanotubes”. *Appl. Mech. Rev*, 55(6):495-532.
2. Tans SJ, Devoret MH, Dai HJ, Thess A, Smalley RE, Geerligs LJ. 1997. “Individual single-wall carbon nanotubes as quantum wires”. *Nature*, 386(6624):474-477

3. Therriault D, White S.R, Lewis J.A. 2003. “Chaotic mixing in three-dimensional microvascular networks fabricated by direct-write assembly”. *Nature Materials*, 2(4): 265-271.
4. Liska R, Schuster M, Infuhr R, Turecek C, Fritscher C, Seidl B, Schmidt V, Kuna L, Haase A, Varga F, Lichtenegger J, Stampfl J. 2007.“Photopolymers for rapid prototyping”. *Journal of Coatings Technology and Research*, 4(4): 505-510.
5. Lebel LL, Aissa B, El Khakani MA, Therriault D., 2010, “Ultraviolet-Assisted Direct-Write Fabrication of Carbon Nanotube/Polymer Nanocomposite Microcoils”, *Advanced Materials*, 22(5):592-596.
6. Lebel LL, Aissa B, El Khakani MA, Therriault D, 2010, “Preparation and mechanical characterization of laser ablated single-walled carbon-nanotubes/polyurethane nanocomposite microbeams” *Composites Science and Technology*, 70(3):518-524.
7. Rahatekar SS, Koziol KKK, Butler SA, Elliott JA, Shaffer MSP, Mackley MR,2006, “Optical microstructure and viscosity enhancement for an epoxy resin matrix containing multiwall carbon nanotubes” *Journal of Rheology*, 50(5):599-610.
8. Moniruzzaman M, Fangming D, Naiffer R, Karen I. W. 2006. “Increased flexural modulus and strength in SWNT/epoxy composites by a new fabrication method. Polymer”, 47(1):293-298.
9. Zhu J, Peng HQ, Rodriguez-Macias F, Margrave JL, Khabashesku VN, Imam AM, 2004, “Reinforcing epoxy polymer composites through covalent integration of functionalized nanotubes” *Advanced Functional Materials*, 14(7):643-648.
10. Thostenson, E.T. and T.W. Chou, 2006, “Processing-structure-multi-functional property relationship in carbon nanotube/epoxy composites” *Carbon*, 44(14):3022-3029.
11. Braidy N, El Khakani M.A, Botton G.A. 2002. “Effect of laser intensity on yield and physical characteristics of single wall carbon nanotubes produced by the Nd : YAG laser vaporization method”. *Carbon*, 40(15):2835-2842.

12. Le Borgne V, Aissa B, Mohamedi M, Kim Y.A, Endo M, El Khakani M.A. 2011. “Pulsed KrF-laser synthesis of single-wall-carbon-nanotubes: effects of catalyst content and furnace temperature on their nanostructure and photoluminescence properties” J. nanopart. Res., 11(51):110409, 1-9.
13. Wang D, Sun G, Xiang B, Chiou BS., 2008, “Controllable biotinylated polyethylene-co-glycidyl methacrylate) (PE-co-GMA) nanofibers to bind streptavidin-horseradish peroxidase (HRP) for potential biosensor applications” *European Polymer Journal*, 44(7):2032-2039.
14. Bruneaux, J., D. Therriault, and M.C. Heuzey, 2008, “Micro-extrusion of organic inks for direct-write assembly”.*Journal of Micromechanics and Microengineering*, 18(11):115020,1-11

Appendix B

Ultraviolet direct-write fabrication of chemically treated single-walled carbon nanotube nanocomposite microfibers: experimental and modeling studies

Rouhollah Dermanaki Farahani[1], Hadi Moussaddy[1], Brahim Aissa[2], My Ali El Khakani[2], Martin Lévesque[1], and Daniel Therriault[1]*

[1]Laboratory of Multiscale Mechanics, Center for applied research on polymers (CREPEC), École Polytechnique de Montreal, C.P. 6079, succ. Centre-Ville, Montreal (QC), H3C 3A7 (Canada)

[2]Institut National de la Recherche Scientifique, INRS-Énergie, Matériaux et Télécommunications, 1650 Blvd. Lionel-Boulet, Varennes (QC), J3X 1S2 (Canada)

Abstract

Nanocomposite microfibers were fabricated by extruding single-walled carbon nanotube (SWCNT)/epoxy suspensions through a micronozzle by means of direct-write technique. The SWCNTs were first purified by acidic treatment and then solubilized in acetone using Zinc proptoporphyrin IX as a surfactant. The nanocomposite suspensions were prepared using an efficient mixing method which involves the simultaneous heating and ultrasonicating of the nanocomposite solution diluted in acetone, followed by solvent evaporation and high shear mixing. Morphological characterization revealed that the SWCNTs and their aggregates with a size of up to ~1.3 μm were fairly dispersed in the epoxy matrix. The mechanical characterization of the nanocomposite fibers showed that, with only 0.5wt% loading of purified SWCNTs, the modulus and strength of the nanocomposite were improved by 33% and 27%, respectively. The overall effective stiffness of the nanocomposites was also estimated using micromechanical

homogenization. Perfect bonding condition between carbon nanotubes and the epoxy matrix was assumed. The SWCNTs were assumed to be straight cylinders having an aspect ratio of 500. Since it is very difficult to control and experimentally determine SWCNTs orientation in the matrix, several orientation distributions were studied for comparison purposes: fully aligned, partially aligned and randomly oriented. The results were obtained for individually dispersed SWCNTs as well as dispersed SWCNT bundles featuring lower aspect ratios (25 to 100). Our experimental measured stiffness were found to be lower than the theoretical estimates for fully aligned SWCNTs or bundles of SWCNTs. However, the measured stiffness remains higher than randomly dispersed bundles of SWCNTS. These results suggest a partial alignment of the carbon nanotubes in the manufactured nanocomposites. The experimental stiffness was found to match with the theoretical results of different configurations of SWCNTs in the nanocomposite. Assuming SWCNTs bundles with an aspect ratio of 50 (10 SWCNTs across its diameter), most bundles would be aligned within +/- 45 degrees. If the SWCNTs were to form bundles with an aspect ratio of 25 (20 SWCNTS across its diameter), bundles would be aligned within a smaller range of +/-19 degrees. These results are based on a perfect bonding assumption between straight SWCNTs and matrix. If imperfect bonding and/or SWCNT waviness are to be considered, the calculated alignment would be even better. This alignment achieved in the fiber manufacturing process along with their chemical treatment and efficient mixing processes proposed help achieve full load transfer across SWCNT/epoxy interface, resulting in a considerable reinforcement of nanocomposite fibers.

Keywords: Carbon nanotubes, Nanocomposites, Mechanical properties, mechanical modeling, homogenization, finite element.

1. Introduction

With their unique high aspect ratio[1], excellent mechanical [2] and electrical properties [3], single-walled carbon nanotubes (SWCNTs) were found to be highly promising candidates for reinforcing polymers toward developing future engineering applications. Both in terms of processing and product, the nanocomposite microstructures is the main parameter affecting the processing conditions as well as the overall properties of the nanocomposites [4]. Among polymer nanocomposites, nanotube-reinforced epoxy systems could offer superior composite materials with high strength and multifunctional features [5, 6]. However, several fundamental processing challenges have to be addressed in order to take the full advantages of the excellent properties of nanotubes. The ability to homogeneously disperse and orient the nanotubes throughout the polymer matrix and tailoring interfacial interaction between nanotubes and the epoxy matrix are the main parameters affecting nanocomposites mechanical performance. For the nanocomposites with a thermosetting matrix like epoxy, various mixing methods such as sonication, high shear mixing in a three-roll mill mixer [7] or a twin-screw batch mixer [8] have been used to disperse intrinsically entangled nanotubes within the polymer matrix. Grafting chemical groups like carboxylic groups to the surface of CNTs can chemically modify the nanotubes surface in order to minimize the nanotube agglomeration and also to enhance their interfacial interaction with the polymer matrix [9, 10]. Non-destructive solubilization of SWCNTs using surfactant also offer functional groups without compromising nanotubes physical structure[11].

To address the nanotube orientation, shear flow [12, 13] and electromagnetic fields [14] have been efficiently used. Although the nanotubes alignment leads to anisotropic mechanical properties, it is an efficient way to maximize their reinforcing effect, particularly in

nanocomposite fibers. Fiber spinning, fiber elecrospinning [15], and extrusion [16] are commonly used for the fabrication of oriented nanotube-reinforced nanocomposite fibers. Similar orientation mechanism as extrusion may occur in the direct-write technique [17, 18]. The direct-write technique consists of the robotized deposition of extruded filaments to fabricate 3D microstructures.

In this paper, functionalized SWCNT reinforced UV-curable epoxy nanocomposites were prepared and used to fabricate nanocomposite microfibers using UV-assisted direct-write fabrication technique. A mixing procedure including chemical treatment of nanotubes surface, ultrasonication and high shear mixing were used to fairly disperse SWCNTs in epoxy matrix. As-produced and functionalized SWCNTs were characterized using X-ray photoelectron spectroscopy (XPS) and transmission electron microscopy (TEM). The nanocomposite was morphologically and mechanically characterized in order to study the effect of mixing procedure and fabrication conditions. Finally, the mechanical properties of the nanocomposite were estimated using the Mori-Tanaka micromechanical model[19]. The model has been adjusted to take into consideration partial alignment of carbon nanotubes. The case of aggregation of SWCNTs into bundles has also been studied. To address the nanoscale behavior of nanotubes, the mechanical properties of SWCNTs and that of bundles of SWCNTs were obtained from atomistic simulations found in literature [20, 21].

2. Experimental Details

2.1. Chemical treatments of SWCNTs and nanocomposite preparation

The SWCNTs were produced by means of the pulsed laser ablation technique, using an excimer KrF laser (248 nm, 20 ns, 50 Hz, 300 mJ) with a Co/Ni-doped graphite target. The as-produced SWCNTs were then subjected to acidic purification treatment (HNO_3 3M, Sigma--

Aldrich) to remove the impurities like metal catalyst particles and covalently functionalize the SWCNTs by the attachment of carboxylic groups at their surface (more details on the SWCNTs growth and purification can be found elsewhere [9]). The SWCNTs were characterized by XPS (Escalab 220i-XL system, VG instruments) and TEM (Jeol JEM-2100F).

The nanocomposites were prepared by blending an ultraviolet/heat curable epoxy (UV-epoxy, UV15DC80, Master Bond Inc.) and purified-SWCNTs (P-SWCNTs) at the load of 0.5wt%. The UV-epoxy used here contains a UV photo-initiator having an optimal absorption at 365 nm and a heat-initiator active in the 60 - 80°C range. Non-covalent functionalization of nanotubes using surfactant was conducted to solubilize nanotube aggregates and offer additional carboxylic groups on the nanotubes surface. The desired amount of P-SWCNTs was added to a solution of 0.1 mM of Zinc protoporphyrin IX (Sigma-Aldrich) in acetone. The suspension was sonicated in an ultrasonic bath (Ultrasonic cleaner 8891, Cole-Parmer) for 30 min. The UV-epoxy was then slowly mixed with the nanotube suspension in acetone over a magnetic stirring hot plate (Model SP131825, Barnstead international) at 50°C for 4 h. After stirring, the nanocomposite mixture was simultaneously sonicated and heated in the ultrasonication bath at 50°C for 4 h in order to evaporate the solvent and prevent re-aggregation of nanotubes. The residual trace of solvent was evaporated by heating the nanocomposite mixture at 30°C for 12 h and at 50°C for 24 h in a vacuumed-oven (Cole Parmer). After the evaporation of the solvent, the nanocomposites were passed through a three-roll mill mixer (Exakt 80E, Exakt Technologies) for final high shear mixing. The gaps between the rolls varied in three batch-wise processing steps including 5 passes at 25 µm, 5 passes at 10 µm and 10 passes at 5 µm, respectively. The speed of the apron roll was set to 250 RPM. The final mixture was then degassed under vacuum for 24 h. For comparison purposes, a nanocomposite mixture without subjecting them to the

ultrasonication (i.e., simultaneous heating/sonication) was also prepared. The solvent was evaporated by placing the nanocomposite under hood at room temperature for 24 h, followed by putting in the vacuumed-oven at 30°C for 12 h and at 50°C for 24 h.

2.2. Nanocomposite characterization

The reinforcing effect of chemically treated SWCNTs in the epoxy matrix were assessed by characterizing the mechanical response of the nanocomposites microfibers, fabricated by the direct-write technique [22]. Figure 1 schematically represents the ultraviolet-assisted direct-write fabrication of microfibers. The direct-write technique consists of a computer-controlled robot (I & J2200-4, I & J Fisnar) that moves a dispensing apparatus (HP-7X, EFD) along the *x*, *y* and *z* axes. Nanocomposite microfibers suspended between two rectangular pads of the same materials were fabricated by extruding the nanocomposites suspension through a micro-nozzle (5127-0.25-B, Precision Stainless Steel Tips, EFD, *ID* = 150 μm) over a 6 mm gap between two nanocomposite pads. The microfibers were cured under UV exposure using two high-intensity UV light-emitting diodes (LED, NCSU033A, Nichia) while being extruded. The same technique was used to deposit a ~20 μm-thick film of the nanocomposites on a glass substrate for optical imaging purposes. The quality of the mixing was observed for the cured nanocomposite film using an optical microscope (BX-61, Olympus) and image analysis software (Image-Pro Plus V5, Media Cybernetics). Mechanical properties (tensile modulus, strength and elongation at break) of the nanocomposites fibers were measured in a dynamic mechanical analyzer (DMA, DMA2980, TA instruments) using a film tension clamp. The fibers were tested with a constant loading rate adjusted to reach failure within 20 ± 3 s according to the ASTM D2256 standard.

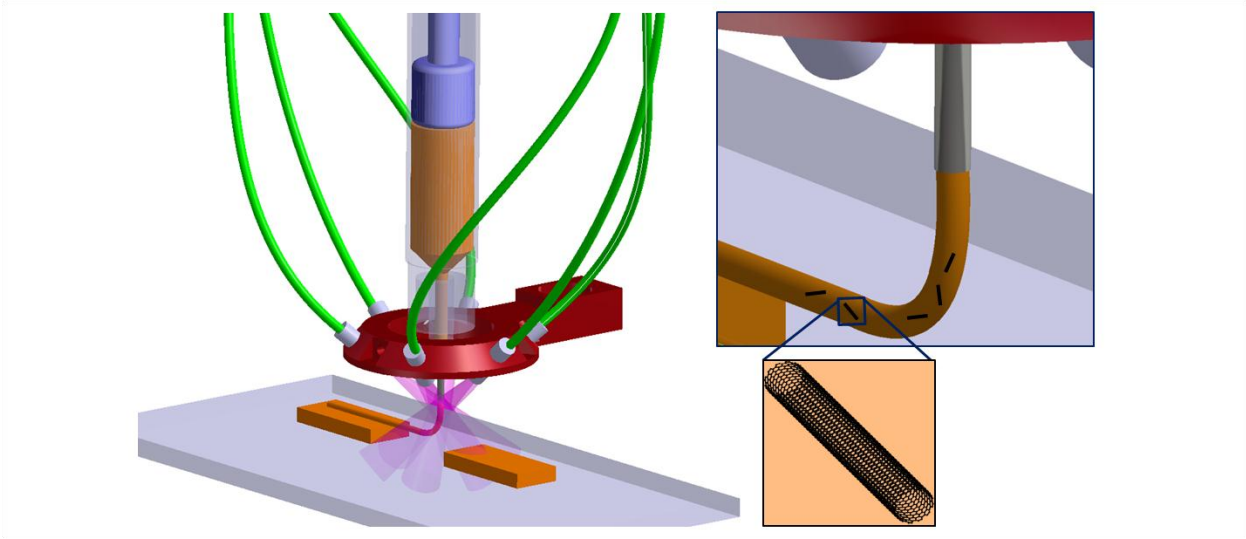

Figure 1. Schematic representation of the UV-assisted direct-writing of nanocomposite microfibers. The microfibers were cured under UV exposure using two high-intensity UV light-emitting diodes (LED, NCSU033A, Nichia) while being extruded through a capillary micronozzle by an applied pressure.

3. Modeling

Several modeling methods have been used in literature to predict the effective mechanical properties of nanocomposites reinforced by SWCNTs[23, 24]. Nanoscale methods, such as molecular dynamics, demand very high computational costs and are limited to very short SWCNTs. Numerical finite element methods have been widely used for the simple case of aligned SWCNTs in nanocomposites. For complex orientations of SWCNTs, finite element calculations become exhaustive. Micromechanical methods, such as the Mori-Tanaka model, reduce considerably the modeling costs. In another study in this same conference, it is shown that the Mori-Tanaka estimations overestimate the finite element results of the effective properties only by up to 5%. This drawback in accuracy is easily accepted considering the gain in computational time and resources. However, care should be taken in micromechanical methods since SWCNTs are not usual fibers, they exhibit a molecular behavior.

In what follows a fourth-order tensor (C_{ijkl}, A_{ijkl} et S_{ijkl}) will be denoted by a bold-faced capital Latin letter (***C***, ***A*** et ***S***).

Following the model of Mori-Tanaka for aligned fibers, the effective elasticity tensor $\boldsymbol{C}^{\boldsymbol{MT}}$ is expressed by [19] :

$$\boldsymbol{C}^{\boldsymbol{MT}} = \boldsymbol{C}_{\boldsymbol{m}} + fv\,\left(\boldsymbol{C}_{\boldsymbol{f}} - \boldsymbol{C}_{\boldsymbol{m}}\right) : \boldsymbol{A}_{\boldsymbol{dil}} : \left[(1-\varphi)\boldsymbol{I} + fv\,\boldsymbol{A}_{\boldsymbol{dil}}\right]^{-1} \qquad \text{(Eq. 1)}$$

where $\boldsymbol{C}_{\boldsymbol{m}}$ and $\boldsymbol{C}_{\boldsymbol{f}}$ are the matrix and the fibre elastic tensor respectively, *fv* is the fiber volume fraction, ***I*** is the 4th order identity tensor and $\boldsymbol{A}_{\boldsymbol{dil}}$ is given by :

$$\boldsymbol{A}_{\boldsymbol{dil}} = \left[\boldsymbol{I} + \boldsymbol{S} : \boldsymbol{C}_{\boldsymbol{m}}^{-1} : \left(\boldsymbol{C}_{\boldsymbol{f}} - \boldsymbol{C}_{\boldsymbol{m}}\right)\right]^{-1} \qquad \text{(Eq.2)}$$

where ***S*** is the Eshelby tensor. The expressions of the Eshelby tensor components are listed in several references, Mura being the most recognizable one [25].

And in the general case of random orientation of fibers, an orientation averaging operation is done:

$$\left\{\boldsymbol{C}^{\boldsymbol{MT}}\right\} = \frac{\int_0^{\theta'}\int_0^{\varphi'}\int_0^{\beta'} \alpha_{ip}\alpha_{jq}\alpha_{kr}\alpha_{ls}\, C^{\boldsymbol{MT}}_{pqrs} \sin(\theta)\, \mathrm{d}\theta\, \mathrm{d}\varphi\, \mathrm{d}\beta}{\int_0^{\theta'}\int_0^{\varphi'}\int_0^{\beta'} \sin(\theta)\, \mathrm{d}\theta\, \mathrm{d}\varphi\, \mathrm{d}\beta} \qquad \text{(Eq. 3)}$$

where $\{\boldsymbol{C}^{\boldsymbol{MT}}\}$ denotes the orientation averaging of $\boldsymbol{C}^{\boldsymbol{MT}}$, and $\boldsymbol{\alpha}$ is the transformation matrix expressed as function of the Euler angles (θ,φ,β) [26]. These three angles can vary between [0; θ'], [0; φ'] and [0; β'] respectively.

Two configurations were studied, the first one is the case of dispersed (10,10) SWCNTs with an aspect ratio of 500 (SWCNTs having a 1.4 nm diameter, and a length of 700 nm). The properties of the nanocomposite were calculated for orientations varying from fully aligned SWCNTs to randomly oriented SWCNTs. This type of SWCNTs, as well as all other armchair and zig-zag nanotube structures, has an axi-symmetric atomic structure. Therefore, they exhibit transverse isotropic material symmetry. The 5 elastic constants, given in Table 1, were obtained by an energetic equivalence between atomic and continuum deformation energies of a discrete atomic model and an equivalent continuum model under given loading conditions[21].

The other configuration is consisted of bundles of SWCNTs dispersed in the epoxy matrix. Depending on the number of its nanotubes, the bundle can have different aspect ratios ranging from 25 (20 SWCNTs across its diameter) to 100 (5 SWCNTs across its diameter). Furthermore, bundles of carbon nanotubes have different elastic properties than individual SWCNTs. Liu et al. [20] have determined the transverse isotropic elastic properties of (10, 10) SWCNTs bundles as a bulk material. The 5 elastic constants are given in Table 1. The effective properties of the nanocomposites reinforced with bundles were calculated for different alignment degrees varying from the ideal case of fully aligned bundles to the opposite case of randomly oriented bundles.

4. Results and discussions

4.2.1. Morphological and mechanical characterizations

Figure 2a shows typical TEM micrographs of the laser-synthesized SWCNTs after their chemical purification. The nanotubes are observed to self-organize most often into bundles, featuring a high aspect ratio since their length can reach up to several microns and their diameter is in the nanometer range. The nanotube chemical purification enabled to remove residual catalyst particles and other carbonaceous structures.

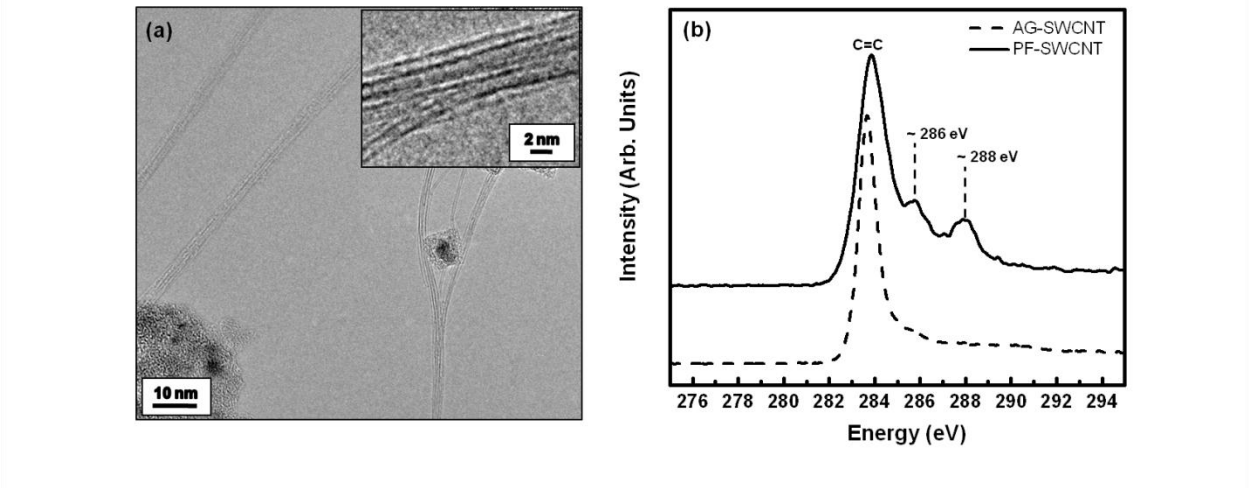

Figure 2. (a) TEM image of P-SWCNTs, and (b) XPS spectrum of as-produced SWCNTs and P-SWCNTs

The presence of functional groups on the surface of SWCNTs was assessed using XPS measurement. Figure 2b shows the XPS spectrum of the as-produced and P-SWCNTs. The XPS results show that the C1s core level peak of purified SWCNTs is consisting of three clear components while that of as-produced samples exhibits only a relatively narrow C=C peak. The main peaks for both curves centered around 284.5 eV are due to the sp^2 bonding for the bulk structure of nanotubes. For the purified nanotubes, the two extra shoulders appearing clearly at ~ 286 eV and ~288 eV are attributed to C-O and/or C-NHx bonds, and to the COO group of carboxylic acid groups [27, 28]. Based on the XPS results, the purification process has led to carboxylic groups grafting onto the SWCNTs surfaces (i.e., covalent functionalization). These functionalized SWCNTs having high aspect ratio are excellent nanofillers for polymer nanocomposites.

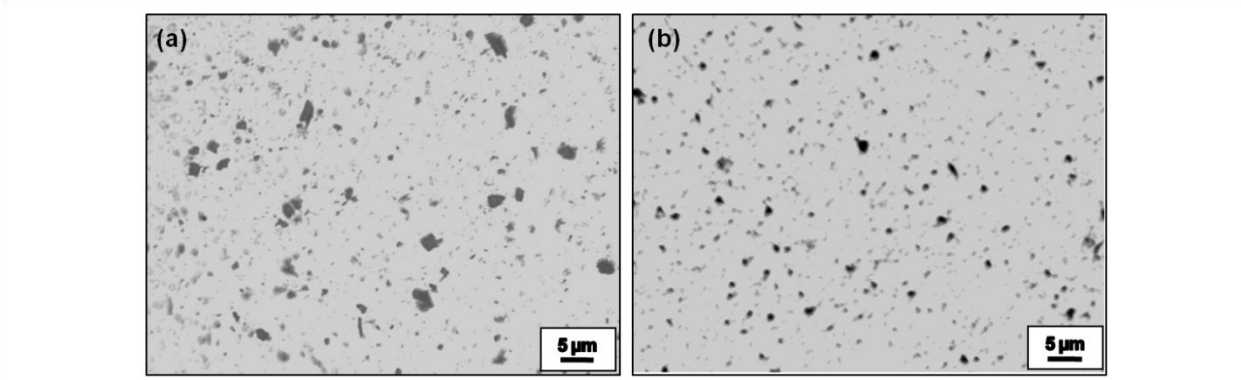

Figure 3. Optical microscopic image of a 20-µm thick film of nanocomposites containing 0.5wt% P-SWCNT prepared by (a) three-roll mill mixing and (b) sonication followed by three-roll mill mixing.

The nanotube dispersion was assessed by optical imaging of nanocomposite films using the optical microscope. Figure 3a shows a typical optical image of the nanocomposites prepared by shear mixing method. The dark spots are believed to be nanotube aggregates and/or carbonaceous materials. Although the majority of the nanotubes have a size in the sub-micron range, micron-size aggregates of up to ~5µm-diameter are also observed. The observed dispersion is due to the enormous shear forces caused by the rotation of rolls with different speeds and also the small gaps between rolls in three-roll mixer. Although the high shear mixing led to breakage of nanotube aggregates, it was not an efficient method to obtain a well-dispersed nanocomposite. Figure 3b shows an optical image of nanocomposite prepared by ultrasonication upon subsequent three-roll mixing. The average size of large aggregates diminished from ~5µm to ~1.3µm-diameter when the nanocomposite suspension subjected to both sonication and high shear mixing. The relatively better dispersion of nanotubes achieved by using this mixing procedure could be attributed to the extra sonication step by preventing re-aggregation of nanotubes in the presence of epoxy molecules while the solvent evaporates.

The reinforcing effect of P-SWCNTs was also assessed by the measurement of the modulus and failure strength. Figure 4 shows the stress-strain curves of the pure UV-epoxy and its

associated nanotube-reinforced nanocomposites microfibers and Table 1 summarizes the results. The incorporation of 0.5wt% P-SWCNTs to the UV-epoxy, by using only three-roll mixer, led to an increase of 24% in modulus and 20% in strength of the nanocomposite fibers. When the nanocomposite was prepared by both ultrasonication and shear mixing methods, the mechanical properties showed higher increase in both modulus (by 33%) and strength (by 27%). The reasonable improvement of mechanical properties of the nanocomposite microfibers suggests that the load is effectively transferred to the nanotubes through interfacial bonding provided by carboxylic groups. Another contribution that might affect the modulus of the nanocomposite microfibers comes from possible beneficial orientation of the nanotubes that may occur during the extrusion of the nanocomposite through the micronozzle. The higher increase in mechanical properties of sonicated/shear-mixed nanocomposite compared to that of shear-mixed nanocomposite might be due to better dispersion of nanotubes, as observed by optical images.

The effective Young modulus results obtained with the Mori-Tanaka model are presented in Figure 5. For each orientation value α, the effective properties are calculated for SWCNTs or bundles of SWCNTs randomly oriented between $[-\alpha; \alpha]$. For the 90 degrees angle value, the effective properties are that of randomly oriented SWCNTs in the nanocomposite. It should be noted that only the longitudinal Young modulus is presented. However, unless the fibers are randomly dispersed, the Young modulus is different in the transverse directions than that of the given longitudinal Young modulus, and the nanocomposite exhibits a transverse isotropic behavior.

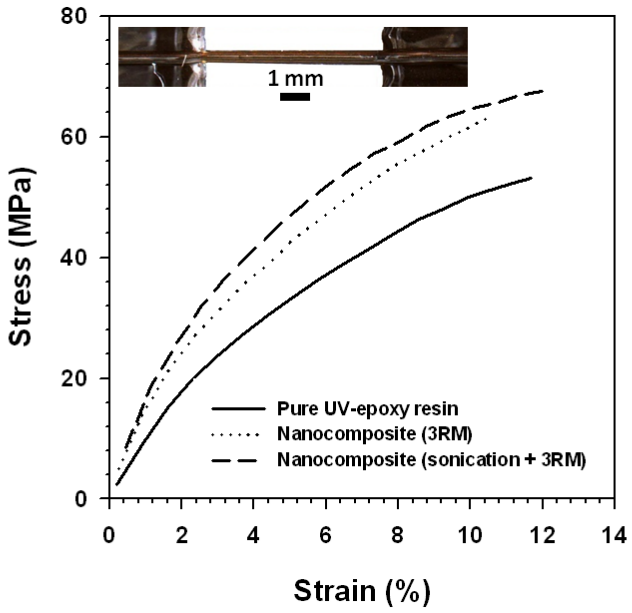

Figure 4. Average stress–strain curves of the UV-epoxy and its nanocomposites fibers.

Depending on the configuration of the reinforcement (individual SWCNTs or bundles) the deducted orientation degree is different. First, it is seen that the individual (10,10) SWCNTs dispersed in the nanocomposite give higher estimations than the experimentally measured stiffness even in the case of full random orientation [-90 ^{o};90^{o}]. For bundles of an aspect ratio of 100 (5 nanotubes across its diameter), the (3RM+Sonication) measured stiffness value corresponds to the nanocomposite with bundles oriented between [-64^{o};64^{o}]. If the SWCNTs were to form bundles having an aspect ratio of 50 (10 SWCNTs across its diameter), the (3RM+Sonication) measured stiffness corresponds to an orientation between [-45^{o},45^{o}]. For bigger bundles with an aspect ratio of 25 (20 SWCNTs across its diameter), the deduced orientation is as close as [-19^{o},19^{o}] for the (3RM+Sonication) measured stiffness. The experimental case with (3RM) is less stiff, hence indicates weaker alignment of the nanotubes and/or bigger bundles having a smaller aspect ratio. The latter is more likely since it was observed in optical images as seen in Figure 3a and 3b.

Table 1. Mechanical properties of (10,10) SWCNTs

	Axial Young modulus (GPa)	Transverse Young modulus (GPa)	Axial Poisson ratio	Transverse Poisson ratio	Axial shear modulus (GPa)
Individual SWCNT	825.0	4.5	0.276	0.389	352.1
Bundle of SWCNTs	621.9	2.7	0.155	0.966	1.22

Table 2. Mechanical properties of the pure UV-epoxy and its nanotube nanocomposites

Type of sample	Modulus (GPa)	Modulus Var. (%)	Strength (MPa)	Strength Var. (%)
UV-epoxy	1.24(± 0.04)	0	53.1(± 2.5)	0
Nanocomposite (3RM)	1.53(± 0.07)	+24	63.3(± 1.7)	+20
Nanocomposite (sonication + 3RM)	1.65(± 0.05)	+33	67.5(± 2.9)	+27

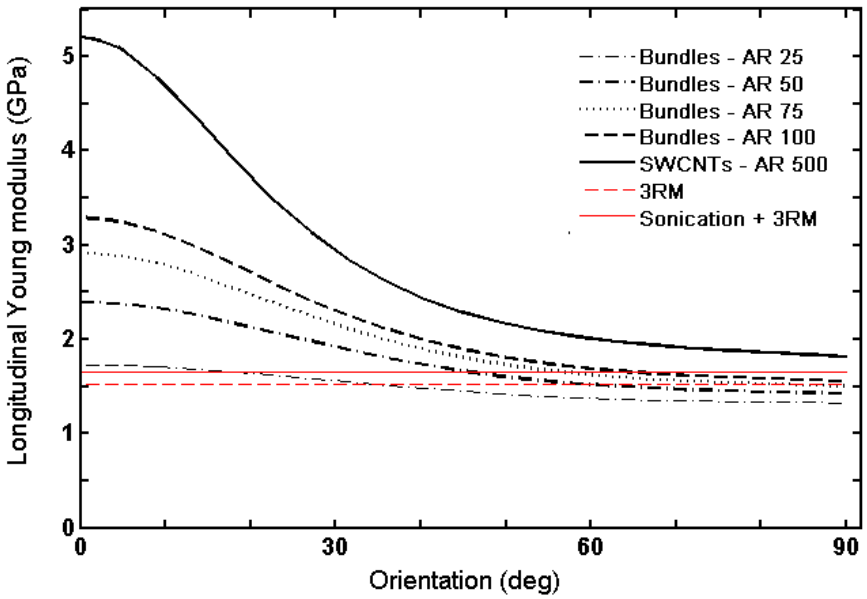

Figure 5. Theoretical estimations and experimental measurements of the longitudinal Young modulus for the SWCNTs/epoxy nanocomposite fibers.

These alignment degrees were deduced only by including the bundling aspect of the SWCNTs. In reality, there are far more defects that can drawback the effective properties of the nanocomposite. First, SWCNTs are wavy and do not stand straight in the nanocomposite. Second, observed carbon nanotubes batches had carbonaceous aggregates. Those aggregates do not have neither the same elastic properties as the SWCNTs, nor the same form and aspect ratio. Furthermore, this relatively weak carbonaceous matter gives place to erroneous SWCNTs volume fractions. Third, perfect bonding was assumed between the nanotubes and the surrounding epoxy matrix. In reality, van der Waals non linear interactions take place between carbon nanotube and surrounding epoxy molecules. However, the perfect bonding assumption is reasonable when studying very long carbon nanotubes [29]. Fourth, carbon nanotubes often have defects in their atomic structure causing a drop in their axial stiffness. The defects can also occur due to the functionalization of SWCNTs. If some or all of these phenomenons were to be considered, higher degree of alignment will be deduced. One can also take into consideration that micromechanical models overestimate the effective properties of nanocomposites, hence will underestimate the alignment of SWCNTs when comparing with experimental results.

5. Conclusions

UV-curable nanocomposite materials reinforced with chemically treated SWCNTs were prepared and then used for the fabrication of nanocomposite microfibers using UV-assisted direct-write fabrication technique. Covalent and non-covalent functionalization of SWCNTs along with an efficient mixing procedure consisting of ultrasonication and three-roll mill mixing led to a considerable enhancement in mechanical properties of the epoxy nanocomposites. According to theoretical predictions, the beneficial orientation of nanotubes that could occur

during the extrusion of the nanocomposites may contribute to the achieved improvement of the modulus of the nanocomposites.

Acknowledgements

The authors acknowledge the financial support from FQRNT (Le Fonds Québécois de la Recherche sur la Nature et les Technologies) and NSERC (Natural Sciences and Engineering Research Council of Canada). The authors would like to thank the technical support of Dr. Brahim Aissa for the nanotube functionalization and characterization, and Maryam Pahlavan Pour for sharing her homogenization Matlab code.

References

[1] D. S. Bethune, *et al.*, "Cobalt-Catalyzed Growth of Carbon Nanotubes with Single-Atomic-Layerwalls," *Nature*, vol. 363, pp. 605-607, Jun 17 1993.

[2] D. Qian, *et al.*, vol. 55, pp. 495-532, November 2002 2002.

[3] S. J. Tans, *et al.*, "Individual single-wall carbon nanotubes as quantum wires," *Nature*, vol. 386, pp. 474-477, Apr 3 1997.

[4] A. W. K. Ma, *et al.*, "The rheology and modeling of chemically treated carbon nanotubes suspensions," *Journal of Rheology*, vol. 53, pp. 547-573, May-Jun 2009.

[5] Y. Ear and E. Silverman, "Challenges and opportunities in multifunctional nanocomposite structures for aerospace applications," *MRS Bulletin*, vol. 32, pp. 328-334, Apr 2007.

[6] J. Zhu, *et al.*, "Reinforcing epoxy polymer composites through covalent integration of functionalized nanotubes," *Advanced Functional Materials*, vol. 14, pp. 643-648, Jul 2004.

[7] E. T. Thostenson and T. W. Chou, "Processing-structure-multi-functional property relationship in carbon nanotube/epoxy composites," *Carbon*, vol. 44, pp. 3022-3029, Nov 2006.

[8] M. Moniruzzaman, *et al.*, "Increased flexural modulus and strength in SWNT/epoxy composites by a new fabrication method," *Polymer,* vol. 47, pp. 293-298, Jan 2006.

[9] L. L. Lebel, *et al.*, "Preparation and mechanical characterization of laser ablated single-walled carbon-nanotubes/polyurethane nanocomposite microbeams," *Composites Science and Technology,* vol. 70, pp. 518-524, Mar 2010.

[10] S. R. Wang, *et al.*, "Effective amino-functionalization of carbon nanotubes for reinforcing epoxy polymer composites," *Nanotechnology,* vol. 17, pp. 1551-1557, Mar 28 2006.

[11] L. Sun, *et al.*, "Mechanical properties of surface-functionalized SWCNT/epoxy composites," *Carbon,* vol. 46, pp. 320-328, Feb 2008.

[12] Z. H. Fan and S. G. Advani, "Characterization of orientation state of carbon nanotubes in shear flow," *Polymer,* vol. 46, pp. 5232-5240, Jun 27 2005.

[13] S. Abbasi, *et al.*, "Flow induced orientation of multiwalled carbon nanotubes in polycarbonate nanocomposites: Rheology, conductivity and mechanical properties," *Polymer,* vol. 51, pp. 922-935, Feb 15 2010.

[14] T. Kimura, *et al.*, "Polymer composites of carbon nanotubes aligned by a magnetic field," *Advanced Materials,* vol. 14, pp. 1380-1383, Oct 2 2002.

[15] I. S. Chronakis, "Novel nanocomposites and nanoceramics based on polymer nanofibers using electrospinning process - A review," *Journal of Materials Processing Technology,* vol. 167, pp. 283-293, Aug 30 2005.

[16] W. Zhou, *et al.*, "Single wall carbon nanotube fibers extruded from super-acid suspensions: Preferred orientation, electrical, and thermal transport," *Journal of Applied Physics,* vol. 95, pp. 649-655, Jan 15 2004.

[17] D. Therriault, *et al.*, "Fugitive inks for direct-write assembly of three-dimensional microvascular networks," *Advanced Materials,* vol. 17, pp. 395-+, Feb 23 2005.

[18] D. Therriault, *et al.*, "Chaotic mixing in three-dimensional microvascular networks fabricated by direct-write assembly," *Nature Materials,* vol. 2, pp. 265-271, Apr 2003.

[19] T. Mori and K. Tanaka, "Average stress in matrix and average elastic energy of materials with misfitting inclusions," *Acta Metallurgica,* vol. 21, pp. 571-4, 1973.

[20] J. Z. Liu, *et al.*, "Mechanical properties of single-walled carbon nanotube bundles as bulk materials," *Journal of the Mechanics and Physics of Solids,* vol. 53, pp. 123-142, 2005.

[21] A. Montazeri, *et al.*, "Computational modeling of the transverse-isotropic elastic properties of single-walled carbon nanotubes," *Computational Materials Science,* vol. 49, pp. 544-551, 2010.

[22] L. L. Lebel, *et al.*, "Ultraviolet-Assisted Direct-Write Fabrication of Carbon Nanotube/Polymer Nanocomposite Microcoils," *Advanced Materials,* vol. 22, pp. 592-+, Feb 2 2010.

[23] G. M. Odegard, *et al.*, "Constitutive modeling of nanotube-reinforced polymer composites," *Composites Science and Technology,* vol. 63, pp. 1671-1687, August 2003 2003.

[24] X. L. Chen and Y. J. Liu, "Square representative volume elements for evaluating the effective material properties of carbon nanotube-based composites," *Computational Materials Science,* vol. 29, pp. 1-11, January 2004 2004.

[25] T. Mura, *Micromechanics of defects in solids,* 2 ed.: Springer, 1982.

[26] J. Schjdt-Thomsen and R. Pyrz, "The Mori-Tanaka stiffness tensor: Diagonal symmetry, complex fibre orientations and non-dilute volume fractions," *Mechanics of Materials,* vol. 33, pp. 531-544, 2001.

[27] S. E. Baker, *et al.*, "Covalently bonded adducts of deoxyribonucleic acid (DNA) oligonucleotides with single-wall carbon nanotubes: Synthesis and hybridization," *Nano Letters,* vol. 2, pp. 1413-1417, Dec 2002.

[28] T. I. T. Okpalugo, *et al.*, "High resolution XPS characterization of chemical functionalised MWCNTs and SWCNTs," *Carbon,* vol. 43, pp. 153-161, 2005.

[29] X. Li, *et al.*, "Reinforcing mechanisms of single-walled carbon nanotube-reinforced polymer composites," *Journal of Nanoscience and Nanotechnology,* vol. 7, pp. 2309-2317, 2007.